The Regulation of Mitochondrial Complex I Biogenesis in *Drosophila* Flight Muscles

Christian Joel Garcia

Submitted in partial fulfillment of the
requirements for the degree of Doctor of Philosophy
under the Executive Committee
of the Graduate School of Arts and Sciences

COLUMBIA UNIVERSITY

2020

Abstract

The Regulation of Mitochondrial Complex I Biogenesis in Drosophila Flight Muscles

Christian Joel Garcia

Mitochondrial Complex I (CI) is composed of 44 distinct subunits that are assembled with eight Fe-S clusters and a single flavin mononucleotide. Mitochondria is highly enriched in the flight muscles of *Drosophila melanogaster,* however the assembly mechanism of *Drosophila* CI has not been described. We report that the mechanism of CI biogenesis in *Drosophila* flight muscles proceeds via the formation of ~315-, ~550-, and ~815 kDa CI assembly intermediates. Additionally, we define specific roles for several CI subunits in the assembly process. In particular, we show that dNDUFS5 is required for converting the ~700 kDa transient CI assembly intermediate into the ~815 kDa assembly intermediate, by stabilizing or promoting the incorporation of dNDUFA10 into the complex. Our findings highlight the potential values of *Drosophila* as a suitable model organism and resource to study the CI biogenesis *in vivo,* and to address questions relevant to CI biogenesis in humans.

CI biogenesis is regulated by transient interactors known as CI assembly factors (CIAFs). To date, about half of CI disorders are attributed to the mutations in the CI subunits and the known CIAFs. The cause for the other half remains to be discovered, warranting the investigation for additional regulators of CI biogenesis such as novel CIAFs. To identify novel regulators, we cataloged interactors of a core subunit, NDUFS3, knocked each one down by RNAi in the *Drosophila* flight muscle, and analyzed its effect in the stability of CI by blue-native PAGE. We identified the Drosophila Fragile X Mental Retardation protein (dFMRP) to destabilize the holoenzyme of CI and cause it to misassemble. Therefore, we report dFMRP as a novel regulator of CI biogenesis, and demonstrate the utilization of *Drosophila* as an effective model system to uncover the mysteries of CI biogenesis.

Table of Contents

List of Figures and Tables

List of Abbreviations

CI	Complex I
CIAF	Complex I assembly factors
dFMRP	*Drosophila* Fragile X Mental Retardation Protein
OMM	Outer mitochondrial membrane
IMM	Inner mitochondrial membrane
IMS	Intermembrane space
mtDNA	Mitochondria DNA
ETC	Electron transport chain
OXPHOS	Oxidative phosphorylation
TCA	Tri-carboxylic acid cycle
MPC	Mitochondrial pyruvate carriers
PDH	Pyruvate dehydrogenase
CPT1	Carnitine palmitoyltransferase 1
CAT	Carnitine translocase
CPT2	Carnitine palmitoyltransferase 2
N	NADH binding site
Q	Ubiquinone binding site
P_P	Proton pumping proximal
P_D	Proton pumping distal
Cryo-EM	Cryo-electron microscopy
RET	Reverse electron transfer flow
PASMCs	Pulmonary artery smooth muscle cells
SIRT3	Sirtuin 3
MCU	Mitochondrial calcium uniporter
MELAS	Mitochondrial encephalomyopathy-lactic acidosis-stroke like episodes
MPTP	1-methyl-4-penyl-1, 2, 3, 6-tetrahydropyridine
FMR1	Fragile X Mental Retardation 1
MCIA	Mitochondrial complex I assembly complex
DIOPT	*Drosophila* ortholog prediction tool
BN-PAGE	Blue native polyacrylamide gel electrophoresis
CIII	Complex III
CV	Complex V

dNDUFS3	*Drosophila* NDUFS3
co-IP	Co-immunoprecipitation
RNAi	RNA interference
UAS	Upstream activating sequence
BDSC	Bloomington *Drosophila* Stock Center
Dmef2	*Drosophila* Muscle Enhancing Factor 2
Mhc	Myosin heavy chain
CRISPRi	CRISPR interference
dCAS9	Dead CAS9
LAI	Lower Assembly Intermediates
OTEs	Off-target effects
FXR1	Fragile X related protein 1
FXR2	Fragile X related protein 2
Scpx	Sterol carrier protein X-related thiolase
Men-b	Malic enzyme b
MCUC	Mitochondrial calcium uniporter complex
BirA	Biotin ligase enzyme
SCAF1	Super complex assembly factor 1

Acknowledgements

I would like to thank my mentor Dr. Edward Owusu-Ansah for giving me the opportunity to work in his lab. Being in a small lab, I had the chance to work side by side with Edward on the scope to learn everything there is about the fruit fly. It was also in these moments, where we had some of the best scientific conversations during my Ph.D. Working in a new lab, I also had the privilege to learn from Edward how to build a lab from the ground up which is something not every grad student gets to do. I will always appreciate everything Edward has done for me that has led to my success as a scientist.

During my time in the Owusu-Ansah lab, I had the opportunity to work with several people who taught me so much and made lab an enjoyable place to be. First and foremost, I would like to thank the first postdoc in the lab, Dr. Jahan Khajeh, who taught me all of the techniques that I have used for my projects. His efforts laid down the foundational work for the scope of my project. Also, I would to thank Drs. Bibhuti Mishra and Anjaneyulu Murari, two other postdocs, who were not only colleagues I could turn to in the lab, but have also become great friends. Other members in the lab I would like to thank are Emmanuel Coulanges, Dr. Kim Lucero, Arden Darko, Sri Goparaju, Maximino Villanueva, Shauna Kay-Rhoomes, and Dr. Rida Gilani for their friendships and hard work behind the scenes to keep the lab running smoothly.

One of the highlights I had as a graduate student was the opportunity to train students. I would especially like to thank Marjana Tafader, John Varriano, and Cindy Osei for not only contributing to my projects but trusting me as a mentor. I learned so much from each of these students and wish them the best in their future endeavors.

Thank you to my collaborators Drs. Emily Chen, Richard Kitsis, Yun Chen, Laura Johnston, Catarina Quinzii, Marcello Ziosi, Jason Fan, Matthew Ulgherait, Mimi Shirazu, Alexander Galkin, Anna Stepanova, and Delfina Larrea for allowing me the opportunity to work with you. I enjoyed all of the conversations we had and look forward to the scientific contributions that will result from our work.

I would like to thank my dissertation research committee: Drs. Estela Area-Gomez, Martin Picard, Eric Schon, and Stavroula Kousteni. I appreciate the time each of you have spent with me and your advice on projects, careers, and life in general that have helped guided me through this Ph.D. journey.

I would also like to acknowledge the Mitochondria Community here at Columbia University who have been so generous from discussing ideas on projects to sharing reagents and resources. In particular, I would like to thank my friend Rishi Agrawal who co-founded the mitochondria group with me. When we first joined our mitochondria labs, no group existed on campus; but after 4 years the group grew from 15 to well over 100 scientists.

During my Ph.D., I was able to partake in co-directing the Science Matters Research Internship and had the chance to work with over 20 high school students to give them the opportunity to work in a CUIMC lab. This was another highlight of the Ph.D. as I got to witness how these internships shaped the lives of these students. I could not have done this without the help of my co-director Elise Flynn. Thank you for being an amazing director and for allowing me to learn from you on how to efficiently run an organization. Also, I would like to thank Drs. John Smerdon and Katherine Xu for having the confidence in me to follow their footsteps as a co-director.

I would like to thank the Institute of Human Nutrition, especially Debra Wolgemuth and Richard Deckelbaum for accepting me into the program and for supporting my career. In addition, I would also like to thank Alex Sosa, Leslie De Pena, Sara Sternglass, and Zachary Corter for their work behind the scenes. Thank you to Zaia Sivo for your guidance throughout the Ph.D.

Thank you to my best friends Jimin Park and Rishi Agrawal for the memorable moments we have accumulated together over these years. From the boardgame nights, brunch, Fort Lee BYOBs, speakeasy hopping and traveling to other countries, I had so much fun in graduate school because of the two of you! Thank you Greg Weissner for sharing my passion of IPAs and throwing Julian an amazing baby shower. Jeewon and I appreciate all you have done for our family. Thank you Bryan Gonzales for getting me hooked on to triathalons. I will never forget our 6 A.M. swim workouts. Calling New York my second home was easier thanks to Brando, my cousin. Thank you for being one of my best friends, my best man, and the best Tio to my son.

My parents, Imelda and Manuel Garcia, my brothers Manuel Jr. and John (JJ) as well as their families. Thank you for instilling my faith in God, for being my role models, for K.I.S.S., for helping me

make the best of my decisions, and for reminding me what the most important things in life are. Thank you all for now being the most amazing grandparents, tios, tias, and primos to Julian. We love you all.

Out of all the events that have happened throughout my Ph.D. journey, the biggest highlight was meeting my wife Jeewon Garcia-So. From our first conversation about IPA beers at Fat Cat, to running the NYC marathon together, to getting married, and then having a child, these past 6 years have been a blessing. Thank you for all the support, sacrifices, and love that you give to Julian and me. I love you and I look forward to starting our next chapter.

Dedication

I dedicate my thesis to my wife Jeewon Garcia-So and my son Julian Noah Garcia-So.

Chapter 1: Introduction

Overview

This chapter is aimed to provide a thorough overview of mitochondria complex I (CI) and the roles it plays inside the cell. First, the localization and the role of CI in the context of metabolism will be discussed. A comprehensive background on the structure, function, and mechanism of CI will follow, going into detail on the proteins involved in the biogenesis of the structure. Next, the role of CI in mitochondria function outside of bioenergetics will be introduced. Finally the known diseases and pathologies that occur due to CI dysfunction, as well as the notion of CI as the hidden nexus of cellular metabolism will be discussed.

Mitochondria

Mitochondria Structure

Over a billion years ago, alpha proteobacteria cells survived endocytosis by a prokaryotic cell, later to be termed mitochondria (Boxma et al., 2005; DiMauro and Schon, 2003; Dyall et al., 2004; Martin, 2010). Through this symbiotic relationship, the eukaryotic cell was born and was enabled to create and expend more energy by using oxygen from the air (Lyons et al., 2014; Spinelli and Haigis, 2018). Because mitochondria originated from bacteria, their structures are quite similar. Mitochondria are dual membrane organelles with an outer mitochondrial membrane (OMM) and an inner mitochondrial membrane (IMM) (DiMauro and Schon, 2003). The space between the OMM and IMM is called the intermembrane space (IMS) and the area enclosed by the IMM is called the matrix (DiMauro and Schon, 2003). Similar to bacterial cells, mitochondria contain their own circular DNA (mtDNA) inside the matrix (Meyer et al., 2018). This is a very unique characteristic of mitochondria, as they are the only organelle besides the nucleus that contain their own DNA. Since mitochondria are thought to predate the eukaryotic cell in evolution, they can be found ubiquitously in eukaryotic cells. However, some cells such as the red blood cell lack mitochondria (Zhang et al., 2011).

Mitochondria DNA

The building blocks of the mitochondria are made up of pieces encoded by both the mtDNA and the nuclear DNA (nDNA). Each individual's mtDNA is maternally inherited with each cell containing several copies. MtDNA is a compact circular genome of 16.5 kb that encodes 11 mRNAs (Jeandard et al., 2019). These are translated to 37 gene products: the 12S and 16S mitochondria ribosomal RNAs, 22 tRNAs required for mitochondrial protein synthesis, and 13 subunits of the protein complexes in the mitochondrial electron transport chain (Jeandard et al., 2019). Mutations in mtDNA can lead to a diverse population of these molecules (termed mtDNA heteroplasmy) among different cells in the same tissue of a person (Stewart and Chinnery, 2015). Interestingly, a person can live normally with up to 80% of mutations in their mtDNA (Stewart and Chinnery, 2015). Recently, mtDNA has been shown to eject itself from the mitochondria into the cytosol and be free floating outside of the cell, suggesting new roles as a signaling molecule (Ingelsson et al., 2018; Trumpff et al., 2018). The nDNA encodes over 1000 gene products that are localized to the mitochondria (Calvo et al., 2016; Pagliarini et al., 2008). The majority of these genes are important for making up the rest of the mitochondrial electron transport chain, the import machinery, the proteins responsible for mitochondrial dynamics, and the proteins involved with metabolism (Jeandard et al., 2019). Although scientists have reported that several of these gene products are localized to the mitochondria, their roles remain to be characterized (Calvo et al., 2016; Pagliarini et al., 2008). Additionally, several nDNA-encoded genes have been shown to be involved in alternative roles to help the cells adapt during mitochondrial dysfunction; these discoveries have shed light on how the nucleus and mitochondria communicate with one another (Haynes and Ron, 2010).

Bioenergetics and Metabolism

Electron Transport Chain

Mitochondria generate ~90% of the cell's energy from the Electron Transport Chain (ETC) (Wallace and Chalkia, 2013). The ETC consists of 4 complexes that are located in the folds of the IMM, also referred to as the cristae. Their names are NADH:ubiquinone oxidoreductase (complex I), succinate dehydrogenase (complex II), ubiquinol-cytochrome c oxidoreductase (complex III), and cytochrome c oxidase (complex IV) **(Figure 1.1)**. The ETC generates ATP through a process known as oxidative phosphorylation (OXPHOS)

(Cogliati et al., 2018; Sazanov, 2015). OXPHOS is the transfer of electrons from high-energy molecules such as NADH or $FADH_2$ to oxygen through electron carriers (i.e. ETC) (Perales-Clemente et al., 2008). These high energy molecules donate their electrons to either complex I or II to initiate the transfer of electrons. NADH is oxidized by complex I and $FADH_2$ is oxidized by complex II (Cogliati et al., 2018). The electrons are passed along to complex III by the electron carrier ubiquinone. After passing through complex III, the electrons are transferred by the electron carrier cytochrome c to complex IV, where the electrons undergo a reaction with oxygen to make water. This process is coupled tightly to the pumping of hydrogen ions, or protons, across the IMM. Complex I and complex III pump 4 protons each and complex IV pumps 2 protons (Perales-Clemente et al., 2008). This creates a proton gradient for the rotor ATP synthase (complex V) to make ATP from ADP and inorganic phosphate (Jonckheere et al., 2012). This process is the underlying theory to the evolution of higher ordered organisms by allowing the cells to perform intricate processes that require more energy (Lyons et al., 2014).

Tri-Carboxylic Acid Cycle

Inside the mitochondrial matrix, the tri-carboxylic acid cycle (TCA) produces the high energy molecules (NADH and $FADH_2$) needed to initiate the ETC (Sharma et al., 2005). The TCA cycle produces 3 NADH and 1 $FADH_2$ from eight reactions and eight intermediates that begins with the oxidization of acetyl-CoA (Sharma et al., 2005). Acetyl-CoA is generated from the carbohydrates, fats, and proteins we consume. Each of these nutrients enter the matrix via different processes. First, carbohydrates are broken down into glucose where it undergoes glycolysis in the cytoplasm of the cell to make pyruvate. Glycolysis will produce 2 ATP per molecule and is the main contributor of ATP production during anaerobic respiration (Rafikov et al., 2015). Interestingly, cancer cells have been known to favor glycolysis (Liberti and Locasale, 2016). Pyruvate is transported into the mitochondria matrix by the mitochondrial pyruvate carriers 1 and 2 (MPC), which form a dimer in the IMM (McCommis and Finck, 2015). Inside the matrix, pyruvate dehydrogenase (PDH) converts pyruvate into acetyl-CoA to initiate the start of the TCA cycle (Sharma et al., 2005). The process of glucose oxidation yields about 32 moles of ATP per molecule of glucose (Schönfeld and Reiser, 2013). Alternatively, acetyl-CoA can be generated from the breakdown of fats into

fatty acids. This process begins in the cytosol where fatty acids are modified to acylcarnitine by carnitine palmitoyltransferase 1 (CPT1) and transported into the IMM by carnitine translocase (CAT) (Schönfeld and Reiser, 2013). In the IMM, acylcarnitine is converted into acyl-CoA by carnitine palmitoyltransferase 2 (CPT2) and imported into the matrix where beta oxidation occurs (Schönfeld and Reiser, 2013). Beta-oxidation produces acetyl-CoA from acyl-CoA for the TCA cycle to use while also making 1 NADH and 1 $FADH_2$. The amount of ATP produced during the oxidation of fatty acids is about 106 moles of ATP per fatty acid (Schönfeld and Reiser, 2013). Finally, the breakdown of proteins into amino acids can be converted into seven different metabolites to power the TCA cycle at various steps. Amino acids that catabolize into acetyl CoA or acetoacetyl coA are known as ketogenic amino acids since they produce ketone bodies or fatty acids (Berg et al., 2002). Other amino acids that are catabolized into pyruvate, alpha ketoglutarate, succinyl CoA, fumarate, or oxaloacetate and are termed glucogenic amino acids (Berg et al., 2002). Alpha ketoglutarate, succinyl CoA, fumarate, and oxaloacetate are all intermediates present in the TCA cycle.

It is important to note that the preference between glucose and fatty acid as precursors of the TCA cycle varies in different tissues. For example, the brain primarily consumes glucose whereas the heart favors the degradation of fatty acids (Schönfeld and Reiser, 2013). Several factors contribute to the reason a certain nutrient is favored over another. First is that since fatty acid oxidation produces more ATP; tissues that require more energy are likely to favor fatty acid oxidation. Another difference is the amount of NADH and $FADH_2$ generated ($FADH_2$/NADH). This ratio is important for dictating whether electrons will be transferred by complex I or complex II. During glucose oxidation a ratio of 0.2 $FADH_2$/NADH will lead to most electrons entering complex I (Schönfeld and Reiser, 2013). Fatty acid oxidation, on the other hand, has a slightly higher ratio of 0.5, which allows for complex II to compete with complex I and thus produce reactive oxygen species from complex I (Schönfeld and Reiser, 2013).

Mitochondria Complex I

Compositions of Mitochondrial Complex I (CI)

Mitochondrial Complex I (I) is the first and largest complex of the electron transport chain. The size of mammalian complex I is about ~1 mDa and has a distinct boot shape, with a peripheral arm extending into the mitochondrial matrix and a membrane arm embedded in IMM (Fiedorczuk et al., 2016; Hirst, 2013). The structure of CI can be divided into three functional modules based on their roles during OXPHOS: the N-module (NADH binding site), the Q module (ubiquinone binding site), and the P module (proton pumping site) (Mimaki et al., 2012). At the tip of the peripheral arm, NADH binds to the N-module, donating two electrons. These electrons pass through a series of iron-sulfur clusters and bind to ubiquinone in the Q module. Concurrently, 4 protons are pumped across the membrane arm from the matrix into the IMS, contributing to the proton gradient for ATP to be made (Hirst, 2013).

Single particle cryo-EM was used to solve the first structural models of mammalian CI (Fiedorczuk et al., 2016; Zhu et al., 2016). These models have provided insights to the positions of each subunit in CI as well as potential roles in regulating complex I. Mammalian CI is made up of 44 different subunits, encoded by both the mitochondrial and nuclear genomes, 7 and 37 subunits respectively **(Figure 1.2)** (Hirst, 2013; Zhu et al., 2016). Fourteen of these subunits are known as the core subunits due to their catalytic functions being conserved throughout all species, while the rest are referred to as the accessory subunits. The 14 core subunits are highly similar structurally to bacteria CI suggesting that the redox mechanism has been evolutionarily conserved across species (Berrisford et al., 2016). The core subunits consist of all 7 mtDNA subunits (ND1-6 and ND4L) and 7 of the nDNA subunits (NDUFS1-3, NDUFS7-NDUFS8, and NDUFV1-2) (Hirst, 2013). The crystal structure of CI from *Thermus thermophilus* identified the positions of all 14 core subunits and showed that they form the foundational boot-shaped structure of CI (Baradaran et al., 2013; Berrisford et al., 2011; Sazanov and Hinchliffe, 2006). The mtDNA-encoded subunits are embedded in the membrane arm and the nDNA-encoded subunits extend into the matrix to make the peripheral arm. In addition to the subunits, the peripheral arm includes a flavin mononucleotide at the tip for the binding of NADH and 8 iron-sulfur clusters that are involved in electron transfer (Fiedorczuk et al., 2016; Zhu et al., 2016). The 30 accessory subunits, which are not present in bacteria CI, form a cage-like structure wrapping around the core subunits. In addition, one of the accessory subunits, NDUFAB1, was found to be present at two different locations to make the total number of subunits in the final complex 45

(Fiedorczuk et al., 2016). The role of these accessory subunits and their requirement for the function of CI is still being explored (Garcia et al., 2017; Stroud et al., 2016).

The roles and the importance of the accessory subunits remain unclear, especially as they seem to have co-evolved with higher-order organisms that demand more energy. One hypothesis is that they play a role in the stabilization of CI. This hypothesis was tested in HEK293 cells using CRISPR to knock out every accessory subunit of CI. Results showed that 25 accessory subunits were strictly required for the stabilization of CI and that NDUFAB1 was required for cell viability (Stroud et al., 2016). Our study performed in *Drosophila* flight muscle knocked down 28 of the 30 accessory subunits found in mammals using RNAi. All 28 accessory subunits were shown to be required for cell viability and stabilization (Garcia et al., 2017). All together, these results have made a strong case that accessory subunits are critical for the function and stabilization of CI.

The characterization of the accessory subunits at atomic resolution have provided great insights to their additional role in regulating CI. In particular, a study of ovine CI identified specific cofactors that bind to accessory subunits that may be important for regulating redox reactions, oxygen sensing, and fatty acid synthesis (Fiedorczuk et al., 2016). Furthermore, in the hydrophobic membrane arm, several lipids, including cardiolipin, bound to several core and accessory subunits and were important for the stabilization of CI (Fiedorczuk et al., 2016). The mechanism regulating the coupling between electron transfer and proton translocation is still a mysterious process, however the CI structure suggests that accessory subunits to play a critical role (Hirst, 2013; Sazanov and Hinchliffe, 2006). The binding site of ubiquinone in CI (Q site) is thought to be the driver of this process, and thus must be tightly regulated. CI regulates the Q site by undergoing a conformational change to block the Q site and prevent ubiquinone from entering (Sazanov, 2014). This state is known as the deactive state of CI and occurs in the absence of substrates (Babot et al., 2014; Blaza et al., 2018). Certain accessory subunits are suggested to flank the Q site during the deactive state to prevent the entry of ubiquinone (Fiedorczuk et al., 2016). As future CI structures increase the atomic resolution of accessory subunits, it will be interesting to see what additional roles are inferred from these structures

Biogenesis of Mitochondrial CI

The assembly of mammalian CI is a step wise process that occurs inside the mitochondria. First, subunits of CI bind to each other to form four distinct assembly intermediates. The N-, Q-, and P- modules make up the core assembly intermediates with the P module split into two different intermediates: P proximal (P_P) (being closer to the membrane arm), and P distal (P_D) (being farther away from the membrane arm) (Formosa et al., 2018; Signes and Fernandez-Vizarra, 2018). Once these assembly intermediates are formed, they integrate in a coordinated sequence to make the final structure. In human 143b osteosarcoma cells, researchers performed a pulse-chase experiment using chloramphenicol to inhibit mitochondria translation. Once the subunits of CI were not detectable, mitochondria translation was turned back on and the assembly of CI was tracked by blue-native PAGE followed by proteomics, the whole process termed "complexome profiling" (Guerrero-Castillo et al., 2017). They found that the Q and P_P modules bind together first, followed by the P_D module. The N module was the last to bind to the Q module to complete the formation of the CI holoenzyme (Guerrero-Castillo et al., 2017). Most CI subunits form one of the assembly intermediates prior to being added to the holoenzyme, but some CI subunits bind the holoenzyme on their own. Our lab published the use of *D. melanogaster* to study CI assembly (Garcia et al., 2017). Using RNAi, 35 of the 37 nuclear encoded subunits were individually knocked down in the flight muscle of *D. melanogaster*. Mitochondria were isolated, and the assembly intermediates were tracked using blue-native PAGE followed by immunoblot analysis. The study showed the steps at which each of these subunits were incorporated into the intermediates and/or the holoenzyme. These results complemented those of the human studies reporting that several of the nuclear-encoded subunits are critical for the formation of specific assembly intermediates. However, interestingly, specific subunits, such as NDUFS5, came in at a later point and did not belong to any specific assembly intermediate, suggesting that certain subunits get inserted into CI on their own (Garcia et al., 2017).

Models of Complex I Biogenesis

Research to uncover the mechanisms of how all 44 subunits come together to form CI has had a setback due to the lack of genetic models as well as the lack of structural knowledge compared to the other

respiratory chain complexes. *Saccharomyces cerevisiae*, which has been a powerful genetic model throughout many areas of scientific research, does not have CI, but has the other four complexes (Mileykovskaya et al., 2012). Although this model served as a foundation for understanding the assembly of complex II-complex V, a different genetic model is necessary to study that of CI (Meunier et al., 2013; Rigby et al., 2007). Therefore, the field turned to other less-known genetic models, such as the fungi *Neurospora crassa* and *Yarrowia lipolytica* (Guerrero-Castillo et al., 2009; Marques et al., 2005). These models were very useful in investigating the core assembly of CI, but were limited due to the lack of certain accessory subunits when compared to mammalian CI (Kerscher et al., 1999; Videira, 1998). In the past decade, the *Drosophila melanogaster* flight muscle has been deemed a relevant model for mitochondria research (Owusu-Ansah et al., 2013; Thomas et al., 2014). In recent years it has been used to understand mammalian CI, as it contains 42 of the 44 human CI subunits, the closest of all models thus far (Garcia et al., 2017). Additionally, recent advancements in genetic tools, such as CRISPR/CAS9, led to the creation of knockout cell lines for each CI subunit (Stroud et al., 2016). These models showed that the accessory subunits are critical for CI assembly and helped elucidate the process.

Another reason that our knowledge of the CI subunits and their assembly has lagged compared to other respiratory chain complexes has to do with the delay in solving the crystal structure of CI. To put things into perspective, the mammalian structures of the other complexes were solved in the late 90s and early 2000s compared to the first atomic resolution mammalian CI structure being identified in 2016 (Abrahams et al., 1994; Fiedorczuk et al., 2016; Iwata et al., 1998; Sun et al., 2005; Tsukihara et al., 1995). The large size of CI is the main reason for this delay, however the development of cyro-electron microscopy (cryo-EM) technology in the past decade contributed to solving the structure of CI (Baker, 2018).

Regulators of CI Biogenesis

In addition to CI subunits, several chaperone proteins known as assembly factors are important for regulating the biogenesis of CI (Formosa et al., 2018). These proteins are involved in the formation and function of CI; however, they are not present in the final holoenzyme. Assembly factors have been shown to play specific roles in regulating the assembly of CI, such as stabilization of the assembly intermediates

by binding to specific subunits, posttranslational modifications of subunits, or stabilizing the expression levels of subunits or other assembly factors (Andrews et al., 2013; Rhein et al., 2013; Sugiana et al., 2008). To date, 15 assembly factors have been identified, with 11 of them shown to have mutations in CI-deficient patients (Formosa et al., 2018). More often than not, patients who are diagnosed with CI deficiency do not know what the causative gene is after exome sequencing. This can be due to mutations happening *de novo*, mutations occurring in untranslated regions, and difficulty in identifying the exact variant that is causing the mutation (Fassone and Rahman, 2012). New technologies, such as RNA sequencing, will be important for identifying such mutations (Kremer et al., 2017). Consequently, new CI assembly factors remain to be discovered (Pagliarini and Rutter, 2013; Taylor et al., 2014).

Supercomplexes

Traditionally, the complexes of the ETC were thought to exist only as discrete enzymes, however the past decade of research has shown evidence that they can exist as supramolecular structures. Cryo-EM has revealed that mammalian CI can bind with complexes III and IV to form supercomplexes. This includes CI bound to a complex III dimer (I_1III_2) and CI bound to a complex III dimer and complex IV ($I_1III_2IV_1$) (Letts et al., 2017). Although the function of supercomplexes is not entirely clear, the current hypothesis of these structures is to increase the efficiency of electron transfer during OXPHOS (Letts and Sazanov, 2017; Milenkovic et al., 2017). Researchers also think that complexes III and IV help stabilize CI and prevent it from oxidative stress. Interestingly, the structures of supercomplexes have revealed accessory subunits of CI to be the main sites where CIII and CIV subunits bind to form supercomplexes (Fiedorczuk et al., 2016; Letts and Sazanov, 2017; Zhu et al., 2016). Such discoveries have proposed an additional role for accessory subunits to be involved in stabilizing and forming supercomplexes.

CI as a Regulator of Mitochondrial Function

As the “front door” for electrons to pass through the ETC and a huge contributor to the proton gradient, CI always had the clearly defined role to be the main driver of ATP production. The past two

decades of mitochondria research have advanced the role of CI beyond bioenergetics, as a central regulator of metabolism. CI is now also implicated in other cellular processes, such as generating reactive oxygen species (ROS) for signaling, regulating the levels of NADH/NAD+, calcium signaling, and regulating apoptosis (Angell et al., 2000; Robb et al., 2018; Santidrian et al., 2013a; Valsecchi et al., 2009). All of these roles that CI is involved in are important for maintaining cellular homeostasis. In pathological states of CI, one or more of these processes in the cell will be the underlying cause (Rodenburg, 2016).

Reactive Oxygen Species Signaling

Mitochondria are key contributors to ROS in the cell (Murphy, 2009). CI is one of the main sites of ROS production, providing superoxides that get converted to hydrogen peroxide by superoxide dismutase (Kussmaul and Hirst, 2006). Hydrogen peroxide has been shown to be an important signaling molecule, regulating metabolic adaptation, cell proliferation and cell differentiation processes (Hamanaka et al., 2013; Wheaton et al., 2014). Although the mechanism by which CI produces ROS during electron transfer flow in the membrane arm is not fully understood, CI can produce ROS via both forward and reverse electron transfer flow (RET) (Hirst et al., 2008; Robb et al., 2018). Forward electron transfer flow is the usual flow of electrons that come from NADH binding to FMN, passing through iron-sulfur clusters and being released to ubiquinone. Studies have shown that most ROS produced this way occurs from the reduction of flavin and an increase of NAD+/NADH ratio (Hirst et al., 2008). Alternatively, RET occurs when there is a high ATP/ADP ratio, reduced ubiquinone pool, and high proton motive force. Instead of electrons being passed onto complex III, ubiquinone will bring the electrons back to complex I where they proceed back through the iron-sulfur clusters and are released to make superoxides due to flavin disassociating from CI (Robb et al., 2018; Stepanova et al., 2017). RET is a common phenomenon in ischemia-reperfusion (Chouchani et al., 2016; Stepanova et al., 2017). During this process CI makes a large amount of superoxides, causing a major oxidative damage in the cell, ultimately leading to damage in the tissue (Chouchani et al., 2016). Although RET is generally perceived as pathological, recently it has been shown to be involved in other physiological processes, such as improved lifespan and cellular differentiation (Lee et al., 2011; Scialò et al., 2016, 2017). As one of the largest sites of superoxide production in the mitochondria, CI may also play

a role in oxygen sensing. NDUFS2, a CI core subunit, was shown to control hydrogen peroxide generation in the carotid body and pulmonary artery smooth muscle cells (PASMCs) during hypoxic conditions (Dunham-Snary et al., 2019; Fernández-Agüera et al., 2015). The knockdown of other CI, CIII, and IV subunits in this study did not alter the levels of peroxide generation or mimic chronic hypoxic conditions, suggesting that this role is unique to NDUFS2 (Dunham-Snary et al., 2019).

NADH metabolism

NADH is a key player in cellular metabolism as a cofactor for several metabolic pathways, including glycolysis and the TCA cycle (Stein and Imai, 2012). For proper mitochondrial function, it is critical to maintain an optimal NAD+/NADH ratio (Zhu et al., 2015). CI oxidizes electrons from NADH to NAD+, and therefore plays an important role in monitoring this ratio. In most cases of CI dysfunction, NADH accumulates in the mitochondria matrix and as a result decreases the NAD+/NADH ratio, eliciting various responses by the cell (Lee et al., 2019). For example, in cardiac-specific NDUFS4 (nuclear encoded subunit of CI) knockout mice, a decrease in the NAD+/NADH ratio led to the inhibition of sirtuin 3 (SIRT3) activity and an increase in protein acetylation, ultimately resulting in an increased sensitivity to cardiac stress (Karamanlidis et al., 2013). SIRT3 is a NAD+ dependent deacetylase that localizes primarily to the mitochondria, and is implicated to be critical in controlling the energy demands of the mitochondria during stress (Ansari et al., 2017)(Ahn et al., 2008). Some CI dysfunction and the consequent decrease of NAD+ has been shown to target SIRT3 activation, leading to an increased level of ROS (Desquiret-Dumas et al., 2013). On the other hand, SIRT3 has been shown to interact with the CI subunit NDUFA9 to regulate its acetylation and thus the CI holoenzyme activity (Ahn et al., 2008). Additionally, while glycolysis favored in cancer cells typically leads to an imbalance of NAD+/NADH ratio, a study showed that increasing CI activity in breast cancer cells prevented tumor growth and metastasis by rebalancing the NAD+/NADH ratio, suggesting that CI activity can regulate tumor growth and metastasis via NADH metabolism (Santidrian et al., 2013b).

Calcium Homeostasis

In the mitochondria, calcium has been shown to affect metabolism, OXPHOS, and apoptosis (Finkel et al., 2015). One driving force for calcium uptake by the mitochondria is the membrane potential created by the respiratory electron transport chain (Griffiths and Rutter, 2009). The pumping of protons across the IMM creates a negative charge in the matrix which induces cations such as calcium to enter the matrix (Griffiths and Rutter, 2009). CI is a critical component to creating this electrochemical proton gradient as it contributes about 40% of the protons being pumped across the IMM (Hirst, 2013). Loss of CI activity leads to decreased ATP production, decreased ATPase activity, lack of calcium uptake by the ER, and finally an accumulation of calcium in the cytoplasm (Valsecchi et al., 2009). The mitochondrial calcium uniporter (MCU), discovered in the past decade, has been suggested to be the main route of entry for calcium into the mitochondria (Giorgi et al., 2018). This protein complex of approximately 480 kDa (Marchi and Pinton, 2014) has been suggested to lead to an accumulation of calcium in the mitochondria in cardiomyopathy mouse models with impaired OXPHOS. In a study done on whole-mitoplast HEK293T cells, chronic inhibition of CI enhanced the MCU activity, suggesting a relationship between CI and the MCU (Balderas-Angeles et al., 2018). As future studies focus on the regulation of the MCU, it will be interesting to see if the uniporter or its regulators are directly involved with the activity or assembly of CI.

Apoptosis

Mitochondria play a key role in activating apoptosis in the cell (Lemarie and Grimm, 2011). Certain subunits of CI have been shown to be directly involved in regulating apoptosis. NDUFA13, also known as GRIM-19 (gene associated with retinoid-interferon-induced-mortality-19), regulates cell death by binding to STAT3 (signal transducer and activator of transcription 3), and inhibiting its ability to bind to DNA (Angell et al., 2000; Huang et al., 2004; Zhang et al., 2003). When STAT3 is active, it binds several anti-apoptotic genes that are transcribed to promote tumor survival (Zhang et al., 2003). NDUFA6, typically downregulated in apoptotic cells, when overexpressed in HIV-infected cells could rescue cells from undergoing apoptosis.(Ladha et al., 2005). The core subunits NDUFS1 and NDUFS3 have also been shown to be implicated in apoptosis. NDUFS1 is cleaved by caspases which are cysteine proteases that initiate apoptosis signaling (Ricci et al., 2004). Similarly, NDUFS3 is cleaved by the protease granzyme A, a

protease that induces cell death (Martinvalet et al., 2008). In both of these cases, an increase of superoxides and disruption in membrane potential leads to apoptosis. CI subunits have previously unknown roles in regulating apoptosis and it will be important to identify any other CI subunits that are involved in these processes.

Diseases of CI

Isolated CI Deficiency

Dysfunction of mitochondria CI has been shown to be involved in several different diseases (Rodenburg, 2016). The most common of these are primary mitochondrial diseases which is a heterogeneous group of diseases that mostly affects the tissues with the highest energy demands. Mutations inherited in the mitochondria-encoded CI subunits, nuclear-encoded CI subunits, or CI assembly factors lead to isolated CI deficiency (Distelmaier et al., 2009). Isolated CI deficiency refers to the severe reduction of CI while the activities of other respiratory chain complexes are normal. Compared to other respiratory chain complexes, isolated CI deficiency accounts for nearly one-third of all OXPHOS disorders (Fassone and Rahman, 2012; Ghezzi and Zeviani, 2018). To date, mutations in all 14 core subunits, 13 of the 30 accessory subunits, and 11 of the 15 assembly factors have been described in patients (Frazier et al., 2019). To diagnose CI deficiency, the CI redox activity in patient biopsies or fibroblasts are measured to be less than 30% compared to the control (Fassone and Rahman, 2012). Most often symptoms involve neurological dysfunction, but can also affect other organs, such as the heart and skeletal muscle, causing multi-system diseases (Fassone and Rahman, 2012). The most common diseases that result from CI deficiency are Leigh Syndrome, fatal infantile lactic acidosis, leukoencephalopathy, mitochondrial encephalomyopathy-lactic acidosis-stroke like episodes (MELAS), and hypertrophic cardiomyopathy (Fassone and Rahman, 2012; Rodenburg, 2016). Interestingly, the correlation between the mutations present in specific CI subunits and their phenotypes did not present any patterns in the clinical outcome (Koene et al., 2012). For example, patients with mutations in NDUFS2, a core subunit of CI found in the Q module, all displayed Leigh Syndrome, but 3 of 5 of the patients also showed hypertrophic cardiomyopathy and the prognosis for these patients varied, with one dying as early as 4 days and another dying at 3 years

old (Ngu et al., 2012). One reason for such heterogenous phenotypes would be that, unlike nuclear DNA mutations which follow the Mendelian laws of inheritance, mtDNA presents heteroplasmy in the various tissues and organs (Alston et al., 2017). These variations have made it difficult for physicians to treat these diseases. Identifying any correlations of phenotypes and prognosis based on the location of CI subunits in the holoenzyme would be an interesting question to pursue.

Complex I Associated Diseases

CI dysfunction is present in several chronic- and age-related diseases, including cardiovascular, diabetes, cancer, and neurodegenerative diseases (Boudina et al., 2007; Hroudová et al., 2014; Siasos et al., 2018; Urra et al., 2017). In most of these diseases CI dysfunction is not due to genetic mutations within CI. Therefore, whether CI is the primary or secondary cause of the disease remains to be debated. For example, CI has long been thought to be the culprit for Parkinson's disease (Area-Gomez et al., 2019). This hypothesis was first suggested when 1-methyl-4-penyl-1, 2, 3, 6-tetrahydropyridine (MPTP), a CI inhibitor, was found to induce parkinsonian syndrome when injected in mice or humans. The resemblance between the MPTP-induced model and the clinical Parkinson's disease led researchers to investigate CI activity in patient samples and find deficiencies in the enzyme (Langston, 2017). However, other observations reporting deficiencies of other respiratory chain enzymes in the muscle, lymphocytes, and platelets of Parkinson's disease patients propose an overall dysfunction in mitochondria, rather than specific to CI (Langston, 2017).

Conclusion

Recent years have unraveled new and foundational components that are required for the function and biogenesis of human CI. In addition, CI has been shown to be involved in other areas of mitochondrial regulation, making it a multifaceted unit in the mitochondria rather than limited to bioenergetics in scope. In the clinical setting, the diagnosis of CI mitochondria diseases still remains to be a challenge due to poor

prognosis and polymorphic phenotypes. Furthermore, CI has been associated with chronic- and age-related diseases that are traditionally not related to mitochondria, however its role remains a mystery. This thesis will be presented in two parts. The first part will focus on the classic assembly process of CI in *Drosophila* and show how the mechanisms are conserved between mammals and flies. The second part will further show how the *Drosophila* model is a powerful genetic model to identify and examine factors that regulate CI. In particular, I will discuss in detail a novel candidate, Fragile X Mental Retardation 1 (FMR1), and its potential role in regulating CI biogenesis. Finally, I will conclude with how *Drosophila* can be used to address future questions of CI.

Figure 1.1: The electron transport chain

Adapted from Sazanov, 2015. The electron transport chain is located in the inner mitochondrial membrane and consists of four different complexes: complex I, complex II, complex III, and complex IV. These four complexes work together to transfer electrons and establish a proton gradient that complex V uses to generate ATP. Complex I or complex II initiate the transfer of electrons when they oxidize NADH or $FADH_2$ respectively. These electrons are first passed along to complex III by the electron carrier ubiquinone and then are passed to complex IV by the electron carrier cytochrome c. These electrons will undergo a reaction with oxygen to make water. To generate the proton gradient, complex I and complex III pump four protons each across the inner mitochondrial membrane and complex IV pumps 2 protons.

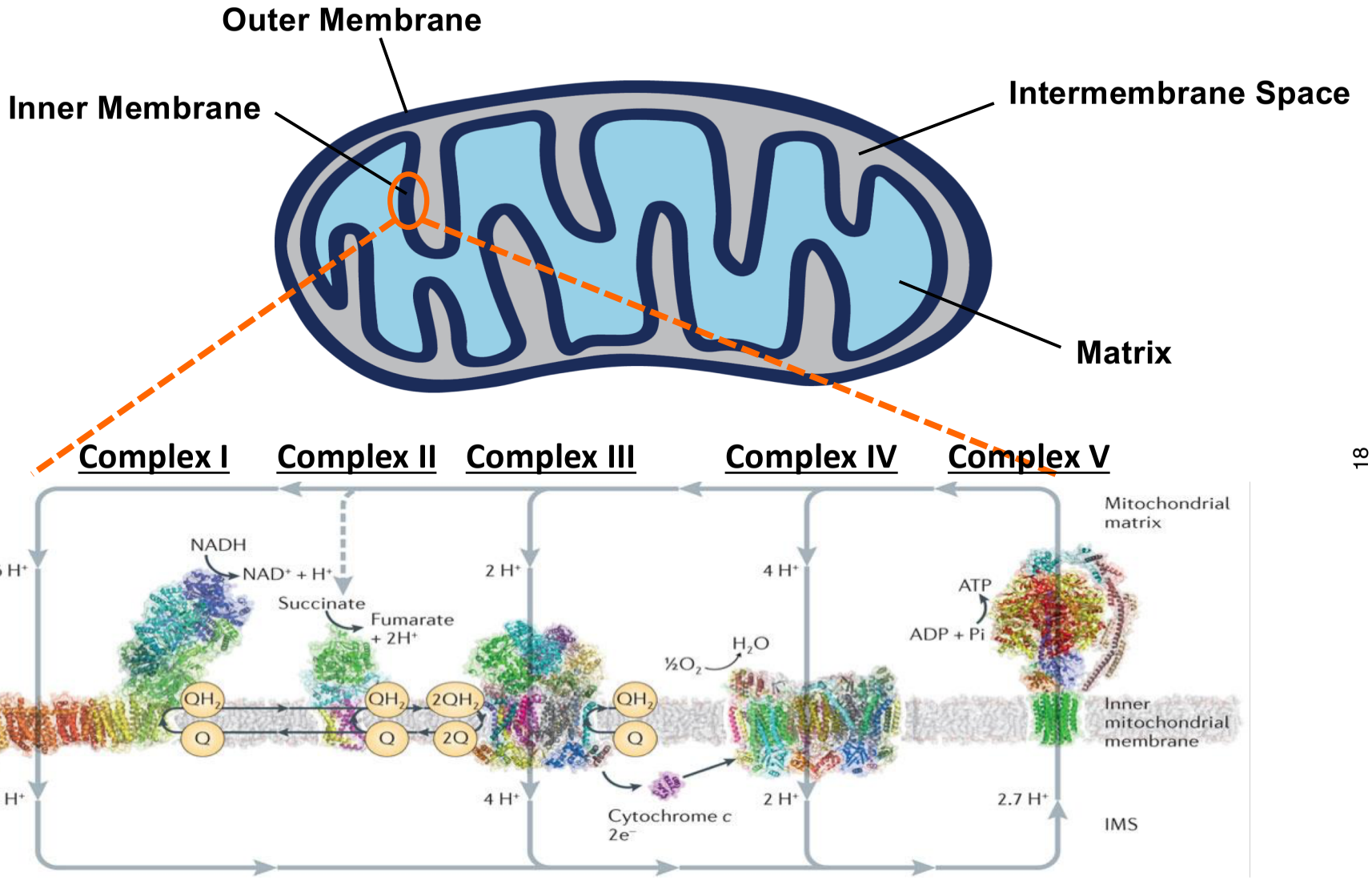
Outer Membrane
Inner Membrane
Intermembrane Space
Matrix
Complex I
Complex II
Complex III
Complex IV
Complex V
Mitochondrial matrix
NADH
NAD+ + H+
6 H+
Succinate
Fumarate + 2H+
2 H+
4 H+
ATP
ADP + Pi
½O2
H2O
QH2
Q
2QH2
2Q
Inner mitochondrial membrane
4 H+
4 H+
Cytochrome c
2e−
2 H+
2.7 H+
IMS

Figure 1.2: Mitochondrial complex I

The function of complex I in the oxidative phosphorylation system can be broken down into three different modules. The N module, Q module and P Module. During OXPHOS, complex I initiates transfer of electrons when NADH binds to a FMN in the N module to donate its electron, these electrons proceeds through 8 iron sulfur clusters where it will then bind to ubiquinone so it can pass the electrons on to Complex III. As this is happening, complex I also contributes to the proton gradient that is important for generating ATP by pumping 4 protons across the inner membrane of the mitochondria at the P modules.

Human complex I has 44 different subunits with some of them located in the membrane and some of the proteins protruding into the matrix. 7 subunits are encoded by the mitochondria and are all found in the inner membrane, while the other 37 subunits are encoded by the nucleus and are found throughout the structure. 14 of the subunits are known as the core proteins and are have been shown to be critical for functions of complex I as they found in all organisms that have complex I. The other 30 accessory subunits found in humans varies between organisms and whether or not they are necessary or required for the assembly and stability of complex I remains to be characterized.

Core Proteins (14)

7 Nuclear-Encoded Core Subunits

7 Mitochondria-Encoded Subunits

Accessory Proteins (Amount Varies)

30 Nuclear-Encoded Accessory Subunits

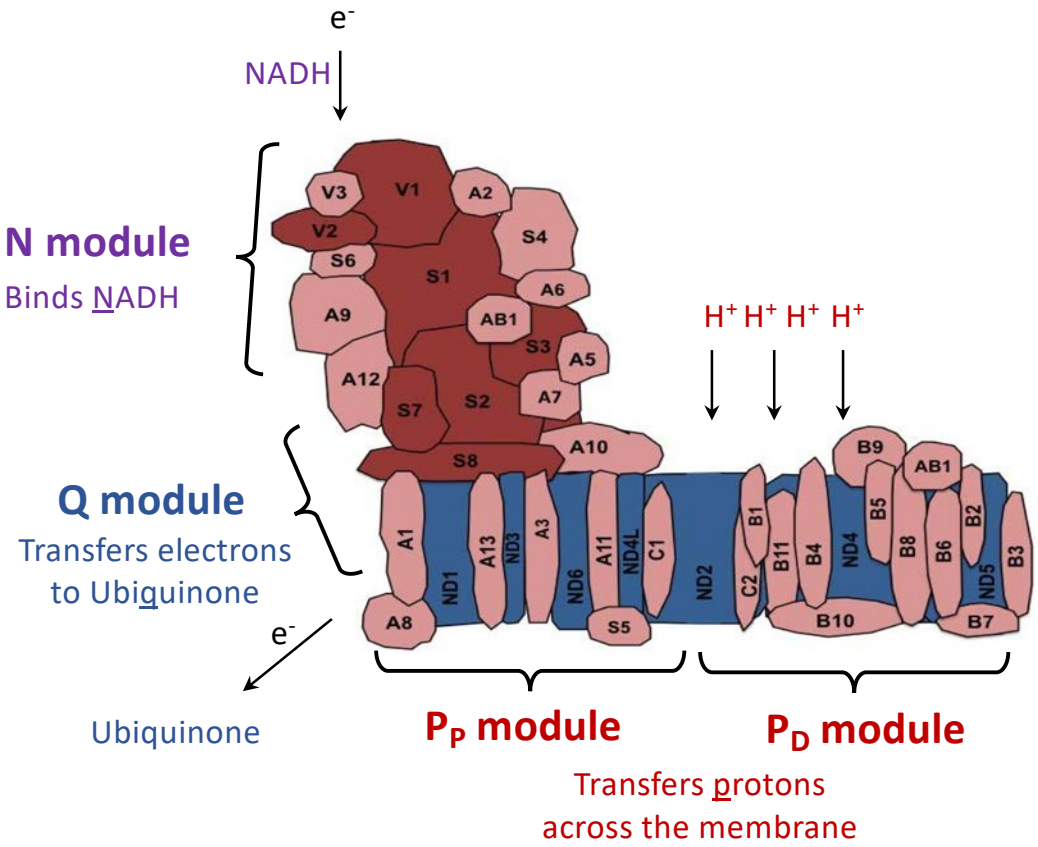

References

Abrahams, J.P., Leslie, A.G., Lutter, R., and Walker, J.E. (1994). Structure at 2.8 A resolution of F1-ATPase from bovine heart mitochondria. Nature *370*, 621–628.

Ahn, B.-H., Kim, H.-S., Song, S., Lee, I.H., Liu, J., Vassilopoulos, A., Deng, C.-X., and Finkel, T. (2008). A role for the mitochondrial deacetylase Sirt3 in regulating energy homeostasis. Proc. Natl. Acad. Sci. USA *105*, 14447–14452.

Alston, C.L., Rocha, M.C., Lax, N.Z., Turnbull, D.M., and Taylor, R.W. (2017). The genetics and pathology of mitochondrial disease. J. Pathol. *241*, 236–250.

Andrews, B., Carroll, J., Ding, S., Fearnley, I.M., and Walker, J.E. (2013). Assembly factors for the membrane arm of human complex I. Proc. Natl. Acad. Sci. USA *110*, 18934–18939.

Angell, J.E., Lindner, D.J., Shapiro, P.S., Hofmann, E.R., and Kalvakolanu, D.V. (2000). Identification of GRIM-19, a novel cell death-regulatory gene induced by the interferon-beta and retinoic acid combination, using a genetic approach. J. Biol. Chem. *275*, 33416–33426.

Ansari, A., Rahman, M.S., Saha, S.K., Saikot, F.K., Deep, A., and Kim, K.-H. (2017). Function of the SIRT3 mitochondrial deacetylase in cellular physiology, cancer, and neurodegenerative disease. Aging Cell *16*, 4–16.

Area-Gomez, E., Guardia-Laguarta, C., Schon, E.A., and Przedborski, S. (2019). Mitochondria, OxPhos, and neurodegeneration: cells are not just running out of gas. J. Clin. Invest.

Babot, M., Birch, A., Labarbuta, P., and Galkin, A. (2014). Characterisation of the active/de-active transition of mitochondrial complex I. Biochim. Biophys. Acta *1837*, 1083–1092.

Baker, M. (2018). Cryo-electron microscopy shapes up. Nature *561*, 565–567.

Balderas-Angeles, E., Sommmakia, S., Deane, S., and Chaudhuri, D. (2018). Complex I inhibition enhances mitochondrial calcium uniporter current. Biophys. J. *114*, 659a.

Baradaran, R., Berrisford, J.M., Minhas, G.S., and Sazanov, L.A. (2013). Crystal structure of the entire respiratory complex I. Nature *494*, 443–448.

Berg, J.M., Tymoczko, J.L., and Stryer, L. (2002). Carbon Atoms of Degraded Amino Acids Emerge as Major Metabolic Intermediates - Biochemistry - NCBI Bookshelf.

Berrisford, J.M., Baradaran, R., and Sazanov, L.A. (2011). Entire Respiratory Complex I from *Thermus Thermophilus*. In Encyclopedia of inorganic and bioinorganic chemistry, R.A. Scott, ed. (Chichester, UK: John Wiley & Sons, Ltd), pp. 1–16.

Berrisford, J.M., Baradaran, R., and Sazanov, L.A. (2016). Structure of bacterial respiratory complex I. Biochim. Biophys. Acta *1857*, 892–901.

Blaza, J.N., Vinothkumar, K.R., and Hirst, J. (2018). Structure of the deactive state of mammalian respiratory complex I. Structure *26*, 312–319.e3.

Boudina, S., Sena, S., Theobald, H., Sheng, X., Wright, J.J., Hu, X.X., Aziz, S., Johnson, J.I., Bugger, H., Zaha, V.G., et al. (2007). Mitochondrial energetics in the heart in obesity-related diabetes: direct evidence for increased uncoupled respiration and activation of uncoupling proteins. Diabetes *56*, 2457–2466.

Boxma, B., de Graaf, R.M., van der Staay, G.W.M., van Alen, T.A., Ricard, G., Gabaldón, T., van Hoek, A.H.A.M., Moon-van der Staay, S.Y., Koopman, W.J.H., van Hellemond, J.J., et al. (2005). An anaerobic mitochondrion that produces hydrogen. Nature *434*, 74–79.

Calvo, S.E., Clauser, K.R., and Mootha, V.K. (2016). MitoCarta2.0: an updated inventory of mammalian mitochondrial proteins. Nucleic Acids Res. *44*, D1251–7.

Chouchani, E.T., Pell, V.R., James, A.M., Work, L.M., Saeb-Parsy, K., Frezza, C., Krieg, T., and Murphy, M.P. (2016). A Unifying Mechanism for Mitochondrial Superoxide Production during Ischemia-Reperfusion Injury. Cell Metab. *23*, 254–263.

Cogliati, S., Lorenzi, I., Rigoni, G., Caicci, F., and Soriano, M.E. (2018). Regulation of mitochondrial electron transport chain assembly. J. Mol. Biol. *430*, 4849–4873.

Desquiret-Dumas, V., Gueguen, N., Leman, G., Baron, S., Nivet-Antoine, V., Chupin, S., Chevrollier, A., Vessières, E., Ayer, A., Ferré, M., et al. (2013). Resveratrol induces a mitochondrial complex I-dependent increase in NADH oxidation responsible for sirtuin activation in liver cells. J. Biol. Chem. *288*, 36662–36675.

DiMauro, S., and Schon, E.A. (2003). Mitochondrial respiratory-chain diseases. N. Engl. J. Med. *348*, 2656–2668.

Distelmaier, F., Koopman, W.J.H., van den Heuvel, L.P., Rodenburg, R.J., Mayatepek, E., Willems, P.H.G.M., and Smeitink, J.A.M. (2009). Mitochondrial complex I deficiency: from organelle dysfunction to clinical disease. Brain *132*, 833–842.

Dunham-Snary, K.J., Wu, D., Potus, F., Sykes, E.A., Mewburn, J.D., Charles, R.L., Eaton, P., Sultanian, R.A., and Archer, S.L. (2019). Ndufs2, a Core Subunit of Mitochondrial Complex I, Is Essential for Acute Oxygen-Sensing and Hypoxic Pulmonary Vasoconstriction. Circ. Res. *124*, 1727–1746.

Dyall, S.D., Brown, M.T., and Johnson, P.J. (2004). Ancient invasions: from endosymbionts to organelles. Science *304*, 253–257.

Fassone, E., and Rahman, S. (2012). Complex I deficiency: clinical features, biochemistry and molecular genetics. J. Med. Genet. *49*, 578–590.

Fernández-Agüera, M.C., Gao, L., González-Rodríguez, P., Pintado, C.O., Arias-Mayenco, I., García-Flores, P., García-Pergañeda, A., Pascual, A., Ortega-Sáenz, P., and López-Barneo, J. (2015). Oxygen sensing by arterial chemoreceptors depends on mitochondrial complex I signaling. Cell Metab. *22*, 825–837.

Fiedorczuk, K., Letts, J.A., Degliesposti, G., Kaszuba, K., Skehel, M., and Sazanov, L.A. (2016). Atomic structure of the entire mammalian mitochondrial complex I. Nature *538*, 406–410.

Finkel, T., Menazza, S., Holmström, K.M., Parks, R.J., Liu, J., Sun, J., Liu, J., Pan, X., and Murphy, E. (2015). The ins and outs of mitochondrial calcium. Circ. Res. *116*, 1810–1819.

Formosa, L.E., Dibley, M.G., Stroud, D.A., and Ryan, M.T. (2018). Building a complex complex: Assembly of mitochondrial respiratory chain complex I. Semin. Cell Dev. Biol. *76*, 154–162.

Frazier, A.E., Thorburn, D.R., and Compton, A.G. (2019). Mitochondrial energy generation disorders: genes, mechanisms, and clues to pathology. J. Biol. Chem. *294*, 5386–5395.

Garcia, C.J., Khajeh, J., Coulanges, E., Chen, E.I.-J., and Owusu-Ansah, E. (2017). Regulation of mitochondrial complex I biogenesis in drosophila flight muscles. Cell Rep. *20*, 264–278.

Ghezzi, D., and Zeviani, M. (2018). Human diseases associated with defects in assembly of OXPHOS complexes. Essays Biochem *62*, 271–286.

Giorgi, C., Marchi, S., and Pinton, P. (2018). The machineries, regulation and cellular functions of mitochondrial calcium. Nat. Rev. Mol. Cell Biol. *19*, 713–730.

Griffiths, E.J., and Rutter, G.A. (2009). Mitochondrial calcium as a key regulator of mitochondrial ATP production in mammalian cells. Biochim. Biophys. Acta *1787*, 1324–1333.

Guerrero-Castillo, S., Vázquez-Acevedo, M., González-Halphen, D., and Uribe-Carvajal, S. (2009). In Yarrowia lipolytica mitochondria, the alternative NADH dehydrogenase interacts specifically with the cytochrome complexes of the classic respiratory pathway. Biochim. Biophys. Acta *1787*, 75–85.

Guerrero-Castillo, S., Baertling, F., Kownatzki, D., Wessels, H.J., Arnold, S., Brandt, U., and Nijtmans, L. (2017). The assembly pathway of mitochondrial respiratory chain complex I. Cell Metab. *25*, 128–139.

Hamanaka, R.B., Glasauer, A., Hoover, P., Yang, S., Blatt, H., Mullen, A.R., Getsios, S., Gottardi, C.J., DeBerardinis, R.J., Lavker, R.M., et al. (2013). Mitochondrial reactive oxygen species promote epidermal differentiation and hair follicle development. Sci. Signal. *6*, ra8.

Haynes, C.M., and Ron, D. (2010). The mitochondrial UPR - protecting organelle protein homeostasis. J. Cell Sci. *123*, 3849–3855.

Hirst, J. (2013). Mitochondrial complex I. Annu. Rev. Biochem. *82*, 551–575.

Hirst, J., King, M.S., and Pryde, K.R. (2008). The production of reactive oxygen species by complex I. Biochem. Soc. Trans. *36*, 976–980.

Hroudová, J., Singh, N., and Fišar, Z. (2014). Mitochondrial dysfunctions in neurodegenerative diseases: relevance to Alzheimer's disease. Biomed Res. Int. *2014*, 175062.

Huang, G., Lu, H., Hao, A., Ng, D.C.H., Ponniah, S., Guo, K., Lufei, C., Zeng, Q., and Cao, X. (2004). GRIM-19, a cell death regulatory protein, is essential for assembly and function of mitochondrial complex I. Mol. Cell. Biol. *24*, 8447–8456.

Ingelsson, B., Söderberg, D., Strid, T., Söderberg, A., Bergh, A.-C., Loitto, V., Lotfi, K., Segelmark, M., Spyrou, G., and Rosén, A. (2018). Lymphocytes eject interferogenic mitochondrial DNA webs in response to CpG and non-CpG oligodeoxynucleotides of class C. Proc. Natl. Acad. Sci. USA *115*, E478–E487.

Iwata, S., Lee, J.W., Okada, K., Lee, J.K., Iwata, M., Rasmussen, B., Link, T.A., Ramaswamy, S., and Jap, B.K. (1998). Complete structure of the 11-subunit bovine mitochondrial cytochrome bc_1 complex. Science *281*, 64–71.

Jeandard, D., Smirnova, A., Tarassov, I., Barrey, E., Smirnov, A., and Entelis, N. (2019). Import of Non-Coding RNAs into Human Mitochondria: A Critical Review and Emerging Approaches. Cells *8*.

Jonckheere, A.I., Smeitink, J.A.M., and Rodenburg, R.J.T. (2012). Mitochondrial ATP synthase: architecture, function and pathology. J. Inherit. Metab. Dis. *35*, 211–225.

Karamanlidis, G., Lee, C.F., Garcia-Menendez, L., Kolwicz, S.C., Suthammarak, W., Gong, G., Sedensky, M.M., Morgan, P.G., Wang, W., and Tian, R. (2013). Mitochondrial complex I deficiency increases protein acetylation and accelerates heart failure. Cell Metab. *18*, 239–250.

Kerscher, S.J., Okun, J.G., and Brandt, U. (1999). A single external enzyme confers alternative NADH:ubiquinone oxidoreductase activity in Yarrowia lipolytica. J. Cell Sci. *112 (Pt 14)*, 2347–2354.

Koene, S., Rodenburg, R.J., van der Knaap, M.S., Willemsen, M.A.A.P., Sperl, W., Laugel, V., Ostergaard, E., Tarnopolsky, M., Martin, M.A., Nesbitt, V., et al. (2012). Natural disease course and genotype-phenotype correlations in Complex I deficiency caused by nuclear gene defects: what we learned from 130 cases. J. Inherit. Metab. Dis. *35*, 737–747.

Kremer, L.S., Bader, D.M., Mertes, C., Kopajtich, R., Pichler, G., Iuso, A., Haack, T.B., Graf, E., Schwarzmayr, T., Terrile, C., et al. (2017). Genetic diagnosis of Mendelian disorders via RNA sequencing. Nat. Commun. *8*, 15824.

Kussmaul, L., and Hirst, J. (2006). The mechanism of superoxide production by NADH:ubiquinone oxidoreductase (complex I) from bovine heart mitochondria. Proc. Natl. Acad. Sci. USA *103*, 7607–7612.

Ladha, J.S., Tripathy, M.K., and Mitra, D. (2005). Mitochondrial complex I activity is impaired during HIV-1-induced T-cell apoptosis. Cell Death Differ. *12*, 1417–1428.

Langston, J.W. (2017). The MPTP Story. J. Parkinsons. Dis. *7*, S11–S19.

Lee, C.F., Caudal, A., Abell, L., Nagana Gowda, G.A., and Tian, R. (2019). Targeting NAD+ metabolism as interventions for mitochondrial disease. Sci. Rep. *9*, 3073.

Lee, S., Tak, E., Lee, J., Rashid, M.A., Murphy, M.P., Ha, J., and Kim, S.S. (2011). Mitochondrial H2O2 generated from electron transport chain complex I stimulates muscle differentiation. Cell Res. *21*, 817–834.

Lemarie, A., and Grimm, S. (2011). Mitochondrial respiratory chain complexes: apoptosis sensors mutated in cancer? Oncogene *30*, 3985–4003.

Letts, J.A., and Sazanov, L.A. (2017). Clarifying the supercomplex: the higher-order organization of the mitochondrial electron transport chain. Nat. Struct. Mol. Biol. *24*, 800–808.

Letts, J.A., Fiedorczuk, K., and Sazanov, L.A. (2017). The architecture of respiratory supercomplexes. Biophys. J. *112*, 278a.

Liberti, M.V., and Locasale, J.W. (2016). The warburg effect: how does it benefit cancer cells? Trends Biochem. Sci. *41*, 211–218.

Lyons, T.W., Reinhard, C.T., and Planavsky, N.J. (2014). The rise of oxygen in Earth's early ocean and atmosphere. Nature *506*, 307–315.

Marchi, S., and Pinton, P. (2014). The mitochondrial calcium uniporter complex: molecular components, structure and physiopathological implications. J. Physiol. (Lond.) *592*, 829–839.

Marques, I., Duarte, M., Assunção, J., Ushakova, A.V., and Videira, A. (2005). Composition of complex I from Neurospora crassa and disruption of two "accessory" subunits. Biochim. Biophys. Acta *1707*, 211–220.

Martin, W. (2010). Evolutionary origins of metabolic compartmentalization in eukaryotes. Philos. Trans. R. Soc. Lond. B, Biol. Sci. *365*, 847–855.

Martinvalet, D., Dykxhoorn, D.M., Ferrini, R., and Lieberman, J. (2008). Granzyme A cleaves a mitochondrial complex I protein to initiate caspase-independent cell death. Cell *133*, 681–692.

McCommis, K.S., and Finck, B.N. (2015). Mitochondrial pyruvate transport: a historical perspective and future research directions. Biochem. J. *466*, 443–454.

Meunier, B., Fisher, N., Ransac, S., Mazat, J.P., and Brasseur, G. (2013). Respiratory complex III dysfunction in humans and the use of yeast as a model organism to study mitochondrial myopathy and associated diseases. Biochim. Biophys. Acta *1827*, 1346–1361.

Meyer, A., Laverny, G., Bernardi, L., Charles, A.L., Alsaleh, G., Pottecher, J., Sibilia, J., and Geny, B. (2018). Mitochondria: an organelle of bacterial origin controlling inflammation. Front. Immunol. *9*, 536.

Milenkovic, D., Blaza, J.N., Larsson, N.-G., and Hirst, J. (2017). The enigma of the respiratory chain supercomplex. Cell Metab. *25*, 765–776.

Mileykovskaya, E., Penczek, P.A., Fang, J., Mallampalli, V.K.P.S., Sparagna, G.C., and Dowhan, W. (2012). Arrangement of the respiratory chain complexes in Saccharomyces cerevisiae supercomplex III2IV2 revealed by single particle cryo-electron microscopy. J. Biol. Chem. *287*, 23095–23103.

Mimaki, M., Wang, X., McKenzie, M., Thorburn, D.R., and Ryan, M.T. (2012). Understanding mitochondrial complex I assembly in health and disease. Biochim. Biophys. Acta *1817*, 851–862.

Murphy, M.P. (2009). How mitochondria produce reactive oxygen species. Biochem. J. *417*, 1–13.

Ngu, L.H., Nijtmans, L.G., Distelmaier, F., Venselaar, H., van Emst-de Vries, S.E., van den Brand, M.A.M., Stoltenborg, B.J.M., Wintjes, L.T., Willems, P.H., van den Heuvel, L.P., et al. (2012). A catalytic defect in mitochondrial respiratory chain complex I due to a mutation in NDUFS2 in a patient with Leigh syndrome. Biochim. Biophys. Acta *1822*, 168–175.

Owusu-Ansah, E., Song, W., and Perrimon, N. (2013). Muscle mitohormesis promotes longevity via systemic repression of insulin signaling. Cell *155*, 699–712.

Pagliarini, D.J., and Rutter, J. (2013). Hallmarks of a new era in mitochondrial biochemistry. Genes Dev. *27*, 2615–2627.

Pagliarini, D.J., Calvo, S.E., Chang, B., Sheth, S.A., Vafai, S.B., Ong, S.-E., Walford, G.A., Sugiana, C., Boneh, A., Chen, W.K., et al. (2008). A mitochondrial protein compendium elucidates complex I disease biology. Cell *134*, 112–123.

Perales-Clemente, E., Bayona-Bafaluy, M.P., Pérez-Martos, A., Barrientos, A., Fernández-Silva, P., and Enriquez, J.A. (2008). Restoration of electron transport without proton pumping in mammalian mitochondria. Proc. Natl. Acad. Sci. USA *105*, 18735–18739.

Rafikov, R., Sun, X., Rafikova, O., Louise Meadows, M., Desai, A.A., Khalpey, Z., Yuan, J.X.-J., Fineman, J.R., and Black, S.M. (2015). Complex I dysfunction underlies the glycolytic switch in pulmonary hypertensive smooth muscle cells. Redox Biol *6*, 278–286.

Rhein, V.F., Carroll, J., Ding, S., Fearnley, I.M., and Walker, J.E. (2013). NDUFAF7 methylates arginine 85 in the NDUFS2 subunit of human complex I. J. Biol. Chem. *288*, 33016–33026.

Ricci, J.-E., Muñoz-Pinedo, C., Fitzgerald, P., Bailly-Maitre, B., Perkins, G.A., Yadava, N., Scheffler, I.E., Ellisman, M.H., and Green, D.R. (2004). Disruption of mitochondrial function during apoptosis is mediated by caspase cleavage of the p75 subunit of complex I of the electron transport chain. Cell *117*, 773–786.

Rigby, K., Zhang, L., Cobine, P.A., George, G.N., and Winge, D.R. (2007). characterization of the cytochrome c oxidase assembly factor Cox19 of Saccharomyces cerevisiae. J. Biol. Chem. *282*, 10233–10242.

Robb, E.L., Hall, A.R., Prime, T.A., Eaton, S., Szibor, M., Viscomi, C., James, A.M., and Murphy, M.P. (2018). Control of mitochondrial superoxide production by reverse electron transport at complex I. J. Biol. Chem. *293*, 9869–9879.

Rodenburg, R.J. (2016). Mitochondrial complex I-linked disease. Biochim. Biophys. Acta *1857*, 938–945.

Santidrian, A.F., Matsuno-Yagi, A., Ritland, M., Seo, B.B., LeBoeuf, S.E., Gay, L.J., Yagi, T., and Felding-Habermann, B. (2013a). Mitochondrial complex I activity and NAD+/NADH balance regulate breast cancer progression. J. Clin. Invest.

Santidrian, A.F., Matsuno-Yagi, A., Ritland, M., Seo, B.B., LeBoeuf, S.E., Gay, L.J., Yagi, T., and Felding-Habermann, B. (2013b). Mitochondrial complex I activity and NAD+/NADH balance regulate breast cancer progression. J. Clin. Invest. *123*, 1068–1081.

Sazanov, L.A. (2014). The mechanism of coupling between electron transfer and proton translocation in respiratory complex I. J Bioenerg Biomembr *46*, 247–253.

Sazanov, L.A. (2015). A giant molecular proton pump: structure and mechanism of respiratory complex I. Nat. Rev. Mol. Cell Biol. *16*, 375–388.

Sazanov, L.A., and Hinchliffe, P. (2006). Structure of the hydrophilic domain of respiratory complex I from Thermus thermophilus. Science *311*, 1430–1436.

Schönfeld, P., and Reiser, G. (2013). Why does brain metabolism not favor burning of fatty acids to provide energy? Reflections on disadvantages of the use of free fatty acids as fuel for brain. J. Cereb. Blood Flow Metab. *33*, 1493–1499.

Scialò, F., Sriram, A., Fernández-Ayala, D., Gubina, N., Lõhmus, M., Nelson, G., Logan, A., Cooper, H.M., Navas, P., Enríquez, J.A., et al. (2016). Mitochondrial ROS produced via reverse electron transport extend animal lifespan. Cell Metab. *23*, 725–734.

Scialò, F., Fernández-Ayala, D.J., and Sanz, A. (2017). Role of mitochondrial reverse electron transport in ROS signaling: potential roles in health and disease. Front. Physiol. *8*, 428.

Sharma, N., Okere, I.C., Brunengraber, D.Z., McElfresh, T.A., King, K.L., Sterk, J.P., Huang, H., Chandler, M.P., and Stanley, W.C. (2005). Regulation of pyruvate dehydrogenase activity and citric acid cycle intermediates during high cardiac power generation. J. Physiol. (Lond.) *562*, 593–603.

Siasos, G., Tsigkou, V., Kosmopoulos, M., Theodosiadis, D., Simantiris, S., Tagkou, N.M., Tsimpiktsioglou, A., Stampouloglou, P.K., Oikonomou, E., Mourouzis, K., et al. (2018). Mitochondria and cardiovascular diseases-from pathophysiology to treatment. Ann Transl Med *6*, 256.

Signes, A., and Fernandez-Vizarra, E. (2018). Assembly of mammalian oxidative phosphorylation complexes I-V and supercomplexes. Essays Biochem *62*, 255–270.

Spinelli, J.B., and Haigis, M.C. (2018). The multifaceted contributions of mitochondria to cellular metabolism. Nat. Cell Biol. *20*, 745–754.

Stein, L.R., and Imai, S. (2012). The dynamic regulation of NAD metabolism in mitochondria. Trends Endocrinol. Metab. *23*, 420–428.

Stepanova, A., Kahl, A., Konrad, C., Ten, V., Starkov, A.S., and Galkin, A. (2017). Reverse electron transfer results in a loss of flavin from mitochondrial complex I: Potential mechanism for brain ischemia reperfusion injury. J. Cereb. Blood Flow Metab. *37*, 3649–3658.

Stewart, J.B., and Chinnery, P.F. (2015). The dynamics of mitochondrial DNA heteroplasmy: implications for human health and disease. Nat. Rev. Genet. *16*, 530–542.

Stroud, D.A., Surgenor, E.E., Formosa, L.E., Reljic, B., Frazier, A.E., Dibley, M.G., Osellame, L.D., Stait, T., Beilharz, T.H., Thorburn, D.R., et al. (2016). Accessory subunits are integral for assembly and function of human mitochondrial complex I. Nature *538*, 123–126.

Sugiana, C., Pagliarini, D.J., McKenzie, M., Kirby, D.M., Salemi, R., Abu-Amero, K.K., Dahl, H.-H.M., Hutchison, W.M., Vascotto, K.A., Smith, S.M., et al. (2008). Mutation of C20orf7 disrupts complex I assembly and causes lethal neonatal mitochondrial disease. Am. J. Hum. Genet. *83*, 468–478.

Sun, F., Huo, X., Zhai, Y., Wang, A., Xu, J., Su, D., Bartlam, M., and Rao, Z. (2005). Crystal structure of mitochondrial respiratory membrane protein complex II. Cell *121*, 1043–1057.

Taylor, R.W., Pyle, A., Griffin, H., Blakely, E.L., Duff, J., He, L., Smertenko, T., Alston, C.L., Neeve, V.C., Best, A., et al. (2014). Use of whole-exome sequencing to determine the genetic basis of multiple mitochondrial respiratory chain complex deficiencies. JAMA *312*, 68–77.

Thomas, R.E., Andrews, L.A., Burman, J.L., Lin, W.-Y., and Pallanck, L.J. (2014). PINK1-Parkin pathway activity is regulated by degradation of PINK1 in the mitochondrial matrix. PLoS Genet. *10*, e1004279.

Trumpff, C., Marsland, A.L., Basualto-Alarcon, C., Martin, J.L., Carroll, J.E., Sturm, G., Vincent, A.E., Mosharov, E.V., Gu, Z., Kaufman, B.A., et al. (2018). Acute Psychological Stress Triggers Circulating Cell-Free Mitochondrial DNA. BioRxiv.

Tsukihara, T., Aoyama, H., Yamashita, E., Tomizaki, T., Yamaguchi, H., Shinzawa-Itoh, K., Nakashima, R., Yaono, R., and Yoshikawa, S. (1995). Structures of metal sites of oxidized bovine heart cytochrome c oxidase at 2.8 A. Science *269*, 1069–1074.

Urra, F.A., Muñoz, F., Lovy, A., and Cárdenas, C. (2017). The mitochondrial complex(i)ty of cancer. Front. Oncol. *7*, 118.

Valsecchi, F., Esseling, J.J., Koopman, W.J.H., and Willems, P.H.G.M. (2009). Calcium and ATP handling in human NADH:ubiquinone oxidoreductase deficiency. Biochim. Biophys. Acta *1792*, 1130–1137.

Videira, A. (1998). Complex I from the fungus Neurospora crassa. Biochimica et Biophysica Acta (BBA) - Bioenergetics *1364*, 89–100.

Wallace, D.C., and Chalkia, D. (2013). Mitochondrial DNA genetics and the heteroplasmy conundrum in evolution and disease. Cold Spring Harb. Perspect. Biol. *5*, a021220.

Wheaton, W.W., Weinberg, S.E., Hamanaka, R.B., Soberanes, S., Sullivan, L.B., Anso, E., Glasauer, A., Dufour, E., Mutlu, G.M., Budigner, G.S., et al. (2014). Metformin inhibits mitochondrial complex I of cancer cells to reduce tumorigenesis. Elife *3*, e02242.

Zhang, J., Yang, J., Roy, S.K., Tininini, S., Hu, J., Bromberg, J.F., Poli, V., Stark, G.R., and Kalvakolanu, D.V. (2003). The cell death regulator GRIM-19 is an inhibitor of signal transducer and activator of transcription 3. Proc. Natl. Acad. Sci. USA *100*, 9342–9347.

Zhang, Z.-W., Cheng, J., Xu, F., Chen, Y.-E., Du, J.-B., Yuan, M., Zhu, F., Xu, X.-C., and Yuan, S. (2011). Red blood cell extrudes nucleus and mitochondria against oxidative stress. IUBMB Life *63*, 560–565.

Zhu, J., Vinothkumar, K.R., and Hirst, J. (2016). Structure of mammalian respiratory complex I. Nature *536*, 354–358.

Zhu, X.-H., Lu, M., Lee, B.-Y., Ugurbil, K., and Chen, W. (2015). In vivo NAD assay reveals the intracellular NAD contents and redox state in healthy human brain and their age dependences. Proc. Natl. Acad. Sci. USA *112*, 2876–2881.

Chapter 2: Mitochondrial Complex I Assembly in *Drosophila* Flight Muscles.

Adapted from **Garcia, C.J., Khajeh, J., Coulanges, E., Chen, E.I.-J., and Owusu-Ansah, E. (2017). Regulation of mitochondrial complex I biogenesis in drosophila flight muscles. Cell Rep. *20*, 264–278.**

Chen E.I-J performed mass spectrometry

Garcia, C.J., Khajeh, J, Coulanges, E., and Owusu-Ansah, E performed the rest of the experiments, analyzed, and discussed results.

Owusu-Ansah, E conceived, designed, secured funding, and wrote the manuscript with feedback from Garcia, C.J. and Khajeh, J.

Introduction

Mitochondrial CI (NADH: ubiquinone oxidoreductase) is the first and largest of the electron transport chain complexes in the mitochondrion, and has a molecular mass approaching 1 MDa [reviewed in (Hirst, 2013)]. Human CI has 44 distinct subunits (**Table 2.1**); 14 of which are directly involved in transferring electrons from NADH to ubiquinone, or in generation of the membrane potential. Because these 14 subunits are conserved from bacteria to humans, and form the catalytic centers of the enzyme, they are referred to as the core or central subunits. The 30 remaining subunits are referred to as accessory subunits, because they are not directly involved in catalysis, and are expressed to varying extents among eukaryotes (**Table 2.1**) [reviewed in (Hirst, 2013)]. A current hypothesis is that the accessory subunits regulate ROS formation, complex assembly or stability, and cellular homeostasis *in vivo*. Of note, disease-causing mutations in several accessory subunits have been identified (Berger et al., 2008; Budde et al., 2000; Hoefs et al., 2008; Hoefs et al., 2011; Kirby et al., 2004; Ostergaard et al., 2011; Scacco et al., 2003); and genetic disruption of some accessory subunits in cell lines impair CI assembly (Guerrero-Castillo et al., 2017; Stroud et al., 2016). However, a definitive role for many of the accessory subunits *in vivo* remains to be established.

CI has two major arms: a hydrophobic membrane arm and a hydrophilic peripheral arm that protrudes into the mitochondrial matrix. The two arms are oriented almost perpendicularly to each other resulting in a characteristic boot or L-shaped structure (Clason et al., 2010; Efremov et al., 2010; Radermacher et al., 2006; Zickermann et al., 2015). Several cryo-electron microscopy density maps and higher resolution atomic structures of CI from various eukaryotes have recently been described (Fiedorczuk et al., 2016; Vinothkumar et al., 2014; Zhu et al., 2016; Zickermann et al., 2015). The accessory subunits were found to form a cage around the core subunits, and were particularly concentrated around the membrane domain. These observations lend further credence to the hypothesis that the accessory subunits are involved in stabilizing the complex during or after biogenesis *in vivo*.

Surprisingly, despite the outstanding genetic capabilities of *Drosophila,* a systematic genetic analysis of CI assembly has not been described in this organism. Instead, previous *in vivo* genetic analyses of the regulation of eukaryotic CI assembly have been performed primarily in the aerobic fungus *Neurospora crassa* (Duarte et al., 1995). Although the *N. crassa* model of CI assembly is renowned for being the first

system for which a model of CI assembly was described, there are notable deviations from the assembly pathway in mammalian systems (Nehls et al., 1992; Tuschen et al., 1990). For instance, several accessory subunits as well as CI assembly intermediates found in mammalian CI are not conserved in *N. crassa* (24). Similarly, CI in *Arabidopsis thaliana* has a carbonic anhydrase domain and several additional subunits that are not present in the human enzyme (21). Thus, it is important to develop additional genetically tractable CI assembly model systems that more closely resemble and recapitulate the human system.

Importantly, *Drosophila* has a comparable number of CI subunits (similar to the human and bovine enzymes) and over a dozen putative assembly factors, all of which have clear human orthologs, making it a suitable model organism for studying CI assembly. Studying CI assembly in *Drosophila* has the added advantage of being in an *in vivo* context, where the effects of both developmental signals and environmental perturbations can be examined. Accordingly, we have analyzed the role of several nuclear-encoded CI subunits in CI assembly in *Drosophila* muscles.

We describe the mechanism of CI assembly in *Drosophila* flight muscles. Specifically, we show that many of the accessory subunits regulate specific stages of CI biogenesis *in vivo*, such that, when their level of expression is reduced, CI activity is diminished due to impaired CI assembly. We demonstrate that CI biogenesis in *Drosophila* involves the formation of ~315-, ~550-, and ~815-kDa assembly intermediates, and that RNAi-mediated knockdown of either dNDUFS2 or dNDUFS3 decreases the amount of the ~315-kDa assembly intermediate that is formed. Furthermore, we show that a specific accessory subunit – dNDUFA5 – is required for the formation and/or stabilization of the ~315-kDa assembly intermediate *in vivo*. Additionally, we define a specific role for another accessory subunit (dNDUFS5); and show that it is required for converting a transient CI assembly intermediate (an ~700-kDa assembly intermediate) into the ~815-kDa assembly intermediate, during one of the terminal steps of CI assembly. Four components of the Mitochondrial Complex I Assembly (MCIA) complex (dECSIT, dNDUFAF1, dACAD9 and dTIMMDC1) were associated with the ~700-kDa assembly intermediate, further confirming that it is a true assembly intermediate in CI biogenesis. Importantly, incorporation of dNDUFS5 into CI is necessary to stabilize or promote incorporation of dNDUFA10 into the complex. We also identify several roles for many of the dNDUFB subunits. Altogether, our analyses reveal how studies of CI biogenesis in *Drosophila* can uncover

mechanisms of CI assembly *in vivo*, and establish *Drosophila* as an important genetically pliable model organism for addressing questions relevant to mammalian CI biogenesis.

Results

Drosophila flight muscles are suitable for studying CI assembly

CI consists of a hydrophilic matrix arm and a hydrophobic membrane arm that are oriented almost orthogonally to each other (**Figure 2.1A**). Subunits with the prefix NDUFA (NDUFA1-3 and NDUFA5-13) were so named as they were originally thought to be part of the matrix arm, whereas the NDUFB subunits (NDUFB1-NDUFB11) are part of the membrane arm. In addition, subunits that are found in the vicinity of the 8 Fe-S clusters (NDUFS) or single Flavoprotein (NDUFV) are also localized in the matrix. All the NDUFA and NDUFB subunits are accessory subunits (**Figure 2.1A**). We used the *Drosophila* RNAi Screening Center Integrative Ortholog Prediction Tool (DIOPT) to identify 42 putative orthologs of the 44 human CI subunits (**Figure 2.1B and Table 2.1**) (Hu et al., 2011). To facilitate comparison with their human orthologs, in this manuscript we refer to *Drosophila* orthologs of the human CI subunits as dNDUFS1, dNDUFS2, etc. Their designated gene nomenclature in *Drosophila* are shown in **Table 2.1**.

To confirm whether the putative CI orthologs identified by DIOPT were *bona fide* CI subunits in *Drosophila* flight muscles, we isolated mitochondria from thoraxes of wild-type flies, solubilized their membranes in 1% digitonin, and resolved their oxidative phosphorylation (OXPHOS) complexes into various bands using blue native polyacrylamide gel electrophoresis (BN-PAGE) (Rera et al., 2011; Wittig et al., 2006). We solubilized the mitochondrial membranes in 1% digitonin because we found that 1% digitonin was the optimal detergent concentration for isolating and resolving OXPHOS complexes in their native state in *Drosophila* (**Figure 2.2**), as has been reported previously (Rera et al., 2011; Wittig et al., 2006). Subsequently, we cut out each of the bands detected by coomassie staining of the gel, and identified their composition by mass spectrometry (**Figure 2.1C**). We confirmed the existence of 37 of the 42 putative CI orthologs based on their presence in the band corresponding to the CI holoenzyme (Band B) and/or supercomplex (Band A) (**Figure 2.1C, Tables 2.1 and 2.2**). Notably, the *Drosophila* ortholog of NDUFA4 (ND-MNLL) – a protein that was previously considered a CI subunit, but has been reassigned as a complex IV (CIV) subunit (Balsa et al., 2012) – co-migrated with the CIV band (Band E) **(Figure 2.1C and Table**

2.2). In addition, 4 of the subunits we were unable to detect are highly hydrophobic membrane-embedded core subunits encoded in the mitochondrion (ND2, ND3, ND4L and ND6); thus they may have escaped detection due to their highly hydrophobic nature. Interestingly, these subunits were not identified in a previous proteomic analysis of CI in mouse cell lines (Balsa et al., 2012).

Coomassie- or silver-stained native gels containing mitochondrial protein complexes from flies expressing RNAi to CI, complex III (CIII), CIV, and complex V (CV) proteins further confirmed the identities of the bands cut for mass spectrometry (**Figure 2.1D**). Because our mass spectrometry data suggested that a portion of CI might be co-migrating with CV and possibly CIII, we tested whether this co-migration was the result of supercomplex formation. We were unable to find antibodies that cross-react with any of the *Drosophila* CIII proteins, but antibodies that cross-react with dNDUFS3 (a CI protein) and dATPsynß (a CV protein) were commercially available, and were used to examine the identity of "band A" *via* western blotting. As is evident in the silver staining gel (**Figure 2.1D**), immunoblotting revealed that "band A" was actually a doublet; and the lower band in the doublet corresponds to a dimer of CV, as has been observed in other contexts (**Figure 2.1E**) (Rera et al., 2011; Wittig et al., 2006). In addition, CI in flight muscles was found to exist predominantly as the holoenzyme, with a relatively small portion involved in CI-CIII supercomplex formation, which migrates as an upper band in the doublet (**Figure 2.1E**). Notably, the observation that CI in *Drosophila* flight/skeletal muscles occurs predominantly as the holoenzyme (i.e. free CI, not involved in supercomplex formation), contrasts markedly with CI in cardiac or skeletal muscles from mice, where a significant portion of CI is trapped in supercomplex formation (**Figure 2.1F**). Thus, in addition to the genetic capabilities of *Drosophila* and the fact that it has a comparable number of CI subunits as the human enzyme, it is a suitable model for studying CI assembly because most of CI in flight muscles exists as the holoenzyme. Accordingly, a defect in CI biogenesis can easily be scored and quantified. Consequently, we decided to examine the role of the nuclear-encoded CI subunits in CI assembly.

Disruption of several CI subunits in flight muscles impair CI assembly

We found that loss-of-function alleles for many *Drosophila* CI genes are lethal (not shown). Therefore, to ascertain which CI subunits are required for CI biogenesis in *Drosophila*, we used the Gal4/UAS system to express transgenic RNAi constructs (henceforth referred to as *UAS-RNAi* lines) to

both core and accessory CI subunits (Brand and Perrimon, 1993). We examined the effect of knocking down the subunits specifically in muscles (using either *Dmef2-Gal4* or *mhc-Gal4*). Transgenic expression of many of the *UAS-RNAi* constructs using *Dmef2-Gal4* – a muscle-restricted Gal4 driver that is expressed strongly throughout development – caused lethality (not shown). However, a genetic cross between each of the *UAS-RNAi* lines and *mhc-Gal4* produced viable flies, as the *mhc-Gal4* driver has a weaker expression relative to *Dmef2-Gal4* during the initial larval stages (**Figure 2.3**). Accordingly, we decided to analyze CI assembly in mitochondria isolated from thoraxes of *mhc-Gal4/UAS-CI$_{RNAi}$* flies (henceforth referred to as *mhc>CI$_{RNAi}$* flies) using BN-PAGE.

We observed that, in general, both core and accessory subunits produced CI assembly defects whenever the extent of transcript knockdown was more than 50% (**Figure 2.4A**). To further assess the extent of the CI assembly deficit for each subunit, we quantified the amount of CI relative to the amount of CV in each lane, and normalized it to the corresponding value in the wild-type lane. Interestingly, this revealed that some of the most robust CI assembly deficits were observed when accessory subunits (such as dNDUFA10-12 and dNDUFB4-6) were genetically impaired (**Figures 2.4A and 2.4B)**. Similar results were obtained with silver staining of the protein complexes in the native gels **(Figure 2.4B)**. Additionally, in-gel CI enzyme activity assay revealed that the assembly deficits correlated with a reduction in CI activity **(Figure 2.4C)**. Finally, we found that knockdown of most accessory and core subunits impaired the climbing ability in these flies **(Figure 2.4D)**. Altogether, these results indicate that many of the core and accessory subunits are essential for viability and biogenesis of the CI holoenzyme or supercomplex in flight muscles. Accordingly, we turned our attention towards elucidating the mechanism of CI assembly in *Drosophila* flight muscles.

Proteomic analyses and immunoblotting identify assembly intermediates of CI

Studies from some mammalian cell lines have shown that CI biogenesis proceeds via a series of assembly intermediates that combine with each other, or other subunits, to form the ~950-kDa boot-shaped holoenzyme. The assembly intermediates generally correspond to partial or complete domains of the 3 functional modules of CI. The NADH Dehydrogenase module (N module) is located at the tip of the matrix arm, and is the site of NADH oxidation. Situated between the N module and the membrane is the Q module,

which is responsible for Ubiquinone reduction. The proton-conducting P module in the membrane arm can be subdivided into a proximal P_P-module (roughly corresponding to the first half of the P-module that connects with the Q-module) and a distal P_D-module (**Figure 2.5A**).

The current model posits that CI assembly in mammalian systems begins with the formation of a small assembly intermediate containing NDUFS2 and NDUFS3, that combines with NDUFS7 and NDUFS8 (**Figure 2.5B**). This assembly intermediate is the primary component of the Q-module; and ultimately combines with ND1 to form an ~315-kDa assembly intermediate that is anchored to the mitochondrial inner membrane. The ~315-kDa assembly intermediate combines with an independently-formed ~370-kDa assembly intermediate to form an ~550-kDa assembly intermediate (**Figure 2.5B**). The ~550-kDa assembly intermediate, which consists of the complete Q-module and a portion of the P-module, grows by the addition of more subunits to form the ~815-kDa assembly intermediate, via mechanisms that are very poorly defined. At this point, the ~815-kDa assembly intermediate is generally considered to be composed of the complete Q- and P-modules. Finally, an independently-formed assembly intermediate consisting of NDUFS1, NDUFV1, NDUFV2, NDUFV3, NDUFS4, NDUFS6 and NDUFA12, which together form the N module, is added as a "cap" to the ~815-kDa assembly intermediate to produce the ~950-kDa holoenzyme [**Figure 2.5B**; the ~315-, ~370-, ~550-, and ~815-kDa assembly intermediates were previously estimated as ~400-, ~460-, ~650- and ~830-kDa subcomplexes respectively (Andrews et al., 2013; Vartak et al., 2014)].

As some flight muscles are formed by 24 hours after pupal formation (Roy and VijayRaghavan, 1999), we decided to ascertain the extent of CI biogenesis starting at 48 hours (i.e. 2 days) post-pupariation. Specifically, we isolated mitochondria at various time points, and examined CI assembly via western blotting of the native complexes. Because current models of mammalian CI assembly postulate that NDUFS3 and ND1 are both part of the ~815-kDa, ~550-kDa, and ~315-kDa assembly intermediates, western blot with anti-NDUFS3 or anti-ND1 antibodies will be expected to detect these 3 assembly intermediates, and possibly lower molecular weight assembly intermediates (if the respective epitopes are not masked when the assembly intermediate is formed). In addition, the fully assembled CI and CI-containing supercomplexes will be expected to be detected as well. Indeed, immunoblotting with anti-NDUFS3 revealed that a portion of CI is assembled during pupal development and continues during the first 48 hours after flies eclose (emerge as adults from pupae) (**Figure 2.5C).** Although we were able to detect the ~315-kDa and ~550-

kDa assembly intermediates with the anti-ND1 antibody (**Figure 2.5C**), the higher molecular weight bands were only weakly detectable, conceivably because the epitope to which this antibody was raised for this hydrophobic subunit becomes less exposed to the aqueous environment during the final stages of CI biogenesis (**Figure 2.5C**). Moreover, while we were able to detect subcomplexes of CV that migrate with an apparent mass of about 100 kDa at this stage of development (**Figure 2.6)**, we were unable to detect dNDUFS3-containing assembly intermediates with an apparent mass of less than 200 kDa. There are at least two possible explanations for this result: (i) the smaller NDUFS3-containing assembly intermediates may not be present at this stage; or (ii) the epitope of dNDUFS3 in the smaller assembly intermediates was inaccessible to the antibody, perhaps as a result of being masked by bound assembly factors and/or other interactors. Therefore, we used proteomic analyses to distinguish between these two possibilities.

Mitochondria were isolated from thoraxes of wild-type flies that had been aged for 24 hours after eclosure, and subjected to BN-PAGE. Subsequently, the region of the gel between ~50 kDa and ~350 kDa, was excised and divided into 14 slices (labeled fraction A1 to A14) for in-gel digestion and subsequent proteomics analyses (**Figure 2.5D**). We observed that dNDUFS2, dNDUFS3 and dNDUFS7 co-migrated in fractions corresponding to a mass of approximately 280-320 kDa (**Figure 2.5D and Table 2.3**). Interestingly, the CI assembly factor, dNDUFAF4, was also found in these fractions (**Figure 2.5D and Table 2.3**). In addition, dNDUFA5 co-migrated with dNDUFS2, dNDUFS3 and dNDUFS7 (**Figure 2.5D**), confirming that it is a component of the ~315-kDa assembly intermediate *in vivo*. Importantly, although several other CI subunits migrated in fractions corresponding to a mass of approximately 50-250 kDa, neither dNDUFS2 nor dNDUFS3 were found in these fractions. Thus, it appears that in an *in vivo* context, in *Drosophila* flight muscles, the constituents of the ~315-kDa assembly intermediate are combined almost synchronously.

Specific subunits regulate the biogenesis or stability of specific assembly intermediates of CI

If the assembly intermediates observed are *bona fide* intermediates in the pathway of CI assembly in *Drosophila*, then at least some of these assembly intermediates will stall and accumulate, or they may disintegrate when specific CI subunits that are required for CI assembly are disrupted (**Figure 2.7A**). To test this hypothesis, we analyzed the CI assembly intermediates from thoraxes of *Mhc>CI$_{RNAi}$* flies, 24 hours

after eclosure using an anti-NDUFS3 antibody. As expected, the various subunits that produced CI assembly deficits in **Figure 4** also resulted in a reduction of the level of the holoenzyme or the CI-containing supercomplex (**Figures 2.7B-F**).

Disruption of dNDUFS1 and dNDUFV1, which are components of the N module of CI, and are thus expected to be added as part of the "cap" during the final step in CI assembly, resulted in a stalling and accumulation of the ~815-kDa assembly intermediate (**Figures 2.7B and 2.7C**). However, unexpectedly, disruption of dNDUFA6 and dNDUFA12, not known to be part of the N module, also stalled the ~815-kDa subcomplex (**Figure 2.7C**). RNAi-mediated knockdown of dNDUFS2, dNDUFS3, dNDUFS5, dNDUFS7, and dNDUFS8 led to a reduction in the amount of the ~815-kDa assembly intermediate (relative to wild type), as they impaired some of the initial steps of CI biogenesis (**Figures 2.7B and 2.7C**). In addition, the amount of the ~315-kDa assembly intermediate was drastically reduced when the expression of dNDUFS2, dNDUFS3, or dNDUFS7 was impaired (**Figure 2.7B**); in line with our proteomic results in **Figure 2.5D** and current mammalian CI assembly models that show that the first step in CI biogenesis involves the formation of an assembly intermediate consisting of NDUFS2 and NDUFS3 (**Figure 2.5B**) [reviewed in (Vartak et al., 2014)]. Notably, we found that RNAi-mediated knockdown of dNDUFA5 depleted the ~315-kDa assembly intermediate (**Figure 2.7C**). Combining this result, with our proteomic data showing that dNDUFA5 co-migrates with dNDUFS2, dNDUFS3 and dNDUFS7 (**Figure 2.5D**), we conclude that although dNDUFA5 is an accessory subunit, it is a critical component of, and required for formation or stabilization of the ~315-kDa assembly intermediate (i.e. the Q module) *in vivo.*

Disruption of most of the dNDUFB subunits did not markedly alter the stability or extent of accretion of the CI assembly intermediates 24 hours after eclosion **(Figure 2.7D)**, but by 48 and 72 hours after eclosion some notable and consistent phenotypes between the two time points were observed **(Figure 2.7E and 2.7F)**. For instance, RNAi-mediated disruption of dNDUFB3 decreased the extent of accumulation of all the assembly intermediates; and the 550-kDa assembly intermediate accumulated when dNDUFB1, dNDUFB8 and dNDUFB11 were impaired at both time points (i.e. 48 and 72 hours post-eclosion). Surprisingly, although none of the NDUFB subunits are known to be part of the 315-kDa assembly intermediate, the extent of accumulation of the 315-kDa assembly intermediate was diminished when the expression of dNDUFB1, dNDUFB4, dNDUFB5, dNDUFB6 and dNDUFB10 were reduced **(Figure 2.7E**

and 2.7F). Taken together, these results indicate that specific subunits regulate the biogenesis or stability of specific CI assembly intermediates during CI assembly in *Drosophila* thoraxes.

Identification of an ~700-kDa assembly intermediate of CI in *Drosophila*

An assembly intermediate that accumulates between the ~550- and ~815-kDa assembly intermediates was detected on immunoblots of samples from *mhc>dNDUFS5$_{RNAi}$* and *mhc>dNDUFC2$_{RNAi}$* thoraxes (**Figure 2.7B**). We estimate its size to be ~700 kDa because it co-migrates with CV, previously estimated to be ~700 kDa in blue native gels (**Figure 2.8A**) (Abdrakhmanova et al., 2006). The accumulation of the ~700-kDa assembly intermediate in samples from *mhc>dNDUFS5$_{RNAi}$* thoraxes was notable, because it suggested that this could be the point of entry of dNDUFS5 during CI assembly. NDUFS5 is a membrane-associated accessory subunit that extends into the intermembrane space; it is currently unclear at what point it becomes incorporated into CI. In contrast to the ~315-, ~550- and ~815-kDa assembly intermediates, the ~700-kDa assembly intermediate was not readily perceptible by anti-NDUFS3 immunoblotting in the wild-type sample or most of the other mutant samples isolated 24 hours after eclosure (**Figure 2.7B**). This raised the possibility that it could simply be a degradation product, perhaps derived from the ~815-kDa assembly intermediate.

To determine whether the ~700-kDa assembly intermediate is a true assembly intermediate, we decided to look at earlier time points (6 and 12 hours post-eclosion) to ascertain whether it ever appears in wild-type samples. Immunoblotting at these time points revealed that accumulation of the ~700-kDa assembly intermediate in *mhc>dNDUFS5$_{RNAi}$* thoraxes is present by the 6-hour time point, and gradually tapers off afterwards (**Figure 2.8B**). Importantly, at the 6-hour time point a faint band corresponding to the ~700-kDa assembly intermediate can be observed in wild-type samples, indicating that the ~700 kDa-assembly intermediate exists in wild-type samples, and rapidly matures to the ~815-kDa assembly intermediate. The stalling of the ~700-kDa assembly intermediate in *mhc>dNDUFS5$_{RNAi}$* thoraxes occurred concurrently with an accumulation of both the ~550-kDa and ~315-kDa assembly intermediates, and a diminution of the ~815-kDa assembly intermediate relative to wild-type levels. Thus, dNDUFS5 may be required for converting the ~700-kDa assembly intermediate into the ~815-kDa assembly intermediate, such that when this fails, there is a backlog of the ~700-, ~550- and ~315-kDa assembly intermediates. To

test this hypothesis, we compared the assembly intermediates that accumulate in *mhc>dNDUFS5$_{RNAi}$,dNDUFS1$_{RNAi}$* and *mhc>dNDUFS5$_{RNAi}$,dNDUFV1$_{RNAi}$* thoraxes with that in *mhc>dNDUFS1$_{RNAi}$* and *mhc>dNDUFV1$_{RNAi}$* thoraxes respectively. We reasoned that because the ~815-kDa assembly intermediate accumulates in *mhc>dNDUFS1$_{RNAi}$* and *mhc>dNDUFV1$_{RNAi}$* thoraxes (**Figure 2.7B**), if dNDUFS5 is required for converting the ~700-kDa assembly intermediate into the ~815-kDa assembly intermediate, then the extent of accumulation of the ~815-kDa assembly intermediate in either *mhc>dNDUFS5$_{RNAi}$,dNDUFS1$_{RNAi}$* and/or *mhc>dNDUFS5$_{RNAi}$,dNDUFV1$_{RNAi}$* thoraxes should be reduced relative to *mhc>dNDUFS1$_{RNAi}$* and *mhc>dNDUFV1$_{RNAi}$* respectively. In agreement with this proposition, we observed that the accumulation of the ~815-kDa assembly intermediate was significantly attenuated *in mhc>dNDUFS5$_{RNAi}$, dNDUFS1$_{RNAi}$* thoraxes relative to *mhc>dNDUFS1$_{RNAi}$* thoraxes (**Figure 2.8C**). This was also accompanied by an accumulation of the ~700-kDa assembly intermediate (**Figure 2.8C**). Similar results were obtained by comparing *mhc>dNDUFS5$_{RNAi}$,dNDUFV1$_{RNAi}$* and *mhc>dNDUFV1$_{RNAi}$* thoraxes (**Figure 2.8C**). Accordingly, we deduce from these results that when dNDUFS5 expression levels are impaired, the transient ~700-kDa assembly intermediate stalls and accumulates, impeding progression of CI biogenesis and ultimately resulting in a bottleneck of the ~550-kDa and ~315-kDa assembly intermediates as well.

To gain further insight into the identity of the ~700-kDa assembly intermediate, a single gel slice encompassing the region shown in **Figure 2.8A** was excised from native gels containing samples from wildtype and *mhc>dNDUFS5$_{RNAi}$* thoraxes. Proteins from the gel slice were digested and analyzed by LC mass spectrometry; and a label-free spectral counting approach was used to generate a heat map for some of the proteins that showed altered expression levels between the samples. In agreement with our results showing a stalling and accumulation of the ~700-kDa assembly intermediate in this portion of the gel, we observed that several CI subunits were upregulated in the *mhc>dNDUFS5$_{RNAi}$* sample relative to wildtype (**Figure 2.8D**). However, in stark contrast to the other CI subunits, we consistently observed (in 6 biological replicates taken at different time points of the day to control for circadian regulation) that dNDUFA10 was downregulated in the *mhc>dNDUFS5$_{RNAi}$* sample; indicating that incorporation of dNDUFS5 into CI is necessary to stabilize or promote incorporation of dNDUFA10 into the complex (**Figure 2.8D)**. In mammalian systems, at least five CI assembly factors – ECSIT, TMEM126B, NDUFAF1, ACAD9 and

TIMMDC1 – are typically found associated with CI assembly intermediates, and have been dubbed the Mitochondrial Complex I Assembly (MCIA) complex (Guarani et al., 2014; Heide et al., 2012; Nouws et al., 2010; Vogel et al., 2007). We found four of these assembly factors (dECSIT, dNDUFAF1, dACAD9 and dTIMMDC1), associated with the 700-kDa assembly intermediate that were upregulated in the *mhc>dNDUFS5$_{RNAi}$* samples, further confirming that it is a true assembly intermediate in CI biogenesis (**Figure 2.8D and Table 2.4**).

The distal portion of the membrane arm of CI is assembled independently of the matrix arm

We noticed that in some instances where CI assembly was impaired, an additional band accumulated between the CIII and CIV bands in both the coomassie- and silver-stained gels (arrows in **Figures 2.4A and 2.4B**). A closer examination revealed that the accumulation of this intermediate was more readily evident in samples where subunits localized to the hydrophilic matrix domain were disrupted (i.e. the dNDUFS, dNDUFV and dNDUFA subunits) (**Figure 2.1A**). In line with our observations described in **Figures 2.5, 2.7 and 2.8**, we hypothesized that this band was likely another CI assembly intermediate that had stalled and accumulated as a result of a block in CI biogenesis. We decided to identify the constituents of this putative assembly intermediate via mass spectrometry.

We cut out the region of the gel corresponding to the stalled assembly intermediate in the wildtype, *mhc>dNDUFS5$_{RNAi}$* and *mhc>dNDUFV1$_{RNAi}$* thoraxes **(Figure 2.9A),** and used label-free quantification of peptides to ascertain which subunits and possibly assembly factors were altered between the two samples. Several components of the ETC machinery were downregulated; but there was a dramatic increase in CI subunits that are part of the distal membrane domain (i.e. all the dNDUFB subunits as well as dNDUFAB1, dNDUFC2, ND4 and ND5) (**Figures 2.9B and 2.9C; Table 2.5**). We note that there was no obvious accumulation of this assembly intermediate in blue native or silver-stained gels when any of these subunits (i.e. the dNDUFB subunits, or NDUFAB1 and NDUFC2 subunits) were disrupted (**Figures 2.4A and 2.4B**). Notably, many of these membrane-associated subunits were present in the corresponding gel slice from the wild-type samples (although at lower levels). All the components of the MCIA complex (i.e. dECSIT, dNDUFAF1, dACAD9, dTMEM126B and dTIMMDC1) were also found associated with this assembly intermediate. Based on current assignments of the various CI subunits, this assembly intermediate is clearly

the distal portion of the membrane arm (Fiedorczuk et al., 2016; Vinothkumar et al., 2014; Zhu et al., 2016; Zickermann et al., 2015).

Proposed model of CI assembly in *Drosophila* muscle

We propose a model for CI assembly in *Drosophila* flight muscles where dNDUFS2, dNDUFS3, dNDUFS7, dNDUFS8 and dNDUFA5 are combined in essentially one step to form the Q module, which is anchored to the membrane by dND1 (**Figure 2.10**). This assembly intermediate corresponds to the assembly intermediate in mammalian systems that was previously referred to as the ~400-kDa subcomplex, but has recently been re-estimated as the ~315-kDa subcomplex (Andrews et al., 2013; Vartak et al., 2014). This is consistent with the observation that assembly intermediates containing dNDUFS2, dNDUFS3, dNDUFS7, dNDUFS8 and dNDUFA5 co-migrate in blue native gels (**Table 2.2**), and that immunoblotting with both anti-ND1 and anti-NDUFS3 detect the ~315-kDa assembly intermediate (**Figure 2.5C**).

Subsequently, another assembly intermediate consisting of some of the subunits in the membrane domain is formed. This assembly intermediate comprises part of the P-module (i.e. Partial P1), and is conjugated to the Q-module to form an assembly intermediate that corresponds to the ~550-kDa (formerly ~650-kDa) assembly intermediate previously described in mammalian systems (**Figure 7**). Although proteomic analyses of the assembly intermediate that accumulates in *mhc>dNDUFS5$_{RNAi}$* and *mhc>dNDUFV1$_{RNAi}$* thoraxes shows that all the dNDUFB subunits as well as dNDUFC1, dNDUFAB1, ND4 and ND5 subunits are present in the subcomplex (see **Table 2.5**), it is unlikely that all the membrane subunits are incorporated into the complex at this stage under normal (wild-type) conditions. We hypothesize that the accumulation of the membrane accessory subunits in response to genetic disruption of the matrix subunits may be a compensatory mitochondrial stress signaling mechanism impinging on the nucleus, and resulting in a system that is poised to rapidly resume CI biogenesis if and when the missing matrix subunit becomes available. The accretion of the Partial P-module under conditions where other components of the CI assembly machinery are impaired provides further evidence that the various modules of the complex (i.e. the Q-, P- and N-modules) are assembled largely independently of each other *in vivo*.

The ~550-kDa assembly intermediate grows by the addition of more subunits to form a transient assembly intermediate of ~700-kDa (**Figure 7**); we postulate that dNDUFS5 is then incorporated at or just

prior to this stage together with possibly dNDUFA10 to rapidly convert the ~700-kDa assembly intermediate to the ~815-kDa assembly intermediate, consisting of the complete P- and Q-modules (**Figure 7**). Finally, the N-module is added to produce the CI holoenzyme (**Figure 7**).

Discussion

We have exploited the genetic capabilities of *Drosophila* to uncover the mechanism of CI assembly *in vivo*, in *Drosophila* flight muscles. Our immunoblotting and proteomic analyses reveal that during CI assembly in *Drosophila*, the first membrane-bound major assembly intermediate that forms contains at least the following six subunits: dND1, dNDUFS2, dNDUFS3, dNDUFS7, dNDUFS8 and dNDUFA5. Based on its constituents and migration pattern in native PAGE, we conclude that this assembly intermediate is the same assembly intermediate traditionally referred to as the ~315-kDa assembly intermediate from studies on mammalian CI assembly; and corresponds to the Q module of CI (Andrews et al., 2013; Vartak et al., 2014). Consistent with their roles in regulating formation of the Q module, we found that genetic disruption of dNDUFS2, dNDUFS3, dNDUFA5, and dNDUFS7 attenuated the amount of the ~315-kDa assembly intermediate formed.

Unexpectedly, we found an ~700-kDa assembly intermediate that is short-lived (at least relative to the ~315-, ~550- and ~815-kDa assembly intermediates), as it is rapidly converted into the ~815-kDa assembly intermediate. Importantly, our proteomic analyses revealed that incorporation of dNDUFS5 into CI around this stage is necessary to stabilize or promote incorporation of dNDUFA10 into the complex. Similar to the ~315-, ~550-, and ~815-kDa assembly intermediates, the ~700-kDa subcomplex is a true assembly intermediate as it can be detected in wild-type muscles as well. Additionally, components of the MCIA complex are associated with the ~700-kDa assembly intermediate, as has been reported for other assembly intermediates observed in mammalian systems. RNAi-mediated disruption of dNDUFS5 led to a stalling and accumulation of this otherwise transient assembly intermediate, to a point where it is readily detectable by western blots; most likely because this is the stage at or around which dNDUFS5 is incorporated into the complex.

It is possible that mutations in some accessory subunits will have both primary and secondary effects. As a case in point, dNDUFS5 disruption may first impair conversion of the ~700-kDa assembly

intermediate to the ~815-kDa assembly intermediate, and consequently, impair CI assembly (as we have shown); but ultimately, the accumulation of the ~700-kDa assembly intermediate can activate the mitochondrial unfolded protein response as well as other stress signaling cascades with far-reaching consequences (Haynes et al., 2013; Jensen and Jasper, 2014; Owusu-Ansah and Banerjee, 2009; Owusu-Ansah et al., 2013; Owusu-Ansah et al., 2008). As another example, when dNDUFB3 was disrupted no specific assembly intermediates were stalled or disintegrated. Instead, there was a general reduction in the level of expression of all assembly intermediates. It is possible that disruption of dNDUFB3 activates stress signaling pathways that induce apoptosis or culminate in a general reduction of protein synthesis, leading to a reduction in CI assembly.

We find that at least 42 of the 44 distinct human CI proteins are conserved in *Drosophila*. The two human CI proteins for which a clear ortholog was not readily identified in *Drosophila* by DIOPT are NDUFA3 (9 kDa) and NDUFC1 (6 kDa), which are two of the smallest subunits of the complex. Interestingly, obvious orthologs of NDUFC1 are not found in *C. elegans* or *Yarrowia lipolytica*; and the orthologs in vertebrates such as Zebrafish and Xenopus have very weak homology (DIOPT score of 1) to the human protein. Therefore it is possible that this subunit has significant sequence divergence in *Drosophila*, and although present, was not recognized by DIOPT. For most of the CI subunits where multiple paralogs were identified by DIOPT (i.e. NDUFS2, NDUFS7, NDUFV2, NDUFA7 and NDUFB2), only one of the paralogs was detected as a *bona fide* CI subunit in flight muscles. However, as an exception to this general rule, two of the three paralogs of NDUFV1 were detected as part of CI in skeletal muscles *via* mass spectrometry. ND-51 (CG9140) appears to be the authentic ortholog of human NDUFV1 as it is highly expressed in skeletal muscles relative to ND-51L (CG11423), and is comparable in size to the human ortholog (both are about 51 kDa). ND-51L is a 77 kDa protein with a stretch of about 200 amino acids at the N-terminus that is not present in either the *Drosophila* paralog (ND-51) or human ortholog (NDUFV1). It remains to be determined whether the expression of the subunits with multiple paralogs are regulated in a tissue-specific manner to generate mitochondria with varied CI activities; or whether they are regulated in the same tissue in response to different environmental conditions to fine-tune the activity of CI.

In summary, we have described the mechanism of CI assembly in *Drosophila* flight muscles, and defined specific roles for some of the accessory subunits in CI assembly. Importantly, although CI

dysfunction has been implicated in a large number of pathologies, we find that knocking down the expression of various antioxidant enzymes or mitochondrial protein quality control genes does not solely impair CI assembly, indicating that destabilization of CI may not be the sole underlying factor in many mitochondrial disorders (**Figure 2.11**). In addition, our proteomic analyses established that incorporation of dNDUFS5 into CI is necessary to stabilize or promote incorporation of dNDUFA10 into the complex. We note that our analyses of CI assembly in an *in vivo* setting, where CI biogenesis is subject to both developmental and environmental cues, revealed that many of the accessory subunits are required for both assembly and viability. Moreover, several NDUFB subunits (dNDUFB1, dNDUFB4, dNDUFB5, dNDUFB6 and dNDUFB10) seem to regulate the stability of the 315-kDa assembly intermediate, in apparent deviation from what will be expected from current models of mammalian CI assembly. However, the mechanism of CI biogenesis in *Drosophila* flight muscles is remarkably similar to what has been described in mammalian systems; and the differences observed here may be due to the fact that we have analyzed CI assembly in an *in vivo* setting. Accordingly, *Drosophila* is a suitable organism for addressing questions relevant to mammalian CI biogenesis. We anticipate that future studies using the full repertoire of genetic tools and resources in *Drosophila* should foster the discovery of novel paradigms for regulating CI assembly in humans.

Materials and Methods

Drosophila Strains and Genetics.

The following fly stocks were used: y w; Dmef2-Gal4 and w; mhc-Gal4 were the Gal4 transgenic lines used to express RNAi lines in muscles. w1118/mhc-Gal4 flies were used as wildtype (wt) controls. Other fly stocks used were: y1 sc*v1 ; P{TRiP.HMS00854}attP2 (Bloomington, #33911), y1 v1 ; P{TRiP.HMS05059}attP2 (Bloomington, #28573), y1 v1 ; P{TRiP.HMC02929}attP40 (Bloomington, #44535), y1 v1 ; P{TRiP.HMC03554}attP40 (Bloomington, #53325), y1 sc*v1 ; P{TRiP.HMC03861}attP40 (Bloomington, #55180), y1 sc*v1 ; P{TRiP.HM05229}attP2 (Bloomington, #30487), y1 sc*v1 ; P{TRiP.HMS01590}attP2 (Bloomington, #36701), y1 v1 ; P{TRiP.HMC03429}attP40 (Bloomington, #51855), y1 sc*v1 ; P{TRiP.HMC03653}attP40 (Bloomington, #52913), y1 sc*v1 ; P{TRiP.GLC01699}attP2 (Bloomington, #50577),y1 sc*v1 ; P{TRiP.HMC03662}attP40 (Bloomington, #52922), y1 sc*v1 ; P{TRiP.HMS00798}attP2 (Bloomington, #32998), y1 sc*v1 ; P{TRiP.HMS01584}attP2 (Bloomington, #36695), y1 sc*v1 ; P{TRiP.HMC02678}attP2/ TM3, Sb1 (Bloomington, #43279), y1 v1 ; P{TRiP.HM05206}attP2 (Bloomington, #29528), y1 v1 ; P{TRiP.HM22452}attP40 (Bloomington, #58322), y1 v1 ; P{TRiP.GLC01422}attP2 (Bloomington, #43235), y1 v1 ; P{TRiP.HMJ23156}attP40 (Bloomington, #61321), y1 sc*v1 ; P{TRiP.HM05255}attP2/TM3, Sb1 (Bloomington, #30511), y1 sc*v1 ; P{TRiP.HMC03242}attP2 (Bloomington, #51357), y1 v1 ; P{TRiP.HMJ22367}attP40 (Bloomington, #58282), y1 sc*v1 ; P{TRiP.HMS00815}attP2 (Bloomington, #33878), y1 v1 ; P{TRiP.JF02892}attP2 (Bloomington, #28056), y1 v1 ; P{TRiP.JF02899}attP2 (Bloomington, #28062) and y1 sc*v1 ; P{TRiP.HMS01560}attP2 (Bloomington, #36672). Transgenic RNAi stocks for disrupting CG8680 (8680R-3), CG9172 (9172R-2), CG6463 (6463R-1), CG9350 (9350R-2), CG9762 (9762R-3), CG13240 (13240R-2), CG3283 (3283R-1) and CG3192 (3192R-3) were from the National Institute of Genetics (NIG, Japan) Drosophila Stock Center. RNAi stocks for disrupting CG12400 (v102590), CG7712 (v100616), CG12859 (v8786), CG4169 (v26405) and CG9306 (v23088) were from the Vienna Drosophila Resource Center.

Mitochondria Purification.

Mitochondrial purification was performed essentially as described by Rera et al 2012 (Rera et al., 2011). Thoraxes were dissected and gently crushed with a pestle homogenizer in 500µl of pre-chilled mitochondrial isolation buffer containing 250 mM sucrose and 0.15 mM MgCl2 in 10 mM Tris.HCl, pH 7.4, on ice. After two rounds of centrifugation at 500g for 5 minutes at 4°C to remove insoluble material, the supernatant was recovered and centrifuged at 5000g for 5 minutes at 4°C. The pellet which is enriched for mitochondria was washed twice in the mitochondrial isolation buffer and stored at -80°C until further processing.

Blue Native Polyacrylamide Gel Electrophoresis (BN-PAGE).

BN-PAGE was performed using NativePAGE gels from Life Technologies, following the manufacturer's instructions. Essentially, mitochondria were suspended in native PAGE sample buffer (Life Technologies) supplemented with 1% digitonin and protease inhibitors, and incubated on ice for 20 minutes. Following centrifugation at 20,000g for 30 minutes, the supernatant was recovered, mixed with the G-250 sample additive (Life Technologies) and Native PAGE Sample Buffer (Life Technologies), and loaded onto 3–12% pre-cast Bis–Tris Native PAGE gels (Life Technologies). The NativeMark Protein standard (Life Technologies), run together with the samples, was used to estimate the molecular weight of the protein complexes. Electrophoreses was performed using the Native PAGE Running buffer (as anode buffer, from Life technologies) and the Native PAGE Running buffer containing 0.4% Coomassie G-250 (cathode buffer). Gels were stained with the Novex Colloidal Blue staining kit (Life Technologies) to reveal the protein complexes.

Silver Staining.

Silver staining of native gels was performed with the SilverXpress staining kit from Life Technologies, following the manufacturer's protocol.

In-gel Complex I Activity.

Complex I activity in native gels was performed by incubating the native gels in 0.1 mg/ml NADH, 2.5 mg/ml Nitrotetrazolium Blue Chloride, 5 mM Tris-HCl (pH 7.4) overnight at room temperature.

Climbing Assay

20 flies were collected in a vial for each CI subunit that was knocked down. Flies were tapped lightly to the bottom of the vial and were allowed 15 seconds to past the midway line in the vial (target line). The percentage of flies to cross the target line was calculated.

Immunoblotting

For immunoblotting of samples in native gels, protein complexes from native gels were transferred to PVDF membranes (BIORAD). For immunoblotting of samples in whole tissue lysates, thoraxes were homogenized in RIPA buffer (150 mM NaCl, 1% Triton X-100, 0.5% Sodium Deoxycholate, 0.1% SDS, 50mM Tris HCl, pH 8) supplemented with Halt protease inhibitors (Pierce), resolved on mini-PROTEAN TGX stain-free gels from BIO-RAD, and transferred to PVDF membranes. In both instances (native and non-native gels), the membrane was subsequently blocked in 5% (w/v) non-fat dry milk in Tris-buffered saline (TBS) for 30minutes, and incubated in the appropriate primary antibody dissolved in 2% BSA, 0.1% Tween 20 in TBS (TBST) overnight at 4°C. Following the overnight incubation, the blot was rinsed 4X10 minutes in 0.1%TBST, blocked for 30 minutes in 5% (w/v) non-fat dry milk in TBST and incubated for two hours with the appropriate HRP-conjugated secondary antibody dissolved in 2% BSA, 0.1% Tween 20 in TBS (TBST). After incubation in the secondary antibody, samples were rinsed 4X10 minutes in 0.1%TBST. Immunoreactivity was detected by enhanced chemiluminescence (ECL) and analyzed by a ChemiDoc Gel imaging system from BIO-RAD. Antibodies used were anti-NDUFS3 (abcam, ab14711), anti-ND1 (abcam, ab74257), anti ATPsynß (Life technologies, A21351) anti-GFP (Life technologies, A6455) and anti-actin (EMD Millipore, MAB1501).

In-Gel Protein Digestion

The dried gel pieces were rehydrated and digested in 80 µL of 12.5 ng/µL Trypsin Gold/50 mM ammonium bicarbonate at 37°C overnight. Following the digestion, condensed evaporated water was collected from tube walls by brief centrifugation using benchtop microcentrifuge (Eppendorf, Hauppauge, NY). The gel pieces and digestion reaction were mixed with 50 µL 2.5% Trifluoroacetic acid (TFA) and rigorously mixed for 15 minutes. The solution with extracted peptides was transferred into a fresh tube, and the remaining peptides were extracted with 80µl of 70% Acetonitrile (ACN)/5% TFA mixture using by rigorously mixing for 15 minutes. The extracts were pooled and dried to completion (1.5–2 hours) in a SpeedVac. The dried peptides were reconstituted in 30 µl of 0.1% TFA by mixing for 5 minutes and stored on ice or at −20 °C prior to analysis.

LC-MS/MS Analysis

The concentrated peptide mix was reconstituted in a solution of 2 % ACN, 2 % Formic acid (FA) for MS analysis. Peptides were eluted from the column using a Dionex Ultimate 3000 Nano LC system with a 10 min gradient from 2% buffer B to 35 % buffer B (100 % ACN, 0.1 % FA). The gradient was switched from 35 % to 85 % buffer B over 1 min and held constant for 2 min. Finally, the gradient was changed from 85 % buffer B to 98 % buffer A (100% water, 0.1% FA) over 1 min, and then held constant at 98 % buffer A for 5 more minutes. The application of a 2.0 kV distal voltage electrosprayed the eluting peptides directly into the Thermo Fusion Tribrid mass spectrometer equipped with an EASY-Spray source (Thermo Scientific). Mass spectrometer-scanning functions and HPLC gradients were controlled by the Xcalibur data system (Thermo Finnigan, San Jose, CA).

Database Search And Interpretation Of MS/MS Data

Tandem mass spectra from raw files were searched against a Drosophila protein database using the Proteome Discoverer 1.4 software (Thermo Finnigan, San Jose, CA). The Proteome Discoverer application extracts relevant MS/MS spectra from the .raw file and determines the precursor charge state and the

quality of the fragmentation spectrum. The Proteome Discoverer probability-based scoring system rates the relevance of the best matches found by the SEQUEST algorithm. The Drosophila protein database was downloaded as FASTA-formatted sequences from Uniprot protein database (database released in May, 2015). The peptide mass search tolerance was set to 10ppm. A minimum sequence length of 7 amino acids residues was required. Only fully tryptic peptides were considered. To calculate confidence levels and false positive rates (FDR), Proteome Discoverer generates a decoy database containing reverse sequences of the non-decoy protein database and performs the search against this concatenated database (non-decoy + decoy). Scaffold (Proteome Software) was used to visualize searched results. The discriminant score was set at less than 1% FDR determined based on the number of accepted decoy database peptides to generate protein lists for this study. Spectral counts were used for estimation of relative protein abundance between samples.

Figure 2.1: *Drosophila* flight muscles are suitable for studying complex I assembly.

(A) Schematic representation of how the 44 distinct subunits of bovine or ovine CI are arranged to produce the L-shaped topology; based on recent CI structures described (Fiedorczuk et al., 2016; Vinothkumar et al., 2014; Zhu et al., 2016; Zickermann et al., 2015). The asterisk denotes subunits for which an ortholog was not identified in *Drosophila* by DIOPT. NDUFAB1 occurs twice in the complex, giving rise to a total of 45 subunits.

(B) Summary of the experimental procedure for studying CI assembly in *Drosophila*. Transgenic RNAi constructs to the nuclear-encoded subunits were expressed specifically in thoracic muscles using the *mhc-Gal4* driver. Mitochondria were isolated from thoraxes of 1 week-old flies, solubilized in 1% digitonin, and analyzed by blue native polyacrylamide gel electrophoresis (BN-PAGE).

(C) The constituents of each of the six major bands observed during BN-PAGE was analyzed by mass spectrometry. 38 subunits of *Drosophila* CI were confirmed by mass spectrometry. The 38 subunits correspond to 37 different orthologs of human CI. Two paralogs of human NDUFV1 were confirmed by mass spectrometry (see **Table 2.1**). See **Table 2.2** for all the peptides identified in the six major bands shown.

(D) BN-PAGE (left panel) and Silver staining (right panel) of samples from thoraxes following RNAi-mediated knockdown of complex I (CI), complex III (CIII), complex IV (CIV) and complex V (CV) proteins to confirm the identities of the bands. SupCI and CV2 denote a supercomplex of CI and a dimer of CV respectively. The exact RNAi constructs expressed starting from left to right were to the white gene (wildtype, WT), dNDUFV1 (CI), dNDUFS1 (CI), dUQCRC-2 (CIII), dUQCRC-Q (CIII), dCox5A (CIV), cyclope (CIV), dATPsyn-β (CV), and ATPsyn-b (CV).

(E) Immunoblotting with anti-NDUFS3 and anti-ATPsynβ antibodies of native gels to detect CI and CV respectively. Note that band A is a doublet consisting predominantly of a dimer of CV, and a supercomplex of CI.

(F) BN-PAGE (top panel) and CI in-gel enzyme activity (lower panel) indicate that most of CI exists as the holoenzyme in *Drosophila melanogaster* (DM) skeletal muscles, in contrast to cardiac, soleus, EDL and tibia muscles from mice where a significant portion of CI exists as a supercomplex.

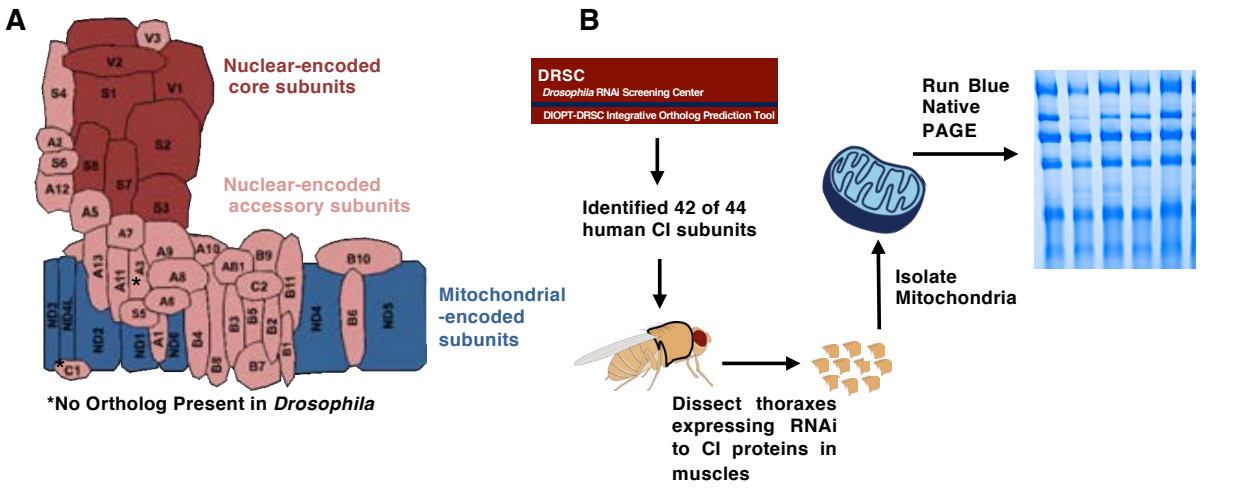
A
Nuclear-encoded core subunits
Nuclear-encoded accessory subunits
Mitochondrial -encoded subunits
*No Ortholog Present in Drosophila
B
DRSC
Drosophila RNAi Screening Center
DIOPT-DRSC Integrative Ortholog Prediction Tool
Identified 42 of 44 human CI subunits
Dissect thoraxes expressing RNAi to CI proteins in muscles
Isolate Mitochondria
Run Blue Native PAGE

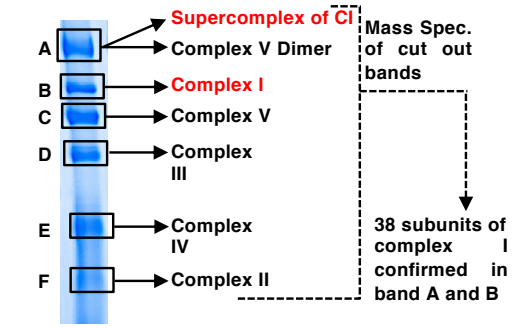
C
A
B
C
D
E
F
Supercomplex of CI
Complex V Dimer
Complex I
Complex V
Complex III
Complex IV
Complex II
Mass Spec. of cut out bands
38 subunits of complex I confirmed in band A and B

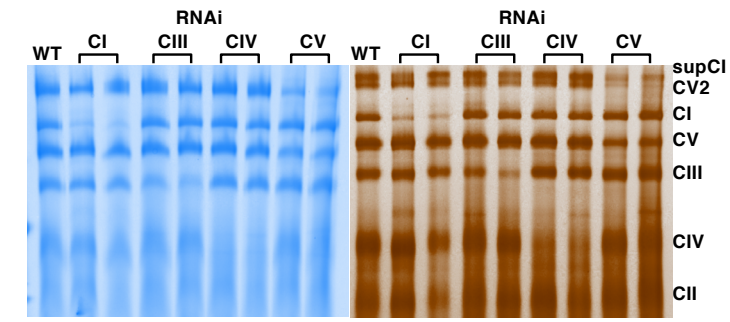
D
RNAi
WT
CI
CIII
CIV
CV
supCI
CV2
CI
CV
CIII
CIV
CII

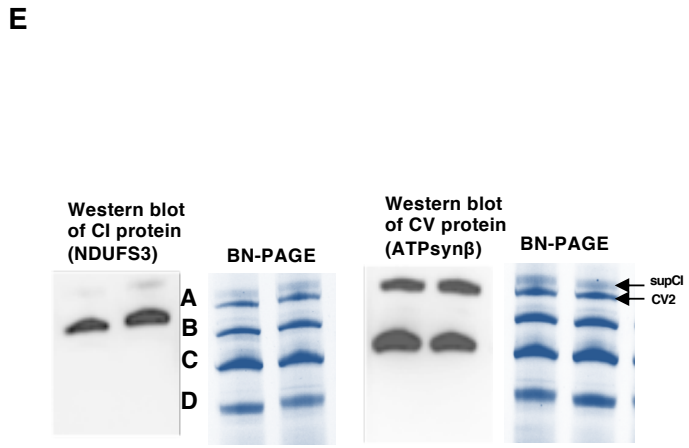
E
Western blot of CI protein (NDUFS3)
BN-PAGE
A
B
C
D
Western blot of CV protein (ATPsynβ)
BN-PAGE
supCI
CV2

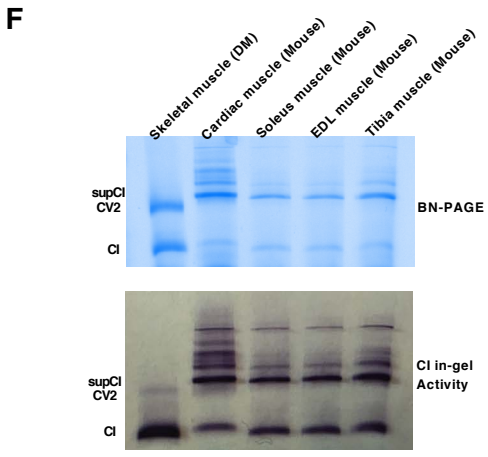
F
Skeletal muscle (DM)
Cardiac muscle (Mouse)
Soleus muscle (Mouse)
EDL muscle (Mouse)
Tibia muscle (Mouse)
supCI
CV2
CI
BN-PAGE
supCI
CV2
CI
CI in-gel Activity

Figure 2.2: 1% digitonin is the optimum detergent concentration for resolving OXPHOS complexes in *Drosophila* thoraxes.

Related to Figure 2.1.

Mitochondrial protein complexes from wild-type thoraxes were solubilized in various concentrations of detergents as shown

(A) Digitonin at 0.25%, 0.5%, 1% and 2%

(B) 1% digitonin, and Triton X-100 concentrations of 0.25%, 0.5%, 1% and 2%

(C) 1% digitonin, and n-Dodecyl β-D-maltoside (DDM) concentrations of 0.25%, 0.5%, 1% and 2%

(D) NP-40 concentrations of 0.25%, 0.5%, 1% and 2%, and

(E) Tween-20 concentrations of 0.25%, 0.5%, 1% and 2%

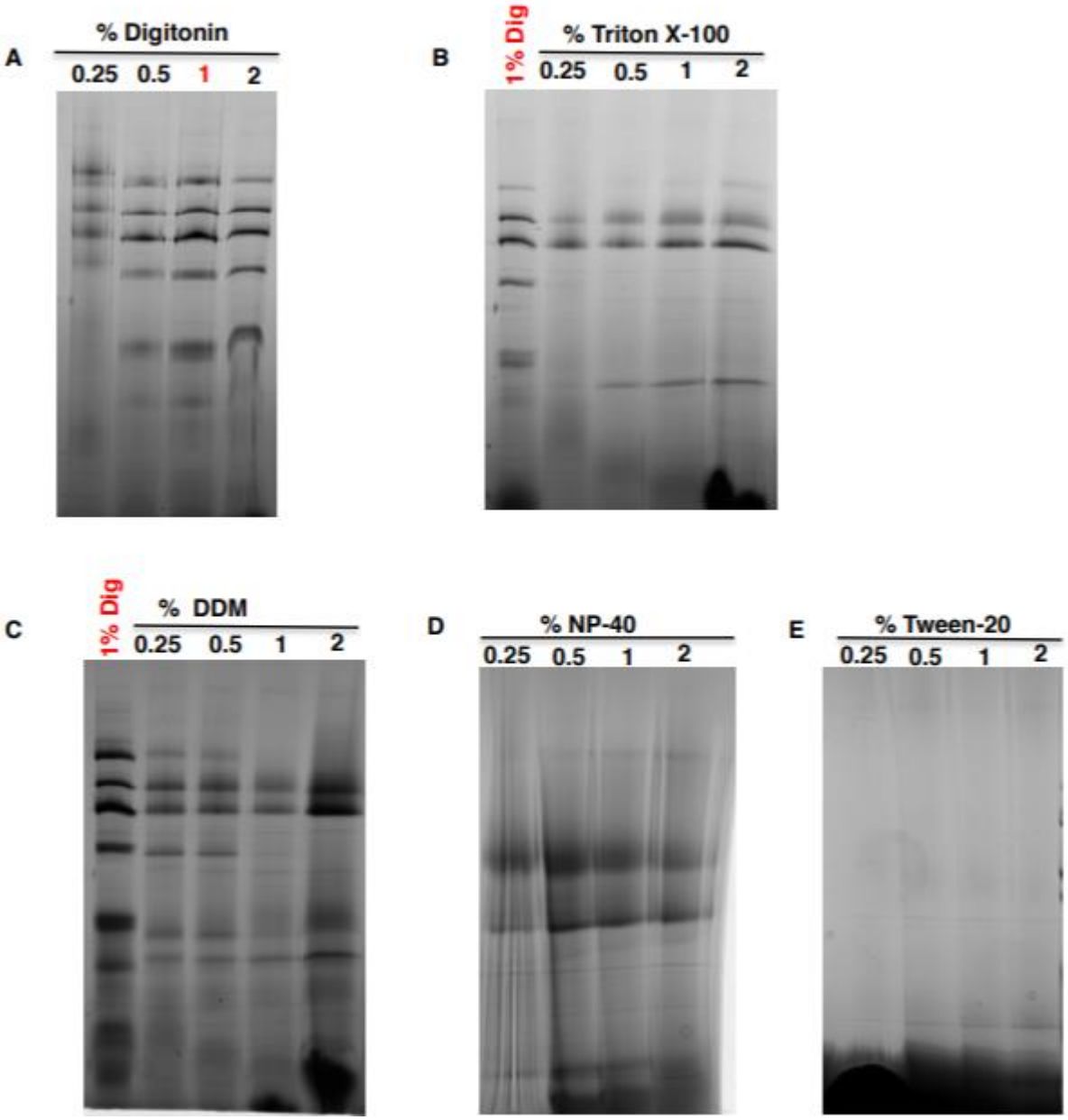
A
% Digitonin
0.25 0.5 1 2
B
1% Dig
% Triton X-100
0.25 0.5 1 2
C
1% Dig
% DDM
0.25 0.5 1 2
D
% NP-40
0.25 0.5 1 2
E
% Tween-20
0.25 0.5 1 2

Figure 2.3: Strong expression of dmef2-gal4 during development.

Related to Figure 2

Western blot showing extent of GFP expression in Dmef2-Gal4; UAS-GFP and mhc-Gal4; UAS-GFP larval somatic and adult thoracic muscles respectively. Expression of β-actin serves as a loading control. Note that the mhc-Gal4 driver has a weaker expression during development relative to the Dmef2-Gal4 driver.

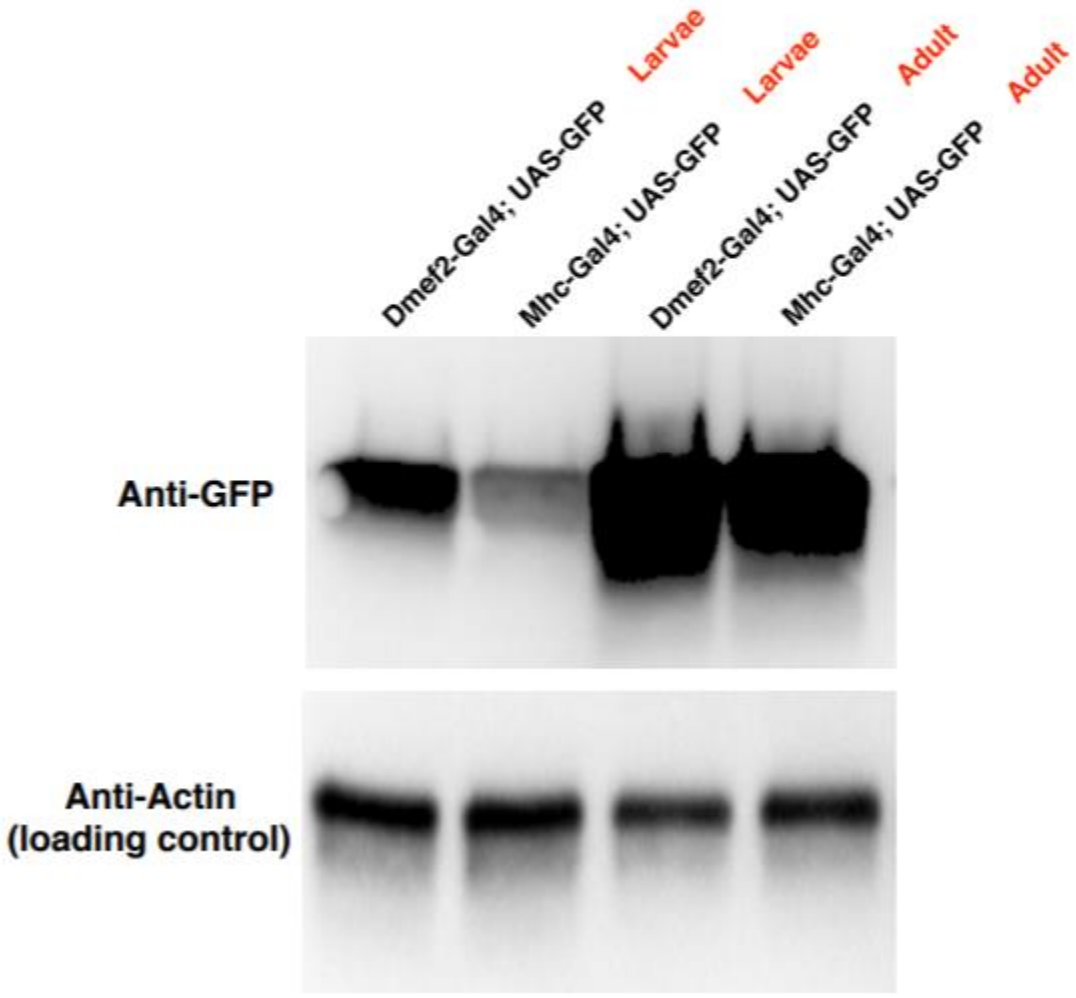
Larvae
Larvae
Adult
Adult
Dmef2-Gal4; UAS-GFP
Mhc-Gal4; UAS-GFP
Dmef2-Gal4; UAS-GFP
Mhc-Gal4; UAS-GFP
Anti-GFP
Anti-Actin
(loading control)

Figure 2.4: Disruption of several CI core and supernumerary subunits impair CI assembly In *Drosophila.*

BN-PAGE **(A)**, Silver staining **(B)**, and CI in-gel enzyme activity **(C)** of mitochondria isolated from thoraxes following RNAi-mediated knockdown of the CI proteins indicated (*mhc-Gal4>dNDUFX^{RNAi}*). The values listed below each lane indicate the residual amount of CI normalized to the amount in the wild-type (*mhc-Gal4>w^{1118}*) lane.

(D) Climbing phenotype after the knockdown of CI subunits. Flies were aged from 0-3 days. Climbing phenotype was calculated by the % of flies able to climb past the target line (halfway point in a vial) in 15 seconds.

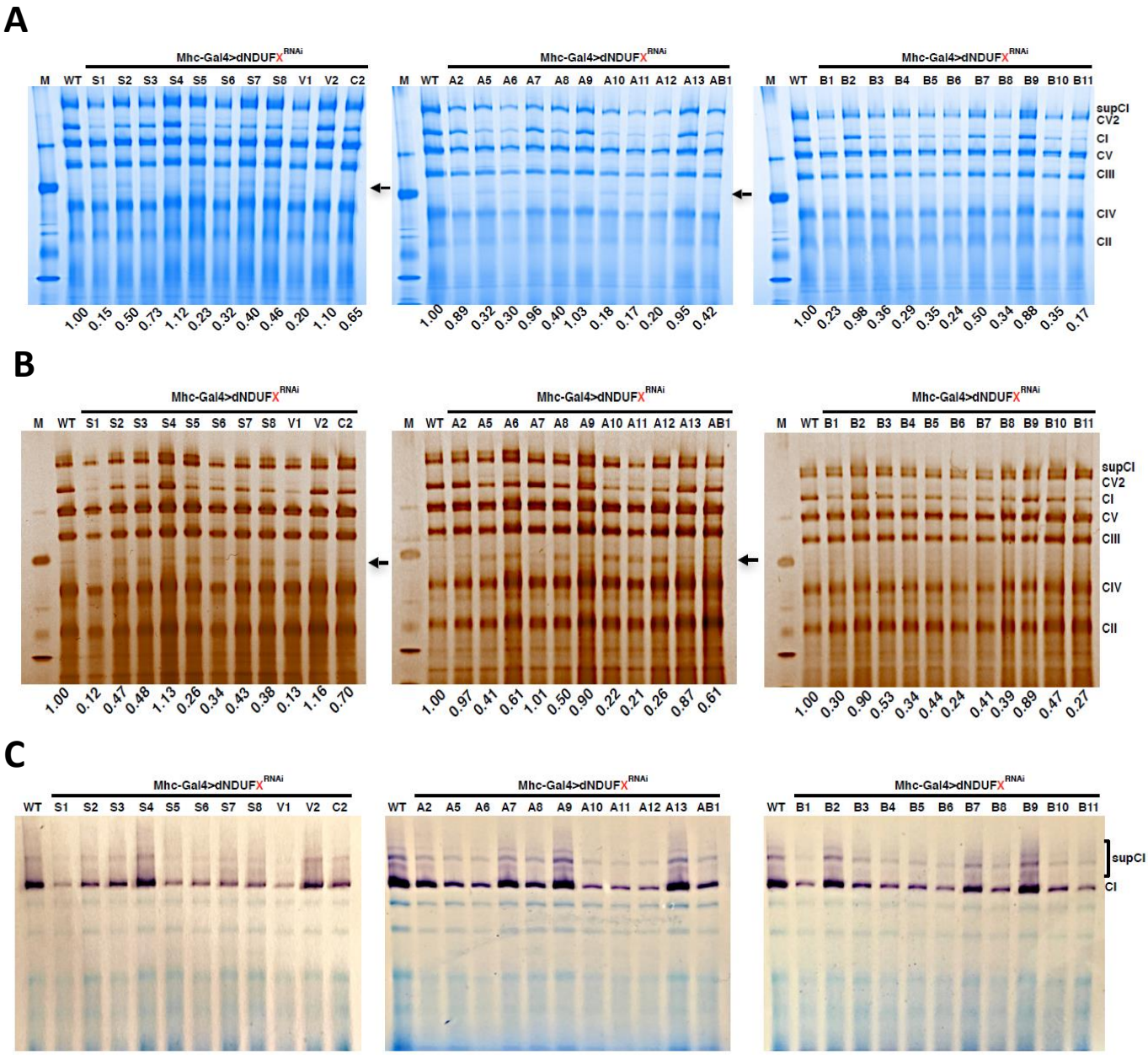
A
Mhc-Gal4>dNDUFX^RNAi
M WT S1 S2 S3 S4 S5 S6 S7 S8 V1 V2 C2
1.00 0.15 0.50 0.73 1.12 0.23 0.32 0.40 0.46 0.20 1.10 0.65
M WT A2 A5 A6 A7 A8 A9 A10 A11 A12 A13 AB1
1.00 0.89 0.32 0.30 0.96 0.40 1.03 0.18 0.17 0.20 0.95 0.42
M WT B1 B2 B3 B4 B5 B6 B7 B8 B9 B10 B11
1.00 0.23 0.98 0.36 0.29 0.35 0.24 0.50 0.34 0.88 0.35 0.17
supCI
CV2
CI
CV
CIII
CIV
CII
B
Mhc-Gal4>dNDUFX^RNAi
M WT S1 S2 S3 S4 S5 S6 S7 S8 V1 V2 C2
1.00 0.12 0.47 0.48 1.13 0.26 0.34 0.43 0.38 0.13 1.16 0.70
M WT A2 A5 A6 A7 A8 A9 A10 A11 A12 A13 AB1
1.00 0.97 0.41 0.61 1.01 0.50 0.90 0.22 0.21 0.26 0.87 0.61
M WT B1 B2 B3 B4 B5 B6 B7 B8 B9 B10 B11
1.00 0.30 0.90 0.53 0.34 0.44 0.24 0.41 0.39 0.89 0.47 0.27
supCI
CV2
CI
CV
CIII
CIV
CII
C
Mhc-Gal4>dNDUFX^RNAi
WT S1 S2 S3 S4 S5 S6 S7 S8 V1 V2 C2
WT A2 A5 A6 A7 A8 A9 A10 A11 A12 A13 AB1
WT B1 B2 B3 B4 B5 B6 B7 B8 B9 B10 B11
supCI
CI

D.

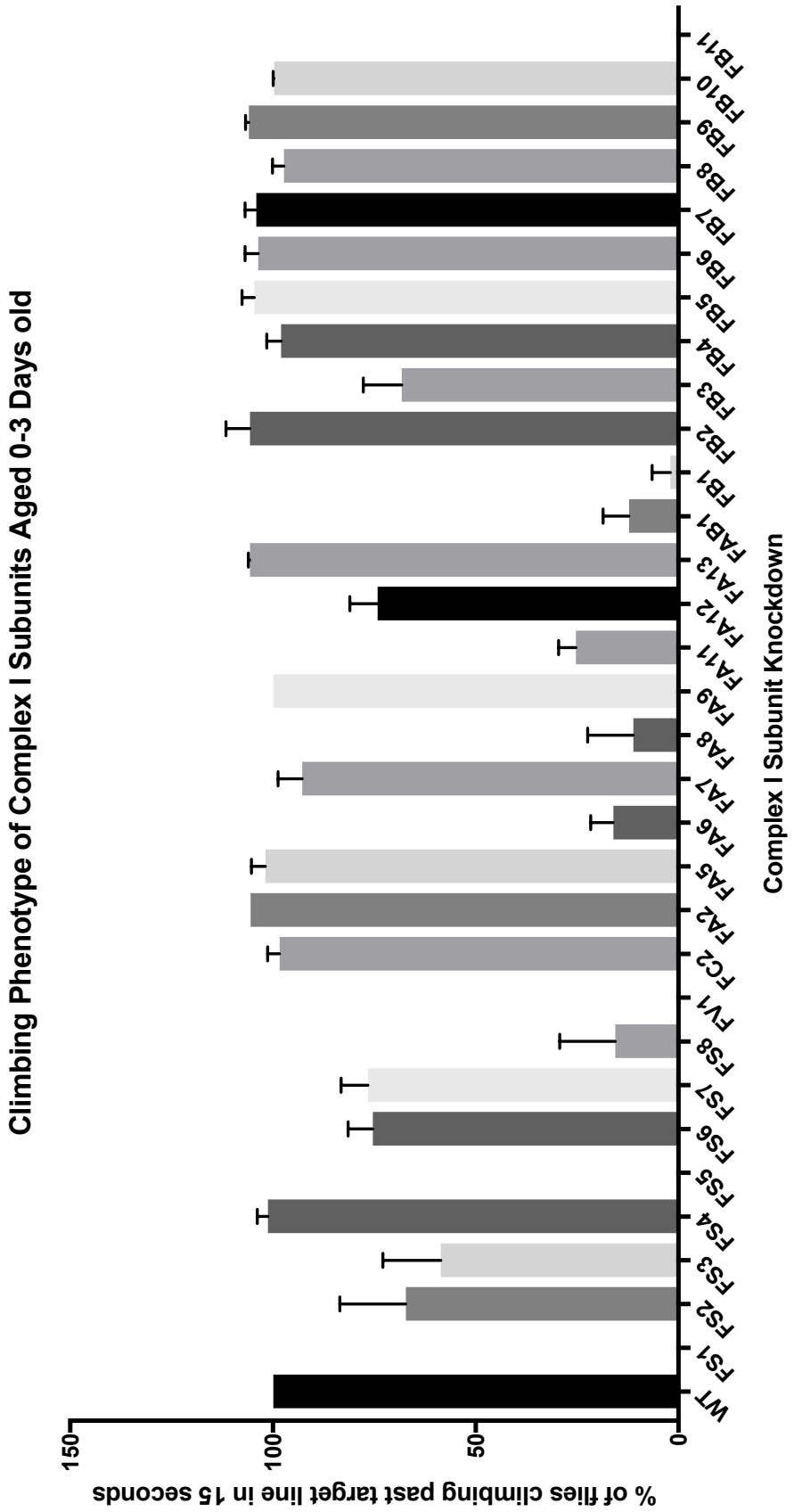
Climbing Phenotype of Complex I Subunits Aged 0-3 Days old
% of flies climbing past target line in 15 seconds
150
100
50
0
Complex I Subunit Knockdown
WT
FS1
FS2
FS3
FS4
FS5
FS6
FS7
FS8
FV1
FC2
FA2
FA5
FA6
FA7
FA8
FA9
FA11
FA12
FA13
FAB1
FB1
FB2
FB3
FB4
FB5
FB6
FB7
FB8
FB9
FB10
FB11

Figure 2.5: Proteomic analyses and immunoblotting identify assembly intermediates of CI.

(A) Schematic of CI showing the three modules of the enzyme. The NADH Dehydrogenase module (N module) is located at the tip of the matrix arm, and is the site of NADH oxidation. Situated between the N module and the membrane arm, is the Q module, which is responsible for Ubiquinone reduction. The proton-conducting P module is in the membrane arm.

(B) The current model of CI assembly in mammalian systems (reviewed in (Vartak et al., 2014). The assembly process begins with the formation of an assembly intermediate containing NDUFS2 and NDUFS3, which combines with NDUFS7 and NDUFS8. The subcomplex of NDUFS2, NDUFS3, NDUFS7 and NDUFS8 ultimately combines with ND1 to form the ~315 kDa assembly intermediate that is anchored to the membrane. The ~315 kDa subcomplex (also called the Q module) combines with an independently-formed ~370 kDa assembly intermediate to form an ~550 kDa assembly intermediate. This assembly intermediate which consists of the Q module and part of the P module grows by the addition of more subunits to form the ~815 kDa assembly intermediate, *via* mechanisms that are very poorly defined. The ~815 kDa assembly intermediate now consists of the complete Q and P modules. Finally, the N module is added to produce the 950kDa fully-assembled complex. Assembly factors or chaperones that assist in this process, but are not present in the fully assembled complex, have been omitted for clarity.

(C) Western blot of samples obtained from thoraxes from pupae aged between 2 and 4 days after pupariation, and of flies from 0.5 hours to 48 hours post-eclosure to detect the assembly intermediates, fully assembled CI, and a supercomplex containing complex I (supCI) after BN-PAGE. The anti-NDUFS3 antibody strongly detects CI and supCI; and weakly detects the ~315 kDa, ~550 kDa and ~815 kDa assembly intermediates after a short exposure. However, after a longer exposure, the ~315 and ~550 kDa assembly intermediates can clearly be seen. In the right panel, the membrane was stripped and re-probed with anti-NDI. Anti-ND1 detects the ~315 kDa and ~550 kDa assembly intermediates, and a very faint band corresponding to CI.

(D) Proteomic analyses of assembly intermediates that form in the native gel sized between ~50 kDa and ~350 kDa. See **Table 2.3** for all the peptides identified.

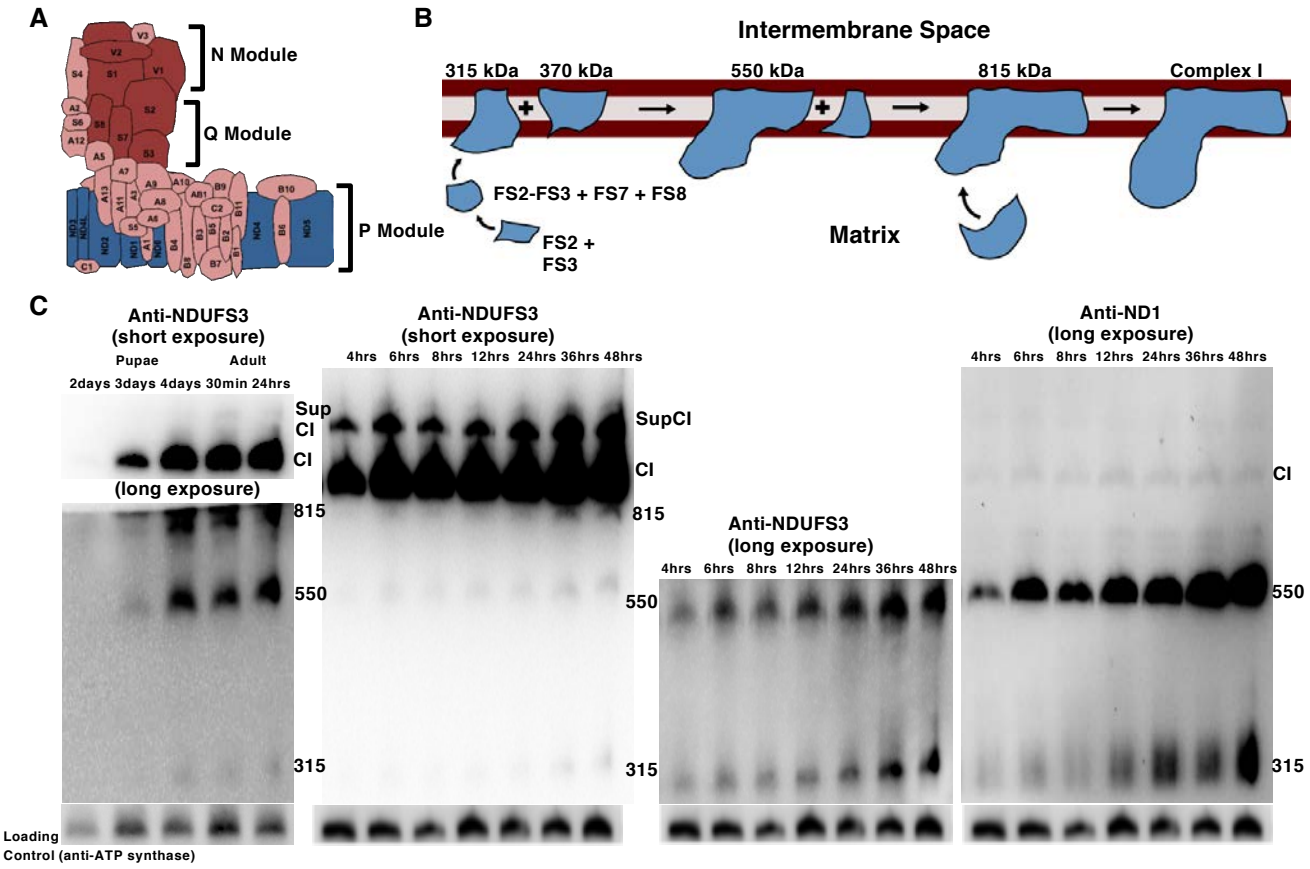

D

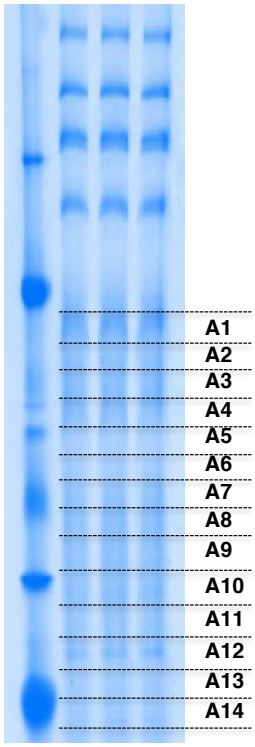

Fraction (approximate size in kDa)	CI Subunits and Assembly Factors Identified In Each Fraction
A1 (400-450)	dNDUFS3
A2 (350-400)	dNDUFAF4, dNDUFS3, dNDUFA5, dNDUFS7
A3 (300-350)	dNDUFAF4, dNDUFS2, dNDUFS3, dNDUFA5, dNDUFS7
A4 (260-300)	dNDUFAF4, dNDUFS2, dNDUFS3, dNDUFA5, dNDUFS7, dACAD9
A5 (220-260)	dNDUFA7, dNDUFS2, dNDUFS3, dNDUFA5, dNDUFS1, dACAD9
A6 (200-220)	dNDUFA7, dNDUFS1, dACAD9
A7 (180-200)	dNDUFA7, dNDUFS1, dACAD9
A8 (160-180)	dNDUFA7, dNDUFS1, dACAD9
A9 (140-160)	dNDUFA10, dNDUFA7, dNDUFA11, dNDUFS1, dACAD9
A10 (120-140)	dNDUFA10, dNDUFA7, dNDUFA11
A11 (100-120)	dNDUFA10, dNDUFA7, dNDUFA12
A12 (85-100)	dNDUFA10, dNDUFA7, dNDUFA12, dNDUFA11
A13 (70-85)	dNDUFA10, dNDUFA7, dNDUFA12, dNDUFA11
A14 (55-70)	dNDUFA10, dNDUFA7, dNDUFA12, dNDUFA11

Figure 2.6: Detection of smaller subcomplexes of CV.

Related to Figure 2.5

Immunoblots of samples obtained from wildtype, mhc>dNDUFS8RNAi and mhc>dNDUFV1RNAi thoraxes of flies aged for 24 hours after eclosure to detect CI and CV assembly intermediates. In the left and right panels, anti-ND1 and anti-NDUFS3 antibodies detect the CI holoenzyme and supercomplex, and the ~315 kDa, ~550 kDa and ~815 kDa CI assembly intermediates; but no assembly intermediates less than about 300 kDa are detected by these antibodies. However, in the middle panel, anti-ATPsynβ detects the CV monomer and dimer as well as several assembly intermediates some of which are smaller than 300 kDa.

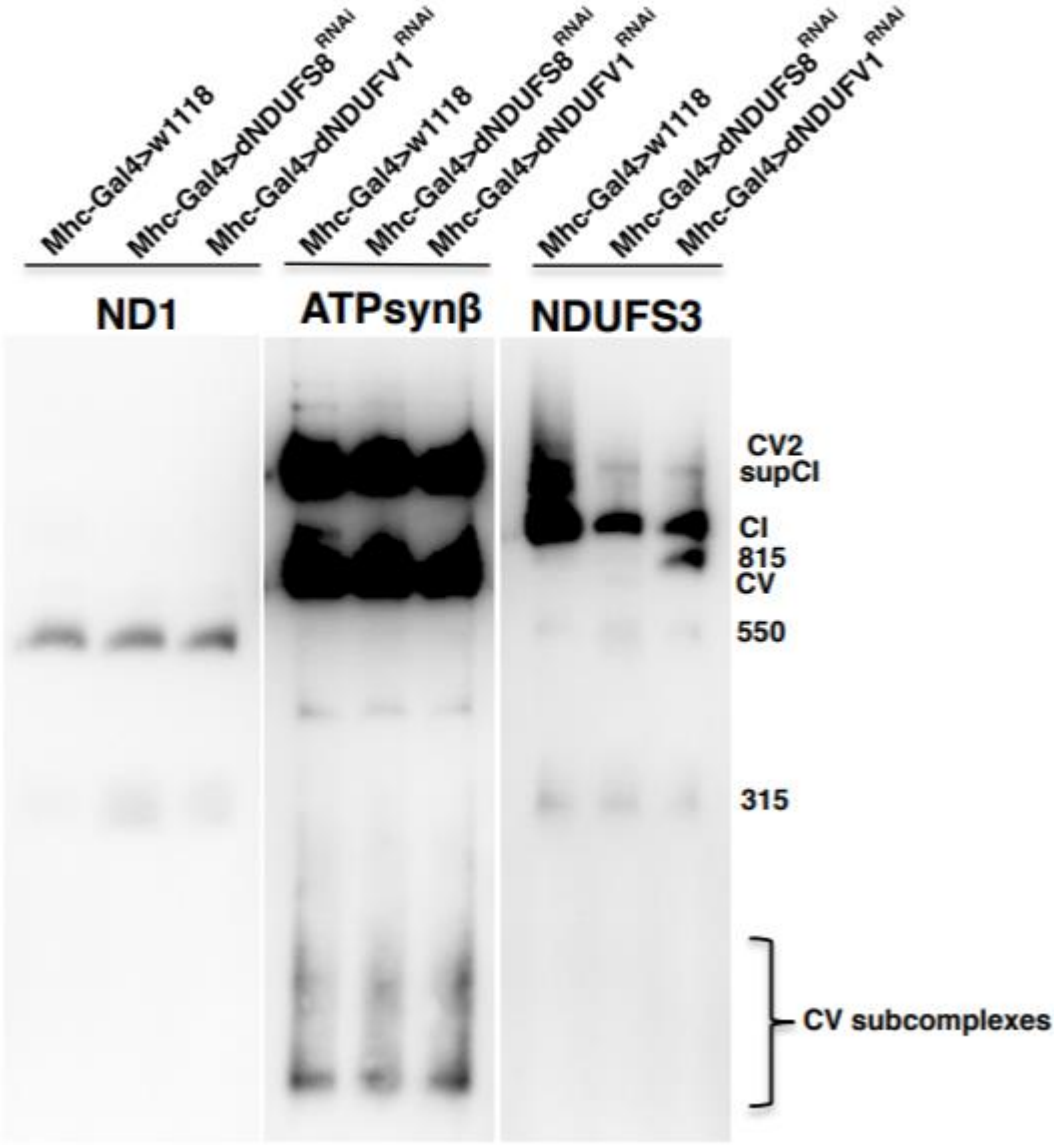
Mhc-Gal4>w1118
Mhc-Gal4>dNDUFS8 RNAi
Mhc-Gal4>dNDUFV1 RNAi
Mhc-Gal4>w1118
Mhc-Gal4>dNDUFS8 RNAi
Mhc-Gal4>dNDUFV1 RNAi
Mhc-Gal4>w1118
Mhc-Gal4>dNDUFS8 RNAi
Mhc-Gal4>dNDUFV1 RNAi
ND1
ATPsynβ
NDUFS3
CV2
supCI
CI
815
CV
550
315
CV subcomplexes

Figure 2.7: Specific subunits regulate the biogenesis or stability of specific assembly intermediates of CI.

(A) The left panel depicts a schematic of the distribution of assembly intermediates on immunoblots as a result of RNAi-mediated disruption of various CI subunits. The right panel describes how various results can be interpreted.

(B-D) Distribution of assembly intermediates in thoraxes dissected 24 hours after eclosion with transgenic RNAi expression of the CI subunits shown. In panels labeled long exposure, the region of the membrane just at or below CI was cut and imaged.

(B) The ~815 kDa assembly intermediate accumulates in thoraxes expressing transgenic RNAi to dNDUFS1 and dNDUFV1; and the ~315 kDa assembly intermediate is decreased in thoraxes expressing transgenic RNAi of dNDUFS2, dNDUFS3 and dNDUFS7. In addition, another assembly intermediate accumulates in thoraxes expressing RNAi to dNDUFS5 and dNDUFC2 (denoted by *). **(C)** The ~815 kDa assembly intermediate stalls in thoraxes expressing transgenic RNAi to dNDUFA6 and dNDUFA12; and the ~315 kDa assembly intermediate is attenuated in thoraxes expressing transgenic RNAi of dNDUFA5. **(D)** There were no overt alterations in assembly intermediates at this time point when the dNDUFB subunits were disrupted.

(E and F) Distribution of assembly intermediates in thoraxes dissected 48 hours **(E)** and 72 hours **(F)** after eclosion with transgenic RNAi expression of the NDUFB subunits shown. RNAi-mediated knockdown of the expression of dNDUFB3 decreased the extent of accumulation of all the assembly intermediates; and the 550 kDa assembly intermediate accumulated when the expression of dNDUFB1, dNDUFB8 and dNDUFB11 were reduced. In addition, the extent of accumulation of the 315 kDa assembly intermediate was diminished following RNAi-mediated disruption of dNDUFB1, dNDUFB4, dNDUFB5, dNDUFB6 and dNDUFB10 at both the 48- and 72-hour time points.

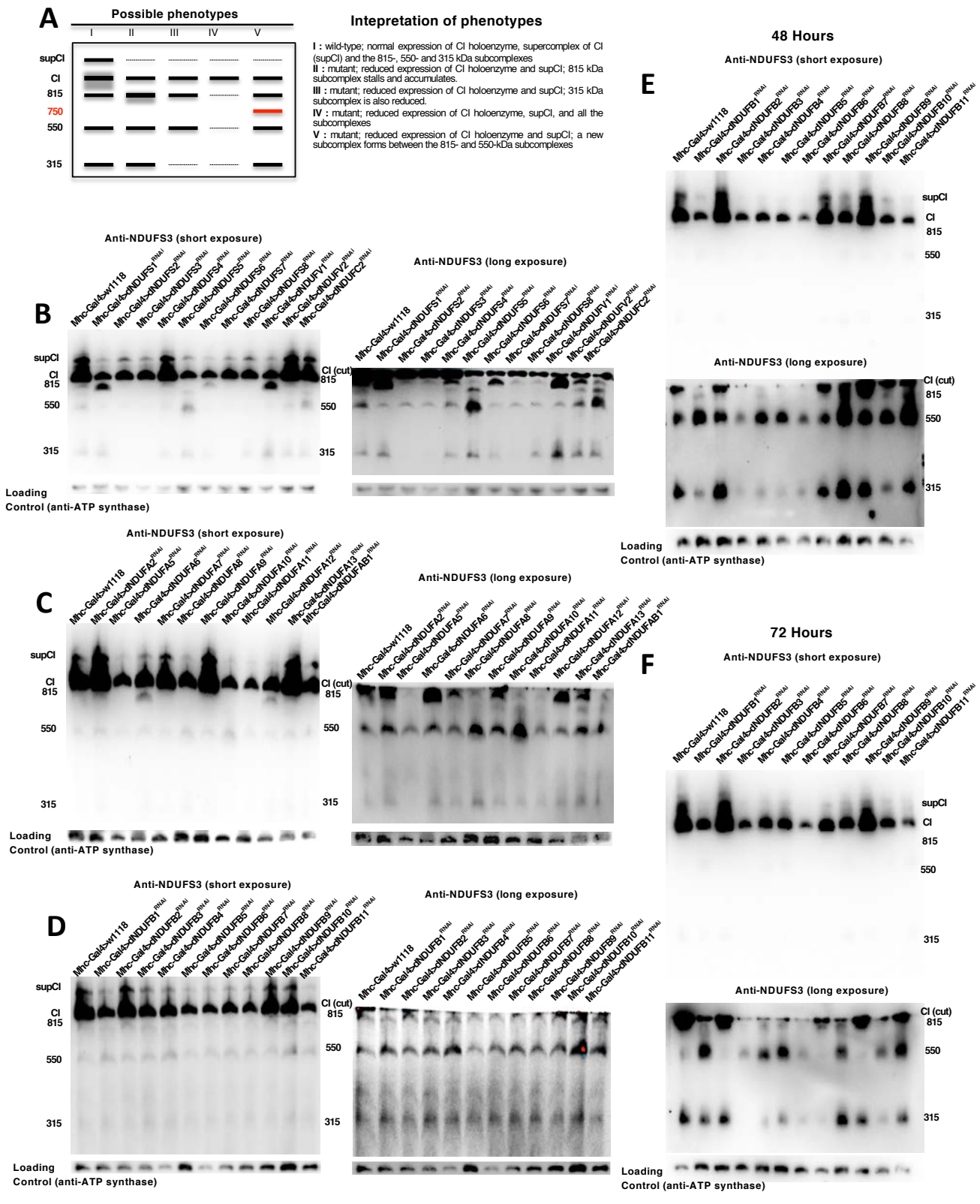
A
Possible phenotypes
I
II
III
IV
V
supCI
CI
815
750
550
315
Intepretation of phenotypes
I : wild-type; normal expression of CI holoenzyme, supercomplex of CI (supCI) and the 815-, 550- and 315 kDa subcomplexes
II : mutant; reduced expression of CI holoenzyme and supCI; 815 kDa subcomplex stalls and accumulates.
III : mutant; reduced expression of CI holoenzyme and supCI; 315 kDa subcomplex is also reduced.
IV : mutant; reduced expression of CI holoenzyme, supCI, and all the subcomplexes
V : mutant; reduced expression of CI holoenzyme and supCI; a new subcomplex forms between the 815- and 550-kDa subcomplexes
B
Anti-NDUFS3 (short exposure)
Anti-NDUFS3 (long exposure)
Mhc-Gal4>w1118
Mhc-Gal4>dNDUFS1 RNAi
Mhc-Gal4>dNDUFS2 RNAi
Mhc-Gal4>dNDUFS3 RNAi
Mhc-Gal4>dNDUFS4 RNAi
Mhc-Gal4>dNDUFS5 RNAi
Mhc-Gal4>dNDUFS6 RNAi
Mhc-Gal4>dNDUFS7 RNAi
Mhc-Gal4>dNDUFS8 RNAi
Mhc-Gal4>dNDUFV1 RNAi
Mhc-Gal4>dNDUFV2 RNAi
Mhc-Gal4>dNDUFC2 RNAi
supCI
CI
815
550
315
CI (cut)
Loading
Control (anti-ATP synthase)
C
Anti-NDUFS3 (short exposure)
Anti-NDUFS3 (long exposure)
Mhc-Gal4>w1118
Mhc-Gal4>dNDUFA2 RNAi
Mhc-Gal4>dNDUFA5 RNAi
Mhc-Gal4>dNDUFA6 RNAi
Mhc-Gal4>dNDUFA7 RNAi
Mhc-Gal4>dNDUFA8 RNAi
Mhc-Gal4>dNDUFA9 RNAi
Mhc-Gal4>dNDUFA10 RNAi
Mhc-Gal4>dNDUFA11 RNAi
Mhc-Gal4>dNDUFA12 RNAi
Mhc-Gal4>dNDUFA13 RNAi
Mhc-Gal4>dNDUFAB1 RNAi
supCI
CI
815
550
315
CI (cut)
Loading
Control (anti-ATP synthase)
D
Anti-NDUFS3 (short exposure)
Anti-NDUFS3 (long exposure)
Mhc-Gal4>w1118
Mhc-Gal4>dNDUFB1 RNAi
Mhc-Gal4>dNDUFB2 RNAi
Mhc-Gal4>dNDUFB3 RNAi
Mhc-Gal4>dNDUFB4 RNAi
Mhc-Gal4>dNDUFB5 RNAi
Mhc-Gal4>dNDUFB6 RNAi
Mhc-Gal4>dNDUFB7 RNAi
Mhc-Gal4>dNDUFB8 RNAi
Mhc-Gal4>dNDUFB9 RNAi
Mhc-Gal4>dNDUFB10 RNAi
Mhc-Gal4>dNDUFB11 RNAi
supCI
CI
815
550
315
CI (cut)
Loading
Control (anti-ATP synthase)
E
48 Hours
Anti-NDUFS3 (short exposure)
Anti-NDUFS3 (long exposure)
Mhc-Gal4>w1118
Mhc-Gal4>dNDUFB1 RNAi
Mhc-Gal4>dNDUFB2 RNAi
Mhc-Gal4>dNDUFB3 RNAi
Mhc-Gal4>dNDUFB4 RNAi
Mhc-Gal4>dNDUFB5 RNAi
Mhc-Gal4>dNDUFB6 RNAi
Mhc-Gal4>dNDUFB7 RNAi
Mhc-Gal4>dNDUFB8 RNAi
Mhc-Gal4>dNDUFB9 RNAi
Mhc-Gal4>dNDUFB10 RNAi
Mhc-Gal4>dNDUFB11 RNAi
supCI
CI
815
550
315
CI (cut)
Loading
Control (anti-ATP synthase)
F
72 Hours
Anti-NDUFS3 (short exposure)
Anti-NDUFS3 (long exposure)
Mhc-Gal4>w1118
Mhc-Gal4>dNDUFB1 RNAi
Mhc-Gal4>dNDUFB2 RNAi
Mhc-Gal4>dNDUFB3 RNAi
Mhc-Gal4>dNDUFB4 RNAi
Mhc-Gal4>dNDUFB5 RNAi
Mhc-Gal4>dNDUFB6 RNAi
Mhc-Gal4>dNDUFB7 RNAi
Mhc-Gal4>dNDUFB8 RNAi
Mhc-Gal4>dNDUFB9 RNAi
Mhc-Gal4>dNDUFB10 RNAi
Mhc-Gal4>dNDUFB11 RNAi
supCI
CI
815
550
315
CI (cut)
Loading
Control (anti-ATP synthase)

Figure 2.8: Identification of an ~700 kDa assembly intermediate of CI in *Drosophila*.

(A) Top Panel: Immunoblots of samples obtained from wildtype and mhc>dNDUFS5^{RNAi} thoraxes of flies aged for 6 hours after eclosure depicting co-migration of the ~700 kDa intermediate and CV. In the left and middle panels, anti-NDUFS3 antibodies detect the fully assembled CI, the ~700 kDa subcomplex, as well as other assembly intermediates in dNDUFS5^{RNAi} thoraxes. Note that in the middle panel, the region of the membrane just below CI was cut and imaged. In the right panel, anti-ATPsynβ detects the CV monomer (700kDa) and dimer as shown. Lower Panel: Mitochondrial protein complexes from wildtype and *mhc>dNDUFS5^{RNAi}* thoraxes were resolved by BN-PAGE and the region corresponding to the ~700 kDa assembly intermediate (i.e. CV, demarcated) was cut out, subjected to tryptic digestion, and analyzed by label-free quantitative LC-MS/MS.

(B) Immunoblots from samples obtained after 6 hours, 12 hours and 24 hours post eclosure from thoraxes where NDUFS1, NDUFS3, NDUFS5 and NDUFV1 were knocked down as a result of transgenic RNAi exression. Note that the ~815 kDa assembly intermediate accumulates as a result of disruption of NDUFS1 and NDUFV1, and the ~700 kDa assembly intermediate stalls and accumulates in NDUFS5 mutants at all time points. Importantly, upon prolonged exposure of the immunoblot, a band corresponding to the ~700 kDa assembly intermediate can also be observed in wild-type samples (denoted with the * in the lower panel), which confirms that it is an authentic, albeit transient assembly intermediate.

(C) The accumulation of the ~815 kDa assembly intermediate was significantly attenuated *in mhc>dNDUFS5^{RNAi},dNDUFS1^{RNAi}* thoraxes relative to *mhc>dNDUFS1^{RNAi}* thoraxes; instead there is an accumulation of the ~700 kDa assembly intermediate. Similar results were obtained when samples from *mhc>dNDUFS5^{RNAi},dNDUFV1^{RNAi}* thoraxes were compared to samples from *mhc>dNDUFV1^{RNAi}* thoraxes.

(D) Proteomic changes in the gel slice sample from wildtype and *mhc>dNDUFS5^{RNAi}* thoraxes corresponding to the ~700 kDa assembly intermediate. Relative protein abundance among biological samples is expressed by spectral counts on a log scale. Several CI subunits and CIAFs, most notably components of the MCIA complex are upregulated in the ~700 kDa assembly intermediate. However, the amount of dNDUFA10 (denoted with an asterisk) is reduced in *mhc>dNDUFS5^{RNAi}* thoraxes relative to wild type. See **Table 2.4** for all the peptides identified.

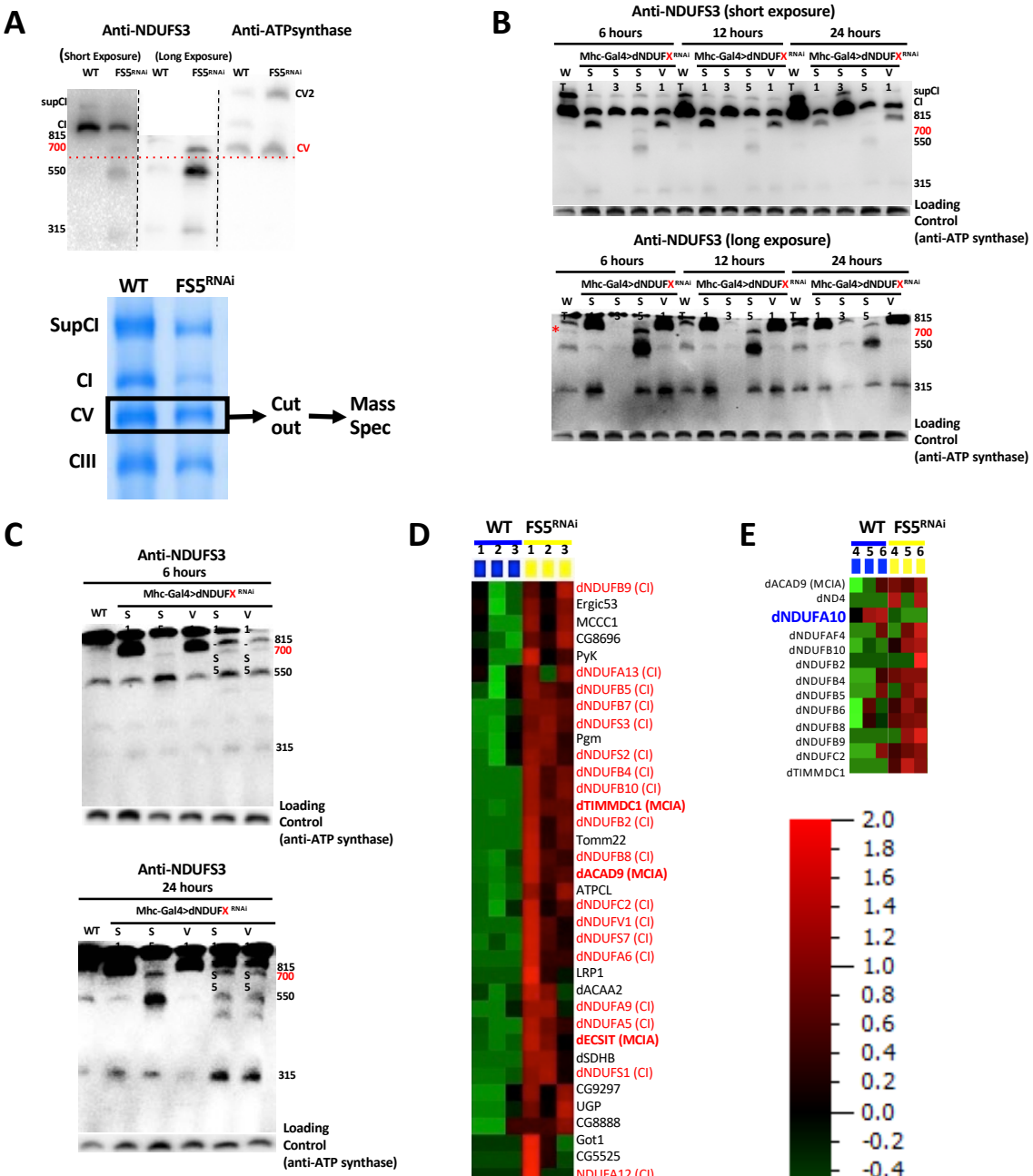
A
Anti-NDUFS3
Anti-ATPsynthase
(Short Exposure)
(Long Exposure)
WT
FS5RNAi
supCI
CI
CV
CV2
815
700
550
315
SupCI
CIII
Cut out
Mass Spec
B
Anti-NDUFS3 (short exposure)
6 hours
12 hours
24 hours
Mhc-Gal4>dNDUFXRNAi
Loading Control (anti-ATP synthase)
Anti-NDUFS3 (long exposure)
C
Anti-NDUFS3
6 hours
24 hours
D
E
dACAD9 (MCIA)
dND4
dNDUFA10
dNDUFAF4
dNDUFB10
dNDUFB2
dNDUFB4
dNDUFB5
dNDUFB6
dNDUFB8
dNDUFB9
dNDUFC2
dTIMMDC1
2.0
1.8
1.6
1.4
1.2
1.0
0.8
0.6
0.4
0.2
0.0
-0.2
-0.4
-0.6
-0.8
-1.0
-1.2
-1.4
-1.6
-1.8
-2.0

Figure 2.9: CI assembly In *Drosophila* involves an assembly intermediate containing several membrane-associated accessory subunits.

(A) Mitochondrial protein complexes from wildtype, *mhc>dNDUFS5*^{RNAi} and *mhc>dNDUFV1*^{RNAi} thoraxes were separated by BN-PAGE and the region corresponding to the accumulated assembly intermediate (demarcated) was cut out, subjected to tryptic digestion, and analyzed by label-free quantitative LC-MS/MS.

(B) Proteomic changes in the gel slice samples from wildtype, *mhc>dNDUFS5*^{RNAi} and *mhc>dNDUFV1*^{RNAi} thoraxes. Relative protein abundance among biological samples is expressed by spectral counts on a log scale. The color scale bar indicates the range of protein expression levels. See additional information in **Table 2.5**.

(C) Schematic representation highlighting the membrane subunits that are upregulated in the gel slice (shown in red font) from the *mhc>dNDUFS5*^{RNAi} and *mhc>dNDUFV1*^{RNAi} thoraxes.

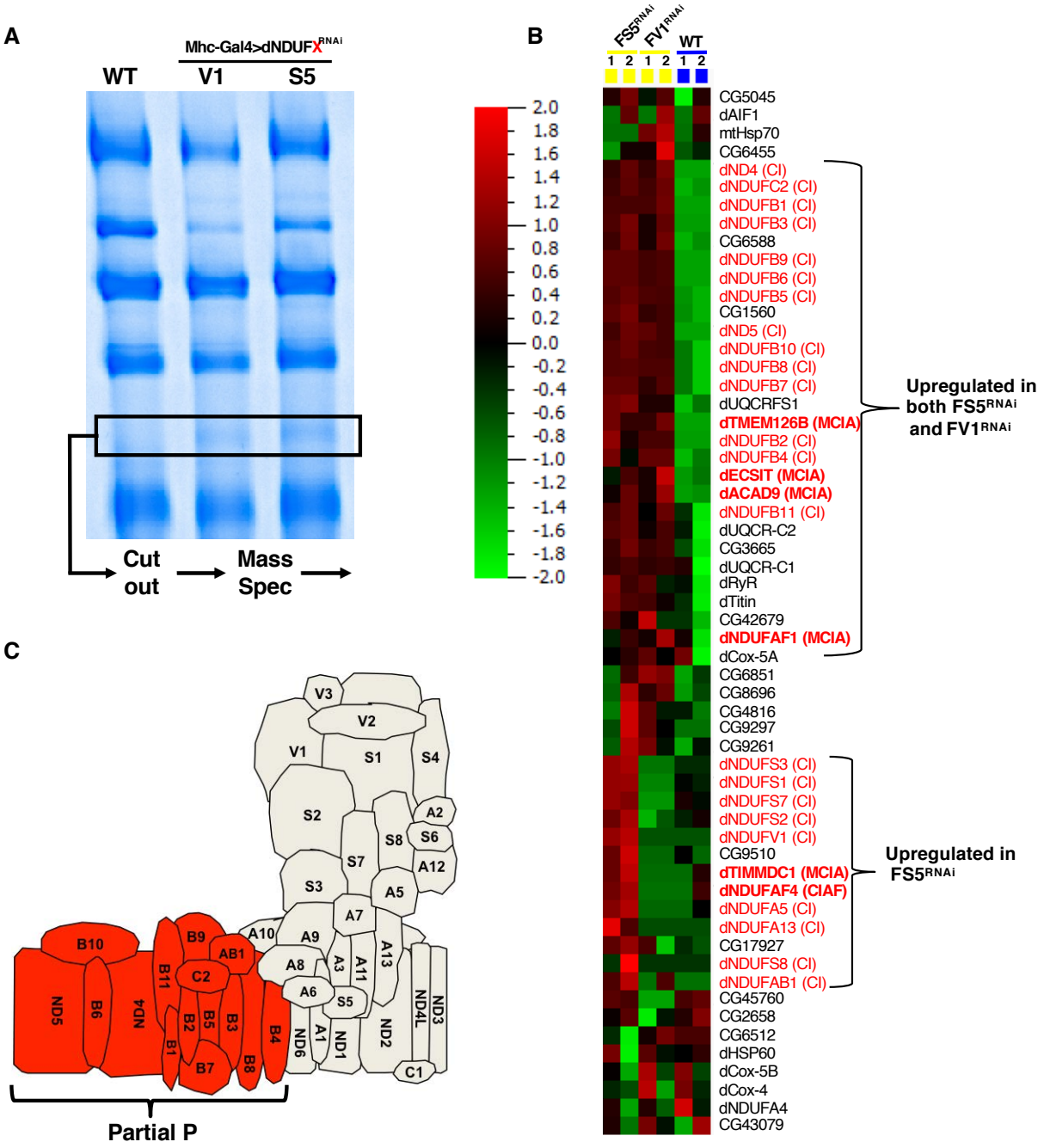
A
Mhc-Gal4>dNDUFX^RNAi
WT
V1
S5
Cut out
Mass Spec
B
FS5^RNAi
FV1^RNAi
WT
1 2 1 2 1 2
2.0
1.8
1.6
1.4
1.2
1.0
0.8
0.6
0.4
0.2
0.0
-0.2
-0.4
-0.6
-0.8
-1.0
-1.2
-1.4
-1.6
-1.8
-2.0
CG5045
dAIF1
mtHsp70
CG6455
dND4 (CI)
dNDUFC2 (CI)
dNDUFB1 (CI)
dNDUFB3 (CI)
CG6588
dNDUFB9 (CI)
dNDUFB6 (CI)
dNDUFB5 (CI)
CG1560
dND5 (CI)
dNDUFB10 (CI)
dNDUFB8 (CI)
dNDUFB7 (CI)
dUQCRFS1
dTMEM126B (MCIA)
dNDUFB2 (CI)
dNDUFB4 (CI)
dECSIT (MCIA)
dACAD9 (MCIA)
dNDUFB11 (CI)
dUQCR-C2
CG3665
dUQCR-C1
dRyR
dTitin
CG42679
dNDUFAF1 (MCIA)
dCox-5A
CG6851
CG8696
CG4816
CG9297
CG9261
dNDUFS3 (CI)
dNDUFS1 (CI)
dNDUFS7 (CI)
dNDUFS2 (CI)
dNDUFV1 (CI)
CG9510
dTIMMDC1 (MCIA)
dNDUFAF4 (CIAF)
dNDUFA5 (CI)
dNDUFA13 (CI)
CG17927
dNDUFS8 (CI)
dNDUFAB1 (CI)
CG45760
CG2658
CG6512
dHSP60
dCox-5B
dCox-4
dNDUFA4
CG43079
Upregulated in both FS5^RNAi and FV1^RNAi
Upregulated in FS5^RNAi
C
V3
V2
V1
S1
S4
S2
A2
S8
S6
S7
A12
S3
A5
A7
A10
A9
A8
A3
A11
A13
A6
S5
ND4L
ND3
ND2
ND6
A1
ND1
C1
B10
B9
AB1
B11
C2
ND5
B6
ND4
B5
B3
B2
B4
B1
B7
B8
Partial P

Figure 2.10: Proposed model of CI assembly in *Drosophila* flight muscle.

An assembly intermediate consisting of dNDUFS2, dNDUS3, dNDUFS7, dNDUFS8 and dNDUFA5 are combined in essentially one step to form the Q module, which is anchored to the membrane by ND1. Subsequently, an independently-formed subcomplex comprising of membrane-associated subunits (Partial P1) is conjugated to the Q module, and possibly other subunits, to form an assembly intermediate comprised of the Q module and part of the P module (Q + Partial P2). This grows by the addition of more subunits to form a transient assembly intermediate of ~700kDa (Q + Partial P3). We propose that dNDUFS5 is then incorporated at this step, to promote incorporation or stabilization of dNDUFA10. Subsequently, the transient ~700 kDa assembly intermediate is rapidly converted to the ~815 kDa assembly intermediate, consisting of the complete P and Q modules (Q + P). Finally, the N module is added to produce the CI holoenzyme.

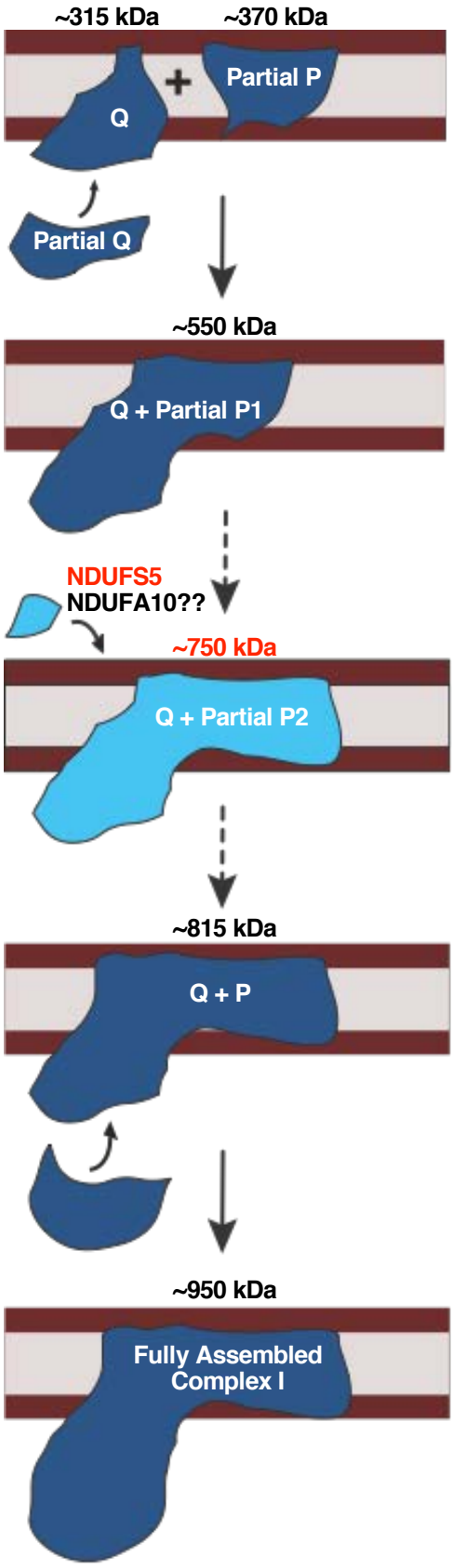
~315 kDa
~370 kDa
Q
Partial P
Partial Q
~550 kDa
Q + Partial P1
NDUFS5
NDUFA10??
~750 kDa
Q + Partial P2
~815 kDa
Q + P
~950 kDa
Fully Assembled
Complex I

Figure 2.11: Destabilization of CI is not specifically linked to stress.

Related to Figure 2.4A

(A) Silver-stained gels containing OXPHOS complexes isolated from wildtype, Dmef2Gal4>PINK1RNAi, Dmef2Gal4>ParkRNAi, Dmef2Gal4>GSTS1RNAi, Dmef2Gal4>Trxr-1RNAi, Dmef2Gal4>Sod1RNAi, Dmef2Gal4>Sod2RNAi and Dmef2Gal4>catalaseRNAi thoraxes of flies aged for 72 hours after eclosure to determine the integrity of the OXPHOS complexes. Lanes marked with an asterisk denote instances where assembly of several OXPHOS complexes were impaired.

(B) BN-PAGE showing mitochondrial protein complexes from mhc>w1118 (wild-type) thoraxes of flies aged for 24 hours; and starved or maintained at 25C, 30C or 37C for 18 or 36 hours. Note that there were no overt alterations in assembly of the OXPHOS complexes.

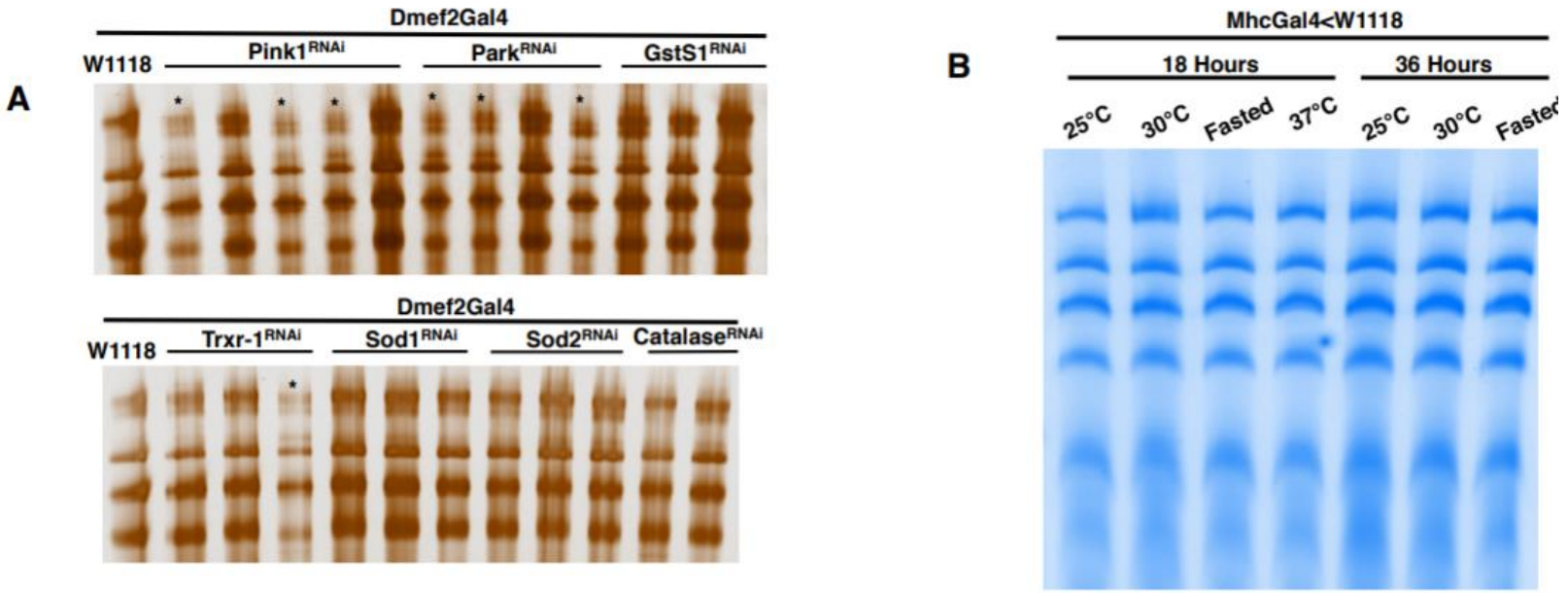
A
Dmef2Gal4
W1118
Pink1RNAi
ParkRNAi
GstS1RNAi
Dmef2Gal4
W1118
Trxr-1RNAi
Sod1RNAi
Sod2RNAi
CatalaseRNAi
B
MhcGal4<W1118
18 Hours
36 Hours
25°C
30°C
Fasted
37°C
25°C
30°C
Fasted

Table 2.1 There are at least 42 orthologs of the 44 human complex I subunits in Drosophila, related to Figure 2.1.

*Shows which protein in a set of paralogs was confirmed by mass spectrometry. Core subunits are shown in bold font.

Human Complex I Protein	Yarrowia lipolytica Complex I Protein	Escherichia coli Complex I Protein	Drosophila Ortholog (DIOPT Score)	Confirmed by Mass Spectrometry
NDUFS1	**NUAM**	**NuoG**	**CG2286 (11)**	+
NDUFS2	**NUCM**	**NuoD**	**CG1970* (11)** **CG11913 (6)**	+
NDUFS3	**NUGM**	**NuoC**	**CG12079 (10)**	+
NDUFS4	NUYM		CG12203 (10)	+
NDUFS5	NIPM		CG11455 (4)	+
NDUFS6	NUMM		CG8680 (11)	+
NDUFS7	**NUKM**	**NuoB**	**CG9172* (9)** **CG2014 (9)**	+
NDUFS8	**NUIM**	**NuoI**	**CG3944 (11)**	+
NDUFV1	**NUBM**	**NuoF**	**CG9140* (10)** **CG11423* (7)** **CG8102 (6)**	+ +
NDUFV2	**NUHM**	**NuoE**	**CG5703* (11)** **CG6485 (7)**	+
NDUFV3			CG11752 (1)	+
NDUFC1				
NDUFC2			CG12400 (8)	+
NDUFA1	NIMM		CG34439 (4)	+
NDUFA2	NI8M		CG15434 (11)	
NDUFA3	NI9M			
NDUFA5	NUFM		CG6463 (9)	+
NDUFA6	NB4M		CG7712 (11)	+
NDUFA7	NUZM		CG3621* (9) CG6914 (7)	+
NDUFA8	NUPM		CG3683 (10)	+
NDUFA9	NUEM		CG6020 (10)	+
NDUFA10			CG6343 (10)	+
NDUFA11	NUJM		CG9350 (7)	+
NDUFA12	N7BM		CG3214 (11)	+
NDUFA13	NB6M		CG3446 (7)	+
NDUFAB1	ACPM1 ACPM2		CG9160 (7)	+
NDUFB1			CG18624 (5)	+
NDUFB2			CG40002* (5) CG40472 (5)	+
NDUFB3	NB2M		CG10320 (8)	+
NDUFB4	NB5M		CG12859 (3)	+
NDUFB5			CG9762 (11)	+
NDUFB6			CG13240 (1)	+
NDUFB7	NB8M		CG5548 (11)	+
NDUFB8	NIAM		CG3192 (10)	+
NDUFB9	NI2M		CG9306 (11)	+
NDUFB10	NIDM		CG8844 (11)	+
NDUFB11	NESM		CG6008 (8)	+
ND1	**NU1M**	**NuoH**	**CG34092 (3)**	+
ND2	**NU2M**	**NuoN**	**CG34063 (6)**	
ND3	**NU3M**	**NuoA**	**CG34076 (7)**	
ND4	**NU4M**	**NuoM**	**CG34085 (3)**	+
ND4L	**NULM**	**NuoK**	**CG34086 (7)**	
ND5	**NU5M**	**NuoL**	**CG34083 (5)**	+
ND6	**NU6M**	**NuoJ**	**CG34089 (1)**	
	NUXM			
	NEBM			
	NUNM			
	NUUM			
	ST1			

Table 2.2: Proteins Identified *via* mass spectrometry of OXPHOS complexes in *Drosophila,* related to Figure 2.1.

The constituents of each of the six major bands observed during BN-PAGE was analyzed by mass spectrometry. Peptides identified in each of bands A to F are shown in the table.

			CV Dimer + SupCI	CI	CV	CIII	CIV	CII	
Identified Proteins	**Accession Number**	**Molecular W**	**Band A**	**Band B**	**Band C**	**Band D**	**Band E**	**Band F**	
ATP synthase subunit alpha, mitochondrial blw	ATPA_DROME	59 kDa	754	189	917	447	179	99	
ATP synthase subunit beta, mitochondrial ATPsyn-beta	ATPB_DROME (+1)	54 kDa	993	191	1049	485	200	139	
Cluster of Calcium-transporting ATPase Ca-P60A (A0A0B4LGB7_DROME)	A0A0B4LGB7_DROME [2]	109 kDa	69	74	84	127	212	898	
AT02348p UQCR-C2	Q9VV75_DROME	45 kDa	44	47	122	763	112	18	
ATP synthase subunit gamma, mitochondrial ATPsyngamma	ATPG_DROME	33 kDa	237	55	321	109	41	11	
Probable citrate synthase, mitochondrial kdn	CISY_DROME	52 kDa	84	88	83	124	121	161	
Glycerol-3-phosphate dehydrogenase Gpo-1	Q7K569_DROME	80 kDa	33	40	45	88	235	144	
Cluster of Sodium/potassium-transporting ATPase subunit alpha Atpalpha (ATNA_DR	ATNA_DROME [2]	116 kDa	22	42	122	98	276	119	
CG3731, isoform A UQCR-C1	Q9VFF0_DROME	52 kDa	48	48	89	321	30	6	
NADH-ubiquinone oxidoreductase 75 kDa subunit, mitochondrial ND-75 (dNDUFS1)	NDUS1_DROME	79 kDa	86	390	6	4	4	6	
Succinate dehydrogenase [ubiquinone] flavoprotein subunit, mitochondrial SdhA	SDHA_DROME	72 kDa	8	10	17	42	106	293	
ATP synthase subunit b, mitochondrial ATPsynB	AT5F1_DROME	27 kDa	141	51	162	18	6	2	
ATP synthase subunit O, mitochondrial ATPsynO	ATPO_DROME	22 kDa	143	31	170	10	0	0	
Cytochrome b-c1 complex subunit Rieske, mitochondrial RFeSP	Q9VQ29_DROME	25 kDa	18	11	39	232	30	12	
Voltage-dependent anion-selective channel porin	VDAC_DROME	31 kDa	12	28	37	54	77	185	
Cluster of Sluggish A, isoform I slgA (M9NFJ2_DROME)	M9NFJ2_DROME [2]	76 kDa	15	19	5	27	83	141	
ADP,ATP carrier protein sesB	ADT_DROME (+1)	34 kDa	29	38	34	48	65	140	
Cluster of Fructose-bisphosphate aldolase Ald (ALF_DROME)	ALF_DROME [2]	39 kDa	57	111	75	45	23	4	
CG1970, isoform B ND-49 (dNDUFS2)	Q9V4E0_DROME	53 kDa	57	176	9	18	11	33	Q module
Apolipophorins Rfabg	APLP_DROME	373 kDa	59	128	36	0	0	0	
ATP synthase subunit d, mitochondrial ATPsynD	ATP5H_DROME	20 kDa	91	40	116	7	5	0	
Cluster of Neural conserved at 73EF, isoform I Nc73EF (A8JNU6_DROME)	A8JNU6_DROME [2]	123 kDa	0	1	6	26	94	181	
CG4769, isoform A Cyt-c1	Q9VRL0_DROME	34 kDa	25	28	35	154	9	4	
IP09655p Mdh2	Q9VEB1_DROME	35 kDa	18	30	24	36	57	97	
Cluster of MICOS complex subunit Mic60 Mitofilin (MIC60_DROME)	MIC60_DROME [2]	82 kDa	29	44	34	22	16	26	
Lethal (1) G0230, isoform A ATPsyndelta	Q9W2X6_DROME	17 kDa	102	18	109	14	7	4	
Pyruvate carboxylase PCB	Q7KN97_DROME	131 kDa	0	4	10	64	84	65	
CG6020, isoform A ND-39 (dNDUFA9)	Q9VPE2_DROME	47 kDa	45	139	3	2	0	0	
Cluster of Calcium-transporting ATPase PMCA (Q9V4C7_DROME)	Q9V4C7_DROME [3]	133 kDa	19	12	6	48	106	0	
Cluster of Ryanodine receptor, isoform J RyR (A0A0B4K715_DROME)	A0A0B4K715_DROME [2]	580 kDa	44	36	8	19	3	0	
Cluster of Glutamate dehydrogenase, mitochondrial Gdh (DHE3_DROME)	DHE3_DROME [2]	63 kDa	3	1	2	29	125	39	
Pyruvate kinase PyK	KPYK_DROME	57 kDa	8	16	15	48	90	25	
NADH dehydrogenase [ubiquinone] 1 alpha subcomplex subunit 10, mitochondrial ND	NDUAA_DROME	47 kDa	37	137	9	5	0	0	
CG12079-PA ND-30 (dNDUFS3)	Q9VZU4_DROME	30 kDa	33	106	7	7	7	27	Q module
CG4389-PB, isoform B Mtpalpha	Q8IPE8_DROME (+1)	80 kDa	1	6	19	55	60	27	
Glycogen phosphorylase GlyP	PYG_DROME	97 kDa	0	0	0	1	109	80	
Enolase Eno	ENO_DROME	54 kDa	0	2	6	24	120	28	
CG7920, isoform A CG7920	Q9VAC1_DROME	52 kDa	36	40	23	34	34	19	
Cluster of Succinate dehydrogenase [ubiquinone] iron-sulfur subunit, mitochondrial S	SDHB_DROME [2]	34 kDa	1	5	3	16	44	77	
Cluster of Titin sls (TITIN_DROME)	TITIN_DROME [4]	2066 kDa	0	2	3	5	5	6	
CG9140, isoform B ND-51 (dNDUFV1)	Q9VMI3_DROME	52 kDa	46	125	0	0	0	0	
Cluster of Alpha-actinin, sarcomeric Actn (ACTN_DROME)	ACTN_DROME [2]	107 kDa	0	1	0	16	141	3	
CG10664-PA, isoform A COX4	Q9VIQ8_DROME	21 kDa	7	8	8	19	87	12	
Cluster of Arginine kinase, isoform E Argk (A8JNP2_DROME)	A8JNP2_DROME [2]	42 kDa	1	8	12	50	42	42	
Cluster of Fasciclin 1, isoform C Fas1 (Q8INA9_DROME)	Q8INA9_DROME [2]	73 kDa	2	9	54	15	35	47	
Cluster of CG9172, isoform A ND-20 (Q9VXK7_DROME) (dNDUFS7)	Q9VXK7_DROME [2]	25 kDa	17	76	9	7	8	20	Q module
Putative ATP synthase subunit f, mitochondrial CG4692	ATPK_DROME	12 kDa	37	11	46	9	4	5	
Aconitate hydratase, mitochondrial Acon	Q9VIE8_DROME	85 kDa	5	9	5	13	48	69	
Cluster of Actin, larval muscle Act79B (ACT4_DROME)	ACT4_DROME [4]	42 kDa	15	14	12	22	31	54	
CG5703, isoform A ND-24 (dNDUFV2)	Q9VX36_DROME	27 kDa	40	105	0	0	0	0	
CG11015-PA COX5B	Q9VMB9_DROME	14 kDa	7	5	14	39	77	5	
Cluster of Tropomyosin-1, isoforms 33/34 Tm1 (TPM4_DROME)	TPM4_DROME [5]	55 kDa	2	3	16	8	81	15	
Cluster of CG9674, isoform F CG9674 (M9NFH8_DROME)	M9NFH8_DROME [2]	232 kDa	0	0	0	0	107	0	
CG9090, isoform A CG9090-RA	Q7JUS9_DROME	41 kDa	8	11	8	19	46	48	

Maltase A1 Mal-A1	MAL1_DROME	66 kDa	9	31	34	45	1	11	
Glucose-6-phosphate isomerase Pgi	G6PI_DROME	62 kDa	15	40	31	43	7	2	
Cluster of CG6512-PA, isoform A CG6512 (Q8T4G5_DROME)	Q8T4G5_DROME [2]	90 kDa	22	48	14	7	6	5	
Cluster of Aralar1, isoform F aralar1 (A0A0B4KHW3_DROME)	A0A0B4KHW3_DROME [3	77 kDa	1	1	1	42	44	28	
RE74917p tobi	Q9VBR6_DROME	75 kDa	8	24	30	19	5	28	
CG4600-PA yip2	Q9VL70_DROME	42 kDa	11	16	10	15	33	36	
Cluster of V-type proton ATPase catalytic subunit A isoform 2 Vha68-2 (VATA2_DROM	VATA2_DROME [2]	68 kDa	49	56	10	44	3	6	
Cluster of Cytochrome b-c1 complex subunit 7 UQCR-14 (Q9VXI6_DROME)	Q9VXI6_DROME [2]	14 kDa	11	11	28	54	0	0	
Cluster of Terribly reduced optic lobes, isoform AI trol (M9NET2_DROME)	M9NET2_DROME [5]	432 kDa	13	9	12	0	1	1	
Cluster of LP02262p l(1)G0255 (Q8IRQ5_DROME)	Q8IRQ5_DROME [2]	50 kDa	0	0	0	0	16	122	
CG3523, isoform C FASN1	B7Z001_DROME (+1)	278 kDa	5	47	12	5	0	0	
Cytochrome c oxidase subunit 2 mt:CoII	COX2_DROME	26 kDa	5	9	11	15	55	9	
Delta-1-Pyrroline-5-carboxylate dehydrogenase 1, isoform A P5CDh1	Q9VNX4_DROME	64 kDa	35	24	13	11	5	0	
Alcohol dehydrogenase Adh	ADH_DROME	28 kDa	9	18	24	26	36	7	
CG6463-PA ND-13B (dNDUFA5)	Q9VTB4_DROME	14 kDa	11	58	3	4	2	10	Q module
Stretchin-Mlck, isoform R Strn-Mlck	A1ZA73_DROME	215 kDa	3	1	4	51	19	18	
ND-ASHI (dNDUFB8)	Q9W3X7_DROME	20 kDa	27	72	1	1	0	0	
Neuroglian, isoform D Nrg	E1JJF9_DROME (+2)	138 kDa	8	55	15	12	0	0	
Cytochrome c oxidase subunit 5A, mitochondrial COX5A	COX5A_DROME	17 kDa	0	5	14	21	45	2	
CG1640, isoform A CG1640	Q7KV27_DROME	63 kDa	7	24	21	15	4	1	
CG6105-PA ATPsynG	Q9VKM3_DROME	11 kDa	22	6	28	6	1	0	
CG7433, isoform A CG7433	Q9VW68_DROME	55 kDa	47	15	2	5	10	7	
Cluster of Glyceraldehyde-3-phosphate dehydrogenase 1 Gapdh1 (G3P1_DROME)	G3P1_DROME [2]	35 kDa	2	2	3	4	25	68	
GM23292p ND-B17 (dNDUFB6)	Q9V3W2_DROME	19 kDa	17	70	5	2	0	0	
GM02062p ND-23 (dNDUFS8)	Q9VF27_DROME	25 kDa	16	46	2	2	1	1	Q module
Cluster of CG9485, isoform B CG9485 (Q9W2H8_DROME)	Q9W2H8_DROME [2]	183 kDa	0	0	0	3	92	0	
V-type proton ATPase subunit B Vha55	VATB_DROME	55 kDa	23	38	12	24	1	2	
Cluster of Shibire, isoform L shi (E1JJA4_DROME)	E1JJA4_DROME [3]	99 kDa	0	0	0	11	50	12	
Cluster of Z band alternatively spliced PDZ-motif protein 52, isoform W Zasp52 (A0A0	A0A0B4LGL0_DROME [2]	227 kDa	1	3	8	21	22	32	
CG3446, isoform B ND-B16.6 (dNDUFA13)	Q9W402_DROME	18 kDa	20	56	3	7	0	0	
Limpet, isoform K Lmpt	Q7KUQ6_DROME	246 kDa	7	2	9	20	11	2	
Cluster of Lethal (2) 01289, isoform F l(2)01289 (E1JGY6_DROME)	E1JGY6_DROME	205 kDa	10	10	5	9	10	1	
LD36265p (Fragment) UGP	A5XCL5_DROME (+1)	58 kDa	2	18	29	17	0	0	
Cluster of Bent, isoform I bt (L0MN91_DROME)	L0MN91_DROME [2]	993 kDa	0	0	0	0	1	3	
Cluster of Reticulon-like protein Rtnl1 (E1JHT6_DROME)	E1JHT6_DROME [4]	65 kDa	5	10	8	12	15	9	
Unc-89, isoform E Unc-89	A0A0B4LGI5_DROME (+2	473 kDa	0	18	20	0	1	1	
Cluster of Myosin heavy chain, isoform P Mhc (E1JHJ5_DROME)	E1JHJ5_DROME [4]	223 kDa	6	6	3	4	8	12	
CG7461, isoform B CG7461	A1ZBJ2_DROME	68 kDa	2	0	0	6	26	44	
Pyruvate dehydrogenase E1 component subunit alpha l(1)G0334	Q9W4H6_DROME	44 kDa	0	2	1	11	28	45	
Cluster of Paramyosin, long form Prm (MYSP1_DROME)	MYSP1_DROME [2]	102 kDa	1	6	16	6	28	3	
CG8036, isoform B CG8036	Q9VHN7_DROME	68 kDa	8	20	18	24	11	4	
Cytochrome b-c1 complex subunit 9 ox	QCR9_DROME	6 kDa	7	8	14	47	2	1	
Cluster of Tropomyosin 2, isoform E Tm2 (A0A0B4KHJ9_DROME)	A0A0B4KHJ9_DROME [2]	33 kDa	1	2	2	6	44	31	
Heat shock 70 kDa protein cognate 3 Hsc70-3	HSP7C_DROME	72 kDa	8	11	6	16	30	31	
Cluster of Kazachoc, isoform G kcc (A0A0B4LGD3_DROME)	A0A0B4LGD3_DROME [2]	120 kDa	1	6	6	55	0	0	
Transferrin 1, isoform A Tsf1	Q9VWV6_DROME	72 kDa	0	0	0	2	36	39	
Cluster of Succinyl-CoA ligase [ADP/GDP-forming] subunit alpha, mitochondrial Scsalp	SUCA_DROME [2]	34 kDa	0	1	2	14	33	40	
NADH dehydrogenase [ubiquinone] 1 subunit C2 ND-B14.5B (dNDUFC2)	Q9VQM2_DROME	13 kDa	21	67	7	0	1	0	
CG32230, isoform B ND-MLRQ	Q8SYJ2_DROME	9 kDa	3	6	13	14	28	13	
Aldehyde dehydrogenase Aldh	Q9VLC5_DROME	57 kDa	0	0	0	2	17	67	
Trehalase Treh	A4UZR3_DROME	64 kDa	0	0	1	6	28	29	
CG5903, isoform A CG5903	Q9VEY5_DROME	24 kDa	18	19	15	13	2	3	
GH13256p Thiolase	Q9W1H8_DROME	51 kDa	2	9	15	19	19	13	
Levy, isoform A levy	Q9W1N3_DROME	12 kDa	2	6	4	8	27	4	
V-type proton ATPase subunit H VhaSFD	VATH_DROME	54 kDa	15	23	0	27	0	2	
Bicoid stability factor bsf	Q9VJ86_DROME	157 kDa	0	0	1	3	39	1	

V-type proton ATPase catalytic subunit A isoform 1 Vha68-1	VATA1_DROME	68 kDa	27	46	9	52	3	6	
LETM1 and EF-hand domain-containing protein anon-60Da, mitochondrial Letm1	A60DA_DROME	114 kDa	1	0	1	5	43	3	
Succinyl-CoA ligase subunit beta skap	Q95U38_DROME (+1)	55 kDa	0	0	0	5	25	40	
LD23292p Mcr	Q9VLT3_DROME	203 kDa	9	34	0	1	0	0	
ATP-dependent 6-phosphofructokinase Pfk	A0A0B4K7L1_DROME	105 kDa	0	1	0	1	13	47	
Probable isocitrate dehydrogenase [NAD] subunit alpha, mitochondrial l(1)G0156	IDH3A_DROME	41 kDa	7	5	4	6	9	28	
CG7712, isoform A ND-B14 (dNDUFA6)	Q7JZK1_DROME	15 kDa	12	45	0	0	0	0	
Prohibitin 2, isoform E Phb2	A8DYI6_DROME	37 kDa	39	4	2	3	0	5	
Phosphoglycerate kinase Pgk	PGK_DROME	44 kDa	0	0	0	2	15	37	
CG11771 CG11771	Q9VC06_DROME	81 kDa	0	1	0	0	16	37	
CG2658, isoform A CG2658	Q9W4W8_DROME	90 kDa	2	0	0	7	37	4	
Cluster of Ade5, isoform B ade5 (F0JAN1_DROME)	F0JAN1_DROME	47 kDa	1	6	8	35	4	4	
V-type proton ATPase subunit a Vha100-2	Q9VE75_DROME	95 kDa	5	11	0	43	0	0	
CG14028-PA cype	Q9VMS1_DROME	8 kDa	3	2	9	10	28	6	
CG8844 protein ND-PDSW (dNDUFB10)	Q9VQR2_DROME	19 kDa	13	48	0	1	0	0	
V-type proton ATPase subunit E Vha26	VATE_DROME	26 kDa	17	13	6	20	0	0	
Cluster of Sodium/potassium-transporting ATPase subunit beta-2 nrv2 (ATPB2_DROM	ATPB2_DROME [2]	37 kDa	0	2	8	8	28	11	
Cluster of V-type proton ATPase subunit a Vha100-1 (Q6NLA3_DROME)	Q6NLA3_DROME [4]	97 kDa	0	0	0	53	0	0	
Microtubule-associated protein futsch futsch	FUTSC_DROME	592 kDa	1	2	4	3	3	2	
Phosphoglucomutase Pgm	PGM_DROME	61 kDa	0	5	11	31	2	0	
Cluster of Discs large 1, isoform R dlg1 (M9PHK8_DROME)	M9PHK8_DROME [5]	107 kDa	7	3	2	5	9	16	
CG30415, isoform A CG30415	Q0E8X7_DROME	10 kDa	6	2	24	0	0	0	
CG9350 ND-B14.7 (dNDUFA11)	Q7JYH3_DROME	18 kDa	14	54	1	0	0	0	
CG9762-PA ND-SGDH (dNDUFB5)	Q9VTU2_DROME	22 kDa	13	37	3	5	1	0	
Cluster of Cheerio, isoform N cher (A0A0B4KHN1_DROME)	A0A0B4KHN1_DROME [4	260 kDa	0	0	0	13	13	0	
Acyl-CoA synthetase long-chain, isoform J Acsl	A0A0B4KFE4_DROME (+3	82 kDa	0	1	2	7	20	20	
CG32649 CG4410	Q9VYI6_DROME	74 kDa	8	2	0	3	26	11	
Cluster of Malic enzyme Men-b (Q9VB69_DROME)	Q9VB69_DROME [2]	69 kDa	0	0	0	1	65	0	
Serine hydroxymethyltransferase CG3011	Q9W457_DROME	59 kDa	0	0	1	11	35	0	
CG6543, isoform A CG6543	Q7JR58_DROME	32 kDa	0	0	0	0	8	54	
Cluster of Elongation factor 1-alpha 2 Ef1alpha100E (EF1A2_DROME)	EF1A2_DROME [2]	51 kDa	1	0	1	1	13	19	
Cluster of Multidrug-Resistance like protein 1, isoform M MRP (Q7KTB7_DROME)	Q7KTB7_DROME [3]	174 kDa	0	0	0	2	28	0	
AT13736p UQCR-Q	Q9VVH5_DROME	10 kDa	2	6	6	29	0	1	
Cluster of Heat shock 70 kDa protein cognate 4 Hsc70-4 (HSP7D_DROME)	HSP7D_DROME [2]	71 kDa	5	5	5	7	26	25	
RH44771p SdhC	Q9VGS3_DROME	19 kDa	3	1	2	3	10	30	
CG13887, isoform C CG13887	Q9W0M4_DROME	26 kDa	0	1	0	16	16	10	
Cluster of CG11876, isoform A CG11876 (Q7K5K3_DROME)	Q7K5K3_DROME	39 kDa	0	1	2	9	19	29	
GH21316p Ssadh	Q9VBP6_DROME	55 kDa	0	3	5	9	29	0	
Cluster of Vesicle-fusing ATPase 1 comt (NSF1_DROME)	NSF1_DROME [2]	83 kDa	0	0	0	0	11	23	
Cluster of FI04632p nrv3 (Q7JS69_DROME)	Q7JS69_DROME [2]	36 kDa	1	0	8	5	27	1	
Protein l(2)37Cc l(2)37Cc	L2CC_DROME	30 kDa	38	5	0	1	0	1	
CG9297, isoform B CG9297	Q8I0D4_DROME	106 kDa	0	5	2	10	18	7	
Malic enzyme Men	Q9VG32_DROME	84 kDa	0	0	0	36	2	0	
Cluster of Stretchin-Mlck, isoform S Strn-Mlck (A0A0B4KF84_DROME)	A0A0B4KF84_DROME	919 kDa	1	1	0	10	2	2	
Cluster of Tubulin beta-1 chain betaTub56D (TBB1_DROME)	TBB1_DROME [6]	50 kDa	0	0	0	1	14	28	
Cluster of TER94, isoform E TER94 (A0A0B4LFZ4_DROME)	A0A0B4LFZ4_DROME [2]	92 kDa	0	0	0	41	0	1	
Amino acid transporter Eaat1	O77062_DROME	52 kDa	2	2	5	9	33	0	
CG5548, isoform B ND-B18 (dNDUFB7)	Q9VXZ0_DROME	14 kDa	9	47	4	2	0	0	
CG5844 CG5844	Q9VG69_DROME	42 kDa	0	0	0	0	0	51	
CG1824 CG1824	Q9VYL5_DROME	84 kDa	1	9	0	5	33	0	
Cluster of Na/Ca-exchange protein, isoform G Calx (A0A0B4K6E2_DROME)	A0A0B4K6E2_DROME [4]	109 kDa	0	0	0	2	31	1	
Putative apoptosis-inducing factor 1, mitochondrial AIF	AIFM1_DROME	81 kDa	3	0	0	2	13	18	Putative Asse
CG3214, isoform B ND-B17.2 (dNDUFA12)	Q9VQD7_DROME	17 kDa	8	36	0	0	0	0	
Transporter Gat	Q9V4E7_DROME	72 kDa	0	0	2	5	7	27	
CG8680, isoform A ND-13A (dNDUFS6)	Q9VMU0_DROME	14 kDa	9	31	0	0	0	0	
CG7470, isoform A CG7470	Q9VNW6_DROME	84 kDa	0	0	0	2	9	18	

Moesin, isoform K Moe	C7LAH9_DROME	76 kDa	0	0	0	4	9	5	
Thioester-containing protein 4, isoform C Tep4	M9PDR0_DROME (+1)	169 kDa	0	0	0	0	0	38	
CG6439, isoform A CG6439	Q9VD58_DROME	40 kDa	2	5	3	4	13	16	
ATP-citrate synthase ATPCL	E2QCF1_DROME	120 kDa	0	1	27	0	0	0	
CG34172, isoform A CG34172	Q6IHY5_DROME	7 kDa	2	2	9	3	31	2	
Cluster of Tubulin alpha-3 chain alphaTub84D (TBA3_DROME)	TBA3_DROME [2]	50 kDa	0	0	0	2	15	26	
Cluster of FI01544p Rab1 (O18332_DROME)	O18332_DROME [4]	23 kDa	1	1	2	1	9	6	
Chaoptin, isoform C chp	A0A0B4KHG5_DROME (+	151 kDa	0	0	0	30	4	0	
Cluster of Basigin, isoform G Bsg (Q7KTJ7_DROME)	Q7KTJ7_DROME [2]	71 kDa	3	3	3	10	22	4	
Ferritin Fer2LCH	A0A0B4KHF0_DROME (+1	26 kDa	0	2	1	37	0	0	
MICOS complex subunit MIC13 homolog CG7603	MIC13_DROME	14 kDa	6	11	10	7	1	4	
ABCB7, isoform B ABCB7	Q7KVB1_DROME (+1)	77 kDa	0	0	0	1	17	16	
CG31195 CG31195-RA	Q8IN49_DROME	94 kDa	1	25	0	0	0	0	
Glycoprotein 93 Gp93	Q9VAY2_DROME	90 kDa	0	0	0	9	4	13	
Catalase Cat	CATA_DROME	57 kDa	14	12	3	6	0	0	
Apolipoprotein lipid transfer particle Apoltp	Q7KTG2_DROME	494 kDa	3	0	0	0	0	0	
CG12203-PA ND-18 (dNDUFS4)	Q9VWI0_DROME	21 kDa	10	33	0	0	0	0	
Nucleoside diphosphate kinase awd	A0A0B4LHX6_DROME (+1	19 kDa	15	2	7	8	10	1	
Vacuolar protein sorting 13, isoform A Vps13	A1Z713_DROME	375 kDa	0	1	10	1	0	0	
AT12494p ND-B22 (dNDUFB9)	Q9VJZ4_DROME	17 kDa	4	16	2	0	0	0	
Probable methylmalonate-semialdehyde dehydrogenase [acylating], mitochondrial C	MMSA_DROME	56 kDa	0	0	0	5	35	0	
9 kD basic protein ATPsynE	O77134_DROME	9 kDa	14	2	16	0	2	2	
Pugilist, isoform E pug	A0A0B4K623_DROME (+1	103 kDa	0	0	0	0	9	16	
ATP synthase protein 8 mt:ATPase8	ATP8_DROME	6 kDa	14	3	17	0	0	0	
3-hydroxyacyl-CoA dehydrogenase type-2 scu	HCD2_DROME	27 kDa	0	1	1	9	16	17	
FI01422p Spn43Ab	A1Z6V5_DROME	43 kDa	1	0	3	7	21	1	
Aspartate aminotransferase Got2	Q8IPY3_DROME	48 kDa	15	8	6	0	0	0	
Protein ROP Rop	ROP_DROME	68 kDa	0	0	0	2	8	14	
Glutamine synthetase Gs2	X2JDA5_DROME	42 kDa	0	0	0	1	10	17	
BcDNA.GH11322 bdl	Q9U4G1_DROME	81 kDa	0	5	2	9	8	7	
CG6851-PA, isoform A Mtch	Q9V3Y4_DROME	35 kDa	0	0	0	9	11	18	
AAA family protein Bor	Q9VEX6_DROME	68 kDa	5	6	0	1	0	0	
CG4908, isoform A CG4908	Q9VL22_DROME	49 kDa	0	2	2	23	0	0	
Cluster of CG10737, isoform R CG10737 (B7YZL6_DROME)	B7YZL6_DROME [4]	97 kDa	5	2	4	2	8	7	
Cluster of Upheld, isoform N up (M9NH07_DROME)	M9NH07_DROME [3]	47 kDa	0	0	0	0	0	3	
Cluster of Dynamin associated protein 160, isoform D Dap160 (M9ND00_DROME)	M9ND00_DROME [3]	132 kDa	0	0	14	2	0	0	
Cluster of Calnexin 99A, isoform A Cnx99A (Q9VAL7_DROME)	Q9VAL7_DROME [2]	68 kDa	0	0	1	3	26	10	
Innexin inx2 Inx2	INX2_DROME	42 kDa	2	9	20	2	0	0	
CG14235-PA, isoform A COX6B	Q9VWD1_DROME	11 kDa	0	1	1	4	17	0	
CG3683 protein ND-19 (dNDUFA8)	Q9W125_DROME	20 kDa	4	23	0	0	0	0	
Mitochondrial import receptor subunit TOM40 homolog 1 Tom40	TO401_DROME	36 kDa	1	1	2	20	3	6	
Cluster of NADPH--cytochrome P450 reductase Cpr (NCPR_DROME)	NCPR_DROME [2]	76 kDa	0	0	0	1	4	21	
Maltase A7, isoform A Mal-A7	A1Z7F2_DROME	67 kDa	0	9	24	15	0	0	
Cytochrome P450 4g1 Cyp4g1	CP4G1_DROME	63 kDa	0	2	0	2	5	14	
Failed axon connections fax	FAXC_DROME (+1)	47 kDa	0	0	0	0	20	8	
Heat shock 70 kDa protein cognate 5 Hsc70-5	HSP7E_DROME	74 kDa	0	0	0	0	8	18	
LD31742p whd	Q7JQH9_DROME (+1)	89 kDa	0	2	2	7	7	12	
Cluster of 60 kDa heat shock protein, mitochondrial Hsp60 (CH60_DROME)	CH60_DROME	61 kDa	0	0	1	4	1	1	
Cluster of CG6603-PA, isoform A Hsc70Cb (Q9VUC1_DROME)	Q9VUC1_DROME [2]	89 kDa	0	0	0	0	0	27	
CG12859 ND-B15 (dNDUFB4)	Q6IDF5_DROME	13 kDa	9	16	1	0	0	0	
CG4984, isoform A CG4975-RB	A1ZAY4_DROME (+1)	51 kDa	2	2	2	5	5	17	
CG10226, isoform B CG10226	M9PEB5_DROME (+1)	134 kDa	0	0	0	12	9	0	
Actin-interacting protein 1 flr	WDR1_DROME	67 kDa	0	0	0	0	29	0	
LP19846p Ndg	A1Z877_DROME	149 kDa	0	0	0	0	0	28	
Sodium/potassium-transporting ATPase subunit beta-1 nrv1	ATPB1_DROME	35 kDa	0	0	0	4	17	11	
LD22449p Tsf2	Q9VTZ5_DROME	92 kDa	4	21	0	0	0	0	

Mitochondrial import inner membrane translocase subunit TIM50-C ttm50	TI50C_DROME	50 kDa	0	0	0	0	14	14	
V-type proton ATPase subunit d 1 VhaAC39-1	VA0D1_DROME	40 kDa	1	4	0	28	1	0	
Cluster of Tripeptidyl-peptidase II, isoform E TppII (A0A0B4LF88_DROME)	A0A0B4LF88_DROME [2]	151 kDa	8	1	0	0	0	0	
CD98 heavy chain, isoform D CD98hc	A0A0B4KFA6_DROME (+1	63 kDa	0	0	0	0	36	0	
CG2918, isoform B EG:25E8.1	O46067_DROME	103 kDa	0	0	0	0	1	19	
Enigma Egm	Q5U117_DROME	71 kDa	0	0	3	16	1	4	Assembly Fac
CG6045 AOX3	Q9VF51_DROME	138 kDa	0	0	0	0	18	0	
Cluster of CG9990, isoform A CG9990 (Q9VAU1_DROME)	Q9VAU1_DROME [2]	89 kDa	0	0	0	4	26	0	
Contactin Cont	CONT_DROME	158 kDa	5	6	0	1	0	0	
Heat shock protein 83 Hsp83	HSP83_DROME	82 kDa	0	0	0	2	9	15	
Protein NDUFAF4 homolog CG11722	NDUF4_DROME	24 kDa	0	0	1	6	7	17	Assembly Fac
Epidermal growth factor receptor pathway substrate clone 15, isoform C Eps-15	Q8MMD3_DROME	120 kDa	0	0	11	4	0	0	
SAM50-like protein CG7639 CG7639	SAM50_DROME	49 kDa	6	4	2	1	7	7	
Cluster of CG9399, isoform A CG9399 (Q9VHB1_DROME)	Q9VHB1_DROME [2]	17 kDa	2	2	2	1	8	23	
NADH-ubiquinone oxidoreductase chain 4 ND4	A0A075E721_DROME	51 kDa	3	26	0	0	0	0	
Optic atrophy 1 ortholog, isoform D Opa1	A0A0B4LFB8_DROME (+3	107 kDa	0	0	0	0	2	8	
Innexin inx3 Inx3	INX3_DROME	45 kDa	0	9	13	0	0	0	
Cluster of Stunted, isoform B sun (Q8IR24_DROME)	Q8IR24_DROME [2]	6 kDa	12	1	15	0	0	0	
CG34439, isoform A ND-MWFE (dNDUFA1)	A8DYC5_DROME	9 kDa	6	23	0	0	0	0	
Transmembrane GTPase Marf Marf	MARF_DROME	91 kDa	0	0	0	2	3	8	
CG13220, isoform A CG13220	Q6NP72_DROME	16 kDa	1	5	5	5	4	7	
GH05862p NP15.6 (dNDUFB11)	Q9V3L7_DROME	17 kDa	11	17	1	1	1	1	
Cytochrome b mt:Cyt-b	CYB_DROME (+1)	43 kDa	2	2	3	15	0	0	
Chitinase-like protein CG5210 CG5210	C5210_DROME	50 kDa	0	0	0	5	22	2	
CG31233 CG5839	Q8MRN5_DROME	107 kDa	0	0	0	3	25	0	
Syntaxin 1A, isoform B Syx1A	A0A0B4JCZ4_DROME (+1	34 kDa	0	3	2	2	9	5	
CG9603, isoform B COX7A	A0A0B4K6C3_DROME (+1	11 kDa	0	0	0	5	13	0	
Neither inactivation nor afterpotential protein C ninaC	NINAC_DROME	174 kDa	0	0	0	0	1	5	
CG8888 CG8888	Q7K3N4_DROME	43 kDa	0	1	0	4	5	2	
Lethal (3) 03670 l(3)03670	Q9VA18_DROME	24 kDa	5	4	9	1	3	0	
V-type proton ATPase subunit C Vha44	VATC_DROME	92 kDa	4	10	0	0	0	0	
Aldehyde dehydrogenase Aldh-III	A0A0B4KEL0_DROME (+2	56 kDa	0	0	0	3	7	8	
CG8399, isoform B CG8399	A0A0B4LGL5_DROME (+1	71 kDa	0	0	0	3	3	18	
Chitinase-like protein Idgf4 Idgf4	IDGF4_DROME	49 kDa	0	0	0	1	7	24	
Innexin inx1 ogre	INX1_DROME	43 kDa	0	2	15	0	0	0	
CG3621, isoform A ND-B14.5A (dNDUFA7)	O97418_DROME	12 kDa	4	18	0	0	0	2	
CG31198 CG31198	Q8IN25_DROME	107 kDa	0	0	0	4	8	7	
Cluster of LP07226p mge (Q9VZL1_DROME)	Q9VZL1_DROME [3]	16 kDa	1	3	3	19	4	0	
Cluster of CG3961, isoform E CG3961 (M9PCX4_DROME)	M9PCX4_DROME [2]	75 kDa	0	0	0	0	5	8	
Cytochrome c-2 Cyt-c-p	CYC2_DROME	12 kDa	0	0	3	3	7	11	
Plexin A, isoform A PlexA	Q9V491_DROME	218 kDa	0	0	0	11	0	0	
Cluster of Mustard, isoform V mtd (A0A0B4K620_DROME)	A0A0B4K620_DROME [2]	146 kDa	0	0	0	1	5	0	
Cluster of Ubiquitin-60S ribosomal protein L40 RpL40 (RL40_DROME)	RL40_DROME [2]	15 kDa	1	1	1	0	7	11	
Cluster of CG18769, isoform G CG18769-RC (E1NZC4_DROME)	E1NZC4_DROME [4]	51 kDa	0	9	0	8	0	0	
Alkaline phosphatase 4 Aph-4	APH4_DROME	65 kDa	0	0	0	1	14	0	
Calcium-dependent secretion activator Caps	CAPS_DROME	163 kDa	0	0	0	1	10	0	
Phenoloxidase 2 PPO2	PPO2_DROME	79 kDa	10	0	0	0	0	0	
CG7052-PD, isoform D Tep2	Q8IPH4_DROME (+4)	157 kDa	0	0	0	0	0	16	
CG4239, isoform A CG4239	Q9VXG9_DROME	30 kDa	4	4	5	3	4	2	
LD12946p MSBP	Q9VXM4_DROME	28 kDa	0	1	0	0	10	10	
CG9512, isoform A CG9512	Q9VY05_DROME	69 kDa	0	0	0	0	0	22	
Protein stoned-B stnB	STNB_DROME (+1)	138 kDa	0	0	5	10	4	0	
Nervous wreck, isoform H nwk	X2J8V0_DROME	110 kDa	2	12	1	0	0	0	
Cluster of Coracle, isoform F cora (A0A0B4LFX4_DROME)	A0A0B4LFX4_DROME [3]	174 kDa	0	2	0	1	6	2	
CG13601, isoform B CG13601	A0A0B4KGV7_DROME (+	31 kDa	0	0	0	13	2	1	
Elongation factor Tu EfTuM	A1Z9E3_DROME	54 kDa	0	0	0	0	3	14	

Rhea, isoform G rhea	M9PBW9_DROME (+1)	305 kDa	0	0	0	4	0	0	
CG13506, isoform A CG13506-RA	Q9W259_DROME	57 kDa	0	0	0	0	4	16	
Adenosylhomocysteinase Ahcy13	SAHH_DROME	47 kDa	0	0	0	0	0	25	
Histone H4 His4	H4_DROME	11 kDa	3	1	2	3	3	0	
FI12817p Nrx-IV	Q8IQH0_DROME	145 kDa	1	2	0	2	0	0	
Cluster of Aspartyl beta-hydroxylase, isoform L Asph (A0A0B4KFS5_DROME)	A0A0B4KFS5_DROME [4]	113 kDa	1	2	0	7	2	1	
Probable medium-chain specific acyl-CoA dehydrogenase, mitochondrial CG12262	ACADM_DROME	46 kDa	0	0	0	0	2	13	
ATP synthase-coupling factor 6, mitochondrial ATPsynCf6	ATP5J_DROME	12 kDa	7	2	12	0	0	0	
Synapsin, isoform D Syn	E2QCY9_DROME (+1)	109 kDa	0	0	0	3	10	0	
Esterase-6 Est-6	EST6_DROME	61 kDa	0	0	0	0	1	14	
GM04645p Ugt86Da	Q9VGT3_DROME	60 kDa	0	0	0	2	2	15	
UDP-glucose:glycoprotein glucosyltransferase Ugt	UGGG_DROME	174 kDa	0	0	0	0	10	0	
ATP synthase subunit a mt:ATPase6	ATP6_DROME (+1)	25 kDa	8	3	17	1	0	0	
Annexin B11 AnxB11	ANX11_DROME	56 kDa	0	0	0	0	0	20	
Peroxiredoxin 1 Jafrac1	PRDX1_DROME	22 kDa	2	1	0	14	1	0	
MIP08013p1 Mpcp	Q0E8E8_DROME	39 kDa	0	0	0	4	7	13	
Ankyrin, isoform B Ank	Q0KIE7_DROME	170 kDa	0	0	0	0	12	0	
Electron transfer flavoprotein-ubiquinone oxidoreductase, isoform A Etf-QO	Q7JWF1_DROME	66 kDa	2	0	0	0	4	18	
CG40002, isoform A ND-AGGG (dNDUFB2)	Q7PL91_DROME	11 kDa	1	17	0	0	0	0	
Dipeptidase B, isoform A Dip-B	Q9VFQ9_DROME	56 kDa	0	2	8	4	0	0	
Triosephosphate isomerase Tpi	TPIS_DROME	27 kDa	1	0	1	2	2	14	
Glutamine synthetase 1, mitochondrial Gs1	GLNA1_DROME	44 kDa	0	0	0	1	6	8	
Integrin alpha-PS2 if	ITA2_DROME	154 kDa	0	0	0	14	0	0	
CG2118, isoform A CG2118	Q9V9T5_DROME	77 kDa	0	4	4	0	0	0	
UDP-glucuronosyltransferase (Fragment) Ugt86Dd	Q9VGT8_DROME	59 kDa	0	0	0	0	1	15	
CG9510, isoform C CG9510	Q9VLG9_DROME	52 kDa	0	0	0	17	0	0	
BcDNA.GH02220 BcDNA.GH02220	Q9Y171_DROME	49 kDa	0	0	0	0	3	14	
CG43163, isoform C CG43163	Q9VSK6_DROME	270 kDa	0	0	0	0	5	0	
Glutamate oxaloacetate transaminase 1, isoform B Got1	A1ZAA5_DROME (+1)	49 kDa	0	0	1	5	10	0	
Probable cytochrome P450 28d1 Cyp28d1	C28D1_DROME	57 kDa	0	0	0	0	4	12	
CG14482, isoform A UQCR-6.4	Q500Y7_DROME	6 kDa	2	2	3	10	4	6	
UDP-glucuronosyltransferase Ugt35b	Q9VGT0_DROME	58 kDa	0	0	0	0	3	18	
UDP-glucuronosyltransferase CG17323	Q9VJ46_DROME	58 kDa	0	0	0	0	4	12	
CG13907, isoform A CG13907	Q9W0L6_DROME	88 kDa	0	0	0	5	15	0	
ATP synthase subunit beta ATPsynbetaL	Q8T4C4_DROME	68 kDa	147	21	169	120	50	0	
Cluster of CG4019, isoform F CG4019 (A0A0B4KFZ1_DROME)	A0A0B4KFZ1_DROME [2]	32 kDa	2	2	2	3	4	1	
Cluster of Axotactin, isoform C axo (M9PE65_DROME)	M9PE65_DROME [2]	242 kDa	0	1	1	5	0	0	
Cluster of CG31075, isoform A CG31075 (Q9VB96_DROME)	Q9VB96_DROME [2]	53 kDa	0	5	7	4	0	0	
CG5028, isoform C CG5028-RC	A8JRB8_DROME (+2)	43 kDa	0	1	2	0	2	10	
Insulin-degrading enzyme Ide	IDE_DROME	114 kDa	0	0	0	0	0	9	
GH04080p PPO1	Q7K2W6_DROME	79 kDa	0	0	0	1	13	0	
Ferritin Fer1HCH	Q7KRU8_DROME	23 kDa	0	1	3	20	0	0	
CG3156 EG:171D11.2	Q8SWW9_DROME	76 kDa	0	0	0	1	3	12	
CG11089, isoform A CG11089	Q9VC18_DROME	63 kDa	0	0	0	0	0	20	
CG14997, isoform A CG14997	Q9VZF6_DROME	51 kDa	0	0	0	1	2	9	
Cluster of V-type proton ATPase subunit D 1 Vha36-1 (VATD1_DROME)	VATD1_DROME [2]	28 kDa	1	5	0	5	0	0	
LD20211p Tudor-SN	Q9W0S7_DROME	103 kDa	0	0	0	0	1	7	
CG1440, isoform A CG1440	Q9W3F6_DROME	55 kDa	0	0	0	0	11	0	
Sphingosine-1-phosphate lyase Sply	SGPL_DROME	60 kDa	0	0	0	2	4	7	
Cluster of Coronin coro (A0A0B4KEJ7_DROME)	A0A0B4KEJ7_DROME [2]	58 kDa	0	0	1	2	8	0	
Peroxisomal multifunctional enzyme type 2 Mfe2	DHB4_DROME	64 kDa	0	0	0	0	1	15	
NADH-ubiquinone oxidoreductase chain 5 mt:ND5	NU5M_DROME	65 kDa	5	17	0	0	0	0	
Pyrroline-5-carboxylate reductase P5cr-2	Q9VEJ3_DROME	28 kDa	1	3	4	8	0	0	
CG18522 AOX1	Q9VF53_DROME	139 kDa	0	0	0	0	12	0	
CG7627, isoform B CG7627-RA	Q9VLN6_DROME	152 kDa	0	0	0	1	4	0	
CG10932, isoform A CG10932	Q9W3N9_DROME	43 kDa	0	0	0	0	3	17	

Synaptosomal-associated protein 25 Snap25	SNP25_DROME	24 kDa	0	0	0	0	3	12	
CG34120, isoform D CG34120	E2QD66_DROME (+2)	222 kDa	0	1	0	3	0	0	
Clathrin heavy chain Chc	CLH_DROME	191 kDa	3	0	0	1	0	0	
CG2076, isoform A CG2076	Q9VZ34_DROME	36 kDa	1	0	0	5	2	5	
CG15011 CG15011	Q9VZF2_DROME	94 kDa	0	0	0	0	2	0	
CG9754 CG9754	Q9W2H9_DROME	61 kDa	2	1	0	5	1	1	
CG32436 CG32436-RA	Q9VP43_DROME	201 kDa	0	0	0	2	0	0	
Cluster of CG11455, isoform A ND-15 (dNDUFS5)	Q7K1C0_DROME [2]	12 kDa	2	15	0	0	0	0	
Neprilysin 2, isoform B Nep2	A0A0B4K692_DROME (+1	88 kDa	0	0	0	0	8	0	
Guanine nucleotide-binding protein subunit beta-1 Gbeta13F	GBB1_DROME	37 kDa	0	0	0	0	9	9	
Probable methylcrotonoyl-CoA carboxylase beta chain, mitochondrial l(2)04524	MCCB_DROME	63 kDa	0	0	3	2	5	0	
CG33970, isoform A CG6166	Q86P18_DROME	86 kDa	0	0	0	2	13	0	
LD30155p lost	Q9VN21_DROME	60 kDa	0	0	0	1	4	9	
FI07923p Karybeta3	Q9VN44_DROME	124 kDa	0	0	0	2	5	0	
BcDNA.GH08860 Tps1	Q9Y119_DROME	91 kDa	0	0	0	0	0	3	
Kinesin heavy chain Khc	KINH_DROME	110 kDa	0	4	2	1	0	0	
Cluster of Heat shock protein 68 Hsp68 (HSP68_DROME)	HSP68_DROME [4]	70 kDa	5	2	3	4	7	5	
Cluster of CG3164, isoform B CG3164 (Q9VPJ9_DROME)	Q9VPJ9_DROME [2]	78 kDa	0	0	0	5	11	0	
Cluster of Like-AP180, isoform I lap (A0A0B4KFE2_DROME)	A0A0B4KFE2_DROME [7]	83 kDa	0	0	0	0	2	15	
Extended synaptotagmin-like protein 2 ortholog, isoform B Esyt2	Q7KS16_DROME (+1)	94 kDa	0	4	0	2	0	0	
NADH-cytochrome b5 reductase CG5946-RB	Q4LDP7_DROME (+1)	36 kDa	0	1	0	2	5	6	
Nckx30C, isoform E Nckx30C	M9MRG0_DROME	94 kDa	0	0	0	0	4	10	
Dihydroorotate dehydrogenase (quinone), mitochondrial Dhod	PYRD_DROME	44 kDa	0	0	0	0	2	4	
CG2254-PA CG2254	Q9W3K9_DROME	36 kDa	0	0	0	0	2	10	
BcDNA.GH10614 BcDNA.GH10614	Q9Y112_DROME	36 kDa	0	0	0	11	0	0	
CG18624, isoform B ND-MNLL (dNDUFB1)	Q9W3N7_DROME	6 kDa	2	5	1	0	0	0	
CG4587, isoform H CG4587	X2J9Z3_DROME	144 kDa	0	0	0	0	4	1	
Multidrug resistance protein homolog 65 Mdr65	MDR65_DROME	144 kDa	0	0	0	0	2	0	
CG41128 CG41128	Q8SY69_DROME	8 kDa	1	2	3	2	0	0	
Cluster of CG42492, isoform A CG11473 (Q9W4A6_DROME)	Q9W4A6_DROME [2]	99 kDa	4	4	1	3	1	0	
Cluster of Acyl carrier protein ND-ACP (dNDUFAB1)	M9PDU4_DROME [2]	21 kDa	3	8	0	0	0	0	
Ubiquinone biosynthesis protein COQ9, mitochondrial Coq9	COQ9_DROME	36 kDa	1	0	0	0	8	2	
NTPase, isoform F NTPase	M9PBV2_DROME	58 kDa	0	0	0	3	1	5	
CG31343 CG5839	Q8SWX4_DROME	108 kDa	0	0	0	5	10	0	
BcDNA.HL02693 CRMP	Q9V3N7_DROME	64 kDa	0	0	0	0	0	9	
CG3999, isoform A CG3999	Q9VH09_DROME	110 kDa	0	0	0	0	0	7	
CG1718, isoform B CG1718	Q9VRG4_DROME	193 kDa	0	0	0	0	3	1	
CG9394, isoform A CG9394	Q9W2L6_DROME	77 kDa	0	0	0	1	8	4	
Stromal interaction molecule homolog Stim	STIM_DROME	65 kDa	1	0	0	4	4	0	
Fat-body protein 1 Fbp1	FBP1_DROME (+1)	120 kDa	0	0	0	0	0	2	
LD45324p Prx5	Q960M4_DROME	20 kDa	0	2	1	6	0	0	
Cytochrome b5-related protein Cyt-b5-r	CYB5R_DROME	50 kDa	1	0	0	2	1	5	
CG32267 CG32267	Q8IRD0_DROME	6 kDa	0	2	4	6	2	5	
Semaphorin-2b, isoform D Sema-2b	A0A0B4KG38_DROME (+1	94 kDa	0	0	0	0	2	0	
Cluster of AMP deaminase, isoform E AMPdeam (Q9VY76_DROME)	Q9VY76_DROME [2]	89 kDa	0	0	0	0	2	0	
Ubiquinone biosynthesis protein COQ4 homolog, mitochondrial CG32174	COQ4_DROME	31 kDa	2	0	0	0	3	1	
Fasciclin-2 Fas2	FAS2_DROME (+4)	97 kDa	0	0	0	4	8	0	
Ferrochelatase, mitochondrial FeCh	HEMH_DROME	44 kDa	0	0	0	0	2	7	
Adaptor protein complex 2, mu subunit, isoform A AP-2mu	O62530_DROME	50 kDa	1	2	2	3	2	0	
CG4123-PA, isoform A Mipp1	Q9VV72_DROME	54 kDa	0	0	0	0	4	6	
FI05212p Sodh-1	O97479_DROME	39 kDa	2	0	1	2	3	2	
G protein alpha o subunit Galphao	GNAO_DROME	40 kDa	0	1	1	3	5	6	
CDGSH iron-sulfur domain-containing protein 2 homolog Cisd2	CISD2_DROME	15 kDa	0	0	0	0	5	9	
UPF0389 protein CG9231 CG9231	U389_DROME	14 kDa	1	2	2	2	2	4	
Mini spindles, isoform E msps	A0A0B4K664_DROME (+1	230 kDa	0	0	0	0	2	0	
CG17360, isoform B CG17360	A0A0B4KH60_DROME (+1	147 kDa	0	0	1	2	0	0	

Cluster of Synaptotagmin 1 Syt1 (SY65_DROME)	SY65_DROME [2]	53 kDa	0	1	0	5	5	2	
Cluster of Non-specific protein-tyrosine kinase Src42A (A1Z6I9_DROME)	A1Z6I9_DROME	176 kDa	0	0	0	0	0	5	
Carboxylic ester hydrolase Ace	A0A0B4KGI5_DROME (+1	71 kDa	0	0	0	0	16	0	
Superoxide dismutase Sod2	A0A0B4LGQ1_DROME (+	25 kDa	0	0	0	1	4	6	
Gelsolin, isoform L Gel	A0A0C4DHG6_DROME	83 kDa	0	0	0	0	0	8	
Protein I'm not dead yet Indy	INDY1_DROME	66 kDa	0	0	0	0	14	0	
Proteasome subunit alpha type-6 Prosalpha1	PSA6_DROME	27 kDa	0	0	5	0	0	0	
CG9629 CG9629	Q8SXQ1_DROME	58 kDa	0	1	6	7	0	0	
CG3699-PA EG:BACR7A4.14	Q9U1L2_DROME	26 kDa	0	0	0	0	5	11	
CG5789, isoform A CG5789-RA	Q9VC63_DROME	157 kDa	0	0	0	0	8	0	
CG2107 CG2107	Q9VZW7_DROME	75 kDa	0	0	0	0	0	6	
FI03690p Gk	Q9W095_DROME	65 kDa	0	2	5	4	0	0	
NADH-ubiquinone oxidoreductase chain 1 mt:ND1	NU1M_DROME (+1)	36 kDa	4	5	0	0	0	0	
CG17734, isoform B CG17734	Q8INK7_DROME (+1)	10 kDa	0	2	1	3	7	2	
RE08173p Tg	Q9VLU2_DROME	87 kDa	0	0	0	0	1	4	
Sodium chloride cotransporter 69, isoform C Ncc69	M9PCA7_DROME (+1)	132 kDa	0	0	2	2	2	0	
Lectin type C (Fragment) lectin-28C	Q9VLW1_DROME	30 kDa	0	0	0	0	5	0	
Facilitated trehalose transporter Tret1-1 Tret1-1	TRE11_DROME	95 kDa	0	1	0	1	3	1	
Cluster of Isocitrate dehydrogenase [NADP] Idh (Q7KUB1_DROME)	Q7KUB1_DROME [2]	53 kDa	0	0	0	0	1	4	
Calpain-A, isoform D CalpA	A0A0B4LG26_DROME (+1	96 kDa	0	0	0	2	9	1	
LD18774p OstDelta	Q7K110_DROME	69 kDa	3	0	5	0	0	0	
CG9416, isoform A CG9416	Q8MT48_DROME	98 kDa	0	0	0	0	0	10	
Peroxiredoxin 3 Prx3	Q9VEJ0_DROME	26 kDa	0	0	0	0	8	0	
Adenylyl cyclase-associated protein capt	Q9VPX6_DROME	84 kDa	0	0	0	0	2	6	
CG2930, isoform A CG2930-RA	Q9W4P6_DROME (+1)	89 kDa	0	0	0	0	3	6	
CG9634, isoform A goe	Q9XZ14_DROME (+1)	100 kDa	0	0	0	4	0	0	
Cytochrome c oxidase subunit 1 mt:Col	COX1_DROME	56 kDa	0	0	0	2	7	0	
Cluster of Glutathione peroxidase PHGPx (Q8IRD3_DROME)	Q8IRD3_DROME [2]	26 kDa	0	1	0	3	0	2	
AP-2 complex subunit alpha AP-2alpha	AP2A_DROME	106 kDa	1	0	0	4	0	0	
Elongation factor 2 EF2	EF2_DROME	94 kDa	0	0	0	0	1	4	
LD47736p Sodh-2	O96299_DROME	39 kDa	0	0	0	0	0	14	
Proteasome subunit alpha type-4 Prosalpha3	PSA4_DROME	29 kDa	0	0	10	0	0	0	
CG31030, isoform B CG31030	Q0KHY8_DROME (+1)	47 kDa	0	0	0	8	0	0	
UDP-glucuronosyltransferase BEST:LD25345	Q9VJ45_DROME	58 kDa	0	0	0	0	0	5	
CG3609, isoform B CG3609	Q9VQB4_DROME	37 kDa	0	0	0	0	3	9	
RH64870p Ucp4A	Q9VX14_DROME	37 kDa	1	0	0	3	1	9	
CG14526 CG14526	Q9Y136_DROME	82 kDa	0	0	0	0	0	9	
High-affinity choline transporter 1 CG7708	SC5A7_DROME	67 kDa	0	0	0	0	0	11	
Uricase Uro	URIC_DROME	40 kDa	0	0	0	0	1	5	
Alpha-mannosidase LManII	Q8IPB7_DROME (+1)	123 kDa	0	0	0	0	3	2	
CG4562, isoform E CG4562	A0A0B4KGI0_DROME	158 kDa	0	0	0	1	5	0	
Holocarboxylase synthetase, isoform B Hcs	A0A0B4KF92_DROME (+1	110 kDa	0	0	0	0	2	1	
Grunge, isoform G Gug	M9NE54_DROME	213 kDa	0	0	0	2	0	0	
Cluster of Serine/threonine-protein phosphatase 2B catalytic subunit 3 CanA-14F (PP2	PP2B3_DROME	64 kDa	0	0	0	0	0	3	
Ubiquinone biosynthesis monooxygenase COQ6, mitochondrial Coq6	COQ6_DROME	52 kDa	7	1	0	0	0	4	
Integrin beta-PS mys	ITBX_DROME (+1)	93 kDa	0	0	0	6	0	0	
CG7834, isoform A CG7834	Q0KHZ6_DROME	27 kDa	0	0	0	0	0	5	
CG1358, isoform A CG1358-RB	Q7K1D7_DROME	52 kDa	0	0	0	0	0	11	
CG17121 CG17121	Q9VCR9_DROME	39 kDa	0	0	0	0	1	6	
CG10639, isoform A CG10639-RA	Q9VJ28_DROME	50 kDa	0	0	0	0	2	5	
CG7752-PA pzg	Q9VP57_DROME	105 kDa	0	0	0	0	3	0	
CG10320, isoform A ND-B12 (dNDUFB3)	Q9W2E8_DROME	12 kDa	3	9	0	0	0	0	
CHOp24, isoform A CHOp24	Q9W4K0_DROME	23 kDa	0	0	0	2	3	6	
Atlastin atl	ATLAS_DROME	61 kDa	1	0	0	0	0	5	
CG10097, isoform B CG10097	Q9VG86_DROME	57 kDa	0	0	0	2	3	1	
Evolutionarily conserved signaling intermediate in Toll pathway, mitochondrial ECSIT	ECSIT_DROME	47 kDa	0	0	0	5	0	0	Assembly Fac

CG10184 CG10184	Q9VCK6_DROME	41 kDa	0	0	0	1	3	0	
CG1742-PA, isoform A Mgstl	Q8SY19_DROME	17 kDa	0	0	0	1	3	3	
Cytoplasmic FMR1-interacting protein Sra-1	CYFIP_DROME	149 kDa	0	0	0	0	2	0	
Mitochondrial import inner membrane translocase subunit Tim16 blp	TIM16_DROME	16 kDa	0	1	0	1	1	3	
Unextended, isoform E uex	A0A0B7P9G0_DROME	93 kDa	0	3	0	0	0	0	
Cluster of Curled, isoform G cu (A0A0C4DHA6_DROME)	A0A0C4DHA6_DROME [3	54 kDa	0	0	0	0	2	3	
Cluster of CG15096, isoform A CG15096 (Q5BIE4_DROME)	Q5BIE4_DROME [2]	53 kDa	0	0	0	0	2	8	
Lachesin Lac	LACH_DROME	40 kDa	0	7	0	0	2	2	
Mitoferrin mfrn	MFRN_DROME	42 kDa	0	0	0	0	1	8	
Proteasome subunit alpha type-7-1 Prosalpha4	PSA71_DROME	28 kDa	0	0	6	0	0	0	
LD46175p sea	Q7KSQ0_DROME	34 kDa	0	0	0	0	0	5	
CG6356 CG6356	Q9VCA0_DROME	63 kDa	0	0	0	0	0	6	
Heavy metal tolerance factor 1 Hmt-1	Q9VF20_DROME	98 kDa	0	0	0	3	0	0	
Carboxylic ester hydrolase alpha-Est7	Q9VIB5_DROME	65 kDa	0	0	0	0	1	5	
Delta-aminolevulinic acid dehydratase Pbgs	Q9VTV9_DROME	36 kDa	0	1	0	0	6	0	
Protein unzipped uzip	UZIP_DROME	54 kDa	0	0	0	0	3	10	
CG4829-PB, isoform B CG4829	Q7KUX2_DROME (+1)	88 kDa	0	0	0	1	5	1	
V-type proton ATPase subunit a Vha100-5	Q9VKF6_DROME	93 kDa	0	0	0	9	0	0	
Probable peroxisomal acyl-coenzyme A oxidase 1 CG5009	ACOX1_DROME	74 kDa	0	0	0	0	0	3	
Phosphoribosylformylglycinamidine synthase ade2	PUR4_DROME	148 kDa	0	0	0	0	0	2	
GH09263p Aats-gly	Q961R8_DROME (+1)	76 kDa	0	0	0	0	0	3	
Glycerol-3-phosphate dehydrogenase [NAD(+)] Gpdh	M9PC43_DROME	39 kDa	0	0	0	0	1	2	
Transmembrane emp24 domain-containing protein bai bai	TMEDA_DROME	24 kDa	0	0	0	0	0	2	
CG5214 CG5214	Q9VGQ1_DROME	50 kDa	0	0	0	0	2	4	
Opsin Rh1 ninaE	OPS1_DROME	41 kDa	0	2	0	4	3	2	
Integrin alpha-PS3 scb	ITA3_DROME	125 kDa	0	0	0	3	1	0	
CG4086-PA Su(P)	Q9V420_DROME	47 kDa	0	0	0	0	1	3	
CG14309 CG14309	Q9VE79_DROME	111 kDa	0	0	0	0	2	0	
Cluster of cAMP-dependent protein kinase type II regulatory subunit Pka-R2 (KAPR2_	KAPR2_DROME	43 kDa	0	0	0	0	3	0	
Cluster of GH13304p Pglym78 (Q9VAN7_DROME)	Q9VAN7_DROME	29 kDa	0	0	0	0	1	5	
Cluster of CG42235, isoform C CG8951 (Q9VBK2_DROME)	Q9VBK2_DROME	74 kDa	0	0	0	0	3	2	
Cluster of CG18135-PD, isoform D CG18135 (Q86BI9_DROME)	Q86BI9_DROME [2]	87 kDa	0	0	0	0	0	6	
Cluster of Proteasome subunit beta type Prosbeta2 (Q9VUJ1_DROME)	Q9VUJ1_DROME	30 kDa	0	0	6	0	0	0	
CG1648, isoform A CG1648	Q7K2P3_DROME	24 kDa	0	0	0	1	5	4	
CG12787-PB, isoform B hoe1	Q8I930_DROME (+2)	91 kDa	0	1	0	8	0	0	
CG31548 CG31548	Q8IPP8_DROME	27 kDa	0	0	0	0	4	9	
CG40042 Tim23	Q8MRW1_DROME	22 kDa	0	0	0	1	4	7	
CG3940, isoform A CG3940	Q9VH26_DROME	34 kDa	0	0	0	0	5	9	
AT14148p CG2604	Q9VN86_DROME	47 kDa	0	0	0	1	2	5	
T-complex protein 1 subunit gamma Cctgamma	TCPG_DROME	59 kDa	0	5	0	0	0	0	
14-3-3 protein zeta 14-3-3zeta	1433Z_DROME	28 kDa	1	2	0	0	0	4	
Cytochrome b5 Cyt-b5	CYB5_DROME	15 kDa	0	0	0	0	5	6	
CG8768 CG8768	Q8T0N5_DROME	33 kDa	0	0	0	0	2	6	
CG16985 protein CG16985	Q9VZZ6_DROME	16 kDa	0	0	0	2	4	6	
Juvenile hormone epoxide hydrolase 1 Jheh1	Q7JRC3_DROME	55 kDa	0	0	0	0	2	3	
Congested-like trachea protein colt	COLT_DROME	33 kDa	1	1	1	1	3	5	
LP14331p Mdr50	Q5BI62_DROME	145 kDa	0	0	0	2	2	0	
CG7382 CG7382	Q9VMR0_DROME	27 kDa	0	0	0	0	3	2	
Protein PTCD3 homolog, mitochondrial CG4679	PTCD3_DROME	74 kDa	1	0	0	3	0	0	
Uncharacterized protein CG7065 CG7065	Y7065_DROME	137 kDa	0	0	0	0	2	0	
Inositol-3-phosphate synthase Inos	INO1_DROME	62 kDa	0	0	0	0	0	7	
Transient receptor potential cation channel protein painless pain	PAIN_DROME	104 kDa	0	1	10	0	0	0	
Proteasome subunit alpha type-1 Prosalpha6	PSA1_DROME	31 kDa	0	0	9	0	0	0	
CG11665, isoform A CG11665	Q7JWI7_DROME	72 kDa	0	0	0	0	10	0	
Proteasome subunit beta type Prosbeta5	Q7K148_DROME	31 kDa	0	0	11	0	0	0	
CG9380, isoform D CG9380	Q8MLN4_DROME	93 kDa	0	0	0	0	2	6	

CG9547 CG9547	Q9VMC6_DROME	46 kDa	0	0	0	0	0	6	
CG3842, isoform A CG3842-RA	Q9W404_DROME	45 kDa	0	0	0	0	1	7	
Transmembrane protein 70 homolog, mitochondrial CG7506	TMM70_DROME	27 kDa	3	0	6	0	0	1	
UNC93-like protein CG4928	UN93L_DROME (+1)	59 kDa	0	0	0	0	2	6	
CG2943, isoform A CG2943	Q9VHY6_DROME	101 kDa	0	0	0	4	0	0	
Transmembrane emp24 domain-containing protein eca eca	TMEDE_DROME	25 kDa	0	0	0	0	2	6	
Vesicular acetylcholine transporter VAChT	VACHT_DROME	64 kDa	0	0	0	0	0	6	
GH24511p Uba1	Q8T0L3_DROME	131 kDa	0	0	0	0	2	3	
Protein jagunal jagn	JAGN_DROME	23 kDa	0	1	1	2	4	4	
CG10075 CG10075	Q9VRZ7_DROME	29 kDa	0	0	0	0	3	3	
Putative cysteine proteinase CG12163 CG12163	CPR1_DROME	69 kDa	0	0	0	0	0	3	
ADP/ATP translocase Ant2	O62526_DROME	34 kDa	3	8	6	8	10	14	
Cluster of CTL-like protein 1 CG1311 (CTLH1_DROME)	CTLH1_DROME [2]	77 kDa	0	0	0	0	0	5	
Cluster of LP11544p Mal-A5 (Q5U124_DROME)	Q5U124_DROME [2]	72 kDa	0	0	0	0	0	2	
Actin-related protein 2 Arp2	ARP2_DROME	45 kDa	0	0	0	0	6	0	
Actin-related protein 2/3 complex subunit 2 Arpc2	ARPC2_DROME	35 kDa	0	0	0	0	6	0	
Glutactin Glt	GLT_DROME	119 kDa	0	0	0	0	5	0	
NADH dehydrogenase (ubiquinone) complex I, assembly factor 6 homolog sicily	NDUF6_DROME	38 kDa	0	0	0	0	1	5	Assembly Fac
Proteasome subunit beta type-4 Prosbeta7	PSB4_DROME	30 kDa	0	0	4	0	0	0	
LP01562p veil	Q7K0L5_DROME	65 kDa	0	0	0	0	1	6	
BcDNA.GH04962 GCS2alpha	Q7KMM4_DROME	106 kDa	0	0	0	0	6	0	
Valyl-tRNA synthetase, isoform C Aats-val	A0A0B4KF06_DROME (+1	119 kDa	0	0	0	0	0	4	
CG3566-PB, isoform B CG3566	Q8IRR0_DROME	13 kDa	0	0	0	0	4	4	
CG17221, isoform C CG17221	Q8IPZ3_DROME	45 kDa	4	1	0	0	0	3	
LD21102p Ugt35a	Q9VGS9_DROME	61 kDa	0	0	0	0	0	3	
Cytochrome c oxidase assembly factor 3, mitochondrial Ccdc56	COA3_DROME	10 kDa	0	0	0	0	2	3	
CG9577 CG9577	Q9W5W8_DROME	34 kDa	0	0	0	1	7	2	
Serine/threonine-protein phosphatase PP2A 65 kDa regulatory subunit Pp2A-29B	2AAA_DROME	65 kDa	0	0	0	0	0	2	
28S ribosomal protein S15, mitochondrial bonsai	RT15_DROME	33 kDa	3	2	0	0	0	0	
Phosrestin-1 Arr2	ARRB_DROME	45 kDa	0	1	0	2	1	3	
Ubiquitin carboxyl-terminal hydrolase 7 Usp7	UBP7_DROME (+1)	130 kDa	0	0	0	0	3	0	
AT01345p CG12736	Q7K3V6_DROME	50 kDa	0	0	0	0	2	3	
CG11752-PA CG11752 (dNDUFV3)	Q9VZ01_DROME	11 kDa	0	3	1	0	4	3	
Scavenger receptor acting in neural tissue and majority of rhodopsin is absent, isoforr	Q9VM10_DROME	63 kDa	0	0	0	0	1	2	
Probable cysteine desulfurase, mitochondrial CG12264	NFS1_DROME	51 kDa	0	0	0	0	0	4	
Protein NipSnap Nipsnap	NIPSN_DROME	32 kDa	0	0	0	0	1	6	
CG8298, isoform A CG8298	Q7JY99_DROME	66 kDa	0	0	2	6	0	0	
CG7888, isoform A CG7888	Q7YTZ0_DROME (+1)	51 kDa	0	0	0	0	2	5	
CG6126 CG6126	Q961R9_DROME	61 kDa	0	0	0	0	0	7	
CG10361 CG10361-RA	Q9VTN9_DROME	46 kDa	0	0	0	0	0	7	
Vacuolar protein sorting-associated protein 26 Vps26	VPS26_DROME	53 kDa	0	0	0	0	4	0	
Proteasome subunit alpha type-3 Prosalpha7	PSA3_DROME	28 kDa	0	0	5	0	0	0	
Glutamate carrier 1, isoform A GC1	Q9VGF7_DROME	35 kDa	0	0	0	0	2	3	
Probable cytochrome P450 6d5 Cyp6d5	CP6D5_DROME	57 kDa	0	0	0	0	1	3	
CG6484 CG6484	Q7K3P6_DROME	50 kDa	0	0	1	0	1	4	
CG7033 CG7033	Q9W392_DROME	58 kDa	0	3	0	0	0	0	
FI02825p VhaM9.7-b	Q9VP18_DROME	10 kDa	0	0	0	11	0	0	
CG11679 CG11679	Q9VXQ8_DROME	48 kDa	0	0	0	3	1	0	
CG11655 CG11655	Q9VXV4_DROME	50 kDa	0	0	0	0	0	3	
Sodium/potassium-transporting ATPase subunit alpha JYalpha	A8QI34_DROME	112 kDa	2	3	12	10	19	11	
Cluster of AT09608p CG30491;CG30495 (Q7JUS1_DROME)	Q7JUS1_DROME [3]	37 kDa	0	0	0	0	2	3	
Cluster of G protein alpha s subunit Galphas (GNAS_DROME)	GNAS_DROME [2]	45 kDa	0	0	0	2	4	4	
Cluster of CG42708, isoform H GLS (Q1RL13_DROME)	Q1RL13_DROME [5]	85 kDa	0	0	0	0	0	3	
Cluster of Glucosamine-6-phosphate isomerase Gnpda1 (GNPI_DROME)	GNPI_DROME [2]	31 kDa	0	0	0	0	2	6	
Cluster of AQP7777 transcript variant D CG7777 (J7K3P9_DROME)	J7K3P9_DROME [2]	28 kDa	0	0	0	1	5	0	
BcDNA.GH03016 Rh50	Q9V3T3_DROME	48 kDa	0	0	0	0	6	0	

CG16986, isoform B CG16986-RA	Q9VZZ5_DROME	16 kDa	0	0	0	1	2	4	
UDP-glucuronosyltransferase BEST:GH09393	Q9W2J4_DROME	60 kDa	0	0	0	0	0	6	
Probable trans-2-enoyl-CoA reductase, mitochondrial CG16935	MECR_DROME	39 kDa	0	0	0	0	1	5	
BcDNA.GH10229 BcDNA.GH10229	Q9Y114_DROME	71 kDa	0	0	0	0	0	3	
Sodium/hydrogen exchanger Nhe3	A8DYW5_DROME	77 kDa	0	0	0	0	3	0	
CG9921, isoform B CG9921	Q9VXH4_DROME	11 kDa	0	0	0	0	7	0	
CG5167 CG5167	Q9VG81_DROME	47 kDa	0	0	0	0	2	4	
CG42497 Tim10-RA	E1JGR3_DROME	7 kDa	0	0	0	0	6	2	
CG9249-PA CG9249	Q9VIF3_DROME	34 kDa	2	0	0	0	0	3	
V-type proton ATPase subunit a Vha100-4	Q9VE77_DROME	97 kDa	0	0	0	5	0	0	
Chitinase-like protein Idgf3 Idgf3	IDGF3_DROME (+1)	49 kDa	0	0	0	1	1	3	
Microtubule-associated protein 205, isoform C Map205	A0A0B4KI71_DROME (+2	118 kDa	0	0	0	3	0	0	
Cytochrome P450 6g1 Cyp6g1	CP6G1_DROME	60 kDa	0	0	0	0	0	2	
Cofilin/actin-depolymerizing factor homolog tsr	CADF_DROME	17 kDa	0	0	0	0	2	3	
Protein windpipe wdp order	WDP_DROME	75 kDa	0	2	0	0	3	0	
CG12858, isoform A CG12858	A1Z9U2_DROME	83 kDa	0	0	0	0	0	8	
Fatty acid (Long chain) transport protein, isoform D Fatp	E1JHE4_DROME (+1)	75 kDa	0	0	0	0	0	5	
Putative hydroxypyruvate isomerase Gip	HYI_DROME	29 kDa	0	0	0	0	0	9	
CG1105 CG1105	Q9VI53_DROME	46 kDa	0	0	0	0	0	5	
Proteasome subunit beta type Prosbeta4	Q9VJJ0_DROME	22 kDa	0	0	5	0	0	0	
CG8323 CG8323	Q7JZE8_DROME	33 kDa	0	0	0	0	0	5	
CG5991, isoform A CG5991	Q9VCE0_DROME	50 kDa	0	0	0	0	2	5	
Calcium/calmodulin-dependent protein kinase II, isoform C CaMKII	A4V133_DROME (+3)	55 kDa	3	0	0	0	0	0	
Alpha-soluble NSF attachment protein alphaSnap	SNAP_DROME	33 kDa	0	0	0	0	0	3	
CG1041, isoform B CRAT	Q0KIA8_DROME (+1)	74 kDa	0	0	0	0	0	4	
Muscle-specific protein 20 Mp20	MP20_DROME	20 kDa	0	0	0	1	4	1	
26S proteasome regulatory complex subunit p48B Rpt1	Q7KMQ0_DROME	49 kDa	3	0	0	0	0	0	
Heat shock protein 23 Hsp23	HSP23_DROME	21 kDa	0	0	0	2	4	2	
No extended memory, isoform C nemy order	Q0E9A2_DROME (+2)	24 kDa	0	2	0	2	2	3	
CG32638 CG32638-RB	Q8IR72_DROME	18 kDa	0	0	0	0	2	6	
CG3902-PA CG3902-RA	Q9VVU1_DROME	45 kDa	0	0	0	0	0	3	
Arc42 Arc42	Q9VDT1_DROME	44 kDa	0	0	0	0	2	3	
Adenylosuccinate lyase AdSL	Q9VEP6_DROME	54 kDa	0	0	0	0	0	4	
FI02870p Jheh2	Q7KB18_DROME	52 kDa	0	0	0	0	0	2	
Maltase A2 Mal-A2	MAL2_DROME	65 kDa	0	0	2	0	0	0	
Calnexin 14D Cnx14D	Q9VXF6_DROME	73 kDa	0	0	0	0	4	0	
Cluster of CG6767, isoform B CG6767 (Q9VT33_DROME)	Q9VT33_DROME [2]	43 kDa	0	0	0	0	2	0	
Cluster of Troponin I wupA (TNNI_DROME)	TNNI_DROME	30 kDa	0	0	0	0	0	2	
Cluster of CG1607, isoform A CG1607 (Q9V9Y0_DROME)	Q9V9Y0_DROME	55 kDa	0	0	0	0	4	0	
Cluster of GH27579p grsm (Q9V3D8_DROME)	Q9V3D8_DROME [2]	60 kDa	0	0	0	0	0	5	
Proteasome subunit alpha type-5 Prosalpha5	PSA5_DROME	27 kDa	0	0	7	0	0	0	
CG7781, isoform B CG7781	Q9VLP2_DROME	16 kDa	0	0	0	0	8	0	
CG3036, isoform A CG3036	Q9VR44_DROME	54 kDa	0	0	0	0	0	7	
Actin-related protein 2/3 complex subunit 3 Arpc3A	Q9VF28_DROME	20 kDa	0	0	0	0	5	0	
Myosin light chain alkali Mlc1	MLC1_DROME	18 kDa	0	0	0	1	2	4	
GH19566p nSyb	Q86BQ0_DROME	15 kDa	0	0	0	0	3	4	
HL04706p wtrw	Q9VHY7_DROME	110 kDa	0	3	0	0	0	0	
Maltase A8 Mal-A8	A1Z7F3_DROME	67 kDa	0	5	6	5	0	0	
Dolichyl-diphosphooligosaccharide--protein glycosyltransferase 48 kDa subunit Ost48	OST48_DROME	50 kDa	0	0	2	0	0	0	
CG16700-PA CG16700-RA	Q9VX84_DROME	51 kDa	0	0	0	0	2	3	
ATP7, isoform B ATP7	Q9VYT4_DROME	136 kDa	0	0	0	0	3	0	
Cytochrome c oxidase subunit 3 mt:CoIII	COX3_DROME	30 kDa	0	0	0	4	4	0	
CG9034, isoform A CG9034	Q9W380_DROME	8 kDa	1	3	0	0	0	0	
CG15631-PA CG15631	Q9VR24_DROME	70 kDa	0	0	0	0	2	0	
CG11423 ND-51L1	A1ZAW7_DROME	77 kDa	2	6	0	0	0	0	
Aconitate hydratase, mitochondrial CG4706	Q8T4D6_DROME	85 kDa	0	0	1	0	4	0	

Asrij, isoform B asrij	A0A0B4KF31_DROME (+1	29 kDa	0	0	0	0	4	0	
CG6028 CG6028	Q95SI7_DROME	32 kDa	0	0	0	0	0	3	
CG8034, isoform A CG8034	Q9VWJ1_DROME	70 kDa	0	0	0	0	3	0	
EG:80H7.2 protein pck	O76899_DROME	30 kDa	0	5	0	0	0	0	
CG6287-PA CG6287	Q9VKI8_DROME	35 kDa	0	0	0	0	0	3	
Hsc70-interacting protein 1 HIP	F10A1_DROME	41 kDa	0	0	0	0	3	2	
CG1275, isoform D CG1275	Q7KV99_DROME (+2)	27 kDa	0	0	0	0	6	2	
Copper transporter 1B Ctr1B	Q9VHS6_DROME	20 kDa	0	0	0	0	0	3	
Multidrug resistance protein 4 ortholog Mrp4	Q9VGM1_DROME	148 kDa	0	0	0	1	3	0	
CG13404 CG13404	Q9VY41_DROME	18 kDa	0	0	0	0	3	3	
Sideroflexin CG11739	Q9VN13_DROME	36 kDa	0	0	0	0	0	3	
Drab11 Rab11	O18335_DROME	24 kDa	0	0	0	0	1	2	
CG31689, isoform H CG31689	M9PBX3_DROME (+1)	70 kDa	0	0	0	2	3	0	
26S proteasome regulatory complex subunit p50 Rpt5	Q9V3V6_DROME	48 kDa	3	0	0	0	0	0	
26S protease regulatory subunit 8 Rpt6	PRS8_DROME	46 kDa	4	1	0	0	0	0	
Actin-related protein 3 Arp3	ARP3_DROME	47 kDa	0	0	0	0	4	0	
Fructose-1,6-bisphosphatase fbp	Q9VIS3_DROME (+1)	36 kDa	0	0	0	6	0	0	
CG10960, isoform C CG10960	Q8IQH6_DROME	51 kDa	0	0	0	0	0	4	
Aldose 1-epimerase CG10467-RA	Q9VRU1_DROME	40 kDa	0	0	0	0	0	4	
Proteasome subunit beta type-1 Prosbeta6	PSB1_DROME	26 kDa	0	0	3	0	0	0	
Proteasome subunit alpha type-2 Prosalpha2	PSA2_DROME	26 kDa	0	0	3	0	0	0	
CG8773 CG8773-RB	Q9VFX0_DROME	111 kDa	0	0	0	3	0	0	
CG9248, isoform A CG9248	Q9VIF2_DROME	56 kDa	0	0	0	0	0	2	
CG1636, isoform A CG1636	Q9W3G7_DROME (+1)	45 kDa	0	0	0	0	3	4	
Amphiphysin Amph	Q7KLE5_DROME	66 kDa	0	0	0	0	1	3	
Tim17b, isoform A Tim17b	Q7PLT4_DROME	18 kDa	0	0	0	0	0	4	
Cysteine string protein, isoform F Csp	D0IQJ8_DROME (+1)	27 kDa	0	0	0	0	0	6	
RIC-3, isoform T RIC-3	A0A0B4KFX1_DROME	38 kDa	0	0	0	3	0	0	
CG17739 CG17739	Q7K3Y9_DROME	98 kDa	0	0	0	2	0	0	
CG4053 CG4053	Q9VEM7_DROME	30 kDa	0	0	0	2	0	0	
Battenin cln3	Q9VVL0_DROME	48 kDa	0	0	0	0	0	3	
RE07815p Ugt58Fa	Q9W228_DROME	59 kDa	0	0	0	0	0	2	
CG9393, isoform B CG9393 order	A0A0B4KGL6_DROME (+1	36 kDa	0	2	0	0	0	0	
CG1090, isoform I CG1090	A0A0B4KGG6_DROME (+	70 kDa	0	0	0	0	0	4	
CG4686, isoform A CG4686	Q9VDT4_DROME	20 kDa	0	0	0	0	0	3	
60S acidic ribosomal protein P0 RpLP0	RLA0_DROME	34 kDa	0	0	0	2	2	0	
CG1665 CG1665-RA	A1Z803_DROME	38 kDa	0	0	0	0	0	3	
CG5103 CG5103-RA	Q9VVP4_DROME	68 kDa	0	2	2	4	2	0	
Cluster of CG42249, isoform B CG42249 (Q9VZ33_DROME)	Q9VZ33_DROME	61 kDa	0	0	0	0	0	2	
CG5915 protein Rab7	O76742_DROME	23 kDa	0	0	0	0	0	3	
Superoxide dismutase [Cu-Zn] Sod	SODC_DROME	16 kDa	0	0	0	0	0	2	
CG1213, isoform A CG1213	Q7JVN6_DROME	53 kDa	0	0	0	0	0	3	
CG15922, isoform A CG15922-RA	Q9VDL5_DROME	7 kDa	0	0	0	0	2	0	
Protein bangles and beads bnb	BNB_DROME	46 kDa	0	0	0	0	3	0	
CG17776, isoform B CG17776	Q9W513_DROME	8 kDa	0	0	0	0	0	4	
Bb in a boxcar, isoform C bbc	A0A0B4K7Y4_DROME (+3	46 kDa	0	0	0	0	2	2	
CG2789-PA Tspo	Q9VPR1_DROME	20 kDa	0	0	0	0	0	3	
Probable Ufm1-specific protease 2 UFSP2	UFSP2_DROME	68 kDa	0	0	0	0	2	0	
CG11857 CG11857	Q9VBU6_DROME	24 kDa	0	0	0	0	2	0	
Organic cation transporter protein Orct	ORCT_DROME	61 kDa	0	0	0	0	0	2	
Serine/threonine-protein phosphatase PP2A mts	PP2A_DROME	35 kDa	0	0	0	0	0	3	
CG2937-PA mRpS2	Q8MSS7_DROME	30 kDa	0	0	0	3	0	0	

CI
CII
CIII
CIV
CV

Table 2.3: Mass spectrometry identifying subcomplexes in *Drosophila* flight muscles, related to Figure 2.5.

The table shows all the peptides identified in the 14 fractions shown in Figure 2.5D

			55-70	70-85	85-100	100-120	120-150	150-180	180-210	210-240	240-260	260-280	280-300	300-320	320-340	340-360	
Identified Proteins (799/836)	**Accession Number**	**Molecular**	**A14**	**A13**	**A12**	**A11**	**A10**	**A9**	**A8**	**A7**	**A6**	**A5**	**A4**	**A3**	**A2**	**A1**	
Cluster of Actin, larval muscle Act79B (ACT4_DROME)	ACT4_DROME [4]	42 kDa	139	131	108	101	72	61	64	49	52	42	39	37	29	28	
ATP synthase subunit beta, mitochondrial ATPsyn-beta	ATPB_DROME (+1)	54 kDa	79	71	66	74	56	47	48	42	40	35	33	37	29	43	
Voltage-dependent anion-selective channel porin	VDAC_DROME	31 kDa	74	65	57	44	30	30	42	39	47	47	52	38	33	31	
Cluster of ADP,ATP carrier protein sesB (ADT_DROME)	ADT_DROME [3]	34 kDa	56	60	61	69	57	62	76	60	64	43	41	26	15	17	
Phosphoglycerate kinase Pgk	PGK_DROME	44 kDa	40	51	51	47	33	31	23	19	21	17	15	8	1	1	
Cluster of PDZ and LIM domain protein Zasp Zasp52 (ZASP_DROME)	ZASP_DROME [4]	238 kDa	49	47	47	57	40	30	37	27	28	28	12	12	11	4	
Cluster of Arginine kinase, isoform E Argk (A8JNP2_DROME)	A8JNP2_DROME [2]	42 kDa	64	46	63	108	136	46	36	31	37	34	29	22	28	18	
CG3731, isoform A UQCR-C1	Q9VFF0_DROME	52 kDa	32	35	12	9	7	7	7	4	3	6	2	2	3	2	
Cluster of Tropomyosin-2 Tm2 (TPM2_DROME)	TPM2_DROME [2]	33 kDa	27	32	37	45	41	34	61	51	43	30	28	31	41	26	
CG9090, isoform A CG9090-RA	Q7JUS9_DROME	41 kDa	35	28	42	66	67	74	89	58	46	25	17	13	6	9	
Cluster of Glycerol-3-phosphate dehydrogenase [NAD(+)] Gpdh (M9PC43_DROME)	M9PC43_DROME [3]	39 kDa	23	28	76	53	15	9	11	9	8	8	7	8	4	5	
GH15296p Scp1	Q8MSI2_DROME	22 kDa	16	28	83	18	8	3	2	1	0	0	0	0	0	0	
Cluster of Glyceraldehyde-3-phosphate dehydrogenase 1 Gapdh1 (G3P1_DROME)	G3P1_DROME [2]	35 kDa	32	26	27	32	35	29	30	25	47	51	26	18	5	6	
Cluster of Pyruvate dehydrogenase E1 component subunit alpha l(1)G0334 (Q9W4H6_	Q9W4H6_DROME [2]	44 kDa	30	26	22	27	18	17	17	31	31	34	23	15	11	8	
Flightin fln	FTN_DROME	21 kDa	23	26	16	22	14	11	9	5	6	6	2	2	3	2	
AT02348p UQCR-C2	Q9VV75_DROME	45 kDa	23	25	29	22	15	16	18	15	15	13	15	9	11	12	
ATP synthase subunit alpha, mitochondrial blw	ATPA_DROME	59 kDa	21	24	26	45	49	59	46	38	32	26	22	24	22	47	
Cluster of Aconitate hydratase, mitochondrial Acon (Q9VIE8_DROME)	Q9VIE8_DROME [2]	85 kDa	22	21	16	14	10	65	70	57	39	24	15	4	6	4	
CG32230, isoform B ND-MLRQ	Q8SYJ2_DROME	9 kDa	27	21	23	23	20	19	18	16	11	11	9	10	13	30	
Alpha-amylase Amy-p	A0A0B4LGS0_DROME (+1)	54 kDa	10	20	13	3	0	0	0	0	0	0	0	0	0	0	
Cluster of Tubulin beta-1 chain betaTub56D (TBB1_DROME)	TBB1_DROME [5]	50 kDa	8	19	36	45	27	16	18	12	13	12	6	7	3	2	
Probable isocitrate dehydrogenase [NAD] subunit alpha, mitochondrial l(1)G0156	IDH3A_DROME	41 kDa	19	19	15	20	10	9	4	6	7	3	2	0	2	0	
Cluster of Succinyl-CoA ligase [ADP/GDP-forming] subunit alpha, mitochondrial Scsalph	SUCA_DROME	34 kDa	17	18	19	24	18	16	18	16	18	17	16	10	11	12	
Cluster of LP07226p mge (Q9VZL1_DROME)	Q9VZL1_DROME [2]	16 kDa	17	18	16	14	11	6	10	7	5	5	2	2	2	5	
Cluster of Calcium-transporting ATPase sarcoplasmic/endoplasmic reticulum type Ca-P	ATC1_DROME [2]	112 kDa	16	17	15	25	19	20	30	60	116	220	346	290	194	123	
Fructose-bisphosphate aldolase Ald	A4V3G1_DROME (+2)	40 kDa	21	17	16	10	3	2	7	3	6	6	8	6	4	12	
CG5903, isoform A CG5903	Q9VEY5_DROME	24 kDa	18	17	15	19	13	15	14	7	7	2	0	1	0	0	
CG5028, isoform C CG5028-RC	A8JRB8_DROME (+2)	43 kDa	13	17	13	12	4	3	4	4	1	1	1	1	1	2	
Muscle LIM protein Mlp84B Mlp84B	MLP2_DROME	54 kDa	13	17	21	14	2	1	3	2	1	2	2	0	0	0	
Electron transfer flavoprotein-ubiquinone oxidoreductase, isoform A Etf-QO	Q7JWF1_DROME	66 kDa	21	16	31	40	33	34	33	30	20	6	5	1	1	1	
Cluster of Tubulin alpha-1 chain alphaTub84B (TBA1_DROME)	TBA1_DROME [2]	50 kDa	12	16	18	22	16	16	15	15	17	12	8	2	0	1	
Cytochrome c-2 Cyt-c-p	CYC2_DROME	12 kDa	16	16	16	14	11	7	10	7	7	5	6	6	5	4	
Alpha-mannosidase LManV	Q9VLI0_DROME	112 kDa	0	16	32	8	0	0	0	0	0	0	0	0	0	0	
Carboxylic ester hydrolase alpha-Est7	Q9VIB5_DROME	65 kDa	11	15	15	18	16	16	14	13	11	4	1	1	1	0	
Cluster of GH13304p Pglym78 (Q9VAN7_DROME)	Q9VAN7_DROME [2]	29 kDa	20	15	17	13	13	13	20	9	8	4	4	2	0	0	
ATP synthase subunit O, mitochondrial ATPsynO	ATPO_DROME	22 kDa	18	15	14	10	11	5	4	6	5	4	3	0	2	0	
Cluster of Glutathione S-transferase S1 GstS1 (GSTS1_DROME)	GSTS1_DROME [2]	28 kDa	45	15	9	7	5	2	2	2	2	2	1	1	1	0	
ATP synthase subunit b, mitochondrial ATPsynB	AT5F1_DROME	27 kDa	19	14	18	20	14	14	15	13	10	8	5	2	4	2	
Glutamine synthetase 2 cytoplasmic Gs2	GLNA2_DROME (+1)	41 kDa	22	14	19	15	9	8	7	5	2	4	3	1	1	2	
Cluster of V-type proton ATPase catalytic subunit A isoform 2 Vha68-2 (VATA2_DROME	VATA2_DROME [2]	68 kDa	31	14	15	27	16	11	11	10	6	3	2	2	1	1	
14-3-3 protein zeta 14-3-3zeta	1433Z_DROME	28 kDa	16	14	13	14	15	11	12	9	5	4	3	1	2	1	
Probable trans-2-enoyl-CoA reductase, mitochondrial CG16935	MECR_DROME	39 kDa	19	14	12	3	2	1	1	3	0	0	0	0	0	0	
Stretchin-Mlck, isoform R Strn-Mlck	A1ZA73_DROME	215 kDa	15	13	17	23	24	38	52	50	56	59	44	46	40	30	
ATP synthase subunit gamma, mitochondrial ATPsyngamma	ATPG_DROME	33 kDa	14	13	15	10	10	6	5	8	6	12	8	8	15	30	
ATP synthase subunit d, mitochondrial ATPsynD	ATP5H_DROME	20 kDa	20	13	9	12	9	6	5	2	2	4	4	2	5	7	
CG1648, isoform B CG1648	A1Z7Z4_DROME (+1)	24 kDa	8	12	22	25	8	6	4	5	4	2	2	0	0	0	
Glutamate dehydrogenase, mitochondrial Gdh	DHE3_DROME	63 kDa	5	11	11	19	13	14	14	15	19	13	12	11	71	85	
Cluster of Ubiquitin-40S ribosomal protein S27a RpS27A (RS27A_DROME)	RS27A_DROME [3]	18 kDa	7	11	19	11	3	3	5	7	6	6	2	0	1	2	
Cluster of Cytochrome b-c1 complex subunit 7 UQCR-14 (Q9VXI6_DROME)	Q9VXI6_DROME	14 kDa	16	11	6	5	1	1	0	3	4	4	6	0	0	0	
Trehalose 6-phosphate phosphatase CG5177	Q9VM18_DROME	31 kDa	13	11	10	10	3	2	1	1	0	1	0	0	0	0	
Fatty acid bindin protein, isoform C fabp	Q8INK3_DROME (+1)	17 kDa	6	11	8	0	0	0	0	0	0	0	0	0	0	0	
Succinate dehydrogenase [ubiquinone] iron-sulfur subunit, mitochondrial SdhB	SDHB_DROME	34 kDa	11	10	10	11	9	31	37	31	33	35	41	25	18	14	
Cluster of Elongation factor 1-alpha 2 Ef1alpha100E (EF1A2_DROME)	EF1A2_DROME [2]	51 kDa	18	10	24	31	24	17	18	16	14	14	11	9	7	5	
Mitochondrial import inner membrane translocase subunit TIM50-C ttm50	TI50C_DROME	50 kDa	10	10	11	12	6	5	9	5	6	5	3	5	4	4	
CG14997, isoform A CG14997	Q9VZF6_DROME	51 kDa	6	10	8	10	6	11	12	6	4	4	2	2	0	0	
CG10639, isoform A CG10639-RA	Q9VJ28_DROME	50 kDa	9	10	6	10	7	5	4	6	2	0	0	0	0	0	
Elongation factor Tu EfTuM	A1Z9E3_DROME	54 kDa	11	10	14	12	7	5	4	3	2	1	0	0	1	0	
Glutathione S-transferase D1 GstD1	GSTD1_DROME	24 kDa	13	10	9	8	4	3	1	1	1	1	0	0	1	1	
V-type proton ATPase subunit B Vha55	VATB_DROME	55 kDa	10	10	8	12	3	4	2	0	0	0	0	0	1	0	
Protein l(2)37Cc l(2)37Cc	L2CC_DROME	30 kDa	10	10	8	3	1	1	1	0	0	0	0	0	0	0	
Protein anoxia up-regulated fau	FAU_DROME	69 kDa	10	10	6	2	4	3	2	2	0	0	0	0	0	0	
CG4769, isoform A Cyt-c1	Q9VRL0_DROME	34 kDa	10	9	12	8	11	9	9	9	11	10	10	7	8	9	
CG30415, isoform A CG30415	Q0E8X7_DROME	10 kDa	5	9	9	10	5	5	5	5	5	0	3	2	0	0	
Prohibitin 2, isoform E Phb2	A8DYI6_DROME (+2)	37 kDa	13	9	9	12	3	5	5	3	2	3	2	2	1	2	
Muscle-specific protein 20 Mp20	MP20_DROME	20 kDa	9	9	7	7	4	3	4	4	3	3	2	2	0	2	

Cluster of Lipid storage droplet-2, isoform D Lsd-2 (Q0KHS6_DROME)	Q0KHS6_DROME [3]	36 kDa	5	9	12	14	5	4	2	1	1	0	0	0	0	0	
Cluster of Peroxiredoxin 2540-2 Prx2540-2 (Q7JX87_DROME)	Q7JX87_DROME [2]	25 kDa	10	9	7	4	0	0	0	0	0	0	0	0	0	0	0	
Cluster of Tropomyosin-1, isoforms 33/34 Tm1 (TPM4_DROME)	TPM4_DROME [4]	55 kDa	10	8	15	25	21	39	55	50	37	20	22	31	48	29		
Cluster of Myosin heavy chain, isoform T Mhc (M9NEP1_DROME)	M9NEP1_DROME [3]	224 kDa	17	8	9	19	12	11	13	9	14	18	18	9	9	8		
Heat shock 70 kDa protein cognate 4 Hsc70-4	HSP7D_DROME	71 kDa	10	8	9	8	13	42	58	46	39	19	15	15	13	10		
Isocitrate dehydrogenase [NADP] Idh	Q7KUB1_DROME	53 kDa	5	8	12	22	30	25	23	13	13	5	4	1	1	0		
Cluster of FI01544p Rab1 (O18332_DROME)	O18332_DROME [8]	23 kDa	14	8	12	15	10	9	12	12	9	9	6	5	2	2		
Probable medium-chain specific acyl-CoA dehydrogenase, mitochondrial CG12262	ACADM_DROME	46 kDa	8	8	8	9	3	1	2	43	34	7	5	2	0	0		
Cytochrome c heme lyase, isoform A Cchl	Q9VD55_DROME	32 kDa	13	8	10	11	14	12	16	12	8	12	5	3	0	1		
LD12946p MSBP	Q9VXM4_DROME	28 kDa	5	8	10	13	11	12	15	15	15	12	10	7	6	4		
Ferrochelatase, mitochondrial FeCh	HEMH_DROME	44 kDa	14	8	7	13	6	9	5	8	6	2	4	1	1	0		
CG3566, isoform D CG3566	M9NEX3_DROME (+2)	12 kDa	10	8	9	12	10	9	10	8	6	2	2	2	0	0		
Protein disulfide-isomerase (Fragment) ERp60	Q3YMU0_DROME	55 kDa	5	8	12	15	9	5	1	1	0	0	0	0	0	0		
CG5355 CG5355	Q9VKW5_DROME	86 kDa	0	8	27	2	1	0	0	0	0	0	0	0	0	0		
Adenylate kinase Adk2	KAD2_DROME	27 kDa	10	8	7	6	0	0	1	0	0	0	0	0	0	0		
AT09608p CG30491;CG30495	Q7JUS1_DROME	37 kDa	10	8	6	5	0	1	3	0	0	0	0	0	0	0		
BcDNA.GH10614 BcDNA.GH10614	Q9Y112_DROME	36 kDa	12	8	4	2	0	0	0	0	0	0	0	0	0	0		
CG10550, isoform B CG10550	Q9VBS7_DROME	49 kDa	2	8	0	0	0	0	0	0	0	0	0	0	0	0		
Cluster of IP16036p Zasp66 (Q058U1_DROME)	Q058U1_DROME [4]	42 kDa	7	8	0	3	2	0	0	0	0	0	0	0	0	0		
RH44771p SdhC	Q9VGS3_DROME	19 kDa	9	8	10	14	11	**12**	**15**	**10**	**12**	**14**	**13**	**12**	7	3		
Cluster of Stretchin-Mlck, isoform S Strn-Mlck (A0A0B4KF84_DROME)	A0A0B4KF84_DROME [4]	919 kDa	6	8	8	11	10	12	15	15	14	13	12	11	8	6		
V-type proton ATPase catalytic subunit A isoform 1 Vha68-1	VATA1_DROME	68 kDa	15	8	12	17	15	10	6	10	4	3	2	1	1	1		
Succinate dehydrogenase [ubiquinone] flavoprotein subunit, mitochondrial SdhA	SDHA_DROME	72 kDa	4	7	19	42	45	**76**	**100**	**80**	**94**	**133**	**127**	**75**	43	26		
Cluster of Reticulon-like protein Rtnl1 (E1JHT6_DROME)	E1JHT6_DROME [5]	65 kDa	11	7	9	20	21	24	31	24	11	5	4	3	5	13		
MIP08013p1 Mpcp	Q0E8E8_DROME	39 kDa	7	7	12	24	21	29	33	21	14	5	4	1	1	1		
CG11876, isoform A CG11876	Q7K5K3_DROME	39 kDa	9	7	8	7	8	7	7	9	9	11	7	4	3	2		
Putative ATP synthase subunit f, mitochondrial CG4692	ATPK_DROME	12 kDa	8	7	7	7	6	6	7	7	7	7	3	2	6	7		
Glutathione peroxidase PHGPx	Q8IRD3_DROME	26 kDa	8	7	6	4	4	4	4	4	1	0	0	0	0	0		
1,4-Alpha-Glucan branching enzyme AGBE	A1Z992_DROME	79 kDa	0	7	43	3	0	0	0	0	0	0	0	0	0	0		
CG6084, isoform D CG6084	M9PI17_DROME (+1)	36 kDa	8	7	4	4	2	2	2	0	0	0	0	0	0	0		
Nucleoside diphosphate kinase awd	A0A0B4LHX6_DROME (+1)	19 kDa	6	7	4	2	0	0	0	0	0	1	4	3	5	6		
CG6439, isoform A CG6439	Q9VD58_DROME	40 kDa	10	7	4	6	3	3	3	2	0	1	1	0	1	0		
40S ribosomal protein S14 RpS14a	RS14_DROME	16 kDa	9	7	5	5	1	0	0	0	0	0	0	0	0	0		
Peptidyl-prolyl cis-trans isomerase Cyp1	PPIA_DROME	25 kDa	10	7	3	2	0	0	0	0	0	0	0	0	0	0		
CG14482, isoform A UQCR-6.4	Q500Y7_DROME	6 kDa	5	7	4	4	4	4	3	4	3	2	2	1	2	2		
CG11752-PA CG11752	Q9VZ01_DROME	11 kDa	6	7	6	6	4	3	1	4	2	1	0	0	1	0	dNDUFV3	
Cluster of CG5174, isoform B CG5174 (A1ZB83_DROME)	A1ZB83_DROME [2]	39 kDa	6	6	8	12	11	5	7	5	2	0	0	0	0	0		
60S acidic ribosomal protein P0 RpLP0	RLA0_DROME	34 kDa	8	6	4	4	4	4	3	4	3	4	5	4	6	4		
C-type lectin 27kD, isoform B Clect27	Q8SZK9_DROME	26 kDa	10	6	8	7	2	2	4	4	4	3	2	1	1	0		
Polyadenylate-binding protein pAbp	PABP_DROME	70 kDa	5	6	11	8	1	3	2	0	0	0	0	0	0	0		
Cluster of Muscle LIM protein at 60A, isoform B Mlp60A (B7YZP9_DROME)	B7YZP9_DROME [2]	53 kDa	4	6	8	4	3	1	1	1	0	1	2	0	0	0		
CG2658, isoform A CG2658	Q9W4W8_DROME	90 kDa	5	6	1	1	1	1	0	0	0	0	0	0	0	1		
40S ribosomal protein S3a RpS3A	RS3A_DROME	30 kDa	4	6	1	1	0	0	0	0	0	0	0	0	0	0		
4-hydroxyphenylpyruvate dioxygenase CG11796	Q9VPF3_DROME	43 kDa	0	6	0	0	0	0	0	0	0	0	0	0	0	0		
Cluster of Paramyosin, long form Prm (MYSP1_DROME)	MYSP1_DROME [2]	102 kDa	5	6	6	11	12	15	15	12	7	7	3	6	9	44		
Succinyl-CoA ligase subunit beta skap	Q95U38_DROME (+1)	55 kDa	4	6	11	9	8	12	15	17	11	8	6	3	4	2		
MICOS complex subunit MIC13 homolog CG7603	MIC13_DROME	14 kDa	11	6	8	5	6	6	6	5	3	1	0	0	0	0		
Peroxiredoxin 3 Prx3	Q9VEJ0_DROME	26 kDa	3	6	5	2	0	0	0	0	0	0	0	0	0	0		
Probable galactose-1-phosphate uridylyltransferase Galt	GALT_DROME	40 kDa	5	6	0	3	0	0	0	0	0	0	0	0	0	0		
CG6459 protein P32	Q7JXC4_DROME	29 kDa	0	6	2	0	0	0	0	0	0	0	0	0	0	0		
NADH dehydrogenase [ubiquinone] 1 alpha subcomplex subunit 10, mitochondrial ND-	NDUAA_DROME	47 kDa	9	6	7	6	1	2	0	1	0	0	0	0	0	0	FA10	
Cytochrome b-c1 complex subunit Rieske, mitochondrial RFeSP	Q9VQ29_DROME	25 kDa	5	6	8	5	5	7	5	7	2	1	0	0	0	0		
IP09655p Mdh2	Q9VEB1_DROME	35 kDa	7	6	5	5	3	24	78	100	95	73	40	25	25	23		
Alpha-mannosidase LManVI	Q9VLH9_DROME	115 kDa	0	6	45	22	0	0	0	0	0	0	0	0	0	0		
CG2720-PA Hop	Q9VPN5_DROME	56 kDa	5	5	5	10	14	11	8	1	2	0	0	0	0	0		
V-type proton ATPase subunit E Vha26	VATE_DROME	26 kDa	11	5	4	7	2	0	1	1	0	0	0	0	0	0		
Transgelin Chd64	Q9VZI1_DROME	21 kDa	11	5	7	5	1	0	0	0	0	0	0	0	0	0		
CG13630 CG13630	Q9VC48_DROME	42 kDa	6	5	4	3	1	2	1	0	0	0	0	0	0	0		
CG9391, isoform C CG9391	Q7KTW5_DROME	31 kDa	3	5	3	0	0	0	0	0	0	0	0	0	0	0		
Ubiquinone biosynthesis monooxygenase COQ6, mitochondrial Coq6	COQ6_DROME	52 kDa	6	5	6	9	4	1	3	1	0	0	0	0	0	0		
Myosin regulatory light chain 2 Mlc2	MLR_DROME	24 kDa	6	5	2	2	2	0	0	0	0	0	0	0	0	0		
Cuticular protein 100A Cpr100A	Q9VA32_DROME	27 kDa	7	5	5	3	0	0	0	0	0	0	0	0	0	0		
Cluster of LD46723p Lmpt (Q9VVB5_DROME)	Q9VVB5_DROME [2]	64 kDa	1	5	6	6	2	0	1	0	1	1	0	0	0	0		
60S ribosomal protein L5 RpL5	RL5_DROME	34 kDa	8	5	3	1	0	0	0	1	0	0	0	0	0	0		
CG8778 CG8778	A1Z934_DROME	32 kDa	0	5	2	0	0	0	1	0	0	0	0	0	0	0		
Glutamine synthetase 1, mitochondrial Gs1	GLNA1_DROME	44 kDa	6	5	7	5	2	1	4	3	3	2	3	3	4	5		
UPF0389 protein CG9231 CG9231	U389_DROME	14 kDa	7	5	7	6	2	3	4	6	2	2	2	2	3	4		

CG11015-PA COX5B	Q9VMB9_DROME	14 kDa	5	5	4	4	4	4	4	4	4	2	8	26	34	51	
CG3621, isoform A ND-B14.5A	O97418_DROME	12 kDa	4	5	5	5	2	2	2	2	3	2	0	0	0	0	FA7
CG7654-PA Tom20	Q95RF6_DROME	19 kDa	2	5	4	2	2	1	2	2	0	1	0	0	0	0	
Heat shock 70 kDa protein cognate 5 Hsc70-5	HSP7E_DROME	74 kDa	8	4	4	8	15	36	58	49	32	16	9	10	5	6	
Cluster of Troponin I wupA (TNNI_DROME)	TNNI_DROME [2]	30 kDa	7	4	6	3	2	2	2	3	2	2	2	0	0	0	
BcDNA.GH02901 pdgy	Q9VXZ8_DROME	66 kDa	4	4	8	2	0	0	0	0	0	0	0	0	0	0	
GH14439p Spn88Ea	Q9VFC2_DROME	48 kDa	0	4	1	0	0	0	0	0	0	0	0	0	0	0	
CG8768 CG8768	Q8T0N5_DROME	33 kDa	8	4	4	3	7	3	4	3	1	0	0	0	0	0	
Cluster of Multifunctional protein ADE2 ade5 (PUR6_DROME)	PUR6_DROME	47 kDa	4	4	3	4	2	1	8	5	5	2	1	2	0	1	
40S ribosomal protein SA sta	RSSA_DROME (+1)	35 kDa	2	4	4	1	0	0	0	0	0	0	0	0	0	0	
Mf4 protein Mf	Q70VI1_DROME (+1)	42 kDa	7	4	4	3	0	0	0	0	0	0	0	0	0	0	
Cluster of LP02262p l(1)G0255 (Q8IRQ5_DROME)	Q8IRQ5_DROME [2]	50 kDa	3	4	5	5	2	2	1	0	0	0	48	41	4	0	
Lethal (1) G0230, isoform A ATPsyndelta	Q9W2X6_DROME	17 kDa	4	4	4	4	1	1	3	1	2	2	2	2	1	5	
Cofilin/actin-depolymerizing factor homolog tsr	CADF_DROME	17 kDa	4	4	3	6	3	1	1	2	1	0	0	0	1	0	
Alcohol dehydrogenase Adh	ADH_DROME	28 kDa	4	4	3	3	0	0	3	1	2	4	0	8	6	5	
Elongation factor 1-gamma Ef1gamma	EF1G_DROME	49 kDa	3	4	6	6	1	3	4	1	1	0	0	0	0	0	
Cytochrome b5 Cyt-b5	CYB5_DROME	15 kDa	6	4	6	8	8	8	7	8	9	6	3	5	5	0	
CathD cathD	Q7K485_DROME	42 kDa	3	4	7	0	0	0	0	0	0	0	0	0	0	0	
CG3609, isoform B CG3609	Q9VQB4_DROME	37 kDa	7	4	5	5	4	0	2	4	4	6	0	0	0	0	
Misexpression suppressor of KSR 2, isoform J MESK2	Q8IGI1_DROME	52 kDa	3	4	4	2	0	2	0	0	0	0	0	0	0	1	
CG1665 CG1665-RA	A1Z803_DROME	38 kDa	4	4	3	5	6	4	3	2	3	0	0	0	0	0	
CG7834, isoform A CG7834	Q0KHZ6_DROME	27 kDa	5	4	6	11	11	7	4	2	4	1	0	0	0	0	
Atilla, isoform B atilla	Q9VK99_DROME	15 kDa	0	4	3	11	7	4	2	1	0	0	0	0	0	0	
40S ribosomal protein S7 RpS7	RS7_DROME	22 kDa	8	4	2	1	0	0	0	0	0	0	0	0	0	0	
CG1635 CG1635	Q95TK5_DROME	51 kDa	4	4	4	4	2	3	2	4	2	4	0	0	1	1	
CG3214, isoform B ND-B17.2	Q9VQD7_DROME	17 kDa	4	4	1	1	0	0	0	0	0	0	0	0	0	0	FA12
Succinate dehydrogenase [ubiquinone] iron-sulfur subunit, mitochondrial SdhBL	Q9VWN3_DROME	47 kDa	0	4	2	0	3	0	9	7	9	9	9	6	0	0	
Cluster of Heat shock protein 68 Hsp68 (HSP68_DROME)	HSP68_DROME [4]	70 kDa	4	4	4	4	6	6	7	6	4	5	6	6	4	4	
Cluster of Bent, isoform F bt (D1YSG0_DROME)	D1YSG0_DROME [2]	1000 kDa	1	3	2	6	12	7	4	2	3	3	6	4	7	11	
40S ribosomal protein S3 RpS3	RS3_DROME	27 kDa	3	3	4	2	1	0	0	0	0	0	0	0	0	0	
CG14235-PB, isoform B COX6B	Q8IQW2_DROME (+1)	9 kDa	1	3	3	5	2	0	2	0	1	0	0	0	0	12	
LD07162p vig	Q9V426_DROME	53 kDa	7	3	3	2	2	3	1	0	0	0	0	0	0	0	
Sallimus, isoform Q sls	M9PDZ6_DROME (+1)	2100 kDa	1	3	2	4	9	19	13	14	12	9	2	1	1	0	
RH54244p yellow-c	Q9VJQ3_DROME	49 kDa	15	3	0	0	0	0	0	0	0	2	2	1	0	0	
CG4847, isoform D CG4847-RD	A1ZAU4_DROME (+1)	44 kDa	8	3	2	3	0	0	0	0	0	0	0	0	0	0	
Ribose-5-phosphate isomerase, isoform B Rpi	Q8MLS2_DROME	27 kDa	0	3	1	0	0	0	0	0	0	0	0	0	0	0	
MIP33278p1 Syb	H1UUB1_DROME	14 kDa	7	3	3	5	5	6	9	7	5	1	2	2	2	2	
Walrus, isoform A wal	Q7KN94_DROME	34 kDa	3	3	3	6	14	3	3	2	1	0	0	0	0	0	
Heterogeneous nuclear ribonucleoprotein 27C Hrb27C	RB27C_DROME	45 kDa	5	3	4	5	0	0	0	0	0	0	0	0	0	0	
Cysteine proteinase-1, isoform D Cp1	A0A0B4JD48_DROME (+1)	27 kDa	7	3	1	2	0	0	0	0	0	0	0	0	0	0	
CG16749 CG16749	Q9VHF7_DROME	28 kDa	0	3	4	2	2	0	0	0	0	0	0	0	0	0	
GDP dissociation inhibitor, isoform A Gdi	Q9VLB7_DROME	50 kDa	3	3	5	10	4	0	0	0	0	0	0	0	0	0	
Eukaryotic translation initiation factor 4E eIF-4E	IF4E_DROME	29 kDa	2	3	4	1	0	0	0	0	0	0	0	0	0	0	
14-3-3 protein epsilon 14-3-3epsilon	1433E_DROME	30 kDa	7	3	4	4	2	2	2	2	2	1	0	0	0	0	
Pyruvate kinase PyK	KPYK_DROME	57 kDa	6	3	17	34	41	22	19	13	13	13	8	10	7	40	
9 kD basic protein ATPsynE	O77134_DROME	9 kDa	4	3	2	4	4	4	3	4	4	2	2	3	2	2	
Opsin Rh1 ninaE	OPS1_DROME	41 kDa	0	3	4	4	4	4	4	4	4	4	4	4	4	4	
CG5167 CG5167	Q9VG81_DROME	47 kDa	0	3	3	4	2	2	3	3	2	3	0	0	2	0	
CG8128, isoform A CG8128	Q9VXR9_DROME	38 kDa	1	3	0	0	0	0	0	0	0	0	0	0	0	0	
Lethal (3) 72Dr l(3)72Dr	Q9VV00_DROME	39 kDa	2	3	0	0	0	0	0	0	0	0	0	0	0	0	
Mitochondrial import inner membrane translocase subunit TIM44 CG11779	Q9VDZ7_DROME	53 kDa	3	3	2	1	1	0	0	0	0	0	0	0	0	0	
Ras-like protein 3 R	RAS3_DROME	21 kDa	1	3	0	1	1	1	1	3	1	0	0	0	0	0	
CG5023 CG5023	Q9I7J0_DROME	19 kDa	7	3	2	2	2	0	0	0	0	0	0	0	0	0	
Cluster of CG44085, isoform O CG44085 (M9PDE7_DROME)	M9PDE7_DROME [2]	267 kDa	1	3	0	1	0	0	0	1	0	0	0	0	0	0	
Superoxide dismutase Sod2	A0A0B4LGQ1_DROME (+1)	25 kDa	4	3	5	4	1	1	2	1	2	2	4	2	2	1	
CG11151, isoform B CG11151	Q9VY92_DROME	12 kDa	2	3	1	1	0	0	0	0	0	0	0	0	0	0	
Levy, isoform A levy	Q9W1N3_DROME	12 kDa	7	3	4	3	4	4	3	3	2	2	2	4	8	19	
CG32267 CG32267	Q8IRD0_DROME	6 kDa	3	3	3	1	2	1	1	0	2	5	4	2	1	1	
Enolase Eno	ENO_DROME	54 kDa	2	3	2	3	2	1	3	3	4	10	30	31	48	25	
LDL receptor protein 1, isoform G LRP1	A1Z7C4_DROME	528 kDa	0	3	0	0	0	0	0	0	0	0	0	0	0	0	
Probable isoaspartyl peptidase/L-asparaginase CG7860 CG7860	ASGL1_DROME	35 kDa	0	3	0	0	0	0	0	0	0	0	0	0	0	0	
CG5590 CG5590	Q9VB10_DROME	44 kDa	2	3	4	2	5	9	11	5	2	1	1	1	0	1	
Synaptosomal-associated protein 25 Snap25	SNP25_DROME	24 kDa	1	3	4	6	4	5	6	3	6	1	1	3	0	0	
CG9336, isoform A CG9336-RA	Q9VII1_DROME	16 kDa	3	3	3	8	5	3	4	1	0	0	0	0	0	0	
Glutathione S transferase O2, isoform B GstO2	Q9VSL4_DROME	29 kDa	3	3	1	1	2	0	0	0	0	0	0	0	0	0	
CG14028-PA cype	Q9VMS1_DROME	8 kDa	3	2	2	2	2	1	1	1	2	4	5	9	13	18	
Dihydroorotate dehydrogenase (quinone), mitochondrial Dhod	PYRD_DROME	44 kDa	3	2	3	6	0	0	1	0	1	0	0	0	0	0	

NADH-cytochrome b5 reductase CG5946-RB	Q4LDP7_DROME (+1)	36 kDa	0	2	0	4	0	1	0	3	0	0	1	2	1	0	
40S ribosomal protein S8 RpS8	RS8_DROME	24 kDa	4	2	3	1	0	0	0	0	0	0	0	0	0	0	
BcDNA.GH05536 CG5867-RA	Q9Y143_DROME	30 kDa	0	2	0	0	0	0	0	0	0	0	0	0	0	0	
Superoxide dismutase [Cu-Zn] Sod	SODC_DROME	16 kDa	2	2	0	3	4	0	6	9	1	0	0	0	0	0	
GH19566p nSyb	Q86BQ0_DROME	15 kDa	0	2	1	3	1	3	3	4	2	0	0	0	0	0	
Drab11 Rab11	O18335_DROME	24 kDa	5	2	5	10	7	8	12	9	4	2	1	0	0	0	
Protein bangles and beads bnb	BNB_DROME	46 kDa	2	2	1	0	0	0	0	1	0	1	0	1	6	2	
CG7920, isoform A CG7920	Q9VAC1_DROME	52 kDa	1	2	4	2	0	0	0	1	2	4	5	9	14	14	
Mitoferrin mfrn	MFRN_DROME	42 kDa	4	2	7	6	4	5	5	9	7	4	2	2	1	0	
Heat shock protein 23 Hsp23	HSP23_DROME	21 kDa	3	2	5	4	1	2	1	1	1	0	0	0	0	0	
Probable citrate synthase, mitochondrial kdn	CISY_DROME	52 kDa	5	2	9	61	142	119	86	70	94	63	91	91	130	59	
Aminomethyltransferase CG6415	Q9VKR4_DROME	43 kDa	1	2	2	2	0	0	0	0	0	0	0	0	0	0	
CG6218, isoform A CG6218	Q9VF86_DROME	38 kDa	0	2	2	0	0	0	0	0	0	0	0	0	0	0	
CG34228 CG34228	Q6IGN6_DROME	10 kDa	4	2	4	2	1	2	0	1	0	0	0	0	0	0	
Ras-like GTP-binding protein Rho1 Rho1	RHO1_DROME	22 kDa	8	2	3	3	2	3	3	2	2	0	0	0	0	0	
GH13256p Thiolase	Q9W1H8_DROME	51 kDa	0	2	0	3	1	0	0	0	0	0	0	4	4	2	
Alpha actinin, isoform G Actn	M9PGA7_DROME	106 kDa	3	2	0	0	0	0	0	0	0	2	2	5	6	93	
Fimbrin Fim	O61604_DROME	72 kDa	1	2	8	6	3	1	2	2	2	2	0	0	0	0	
GrpE protein homolog, mitochondrial Roe1	GRPE_DROME	24 kDa	4	2	3	2	2	1	2	0	0	0	0	0	0	0	
Palmitoyl-protein thioesterase 1 Ppt1	PPT1_DROME	36 kDa	1	2	1	3	1	0	2	0	0	0	0	0	0	0	
Cdc42 homolog Cdc42	CDC42_DROME	21 kDa	1	2	3	2	1	0	0	0	0	0	0	0	0	0	
Protein lethal(2)essential for life l(2)efl	L2EFL_DROME	21 kDa	7	2	2	2	1	2	1	0	0	0	0	0	0	0	
Triosephosphate isomerase Tpi	TPIS_DROME	27 kDa	2	2	9	12	15	12	22	12	14	10	8	3	2	1	
CG17221, isoform C CG17221	Q8IPZ3_DROME	45 kDa	2	2	1	3	3	4	2	2	1	0	0	0	0	0	
Amphiphysin Amph	Q7KLE5_DROME	66 kDa	3	2	4	2	2	1	1	4	0	0	0	0	0	0	
LD24721p Sgt	Q9VJD4_DROME	36 kDa	3	2	2	5	0	1	0	1	0	0	0	0	0	0	
Cluster of Congested-like trachea protein colt (COLT_DROME)	COLT_DROME	33 kDa	4	2	4	3	4	3	4	5	4	3	2	1	2	1	
CDGSH iron-sulfur domain-containing protein 2 homolog Cisd2	CISD2_DROME	15 kDa	4	2	8	10	10	8	13	13	11	7	4	2	0	0	
UDP-glucose 4-epimerase Gale	GALE_DROME	39 kDa	3	2	2	0	0	0	0	0	0	0	0	0	0	0	
Protein NDUFAF4 homolog CG11722	NDUF4_DROME	24 kDa	6	2	1	3	0	0	0	0	0	0	5	4	1	0	CI Assembly
CG9399, isoform A CG9399	Q9VHB1_DROME	17 kDa	4	2	3	4	3	8	12	17	10	7	4	3	1	2	
CG9914, isoform A CG9914	Q9VXI1_DROME	35 kDa	3	2	0	4	5	3	0	0	0	0	0	0	0	0	
Alpha-soluble NSF attachment protein alphaSnap	SNAP_DROME	33 kDa	3	2	4	3	2	0	0	0	0	0	0	0	0	0	
Cluster of Synapse-associated protein 47kD, isoform K Sap47 (A0A0B4LH71_DROME)	A0A0B4LH71_DROME [2]	35 kDa	1	2	2	7	4	0	0	0	0	0	0	0	0	0	
Synaptosomal-associated protein Snap24	Q9VH76_DROME	24 kDa	3	2	1	5	3	2	5	5	4	3	3	3	0	1	
Glutamate carrier 1, isoform A GC1	Q9VGF7_DROME	35 kDa	1	2	2	2	0	0	4	3	2	1	0	0	0	0	
CG6512-PB, isoform B CG6512	Q8IQQ9_DROME (+1)	76 kDa	2	2	3	4	1	1	0	0	0	0	0	0	0	0	
Tetraspanin Tsp42Ea	Q7K1I4_DROME	26 kDa	0	2	1	2	2	2	4	2	2	2	0	0	0	0	
CG7675, isoform B CG7675	Q9VE80_DROME	37 kDa	2	2	3	2	2	1	1	2	0	0	0	0	0	0	
CG9338, isoform B CG9338	Q9VIH9_DROME	16 kDa	2	2	3	3	2	0	2	0	0	0	0	0	0	0	
Squid, isoform E sqd	A0A0B4K6U6_DROME (+1)	33 kDa	2	2	2	0	0	0	0	0	0	0	0	0	0	0	
CG9350 ND-B14.7	Q7JYH3_DROME	18 kDa	5	2	2	0	1	1	0	0	0	0	0	0	0	0	FA11
CG4086-PA Su(P)	Q9V420_DROME	47 kDa	4	2	4	4	2	2	2	0	1	0	0	0	0	0	
Neural lazarillo, isoform B NLaz	M9PBN2_DROME	27 kDa	0	2	4	2	0	0	0	0	0	1	0	0	0	0	
Heterogeneous nuclear ribonucleoprotein at 98DE, isoform F Hrb98DE	A4V3J6_DROME (+1)	39 kDa	3	2	1	0	0	0	0	0	0	0	0	0	0	0	
DJ-1 beta dj-1beta	Q9VA37_DROME	21 kDa	1	2	3	0	0	0	0	0	0	0	0	0	0	0	
Calcium-binding protein 1, isoform A CaBP1	Q9V438_DROME	47 kDa	2	2	4	2	2	2	1	2	2	2	0	0	0	0	
Eukaryotic initiation factor 4A-III eIF4AIII	IF4A3_DROME	46 kDa	3	2	4	7	5	0	0	0	0	0	0	0	0	0	
CG2064 CG2064	A1Z729_DROME	37 kDa	6	2	1	4	0	2	3	1	2	0	0	0	0	0	
CG2065, isoform A CG2065	Q7JYX2_DROME	33 kDa	3	2	0	3	0	2	2	0	0	0	0	0	0	0	
Heat shock 70 kDa protein cognate 3 Hsc70-3	HSP7C_DROME	72 kDa	3	2	4	4	6	21	40	30	25	17	12	11	11	9	
Eukaryotic initiation factor 4A eIF-4a	IF4A_DROME	46 kDa	3	2	5	6	5	0	0	0	0	0	0	0	0	0	
Tubulin alpha-4 chain alphaTub67C	TBA4_DROME	51 kDa	2	2	2	3	2	2	2	2	2	2	2	2	0	0	
Alpha-mannosidase LManIII	Q9VLI2_DROME	114 kDa	0	2	9	1	0	0	0	0	0	0	0	0	0	0	
CG1009-PE, isoform E Psa	Q8IRH0_DROME	120 kDa	0	1	35	10	0	0	0	0	0	0	0	0	0	0	
Transferrin 1, isoform A Tsf1	Q9VWV6_DROME	72 kDa	1	1	2	2	1	3	7	8	20	25	29	20	15	14	
Cluster of 60 kDa heat shock protein, mitochondrial Hsp60 (CH60_DROME)	CH60_DROME [2]	61 kDa	0	1	2	4	4	16	22	20	7	1	0	2	0	3	
CG14207-PB, isoform B HspB8	Q8IQW5_DROME	22 kDa	3	1	2	3	0	0	0	0	0	0	0	0	0	0	
CG2862, isoform C CG2862	Q8STA5_DROME	17 kDa	0	1	0	0	2	1	3	0	0	0	0	0	0	0	
FI04632p nrv3	Q7JS69_DROME	36 kDa	2	1	1	2	0	1	4	4	3	2	2	1	6	14	
Protein disulfide-isomerase Pdi	PDI_DROME	56 kDa	9	1	1	2	1	0	10	5	2	2	0	0	0	0	
Ras-related protein Rac2 Rac2	RAC2_DROME	21 kDa	2	1	3	3	1	1	1	0	1	0	0	0	0	0	
Sodium/potassium-transporting ATPase subunit beta-2 nrv2	ATPB2_DROME	37 kDa	1	1	2	0	2	1	4	2	1	0	4	12	18	18	
Cabeza, isoform D caz	M9PH94_DROME	34 kDa	0	1	2	0	0	0	0	0	0	0	0	0	0	0	
Transmembrane protein 70 homolog, mitochondrial CG7506	TMM70_DROME	27 kDa	3	1	1	1	0	0	0	1	1	1	0	0	0	0	
CG13887, isoform C CG13887	Q9W0M4_DROME	26 kDa	1	1	1	2	0	2	4	5	4	7	6	11	9	6	
CG3902-PA CG3902-RA	Q9VVU1_DROME	45 kDa	0	1	1	0	0	0	1	17	12	5	3	2	1	0	

Babos, isoform A babos	Q9W258_DROME	20 kDa	2	1	3	4	3	5	4	4	2	0	0	0	0	0	
LD37574p yps	Q95RE4_DROME	38 kDa	1	1	5	11	18	23	11	7	4	3	0	1	0	0	
Inorganic pyrophosphatase Nurf-38	IPYR_DROME	38 kDa	0	1	6	17	7	1	0	0	0	0	0	0	0	0	
Fat-body protein 1 Fbp1	FBP1_DROME (+1)	120 kDa	3	1	2	5	3	0	1	2	1	0	0	0	0	0	
CG5991, isoform A CG5991	Q9VCE0_DROME	50 kDa	0	1	1	3	1	0	4	1	2	1	0	0	0	1	
Ubiquinone biosynthesis protein COQ9, mitochondrial Coq9	COQ9_DROME	36 kDa	2	1	0	1	0	1	0	0	0	0	0	0	0	0	
AT13736p UQCR-Q	Q9VVH5_DROME	10 kDa	1	1	0	2	0	0	2	1	2	2	3	1	0	2	
CG5915 protein Rab7	O76742_DROME	23 kDa	2	1	1	3	0	4	3	6	5	3	2	0	0	0	
Trehalase Treh	A4UZR3_DROME	64 kDa	0	1	1	3	2	4	7	13	15	12	12	12	13	7	
40S ribosomal protein S19a RpS19a	RS19A_DROME	17 kDa	3	1	0	0	0	0	0	0	0	0	0	0	1	0	
LD46175p sea	Q7KSQ0_DROME	34 kDa	4	1	3	2	1	4	2	5	2	2	2	0	0	0	
GH10642p hebe	Q7K568_DROME	48 kDa	1	1	0	4	3	0	1	0	3	2	0	0	0	0	
CG40042 Tim23	Q8MRW1_DROME	22 kDa	6	1	3	2	1	0	5	0	2	2	0	4	4	2	
CG7636-PA mRpL2	Q9VTF8_DROME	33 kDa	4	1	1	1	0	0	0	0	0	0	0	0	0	0	
CG32209-PB serp	Q9VW34_DROME	62 kDa	0	1	6	0	0	0	0	0	0	0	0	0	0	0	
CCHC-type zinc finger protein CG3800 CG3800	Y3800_DROME	18 kDa	1	1	2	4	0	1	0	0	0	0	0	0	0	0	
Phosphatidylglycerophosphatase and protein-tyrosine phosphatase 1 Plip	PTPM1_DROME	23 kDa	2	1	1	2	0	0	0	0	0	0	0	0	0	0	
MICOS complex subunit Mic60 Mitofilin	MIC60_DROME	82 kDa	1	1	0	2	2	0	1	2	3	0	1	0	0	0	
CG4600-PA yip2	Q9VL70_DROME	42 kDa	1	1	0	0	1	0	2	1	2	16	18	19	14	20	
Maltase A1 Mal-A1	MAL1_DROME	66 kDa	7	1	0	0	0	0	0	0	0	0	0	0	0	0	
Mitochondrial transcription factor A, isoform B TFAM	Q86BR8_DROME (+1)	33 kDa	9	1	1	0	0	0	0	0	0	0	0	0	0	0	
CG6287-PA CG6287	Q9VKI8_DROME	35 kDa	0	1	0	1	3	4	7	6	3	0	0	0	0	0	
Transmembrane protein 14 homolog CG5532	TM14_DROME	12 kDa	1	1	2	3	3	4	4	4	4	0	0	0	0	0	
Guanine nucleotide-binding protein subunit beta-1 Gbeta13F	GBB1_DROME	37 kDa	0	1	1	4	6	4	4	4	2	2	1	0	0	0	
Malate dehydrogenase Mdh1	Q9VKX2_DROME	36 kDa	1	1	1	8	6	3	0	0	0	0	0	0	0	0	
CG7138-PA r2d2	Q9VLW8_DROME	35 kDa	0	1	0	0	0	0	0	2	0	0	1	0	0	0	
Deoxyribonuclease II DNaseII	Q9VED8_DROME	41 kDa	0	1	2	2	3	1	1	0	0	0	0	0	0	0	
LD43175p yellow-b	Q9VJI5_DROME	51 kDa	1	1	0	1	0	1	7	10	11	11	5	0	0	0	
Cluster of Ryanodine receptor, isoform J RyR (A0A0B4K715_DROME)	A0A0B4K715_DROME [2]	580 kDa	0	0	0	0	0	0	0	0	0	0	0	0	2	6	
Eb1, isoform A Eb1	Q7JZD3_DROME (+1)	33 kDa	3	0	2	0	1	1	1	0	0	0	0	0	0	0	
CG5676-PA CG5676	Q9VL16_DROME	17 kDa	2	0	2	3	3	1	0	2	0	0	0	0	0	0	
Annexin B11 AnxB11	ANX11_DROME	56 kDa	1	0	1	1	0	2	3	4	13	28	20	4	1	0	
CG4123-PA, isoform A Mipp1	Q9VV72_DROME	54 kDa	0	0	2	2	5	9	19	21	19	8	6	4	2	2	
Cluster of Cheerio, isoform M cher (A0A0B4KGT8_DROME)	A0A0B4KGT8_DROME [4]	263 kDa	0	0	0	0	0	0	0	18	19	9	2	1	6	3	
Cluster of Unc-89, isoform E Unc-89 (A0A0B4LGI5_DROME)	A0A0B4LGI5_DROME [4]	473 kDa	0	0	0	5	4	2	3	3	3	4	2	5	8	2	
Microtubule-associated protein futsch futsch	FUTSC_DROME	592 kDa	0	0	0	0	0	1	1	2	2	0	0	2	1	2	
Heme oxygenase Ho	Q9VGJ9_DROME	34 kDa	1	0	0	0	1	1	2	0	0	0	0	0	0	0	
Peroxisomal multifunctional enzyme type 2 Mfe2	DHB4_DROME	64 kDa	0	0	0	0	0	0	0	0	3	4	2	1	0	0	
Pyruvate carboxylase PCB	Q0E9E2_DROME (+1)	133 kDa	0	0	0	0	0	0	6	20	42	38	42	34	31	21	
Cluster of ATP-dependent 6-phosphofructokinase Pfk (A0A0B4K7L1_DROME)	A0A0B4K7L1_DROME [2]	105 kDa	0	0	0	1	12	23	25	23	30	13	12	4	1	0	
Cluster of Disks large 1 tumor suppressor protein dlg1 (DLG1_DROME)	DLG1_DROME [7]	107 kDa	0	0	0	2	3	2	6	2	4	4	3	1	0	1	
Laminin subunit alpha LanA	LAMA_DROME	411 kDa	0	0	0	0	0	0	0	0	0	0	0	0	6	6	
Limpet, isoform K Lmpt	Q7KUQ6_DROME	246 kDa	0	0	0	1	1	3	8	5	6	1	0	0	2	5	
Cluster of Shibire, isoform L shi (E1JJA4_DROME)	E1JJA4_DROME [2]	99 kDa	1	0	0	1	0	0	0	1	1	0	0	0	3	2	
Cluster of CG9674, isoform F CG9674 (M9NFH8_DROME)	M9NFH8_DROME [2]	232 kDa	0	0	0	0	0	0	0	0	1	0	0	0	23	28	
Heat shock protein 83 Hsp83	HSP83_DROME	82 kDa	0	0	1	4	10	16	20	15	5	6	5	3	0	2	
CG17776, isoform B CG17776	Q9W513_DROME	8 kDa	1	0	0	1	0	1	0	3	3	2	0	1	0	0	
Cluster of Basigin, isoform G Bsg (Q7KTJ7_DROME)	Q7KTJ7_DROME [3]	71 kDa	0	0	4	5	5	8	14	10	10	5	7	6	6	14	
Chitinase-like protein Idgf4 Idgf4	IDGF4_DROME	49 kDa	1	0	0	0	0	3	6	13	18	4	5	1	0	1	
3-hydroxyacyl-CoA dehydrogenase type-2 scu	HCD2_DROME	27 kDa	4	0	3	5	2	8	12	14	8	7	6	6	6	5	
CG2915, isoform A CG2915-RB	Q0E9F9_DROME	51 kDa	0	0	0	0	0	0	0	20	1	0	0	0	0	0	
Cluster of Syncrip, isoform H Syp (A8JR54_DROME)	A8JR54_DROME [4]	60 kDa	0	0	2	3	2	1	0	0	0	0	0	0	0	0	
Cluster of CG14526 CG14526 (Q9Y136_DROME)	Q9Y136_DROME	82 kDa	0	0	0	0	0	4	8	5	5	2	10	2	0	0	
CG9331, isoform B CG9331	Q7KT11_DROME (+2)	36 kDa	0	0	4	4	0	0	0	0	0	0	0	0	0	0	
CG7461, isoform B CG7461	A1ZBJ2_DROME	68 kDa	0	0	0	0	0	0	6	12	7	4	2	2	1	1	
Adenylosuccinate synthetase AdSS	PURA_DROME	49 kDa	0	0	12	20	5	0	0	0	0	0	0	0	0	0	
Alpha-mannosidase LManI	Q9VKV2_DROME	108 kDa	0	0	0	0	0	0	0	0	0	3	0	2	1	0	
LP14331p Mdr50	Q5BI62_DROME	145 kDa	0	0	0	0	0	0	0	0	0	0	0	5	3	0	
Cluster of Piezo-type mechanosensitive ion channel component Piezo (E1JHB4_DROME	E1JHB4_DROME	305 kDa	0	0	0	0	0	0	2	0	0	0	0	0	0	0	
Lamin-C LamC	LAMC_DROME	70 kDa	2	0	2	0	0	0	0	0	0	0	0	0	0	1	
Cluster of Terribly reduced optic lobes, isoform AI trol (M9NET2_DROME)	M9NET2_DROME [6]	432 kDa	0	0	0	0	0	0	0	1	5	4	3	4	0	0	
Microsomal triacylglycerol transfer protein Mtp	Q9VIH3_DROME	99 kDa	0	0	0	0	0	0	13	0	0	0	0	0	0	0	
Cluster of Multiple ankyrin repeats single KH domain, isoform C mask (A0A0B4K725_DI	A0A0B4K725_DROME [5]	424 kDa	0	0	0	0	0	0	0	0	0	0	2	0	0	0	
Cytochrome P450 4g1 Cyp4g1	CP4G1_DROME	63 kDa	0	0	1	4	8	12	23	21	19	10	8	5	3	2	
CG11980, isoform C CG11980	Q8INP9_DROME	41 kDa	0	0	0	0	2	0	0	0	0	0	0	0	0	0	
GH13725p Tcp-1zeta	Q9VXQ5_DROME	58 kDa	0	0	0	3	2	2	2	0	0	0	0	0	0	0	
GH01829p Tep2	Q9NFV7_DROME	158 kDa	0	0	0	0	0	0	0	0	0	1	6	9	3	0	

40S ribosomal protein S4 RpS4	RS4_DROME	29 kDa	3	0	0	0	0	0	0	0	0	0	0	0	0	0	
CG8323 CG8323	Q7JZE8_DROME	33 kDa	3	0	2	1	1	2	3	2	0	1	0	0	0	0	
Glycogen phosphorylase GlyP	PYG_DROME	97 kDa	0	0	0	0	15	61	73	55	56	43	35	31	47	40	
Cluster of Fat body protein 2 Fbp2 (FBP2_DROME)	FBP2_DROME [2]	29 kDa	1	0	0	4	1	1	6	8	19	4	0	0	0	3	
CG9603, isoform B COX7A	A0A0B4K6C3_DROME (+1)	11 kDa	1	0	0	0	0	0	0	0	0	0	0	0	2	5	
Sideroflexin CG6812-RA	Q9VVW3_DROME	36 kDa	0	0	2	0	0	2	7	2	1	0	0	0	0	0	
CG5844 CG5844	Q9VG69_DROME	42 kDa	0	0	0	0	0	0	0	0	1	5	1	0	0	0	
Peroxiredoxin 1 Jafrac1	PRDX1_DROME	22 kDa	3	0	0	0	0	0	1	0	0	0	0	0	0	1	
GM04645p Ugt86Da	Q9VGT3_DROME	60 kDa	0	0	0	0	0	0	0	0	0	2	4	3	2	2	
AT14148p CG2604	Q9VN86_DROME	47 kDa	0	0	0	2	0	0	4	2	2	3	2	1	2	0	
CG4752 CG4752-RA	Q9W247_DROME	140 kDa	0	0	0	0	0	0	0	0	2	2	0	0	3	0	
Dipeptidyl peptidase 3 DppIII	DPP3_DROME	89 kDa	0	0	0	5	8	24	30	1	0	0	0	0	0	0	
Chitinase-like protein Idgf5 Idgf5	IDGF5_DROME	50 kDa	0	0	3	5	4	0	0	0	0	0	0	0	0	0	
Cluster of CG42666, isoform E CG14801-RA (C7LAE5_DROME)	C7LAE5_DROME [2]	94 kDa	0	0	0	2	0	0	0	0	0	0	0	0	0	0	
Aminoacylase-1 CG6733	Q9VCQ9_DROME	45 kDa	0	0	0	0	0	1	2	2	0	0	0	0	0	0	
Cluster of Sodium/potassium-transporting ATPase subunit alpha Atpalpha (ATNA_DRO	ATNA_DROME [2]	116 kDa	3	0	0	0	0	1	3	1	3	9	41	95	149	126	
Cluster of Curled, isoform G cu (A0A0C4DHA6_DROME)	A0A0C4DHA6_DROME [3]	54 kDa	0	0	2	1	0	0	0	0	0	0	0	0	0	0	
CG6225, isoform A CG6225	Q9VG44_DROME	80 kDa	0	0	0	0	0	0	0	2	11	9	0	0	0	0	
LD04933p ste24a	Q7K172_DROME	52 kDa	0	0	0	0	0	0	0	3	4	0	0	0	0	0	
BcDNA.GH02220 BcDNA.GH02220	Q9Y171_DROME	49 kDa	0	0	1	2	2	2	2	2	3	2	1	1	2	0	
GH01724p p47	Q7K3Z3_DROME	43 kDa	0	0	1	1	2	0	0	0	0	0	0	0	0	0	
Lipid storage droplet-1, isoform D Lsd-1	A0A0B4KHZ1_DROME (+1)	46 kDa	0	0	2	4	0	2	0	1	0	0	0	0	0	0	
CG6878-PA CG6878	Q9VUM2_DROME	8 kDa	0	0	0	0	0	0	0	3	0	0	0	0	0	0	
Insulin-degrading enzyme Ide	IDE_DROME	114 kDa	0	0	0	0	0	0	0	0	0	1	4	0	0	0	
CG7322, isoform B CG7322	Q9VWP2_DROME	26 kDa	0	0	0	0	0	0	0	3	4	2	0	0	0	0	
CG31676, isoform B CG31676-RA	Q9VII5_DROME	18 kDa	0	0	1	1	3	2	0	0	0	0	0	0	0	0	
Transporter Gat	Q9V4E7_DROME	72 kDa	0	0	0	0	0	0	0	2	3	8	15	7	2	2	
Protein windpipe wdp	WDP_DROME	75 kDa	0	0	0	0	0	1	2	2	4	3	1	0	2	2	
Moesin, isoform K Moe	C7LAH9_DROME	76 kDa	0	0	0	0	0	2	3	3	3	3	1	2	0	1	
CG2736 CG2736	Q9W0X1_DROME	58 kDa	0	0	0	0	0	0	0	1	2	2	0	0	0	0	
Cluster of CG4389-PB, isoform B Mtpalpha (Q8IPE8_DROME)	Q8IPE8_DROME [2]	80 kDa	0	0	0	0	0	3	13	6	3	6	2	4	6	12	
Aromatic-L-amino-acid decarboxylase Ddc	DDC_DROME	57 kDa	0	0	14	0	0	0	0	0	0	0	0	0	0	0	
Fasciclin 1, isoform G Fas1	A0A0B4KH94_DROME (+6)	74 kDa	0	0	0	0	0	15	21	14	15	19	13	5	2	2	
Cluster of CG6603-PA, isoform A Hsc70Cb (Q9VUC1_DROME)	Q9VUC1_DROME [2]	89 kDa	0	0	0	0	0	0	0	0	2	26	4	1	0	1	
Granny smith, isoform F grsm	A0A0C4FEI8_DROME (+1)	71 kDa	0	0	0	0	0	0	0	0	0	0	0	17	2	0	
Aldehyde dehydrogenase Aldh-III	A0A0B4KEL0_DROME (+4)	56 kDa	0	0	0	0	0	0	3	4	9	7	5	4	4	4	
Alkaline phosphatase 4 Aph-4	APH4_DROME	65 kDa	0	0	0	0	0	0	0	0	0	0	0	0	12	6	
CG9512, isoform A CG9512	Q9VY05_DROME	69 kDa	0	0	0	0	0	0	0	3	25	37	3	2	3	0	
CG1970, isoform B ND-49	Q9V4E0_DROME	53 kDa	0	0	0	0	0	0	0	0	0	1	8	4	0	0	FS2
Glutamate decarboxylase Gad1	DCE_DROME	58 kDa	0	0	0	0	8	20	4	0	0	0	0	0	0	0	
CG11267-PA CG11267	Q9VU35_DROME	11 kDa	0	0	0	0	2	3	1	0	0	0	0	0	0	0	
Cluster of Proline dehydrogenase 1, mitochondrial slgA (PROD_DROME)	PROD_DROME [2]	77 kDa	0	0	0	0	4	22	31	35	42	25	17	11	9	3	
LD22449p Tsf2	Q9VTZ5_DROME	92 kDa	1	0	0	0	0	0	0	0	1	3	4	0	0	0	
Non-lysosomal glucosylceramidase CG33090	C3390_DROME (+1)	108 kDa	0	0	0	0	0	0	0	0	3	1	0	0	0	0	
Osiris 21 Osi21	Q9VKH5_DROME	30 kDa	0	0	0	0	0	0	2	0	1	0	0	0	0	0	
CG15347, isoform B CG15347-RB	F0JAP7_DROME (+1)	25 kDa	0	0	0	0	0	0	4	5	3	0	0	0	0	0	
Cluster of CG15096, isoform A CG15096 (Q5BIE4_DROME)	Q5BIE4_DROME [2]	53 kDa	0	0	0	0	0	0	1	6	9	9	5	2	1	1	
Probable sodium/potassium/calcium exchanger CG1090 CG1090	NCKXH_DROME	71 kDa	0	0	0	0	0	0	0	0	0	0	4	4	3	0	
Dihydropyrimidine dehydrogenase su(r)	Q9W374_DROME	111 kDa	0	0	0	1	0	0	0	0	1	0	0	4	6	0	
Alanine--tRNA ligase, cytoplasmic Aats-ala	SYAC_DROME	108 kDa	0	0	0	0	0	0	2	12	6	2	0	0	0	0	
Larval serum protein 1 beta chain Lsp1beta	LSP1B_DROME	96 kDa	0	0	0	5	8	4	5	4	3	1	0	0	0	0	
CG3835, isoform A EG:87B1.3	Q7K511_DROME	58 kDa	0	0	2	9	0	0	0	0	0	0	0	0	0	0	
CG7382 CG7382	Q9VMR0_DROME	27 kDa	0	0	0	1	2	0	2	2	1	0	0	0	1	0	
Probable glutamine--tRNA ligase Aats-gln	SYQ_DROME	88 kDa	0	0	0	0	0	0	5	0	0	0	0	0	0	0	
Ras-like protein 1 Ras85D	RAS1_DROME	22 kDa	0	0	0	3	1	0	0	0	0	0	0	0	0	0	
CG12079-PA ND-30	Q9VZU4_DROME	30 kDa	0	0	0	0	0	0	0	0	0	3	9	4	1	1	FS3
NTPase, isoform F NTPase	M9PBV2_DROME	58 kDa	0	0	0	1	0	0	2	2	2	0	1	0	0	0	
Larval serum protein 2 Lsp2	LSP2_DROME	83 kDa	0	0	31	25	7	2	1	0	0	0	0	0	23	0	
CG4598, isoform B CG4598	Q9VL68_DROME	31 kDa	0	0	0	0	0	8	14	14	10	1	0	0	0	0	
Dihydrolipoyl dehydrogenase CG7430	Q9VVL7_DROME	53 kDa	0	0	0	19	72	91	33	11	7	2	1	0	0	0	
Protein unzipped uzip	UZIP_DROME	54 kDa	0	0	0	0	0	0	0	0	0	2	5	4	2	0	
CG5390, isoform A CG5390-RA	Q9VL01_DROME	45 kDa	0	0	1	0	3	2	1	0	0	0	0	0	0	0	
Cluster of Aspartyl beta-hydroxylase, isoform L Asph (A0A0B4KFS5_DROME)	A0A0B4KFS5_DROME [3]	113 kDa	0	0	0	0	0	0	0	0	0	2	2	1	4	1	
CG3940, isoform A CG3940	Q9VH26_DROME	34 kDa	1	0	2	2	1	3	7	7	12	9	11	6	5	0	
LP11544p Mal-A5	Q5U124_DROME (+1)	72 kDa	0	0	0	0	0	0	0	0	2	2	3	0	0	0	
CG4199, isoform B EG:22E5.5	Q960D4_DROME	65 kDa	0	0	0	0	0	0	2	2	1	0	0	0	0	0	
CG4753, isoform A CG4753	Q9VV49_DROME	43 kDa	0	0	0	0	1	2	3	3	0	0	1	0	0	0	

Cluster of Na/Ca-exchange protein, isoform D Calx (A0A0B4K6R7_DROME)	A0A0B4K6R7_DROME [4]	106 kDa	0	0	0	0	0	0	0	0	0	0	0	7	27	18	
Cluster of CAP, isoform X CAP (A0A0B4K7L3_DROME)	A0A0B4K7L3_DROME	283 kDa	0	0	0	2	0	0	0	0	0	0	0	0	0	0	
RE63021p Rap2l	O96692_DROME	20 kDa	1	0	0	2	1	2	3	1	0	0	0	0	0	0	
CG8036, isoform B CG8036	Q9VHN7_DROME	68 kDa	0	0	0	0	0	0	0	0	0	2	1	3	2	8	
Cluster of Troponin T, skeletal muscle up (TNNT_DROME)	TNNT_DROME [2]	47 kDa	0	0	0	2	1	0	1	4	5	2	2	0	0	0	
FI02870p Jheh2	Q7KB18_DROME	52 kDa	0	0	0	0	0	0	0	0	2	2	0	0	0	0	
Cluster of Zormin, isoform K zormin (Q0E8J5_DROME)	Q0E8J5_DROME [5]	335 kDa	0	0	2	2	0	0	2	2	0	0	2	0	0	0	
LETM1 and EF-hand domain-containing protein anon-60Da, mitochondrial Letm1	A60DA_DROME	114 kDa	0	0	0	0	0	0	1	1	1	3	1	1	2	5	
Multidrug-Resistance like protein 1, isoform H MRP	Q7KTC4_DROME (+7)	173 kDa	0	0	0	0	0	0	0	0	0	0	0	0	0	12	
CG13220, isoform A CG13220	Q6NP72_DROME	16 kDa	1	0	4	3	3	6	6	7	6	5	3	2	1	3	
CG3156 EG:171D11.2	Q8SWW9_DROME	76 kDa	0	0	0	0	0	0	0	0	0	0	0	3	2	0	
Elongation factor 2 EF2	EF2_DROME	94 kDa	0	0	0	2	0	8	29	28	13	10	10	4	2	0	
Cluster of Calnexin 99A, isoform A Cnx99A (Q9VAL7_DROME)	Q9VAL7_DROME [2]	68 kDa	0	0	0	0	0	0	1	3	11	10	10	11	13	21	
Calnexin 14D Cnx14D	Q9VXF6_DROME	73 kDa	0	0	0	0	0	0	0	0	1	1	1	0	2	3	
Glycerol-3-phosphate dehydrogenase Gpo-1	Q7K569_DROME	80 kDa	4	0	0	0	6	11	23	31	53	58	67	92	138	99	
Cluster of Neural conserved at 73EF, isoform I Nc73EF (A8JNU6_DROME)	A8JNU6_DROME [2]	123 kDa	0	0	0	0	0	3	9	15	17	32	106	79	50	34	
NADPH--cytochrome P450 reductase Cpr	NCPR_DROME	76 kDa	0	0	2	20	9	22	26	35	25	16	10	3	2	1	
CG10664-PA, isoform A COX4	Q9VIQ8_DROME	21 kDa	3	0	0	1	0	0	4	5	8	**8**	**15**	**21**	**20**	**33**	
Acyl-CoA synthetase long-chain, isoform J Acsl	A0A0B4KFE4_DROME (+3)	82 kDa	0	0	0	0	2	16	16	16	21	18	17	9	6	6	
CG6543, isoform A CG6543	Q7JR58_DROME	32 kDa	0	0	0	0	0	0	0	0	1	23	58	35	4	0	
NADH-ubiquinone oxidoreductase 75 kDa subunit, mitochondrial ND-75	NDUS1_DROME	79 kDa	0	0	0	0	2	14	21	16	21	17	3	3	1	1	FS1
LP19846p Ndg	A1Z877_DROME	149 kDa	0	0	0	1	0	0	3	0	0	0	53	34	9	2	
Sodium/potassium-transporting ATPase subunit beta-1 nrv1	ATPB1_DROME	35 kDa	0	0	1	3	4	5	9	4	5	4	5	14	17	12	
CG4984, isoform A CG4975-RB	A1ZAY4_DROME (+1)	51 kDa	0	0	0	0	0	6	13	16	18	13	9	5	5	6	
Cluster of Calcium-transporting ATPase PMCA (E6EK15_DROME)	E6EK15_DROME [4]	132 kDa	0	0	0	0	0	0	0	0	1	0	0	0	9	79	
Aldehyde dehydrogenase Aldh	Q9VLC5_DROME	57 kDa	0	0	0	0	0	0	0	0	0	3	28	24	23	7	
Vinculin Vinc	VINC_DROME	106 kDa	0	0	0	0	0	0	0	1	33	39	8	0	0	0	
CG13506, isoform A CG13506-RA	Q9W259_DROME	57 kDa	0	0	1	6	5	0	0	6	22	25	17	4	2	3	
Failed axon connections fax	FAXC_DROME (+1)	47 kDa	0	0	0	0	0	10	19	15	12	7	6	4	3	7	
CG31198 CG31198	Q8IN25_DROME	107 kDa	0	0	0	0	0	0	0	0	0	0	21	29	20	7	
Cytochrome c oxidase subunit 2 mt:CoII	COX2_DROME	26 kDa	0	0	0	2	2	2	2	2	2	4	**10**	**12**	**16**	**18**	
CG2107 CG2107	Q9VZW7_DROME	75 kDa	0	0	4	10	12	10	9	11	3	3	1	0	0	1	
Putative apoptosis-inducing factor 1, mitochondrial AIF	AIFM1_DROME	81 kDa	0	0	0	1	3	9	10	11	9	5	9	6	3	3	
Cluster of CG9485, isoform B CG9485 (Q9W2H8_DROME)	Q9W2H8_DROME [2]	183 kDa	0	0	0	0	0	0	0	0	0	0	0	0	0	56	
Alpha-mannosidase LManII	Q9VKV1_DROME	123 kDa	0	0	0	0	1	0	0	0	29	10	3	2	4	0	
Cluster of Serine/threonine-protein phosphatase 2B catalytic subunit 3 CanA-14F (PP2E	PP2B3_DROME [4]	64 kDa	0	0	0	21	21	8	4	1	0	1	0	0	0	0	
Imaginal disc growth factor 2, isoform B Idgf2	D4G7B1_DROME (+1)	41 kDa	0	0	0	0	4	11	20	18	9	3	6	0	1	0	
Pugilist, isoform E pug	A0A0B4K623_DROME (+1)	103 kDa	0	0	0	0	0	0	0	0	0	0	0	25	14	0	
Chitinase-like protein Idgf3 Idgf3	IDGF3_DROME (+1)	49 kDa	0	0	0	0	0	1	4	7	3	7	2	3	3	4	
Esterase-6 Est-6	EST6_DROME	61 kDa	0	0	0	0	1	0	0	3	24	19	1	0	0	0	
Aconitate hydratase Irp-1B	Q9VGZ3_DROME	99 kDa	0	0	4	47	30	1	3	2	0	0	0	0	0	0	
LD20211p Tudor-SN	Q9W0S7_DROME	103 kDa	0	0	0	1	0	1	0	2	10	6	9	2	1	0	
Malic enzyme Men-b	Q9VB69_DROME	69 kDa	0	0	0	0	0	0	0	0	0	0	0	1	15	39	
Probable cytochrome P450 6d5 Cyp6d5	CP6D5_DROME	57 kDa	0	0	0	0	0	2	6	6	8	2	1	0	0	0	
Thioester-containing protein 4, isoform B Tep4	M9PD73_DROME (+1)	166 kDa	0	0	0	0	0	0	0	0	0	0	11	10	7	0	
Cluster of CG9297, isoform B CG9297 (Q8I0D4_DROME)	Q8I0D4_DROME	106 kDa	2	0	3	2	2	1	3	4	4	2	5	6	4	1	
CG31233 CG5839	Q8MRN5_DROME	107 kDa	0	0	0	0	0	0	0	0	0	0	8	0	5	31	
CG8839, isoform A CG8839	Q7K2E1_DROME	58 kDa	0	0	1	3	2	7	8	8	6	5	1	0	1	0	
Actin-interacting protein 1 flr	WDR1_DROME	67 kDa	0	0	0	0	0	0	0	0	0	0	0	0	5	21	
Protein ROP Rop	ROP_DROME	68 kDa	0	0	1	9	9	7	5	0	0	2	0	0	0	0	
CG8399, isoform B CG8399	A0A0B4LGL5_DROME (+1)	71 kDa	0	0	0	0	0	0	0	1	2	5	18	11	1	0	
CG11771 CG11771	Q9VC06_DROME	81 kDa	0	0	0	1	2	1	3	4	10	9	3	1	0	0	
Adenylyl cyclase-associated protein capt	Q9VPX6_DROME	84 kDa	0	0	0	0	0	0	1	0	0	5	8	5	3	6	
Krueppel homolog 2 Kr-h2	KRH2_DROME	31 kDa	0	0	0	1	4	4	5	5	5	6	4	4	4	4	
Sideroflexin CG11739	Q9VN13_DROME	36 kDa	1	0	2	2	1	5	9	8	3	0	0	0	0	0	
CHOp24, isoform A CHOp24	Q9W4K0_DROME	23 kDa	0	0	0	0	0	0	0	0	2	8	13	10	2	2	
Valyl-tRNA synthetase, isoform C Aats-val	A0A0B4KF06_DROME (+1)	119 kDa	0	0	0	0	0	0	7	3	10	4	0	0	0	0	
Bicoid stability factor bsf	Q9VJ86_DROME	157 kDa	0	0	0	1	0	0	0	0	0	0	0	0	2	13	
RH64870p Ucp4A	Q9VX14_DROME	37 kDa	0	0	0	0	1	2	8	10	7	3	0	0	0	0	
Serine hydroxymethyltransferase CG3011	B7Z0X1_DROME (+1)	51 kDa	0	0	0	0	0	0	0	0	0	0	0	1	16	13	
Carnitine palmitoyltransferase I whd	Q9V3K9_DROME	90 kDa	0	0	0	1	0	0	0	2	5	5	6	4	5	3	
CG17337, isoform A CG17337	Q8MT58_DROME	53 kDa	0	0	0	26	6	0	0	0	0	0	0	0	0	0	
Adenosylhomocysteinase Ahcy13	SAHH_DROME	47 kDa	0	0	0	0	0	0	0	0	0	0	30	7	0	0	
CG1742-PA, isoform A Mgstl	Q8SY19_DROME	17 kDa	0	0	0	0	1	3	4	6	6	6	6	3	1	2	
CG34355, isoform E CG34355	A0A0B4K709_DROME (+1)	85 kDa	0	0	0	0	0	0	3	6	4	11	8	0	0	0	
CG1907 CG1907	Q9VAJ9_DROME	35 kDa	0	0	1	1	3	7	11	5	3	0	0	0	0	0	
CG2918, isoform B EG:25E8.1	O46067_DROME	103 kDa	0	0	0	0	0	0	0	0	0	19	1	0	0	0	

Enigma Egm	Q5U117_DROME	71 kDa	0	0	0	0	0	3	6	6	7	6	2	0	0	0	ACAD9
Cytochrome c oxidase subunit 5A, mitochondrial COX5A	COX5A_DROME	17 kDa	1	0	0	0	0	0	0	0	0	3	4	5	6	9	
CG9509, isoform A CG9509	Q9VY04_DROME	71 kDa	0	0	0	0	0	0	0	2	28	0	1	0	0	0	
Cluster of Coronin coro (A0A0B4KEJ7_DROME)	A0A0B4KEJ7_DROME [3]	58 kDa	0	0	1	2	5	1	0	0	0	0	2	2	4	6	
GH09263p Aats-gly	Q961R8_DROME (+1)	76 kDa	0	0	0	0	0	1	6	3	1	1	3	10	0	0	
LD30155p lost	Q9VN21_DROME	60 kDa	0	0	0	2	2	4	5	6	5	4	4	3	0	0	
Cluster of Cysteine string protein, isoform F Csp (D0IQJ8_DROME)	D0IQJ8_DROME [3]	27 kDa	0	0	0	0	0	1	7	7	8	5	1	1	0	0	
Presequence protease, mitochondrial CG3107	PREP_DROME	119 kDa	0	0	0	0	0	2	7	2	0	0	0	0	0	0	
GH24511p Uba1	Q8T0L3_DROME	131 kDa	0	0	0	0	4	2	4	4	4	3	3	3	3	1	
CG4829, isoform E CG4829	A8JV19_DROME (+3)	78 kDa	0	0	0	0	0	0	0	1	1	3	0	6	8	3	
Heat shock 70 kDa protein cognate 1 Hsc70-1	HSP7A_DROME	71 kDa	0	0	2	0	4	12	18	11	10	5	3	3	3	2	
CG9416, isoform A CG9416	Q8MT48_DROME	98 kDa	0	0	0	0	0	0	0	0	2	7	10	5	2	2	
CG5112 CG5112	Q9VBQ5_DROME	58 kDa	0	0	0	0	0	4	6	5	4	3	2	0	0	1	
CG11089, isoform A CG11089	Q9VC18_DROME	63 kDa	0	0	0	0	0	0	0	0	3	11	10	3	3	0	
Cluster of Thioredoxin reductase 1, mitochondrial Trxr-1 (TRXR1_DROME)	TRXR1_DROME	64 kDa	0	0	0	2	21	3	0	0	0	0	0	0	0	0	
FI01422p Spn43Ab	A1Z6V5_DROME	43 kDa	0	0	0	0	0	0	0	0	0	0	5	3	5	9	
Arc42 Arc42	Q9VDT1_DROME	44 kDa	0	0	0	0	0	0	10	13	2	0	0	0	0	0	
CG8602, isoform B CG8602	Q9VS47_DROME	53 kDa	0	0	0	0	0	0	0	6	8	8	7	1	1	0	
CG16986, isoform B CG16986-RA	Q9VZZ5_DROME	16 kDa	0	0	0	2	1	3	2	2	0	2	4	1	1	0	
CG1105 CG1105	Q9VI53_DROME	46 kDa	0	0	0	0	0	0	1	7	9	5	2	1	0	1	
CG10932, isoform A CG10932	Q9W3N9_DROME	43 kDa	1	0	0	0	0	0	0	0	0	9	9	1	0	0	
Cytochrome b5-related protein Cyt-b5-r	CYB5R_DROME	50 kDa	0	0	0	0	0	2	2	2	3	2	2	1	1	0	
Phosphoribosylformylglycinamidine synthase ade2	PUR4_DROME	148 kDa	0	0	0	0	0	0	0	0	0	0	9	8	0	0	
CG4721 CG4721-RA	Q9VCU1_DROME	81 kDa	0	0	0	0	0	3	7	2	4	1	0	0	0	0	
CG6045 AOX3	Q9VF51_DROME	138 kDa	0	0	0	0	0	0	0	0	0	0	0	0	5	17	
Probable cytochrome P450 28d1 Cyp28d1	C28D1_DROME	57 kDa	0	0	0	0	1	2	4	3	1	0	0	0	0	0	
AT07710p CG7910	Q9VHW0_DROME	58 kDa	0	0	0	0	0	0	7	5	2	2	1	1	0	0	
CG31343 CG5839	Q8SWX4_DROME	108 kDa	0	0	0	0	0	0	0	0	0	0	0	3	3	15	
CG9577 CG9577	Q9W5W8_DROME	34 kDa	0	0	0	0	0	0	0	2	3	1	1	1	4	7	
Aralar1, isoform E aralar1	A0A0B4K6V1_DROME (+1)	78 kDa	0	0	0	0	0	0	0	0	2	0	1	0	0	2	
Cluster of Mitochondrial import receptor subunit TOM40 homolog 1 Tom40 (TO401_D	TO401_DROME	36 kDa	0	0	0	0	0	0	1	2	3	3	5	3	1	2	
CG3961, isoform D CG3961-RD	E2QCY2_DROME (+1)	73 kDa	0	0	0	0	0	0	0	0	2	4	1	0	0	1	
CG3699-PA EG:BACR7A4.14	Q9U1L2_DROME	26 kDa	0	0	4	3	3	2	2	3	1	2	0	0	0	0	
Glutactin Glt	GLT_DROME	119 kDa	0	0	0	0	0	0	0	0	6	9	0	0	0	4	
GH04080p PPO1	Q7K2W6_DROME	79 kDa	0	0	0	0	0	0	0	0	0	0	0	0	0	22	
CG9380, isoform D CG9380	Q8MLN4_DROME	93 kDa	0	0	0	0	0	0	0	0	2	8	7	4	2	0	
V-type proton ATPase subunit H VhaSFD	VATH_DROME	54 kDa	0	0	0	0	0	0	1	2	6	3	1	1	0	0	
CG6463-PA ND-13B	Q9VTB4_DROME	14 kDa	0	0	0	0	0	0	0	0	0	1	6	5	2	0	FA5
Tetraspanin Tsp5D	M9PDV2_DROME (+1)	32 kDa	0	0	0	1	1	4	6	3	2	2	1	1	2	0	
RE74917p tobi	Q9VBR6_DROME	75 kDa	4	0	0	0	0	0	0	0	0	5	9	1	0	0	
Aquaporin, isoform B AQP	E1JH55_DROME (+1)	29 kDa	1	0	0	2	0	0	2	2	4	3	3	1	2	0	
Tyrosine--tRNA ligase Aats-tyr	Q9VV60_DROME	58 kDa	0	0	1	0	0	0	4	1	2	1	0	0	0	0	
CG12119, isoform A CG12119	Q9W373_DROME	56 kDa	0	0	0	2	4	2	2	2	4	0	0	0	0	0	
CG1275, isoform D CG1275	Q7KV99_DROME (+2)	27 kDa	0	0	0	0	0	0	0	1	2	2	4	4	6	6	
FI18644p1 Hmu	Q9VB46_DROME	63 kDa	0	0	0	0	0	2	4	4	3	1	1	0	0	0	
Cluster of CG2930, isoform A CG2930-RA (Q9W4P6_DROME)	Q9W4P6_DROME [2]	89 kDa	0	0	0	0	0	0	0	0	4	7	4	5	6	0	
Transmembrane emp24 domain-containing protein bai bai	TMEDA_DROME	24 kDa	0	0	0	0	0	0	0	2	3	5	1	4	2	0	
LP01981p p24-2	Q86BA5_DROME	28 kDa	0	0	0	0	0	0	0	0	0	6	4	5	3	0	
CG6851-PA, isoform A Mtch	Q9V3Y4_DROME	35 kDa	0	0	0	0	0	1	4	5	4	2	0	0	0	0	
UDP-glucuronosyltransferase CG17323	Q9VJ46_DROME	58 kDa	0	0	0	0	0	0	0	0	0	0	2	6	7	1	
Aminopeptidase P ApepP	Q9VJG0_DROME	69 kDa	0	0	0	0	0	0	0	0	11	2	0	0	0	0	
CG9149 CG9149	Q9W0H6_DROME	41 kDa	0	0	0	0	0	0	5	11	3	0	0	0	0	0	
Glycoprotein 93 Gp93	Q9VAY2_DROME	90 kDa	0	0	0	1	0	0	1	1	1	1	5	3	1	0	
CG33123, isoform A CG33123	Q9VQR8_DROME	135 kDa	0	0	0	0	0	0	0	0	0	0	2	1	0	0	
Cluster of Fasciclin 3, isoform G Fas3 (X2JAT7_DROME)	X2JAT7_DROME [2]	61 kDa	0	0	0	0	0	1	0	3	4	6	3	4	1	0	
Fatty acid (Long chain) transport protein, isoform D Fatp	E1JHE4_DROME (+1)	75 kDa	0	0	0	0	0	0	0	1	2	5	2	1	0	0	
Glucosamine-6-phosphate isomerase Oscillin	M9ND31_DROME	31 kDa	0	0	0	0	0	0	0	0	2	3	7	0	0	1	
Neutral ceramidase CDase	NCASE_DROME	78 kDa	0	0	0	0	0	0	2	2	2	4	1	1	1	0	
CG5789, isoform A CG5789-RA	Q9VC63_DROME	157 kDa	0	0	0	0	0	0	0	0	0	0	0	0	5	3	
CG9172, isoform A ND-20	Q9VXK7_DROME	25 kDa	0	0	0	0	0	0	0	0	0	0	9	5	2	0	FS7
CG13907, isoform A CG13907	Q9W0L6_DROME	88 kDa	0	0	0	0	0	0	0	0	0	0	0	1	4	8	
Probable cytochrome P450 6a20 Cyp6a20	C6A20_DROME	58 kDa	0	0	0	0	0	2	4	3	2	0	0	0	0	0	
Cytochrome P450 9b2 Cyp9b2	CP9B2_DROME	59 kDa	0	0	0	0	0	0	1	1	5	0	0	0	0	0	
CG10960, isoform C CG10960	Q8IQH6_DROME (+1)	51 kDa	0	0	0	0	0	0	4	5	6	5	0	1	0	0	
Alcohol dehydrogenase class-3 Fdh	ADHX_DROME	40 kDa	0	0	0	0	2	6	8	2	0	0	0	0	0	0	
Probable 2-oxoglutarate dehydrogenase E1 component DHKTD1 homolog, mitochondr	DHTK1_DROME	104 kDa	0	0	0	0	0	0	0	0	7	3	0	0	0	0	
Gelsolin Gel	GELS_DROME	88 kDa	0	0	0	0	0	0	0	0	3	5	6	1	0	0	

ABCB7, isoform B ABCB7	Q7KVB1_DROME (+1)	77 kDa	0	0	0	0	0	0	0	0	0	0	0	2	6	1		
Calpain-A, isoform D CalpA	A0A0B4LG26_DROME (+1)	96 kDa	0	0	0	0	1	1	4	1	0	0	2	1	3	1		
CD98 heavy chain, isoform D CD98hc	A0A0B4KFA6_DROME (+1)	63 kDa	0	0	0	0	0	0	0	0	0	0	0	0	1	8		
CG5482, isoform A CG5482	Q7K3D4_DROME	45 kDa	0	0	0	4	4	4	1	0	0	0	0	0	0	0		
Amino acid transporter Eaat1	O77062_DROME	52 kDa	0	0	0	0	0	0	2	2	2	2	2	1	2	3		
Cluster of CG32473, isoform B CG32473-RB (Q8INH5_DROME)	Q8INH5_DROME [3]	103 kDa	0	0	0	0	0	0	0	5	8	0	0	0	0	2		
CG3036, isoform A CG3036	Q9VR44_DROME	54 kDa	0	0	0	0	0	0	0	2	3	8	4	2	0	0		
Probable phosphoserine aminotransferase CG11899	SERC_DROME	40 kDa	0	0	0	0	0	0	3	4	4	1	0	0	0	0		
CG9691, isoform B CG9691	Q9W306_DROME	13 kDa	0	0	1	6	4	1	0	0	0	0	0	0	0	0		
UNC93-like protein CG4928	UN93L_DROME (+1)	59 kDa	0	0	0	0	0	0	0	0	4	6	3	0	1	0		
Maltase A6, isoform C Mal-A6	A1Z7F1_DROME	68 kDa	0	0	0	0	0	1	9	4	1	0	0	0	0	0		
LP01562p veil	Q7K0L5_DROME	65 kDa	0	0	0	0	0	0	0	0	0	0	4	5	3	0		
UDP-glucuronosyltransferase Ugt35b	Q9VGT0_DROME	58 kDa	0	0	0	0	0	0	0	0	0	0	7	10	0	0		
CG2254-PA CG2254	Q9W3K9_DROME	36 kDa	0	0	0	0	0	0	1	2	3	0	0	0	0	0		
Carboxylic ester hydrolase Ace	A0A0B4KGI5_DROME (+1)	71 kDa	0	0	0	0	0	0	0	1	2	2	0	1	9	2		
CG18522 AOX1	Q9VF53_DROME	139 kDa	0	0	0	0	0	0	0	0	0	0	0	0	0	10		
CG9248, isoform A CG9248	Q9VIF2_DROME	56 kDa	0	0	0	1	0	1	2	4	4	3	0	0	0	0		
No extended memory, isoform A nemy	Q7JR72_DROME	33 kDa	0	0	0	0	0	0	1	2	0	2	4	2	2	3		
Cluster of CG1440, isoform A CG1440 (Q9W3F6_DROME)	Q9W3F6_DROME [2]	55 kDa	0	0	0	0	0	0	0	0	0	0	0	1	0	2		
CG17259, isoform A CG17259	Q9VQL1_DROME	56 kDa	0	0	0	0	0	0	0	2	6	3	0	0	0	0		
Ecto-5'-nucleotidase 2, isoform A NT5E-2	Q8SZY4_DROME	64 kDa	0	0	0	0	0	0	0	0	0	0	0	2	2	0		
Putative fatty acyl-CoA reductase CG8306 CG8306	FACR3_DROME	58 kDa	0	0	0	0	0	0	0	2	5	0	0	0	0	2		
CG10650, isoform A BEST:GH09876	Q9VJ22_DROME	44 kDa	0	0	0	0	0	0	4	2	4	2	0	0	0	0		
CG1718, isoform C CG1718	M9PFD0_DROME (+2)	193 kDa	0	0	0	0	0	0	0	0	0	0	0	0	0	6		
Aminoacylase-1 CG6726	Q9VCR2_DROME	45 kDa	0	0	0	0	0	4	13	2	0	0	0	0	0	0		
Epithelial membrane protein, isoform B emp	Q9W0X0_DROME	62 kDa	0	0	0	0	0	0	0	2	2	2	0	0	0	0		
Lethal (3) 87Df l(3)87Df	Q9VG00_DROME	13 kDa	0	0	0	3	0	2	2	2	2	1	0	0	0	0		
6-phosphogluconate dehydrogenase, decarboxylating Pgd	6PGD_DROME (+1)	52 kDa	0	0	0	1	4	3	0	0	0	0	0	0	0	0		
CG14935-PA, isoform A Mal-B2	Q8IPA2_DROME	65 kDa	0	0	0	0	9	0	0	0	0	0	0	0	0	0		
CG3999, isoform A CG3999	Q9VH09_DROME	110 kDa	0	0	0	0	0	0	0	0	0	1	5	1	0	0		
Dietary and metabolic glutamate transporter dmGlut	Q9VKC9_DROME	54 kDa	0	0	0	0	0	0	1	3	4	2	1	0	0	0		
CG1636, isoform A CG1636	Q9W3G7_DROME (+1)	45 kDa	0	0	0	0	0	0	0	0	4	4	3	0	2	0		
CG9796 GILT1	Q95RA9_DROME	28 kDa	0	0	0	1	4	2	3	0	0	0	0	0	0	0		
EH domain containing protein Past1	Q8T6I0_DROME (+1)	61 kDa	0	0	0	0	1	2	1	1	0	0	0	0	0	0		
CG6126 CG6126	Q961R9_DROME	61 kDa	0	0	0	0	0	0	0	0	4	6	1	0	0	0		
CG13850, isoform A CG13850	Q9VD14_DROME	62 kDa	0	0	0	4	0	2	1	0	1	0	0	0	0	0		
Alkyldihydroxyacetonephosphate synthase CG10253	ADAS_DROME	71 kDa	0	0	0	0	0	0	0	0	0	0	1	3	4	2		
CG10512, isoform A CG10512	Q9VP68_DROME	47 kDa	0	0	0	1	4	0	0	0	0	0	0	0	0	0		
CG1213, isoform A CG1213	Q7JVN6_DROME	53 kDa	0	0	0	0	0	0	1	1	5	3	0	0	0	0		
Tetraspanin Tsp96F	A0A0B4KH03_DROME (+1)	32 kDa	0	0	0	0	1	2	4	3	2	0	0	0	0	0		
CG2789-PA Tspo	Q9VPR1_DROME	20 kDa	0	0	0	2	0	1	1	3	0	0	0	0	0	0		
Histidyl-tRNA synthetase, isoform C Aats-his	M9PHI2_DROME (+1)	61 kDa	0	0	2	2	0	0	3	0	1	0	0	0	0	0		
Cluster of CG1674, isoform M CG1674 (L0MLJ3_DROME)	L0MLJ3_DROME [4]	93 kDa	1	0	2	2	0	0	0	0	0	0	1	0	0	0		
Putative hydroxypyruvate isomerase Gip	HYI_DROME	29 kDa	0	0	0	0	0	0	0	0	4	4	2	0	0	0		
Probable methylmalonate-semialdehyde dehydrogenase [acylating], mitochondrial CG	MMSA_DROME	56 kDa	0	0	0	1	2	0	0	0	0	0	0	0	1	6		
Probable sulfite oxidase, mitochondrial CG7280	SUOX_DROME	64 kDa	0	0	0	9	1	0	0	0	0	0	0	0	0	0		
Leukotriene A(4) hydrolase CG10602	Q9VJ39_DROME	68 kDa	0	0	0	7	5	0	0	0	0	0	0	0	0	0		
Adenylosuccinate lyase AdSL	Q9VEP6_DROME	54 kDa	0	0	0	0	0	0	0	0	0	5	4	1	0	0		
Chitinase-like protein Idgf1 Idgf1	IDGF1_DROME	49 kDa	0	0	0	0	0	0	2	2	3	0	0	0	0	0		
Acyl-coenzyme A oxidase CG9527	B7ZG28_DROME (+1)	81 kDa	0	0	0	0	2	0	0	0	3	2	2	1	1	0		
Tetraspanin Tsp42Ee	Q7KJ73_DROME	25 kDa	0	0	0	2	2	3	3	1	1	0	0	0	0	0		
CG5399, isoform A CG5399	Q9VF46_DROME	23 kDa	0	0	0	0	0	2	2	2	3	2	0	0	1	0		
Endonuclease G EndoG	Q7JXB9_DROME	35 kDa	0	0	0	0	2	9	0	0	0	0	0	0	0	0		
CG17121 CG17121	Q9VCR9_DROME	39 kDa	0	0	0	0	0	0	0	0	0	1	5	3	0	0		
Syntaxin 1A, isoform B Syx1A	A0A0B4JCZ4_DROME (+1)	34 kDa	0	0	0	0	0	0	0	0	0	2	3	2	0	0		
Rad23, isoform B Rad23	Q8IMB7_DROME (+1)	38 kDa	0	0	0	1	5	4	3	0	0	0	0	0	0	0		
Transglutaminase, isoform B Tg	Q8IPH0_DROME (+1)	87 kDa	0	0	0	0	0	1	2	0	0	2	0	0	0	0		
Fasciclin-2 Fas2	FAS2_DROME	97 kDa	0	0	0	0	0	0	0	0	0	0	0	0	0	2		
CG16985 protein CG16985	Q9VZZ6_DROME	16 kDa	0	0	0	0	0	2	1	2	1	0	1	0	1	0		
CG12531, isoform B CG12531	M9PHM0_DROME	87 kDa	0	0	0	0	2	0	0	0	0	0	0	0	0	0		
L-lactate dehydrogenase ImpL3	LDH_DROME	36 kDa	0	0	0	0	0	2	2	4	3	1	0	0	0	0		
BcDNA.GH04962 GCS2alpha	Q7KMM4_DROME	106 kDa	0	0	0	0	0	0	0	0	0	0	0	0	0	7		
HMG coenzyme A synthase, isoform A Hmgs	Q7K4Q9_DROME	51 kDa	0	0	0	3	3	0	0	0	0	0	0	0	0	0		
Xanthine dehydrogenase ry	XDH_DROME	147 kDa	0	0	0	0	0	0	0	0	0	0	0	2	0	0		
CG14523 CG14523	Q9VAS1_DROME	77 kDa	0	0	0	0	0	3	0	0	0	0	0	0	0	0		
Dipeptidase C, isoform A Dip-C	Q9VG79_DROME	55 kDa	0	0	0	0	0	0	3	0	0	0	0	0	0	0		
Cluster of CG8834, isoform A CG8834 (A1Z8Z9_DROME)	A1Z8Z9_DROME [2]	59 kDa	0	0	2	7	1	0	1	0	0	0	0	0	0	0		

LD47736p Sodh-2	O96299_DROME	39 kDa	0	0	0	0	0	0	0	0	0	7	6	0	0	0		
Aconitate hydratase Irp-1A	Q9VCV4_DROME	99 kDa	0	0	5	13	8	0	2	1	0	0	0	0	0	0		
CG4019, isoform F CG4019	A0A0B4KFZ1_DROME (+3)	32 kDa	0	0	0	0	0	0	0	0	0	0	0	1	2	5		
Malic enzyme Men	Q9VG31_DROME	85 kDa	0	0	0	0	0	0	0	0	0	0	0	0	0	4		
Adenosylhomocysteinase CG9977-RA	Q9VZX9_DROME	57 kDa	0	0	0	0	0	0	0	0	0	0	0	2	0	0		
I'm not dead yet, isoform D Indy	E1JI19_DROME (+1)	64 kDa	0	0	0	0	0	0	0	0	0	0	0	0	3	4		
CG18374-PB, isoform B Gyk	Q8IRJ9_DROME	52 kDa	0	0	0	3	0	0	0	0	0	0	0	0	0	0		
FI02050p ninaD	Q8INY3_DROME	58 kDa	0	0	0	0	0	0	0	3	4	0	0	0	0	0		
Ornithine aminotransferase, mitochondrial Oat	OAT_DROME	47 kDa	0	0	0	2	0	0	2	2	4	0	0	0	0	0		
Vanin-like protein 1 CG32754	VNNL1_DROME	62 kDa	0	0	0	0	0	0	0	3	4	0	0	0	0	0		
CG4408, isoform B CG4408	Q7JVX3_DROME (+1)	53 kDa	0	0	0	0	0	0	0	0	3	3	1	0	0	0		
MIP04528p path	Q9VT04_DROME	52 kDa	0	0	0	0	0	0	1	2	4	0	0	0	0	0		
Catalase Cat	CATA_DROME	57 kDa	0	0	0	0	0	0	0	0	0	0	0	0	0	5		
Histone H4 His4	H4_DROME	11 kDa	0	0	0	6	0	0	0	0	1	0	0	0	1	1		
UDP-glucuronosyltransferase (Fragment) Ugt86Dd	Q9VGT8_DROME	59 kDa	0	0	0	0	0	0	0	0	0	0	6	2	0	0		
CG11655 CG11655	Q9VXV4_DROME	50 kDa	0	0	0	0	0	0	0	0	4	4	3	0	0	0		
CG1910, isoform D CG1910	Q8I0J1_DROME (+2)	46 kDa	0	0	0	0	0	0	3	0	0	0	0	0	0	0		
CG2493, isoform A CG2493	Q9VIM0_DROME	54 kDa	0	0	0	0	0	0	0	0	0	0	0	1	3	1		
Cytochrome P450 4d1 Cyp4d1	CP4D1_DROME	59 kDa	0	0	0	0	0	0	3	0	0	0	0	0	0	0		
Sphingomyelin phosphodiesterase CG15533	Q9VA78_DROME	78 kDa	0	0	0	2	0	0	0	0	0	0	1	1	0	0		
Cluster of Menage a trois, isoform D metro (A0A0B4LF49_DROME)	A0A0B4LF49_DROME [2]	62 kDa	0	0	0	0	0	0	2	0	1	0	0	0	0	0		
CG9119 CG9119	Q9W0J9_DROME	36 kDa	0	0	0	5	0	0	3	0	0	0	0	0	0	0		
Lachesin Lac	LACH_DROME	40 kDa	0	0	0	0	0	0	0	2	5	1	0	0	0	0		
CG5126 CG5126	Q9VPY7_DROME	53 kDa	4	0	0	0	0	0	0	0	0	0	0	0	0	0		
RE07815p Ugt58Fa	Q9W228_DROME	59 kDa	0	0	0	0	0	0	0	0	0	0	0	4	0	0		
CG8773 CG8773-RB	Q9VFX0_DROME	111 kDa	0	0	0	0	0	0	0	2	0	0	0	0	0	6		
Heterogeneous nuclear ribonucleoprotein 87F Hrb87F	RB87F_DROME	39 kDa	4	0	2	1	0	0	0	0	0	0	0	0	0	0		
BcDNA.GH03016 Rh50	Q9V3T3_DROME	48 kDa	0	0	0	0	0	0	0	0	0	0	0	0	2	3		
Juvenile hormone epoxide hydrolase 3 Jheh3	Q7K1W4_DROME	54 kDa	0	0	0	0	0	0	0	0	0	2	0	0	0	0		
CG4562, isoform E CG4562	A0A0B4KGI0_DROME (+1)	158 kDa	0	0	0	0	0	0	0	0	0	0	0	0	0	4		
Angiotensin-converting enzyme-related protein Acer	ACER_DROME	73 kDa	0	0	0	0	0	0	3	0	0	0	0	0	0	0		
CG7966 CG7966	Q9VFZ4_DROME	55 kDa	3	0	0	0	0	0	0	0	0	0	0	0	0	0		
Methylthioribose-1-phosphate isomerase CG11334	MTNA_DROME	39 kDa	0	0	0	4	2	0	0	0	0	0	0	0	0	0		
Ance-4, isoform A Ance-4	A1Z7M8_DROME	70 kDa	0	0	0	0	0	2	0	0	0	0	0	0	0	0		
Eukaryotic translation initiation factor 3 subunit I Trip1	EIF3I_DROME	36 kDa	2	0	1	1	0	0	0	0	0	0	0	0	0	0		
CG10924, isoform B CG10924	A8DYI3_DROME (+1)	62 kDa	0	0	2	0	0	0	0	0	0	0	0	0	0	0		
Lethal (3) 03670 l(3)03670	Q9VA18_DROME	24 kDa	4	0	0	1	0	0	0	0	0	0	0	0	0	0		
Probable peroxisomal acyl-coenzyme A oxidase 1 CG5009	ACOX1_DROME	74 kDa	0	0	0	0	0	0	0	0	0	2	0	0	0	0		
CG2003, isoform A CG2003-RA	Q9V9S4_DROME	54 kDa	0	0	0	0	0	0	0	0	2	0	0	0	0	0		
CG11208 CG11208	Q7K3B7_DROME	62 kDa	0	0	0	0	0	0	0	0	0	0	0	0	5	0		
GH21316p Ssadh	Q9VBP6_DROME	55 kDa	0	0	0	0	0	0	0	0	0	0	0	0	3	0		
CG6180 CG6180	Q9VK60_DROME	29 kDa	0	0	1	3	0	0	0	0	0	0	0	0	0	0		
CG9921, isoform B CG9921	Q9VXH4_DROME	11 kDa	0	0	0	0	0	0	1	0	1	0	0	0	0	4		
CG1824 CG1824	Q9VYL5_DROME	84 kDa	0	0	0	0	0	0	0	0	0	0	0	0	1	3		
CG8774, isoform A CG8774	Q9VFW9_DROME	107 kDa	0	0	0	0	0	0	0	0	0	0	0	0	0	3		
Fumarylacetoacetase Faa	Q9VZI8_DROME	46 kDa	0	0	0	4	0	0	0	0	0	0	0	0	0	0		
CG9148-PA, isoform A scf	Q9W0H8_DROME	38 kDa	0	0	2	2	0	0	0	0	0	0	0	0	0	0		
Signal peptidase complex subunit 3 Spase22-23	SPCS3_DROME	20 kDa	0	0	0	0	0	0	0	0	0	3	2	0	0	0		
LD21102p Ugt35a	Q9VGS9_DROME	61 kDa	0	0	0	0	0	0	0	0	0	0	2	2	0	0		
Multidrug resistance protein 4 ortholog Mrp4	Q9VGM1_DROME	148 kDa	0	0	0	0	0	0	0	0	0	0	0	0	0	3		
CG3164, isoform C CG3164	Q8IPV3_DROME (+1)	78 kDa	0	0	0	0	0	0	0	0	0	0	0	0	0	3		
CG10592 CG10592	Q9VRM8_DROME	58 kDa	0	0	4	0	0	0	0	0	0	0	0	0	0	0		
CG9547 CG9547	Q9VMC6_DROME	46 kDa	0	0	0	0	0	0	0	0	0	0	3	0	0	0		
Procollagen lysyl hydroxylase, isoform A Plod	Q9VTH0_DROME	83 kDa	0	0	0	0	0	0	0	0	0	0	3	1	0	0		
LD21404p mRpL16	Q9W547_DROME	28 kDa	2	0	0	0	0	0	0	0	0	0	0	0	0	0		
Aldose 1-epimerase CG10467-RA	Q9VRU1_DROME	40 kDa	0	0	0	0	1	0	0	0	3	1	0	0	0	0		
Chitinase-like protein CG5210 CG5210	C5210_DROME	50 kDa	0	0	0	0	0	0	0	2	2	0	0	0	0	6		
CG4603, isoform B CG4603	M9PED6_DROME (+1)	41 kDa	5	0	0	0	0	0	0	0	0	0	0	0	0	0		
Delta-aminolevulinic acid dehydratase Pbgs	Q9VTV9_DROME	36 kDa	0	0	0	0	0	0	0	0	0	0	0	0	0	5		
FI05212p Sodh-1	O97479_DROME	39 kDa	0	0	0	0	0	0	0	0	0	3	3	0	0	3		
CG4872-PA CG4872	Q8SY58_DROME	39 kDa	0	0	0	2	0	0	0	0	0	0	0	0	0	0		
CG6656 CG6656	Q9VD68_DROME	45 kDa	0	0	0	0	0	0	0	0	2	1	0	0	0	0		
Sphingomyelin phosphodiesterase CG15534	Q9VA77_DROME	75 kDa	0	0	2	0	0	0	0	0	0	0	0	0	0	0		
Heat shock 70 kDa protein cognate 2 Hsc70-2	HSP7B_DROME	70 kDa	0	0	0	0	4	4	4	4	3	3	0	2	0	0		
CG8239, isoform A CG8239	Q9VXQ3_DROME	43 kDa	0	0	2	2	0	0	0	0	0	0	0	0	0	0		
CG17029, isoform A CG17029	Q9VUW2_DROME	31 kDa	0	0	2	0	0	0	0	0	0	0	0	0	0	0		
CG7882, isoform A CG7882	Q0IGX4_DROME	57 kDa	0	0	0	0	0	0	1	3	0	0	0	0	0	0		

CG7638-PA CG7638	Q9VTF5_DROME	56 kDa	0	0	0	0	0	0	0	2	0	0	0	0	0	0	
CG11665, isoform A CG11665	Q7JWI7_DROME	72 kDa	0	0	0	0	0	0	0	0	0	0	0	0	2	2	
Tetraspanin Tsp42Ed	Q7JWV7_DROME	25 kDa	0	0	0	0	0	0	2	0	0	0	0	0	0	0	
CG1358, isoform A CG1358-RB	Q7K1D7_DROME	52 kDa	0	0	0	0	0	0	0	0	0	2	0	0	0	0	
LD45324p Prx5	Q960M4_DROME	20 kDa	2	0	0	0	0	0	0	0	0	0	0	0	0	0	
CG17026-PA CG17026-RA	Q9VUW1_DROME	31 kDa	0	0	0	2	0	0	0	0	0	0	0	0	0	0	

Table 2.4: Mass spectrometry identifying constituents of the 700 kDa subcomplex in *Drosophila* flight muscles, related to Figure 2.8.

The table shows the total number and identity of peptides found in the 700 kDa assembly intermediate.

			WT	WT	WT	Mutant	Mutant	Mutant
Identified Proteins	Accession N	Molecular	MWA	MWB	MWC	F5A	F5B	F5C
ATP synthase subunit alpha, mitochondrial blw	ATPA_DRO	59 kDa	237	224	236	342	290	283
Cluster of ATP synthase subunit beta, mitochondrial ATPsyn-beta (ATPB	ATPB_DRO	54 kDa	207	208	200	375	286	285
ATP synthase subunit gamma, mitochondrial ATPsyngamma	ATPG_DRO	33 kDa	97	93	97	117	103	97
Calcium-transporting ATPase Ca-P60A	A0A0B4LG	109 kDa	55	36	63	82	55	73
Unc-89, isoform E Unc-89	A0A0B4LG	473 kDa	50	22	46	88	47	56
ATP synthase subunit d, mitochondrial ATPsynD	ATP5H_DR	20 kDa	50	47	41	59	50	49
Cluster of Sodium/potassium-transporting ATPase subunit alpha Atpalp	ATNA_DRO	116 kDa	49	26	55	49	39	50
AT02348p UQCR-C2	Q9VV75_D	45 kDa	47	36	35	49	37	42
ATP synthase subunit O, mitochondrial ATPsynO	ATPO_DRO	22 kDa	45	36	47	53	38	40
CG3731, isoform A UQCR-C1	Q9VFF0_DI	52 kDa	45	42	49	51	43	36
ATP synthase subunit b, mitochondrial ATPsynB	AT5F1_DR	27 kDa	41	42	47	72	57	52
Fructose-bisphosphate aldolase Ald	ALF_DROM	39 kDa	37	46	42	48	48	56
Probable citrate synthase, mitochondrial kdn	CISY_DROM	52 kDa	34	22	28	39	29	28
Neuroglian, isoform D Nrg	E1JJF9_DR	138 kDa	31	13	25	34	20	22
Lethal (1) G0230, isoform A ATPsyndelta	Q9W2X6_D	17 kDa	30	32	32	37	33	35
Glycerol-3-phosphate dehydrogenase Gpo-1	Q7K569_D	80 kDa	28	14	22	44	36	35
Proteasome subunit alpha type-1 Prosalpha6	PSA1_DRO	31 kDa	28	19	24	28	23	31
Cluster of Proteasome subunit beta type Prosbeta2 (Q9VUJ1_DROME)	Q9VUJ1_DI	30 kDa	27	8	14	19	16	21
Fasciclin 1, isoform G Fas1	A0A0B4KH	74 kDa	26	2	27	24	20	33
CG4769, isoform A Cyt-c1	Q9VRL0_DI	34 kDa	20	14	18	27	23	18
Stretchin-Mlck, isoform R Strn-Mlck	A1ZA73_DI	215 kDa	20	2	6	11	5	0
Cluster of Actin-42A Act42A (ACT2_DROME)	ACT2_DRO	42 kDa	19	24	23	12	12	17
Glucose-6-phosphate isomerase Pgi	G6PI_DRO	62 kDa	18	18	26	28	28	22
Cytochrome b-c1 complex subunit Rieske, mitochondrial RFeSP	Q9VQ29_D	25 kDa	18	9	18	18	9	15
Proteasome subunit alpha type-5 Prosalpha5	PSA5_DRO	27 kDa	18	8	13	18	13	19
Proteasome subunit beta type-1 Prosbeta6	PSB1_DRO	26 kDa	17	9	13	16	14	16
Voltage-dependent anion-selective channel porin	VDAC_DRO	31 kDa	16	15	18	22	22	19
Proteasome subunit beta type Prosbeta5	Q7K148_D	31 kDa	16	9	12	14	14	15
Cluster of Arginine kinase, isoform E Argk (A8JNP2_DROME)	A8JNP2_DI	42 kDa	15	9	18	27	20	17
Cluster of Proteasome subunit alpha type-4 Prosalpha3 (PSA4_DROME)	PSA4_DRO	29 kDa	15	7	12	10	12	15
Proteasome subunit beta type-4 Prosbeta7	PSB4_DRO	30 kDa	15	5	9	13	10	11
CG7920, isoform A CG7920	Q9VAC1_D	52 kDa	14	12	13	9	13	8
CG30415, isoform A CG30415	Q0E8X7_DI	10 kDa	13	12	12	12	15	8
ADP,ATP carrier protein sesB	ADT_DROM	34 kDa	13	8	21	22	19	20
CG8036, isoform D CG8036	Q7KSU6_D	63 kDa	13	5	11	17	11	10
Cluster of Paramyosin, long form Prm (MYSP1_DROME)	MYSP1_DR	102 kDa	13	4	15	8	3	1
Dipeptidase B, isoform A Dip-B	Q9VFQ9_D	56 kDa	13	3	8	11	7	5
CG11015-PA COX5B	Q9VMB9_D	14 kDa	13	7	11	13	10	14
Putative ATP synthase subunit f, mitochondrial CG4692	ATPK_DRO	12 kDa	12	16	14	22	15	17

Cluster of Myosin heavy chain, isoform P Mhc (E1JHJ5_DROME)	E1JHJ5_DR	223 kDa	12	4	9	21	10	5
Innexin inx2 Inx2	INX2_DRO	42 kDa	12	10	14	16	16	12
Cytochrome b-c1 complex subunit 7 UQCR-14	Q9VXI6_DR	14 kDa	12	7	11	21	11	10
CG10664-PA, isoform A COX4	Q9VIQ8_DR	21 kDa	12	7	12	13	9	13
Catalase Cat	CATA_DRO	57 kDa	12	7	9	12	7	9
CG31075, isoform B CG31075	A0A0B4K6	55 kDa	12	3	17	13	10	4
Proteasome subunit alpha type-6 Prosalpha1	PSA6_DRO	27 kDa	12	5	10	11	11	14
Proteasome subunit beta type Prosbeta1	A0AQH0_D	24 kDa	12	6	6	7	11	13
Cluster of Heat shock 70 kDa protein cognate 3 Hsc70-3 (HSP7C_DROM	HSP7C_DR	72 kDa	11	4	8	19	13	9
Proteasome subunit alpha type-3 Prosalpha7	PSA3_DRO	28 kDa	11	6	7	10	6	12
Proteasome subunit alpha type-2 Prosalpha2	PSA2_DRO	26 kDa	11	6	7	12	7	8
Proteasome subunit alpha type-7-1 Prosalpha4	PSA71_DR	28 kDa	11	4	6	8	7	9
Proteasome subunit beta type Prosbeta4	Q9VJJ0_DR	22 kDa	10	4	4	6	4	7
AT13736p UQCR-Q	Q9VVH5_D	10 kDa	10	8	7	9	8	7
Heat shock protein 83 Hsp83	HSP83_DR	82 kDa	8	1	3	10	5	4
NADH dehydrogenase [ubiquinone] 1 alpha subcomplex subunit 10, mi	NDUAA_DR	47 kDa	8	1	8	1	0	0
Contactin Cont	CONT_DRO	158 kDa	7	2	12	17	11	13
Neurexin-4 Nrx-IV	NRX4_DRO	145 kDa	7	3	9	7	3	10
Nucleoside diphosphate kinase awd	A0A0B4LH	19 kDa	7	2	4	8	6	6
Levy, isoform A levy	Q9W1N3_D	12 kDa	7	3	4	6	4	4
Cluster of Terribly reduced optic lobes, isoform AI trol (M9NET2_DROM	M9NET2_D	432 kDa	6	3	16	14	7	6
CG9762-PA ND-SGDH	Q9VTU2_D	22 kDa	6	3	8	11	10	9
Enigma Egm	Q5U117_D	71 kDa	6	5	7	20	14	15
Cluster of Calcium-transporting ATPase PMCA (E6EK15_DROME)	E6EK15_DR	132 kDa	6	2	8	12	8	7
CG32230, isoform B ND-MLRQ	Q8SYJ2_DR	9 kDa	6	5	5	12	4	6
CG14028-PA cype	Q9VMS1_D	8 kDa	6	6	5	4	3	7
Proteasome subunit beta type-3 Prosbeta3	PSB3_DRO	23 kDa	6	6	6	6	5	6
Stunted, isoform B sun	Q8IR24_DR	6 kDa	6	4	6	6	3	3
IP09655p Mdh2	Q9VEB1_DI	35 kDa	6	5	8	14	10	10
CG3446, isoform B ND-B16.6	Q9W402_D	18 kDa	6	4	6	7	5	7
Cluster of Sodium/potassium-transporting ATPase subunit beta-2 nrv2 (	ATPB2_DR	37 kDa	6	2	6	7	7	4
9 kD basic protein ATPsynE	O77134_D	9 kDa	6	4	4	6	6	6
CG13492 CG13492	Q8MLU9_D	321 kDa	5	0	2	1	0	0
Innexin inx1 ogre	INX1_DRO	43 kDa	5	4	11	15	5	5
Flightin fln	FTN_DROM	21 kDa	5	2	4	2	4	1
Pyruvate carboxylase PCB	Q0E9E2_DR	133 kDa	5	0	3	6	3	5
CG1970, isoform B ND-49	Q9V4E0_DI	53 kDa	5	3	8	13	12	10
FI04632p nrv3	Q7JS69_DR	36 kDa	5	1	3	4	2	5
Cytochrome c oxidase subunit 2 mt:CoII	COX2_DRO	26 kDa	5	6	6	5	6	5
Cluster of Tropomyosin-1, isoforms 33/34 Tm1 (TPM4_DROME)	TPM4_DRO	55 kDa	4	12	16	10	5	6
Albumin	ALBU_RABI	69 kDa	4	0	0	0	0	0

Cluster of CG9090, isoform A CG9090-RA (Q7JUS9_DROME)	Q7JUS9_DR	41 kDa	4	1	5	2	3	5
CG4389-PB, isoform B Mtpalpha	Q8IPE8_DR	80 kDa	4	0	3	8	2	2
Cluster of Glyceraldehyde-3-phosphate dehydrogenase 1 Gapdh1 (G3P1	G3P1_DRO	35 kDa	4	2	3	3	3	3
CG9629 CG9629	Q8SXQ1_D	58 kDa	4	1	6	3	1	2
NADH dehydrogenase [ubiquinone] 1 beta subcomplex subunit 8, mitoc	Q9W3X7_D	20 kDa	4	3	6	17	12	11
CG6105-PA ATPsynG	Q9VKM3_D	11 kDa	4	4	9	9	6	7
FI19426p1 SP1173	Q0E8H7_D	82 kDa	4	0	1	3	2	1
Z band alternatively spliced PDZ-motif protein 52, isoform W Zasp52	A0A0B4LGI	227 kDa	3	1	5	3	8	0
Alcohol dehydrogenase Adh	ADH_DRON	28 kDa	3	1	4	8	3	5
Cytochrome c oxidase subunit 5A, mitochondrial COX5A	COX5A_DR	17 kDa	3	4	2	2	2	3
Basigin, isoform B Bsg	Q8IPG9_DR	29 kDa	3	2	2	4	3	2
CG3734, isoform A CG3734	Q8SXS7_DR	53 kDa	3	0	1	0	0	0
CG6020, isoform A ND-39	Q9VPE2_DI	47 kDa	3	3	4	6	6	4
Eip55E, isoform A Eip55E	Q7JXZ2_DR	43 kDa	3	1	3	4	2	1
CG12079-PA ND-30	Q9VZU4_D	30 kDa	3	2	7	11	12	10
Ferritin Fer2LCH	A0A0B4KH	26 kDa	3	1	4	4	3	4
Pyruvate kinase PyK	KPYK_DRO	57 kDa	3	1	1	6	3	4
AT12494p ND-B22	Q9VJZ4_DR	17 kDa	3	1	2	4	3	5
FI01422p Spn43Ab	A1Z6V5_DR	43 kDa	3	2	3	5	3	3
CG9172, isoform A ND-20	Q9VXK7_D	25 kDa	3	4	3	10	7	6
Integrin beta-PS mys	ITBX_DRON	93 kDa	3	0	0	2	1	0
Stretchin-Mlck, isoform S Strn-Mlck	A0A0B4KF8	919 kDa	3	0	2	3	0	0
Innexin inx3 Inx3	INX3_DRO	45 kDa	2	2	11	10	13	7
Phosphoglucomutase Pgm	PGM_DRO	61 kDa	2	1	5	8	8	6
Reticulon-like protein Rtnl1	E1JHT6_DR	65 kDa	2	0	4	6	3	2
Cluster of Elongation factor 1-alpha 2 Ef1alpha100E (EF1A2_DROME)	EF1A2_DRO	51 kDa	2	7	4	5	6	5
Mitochondrial import receptor subunit TOM40 homolog 1 Tom40	TO401_DR	36 kDa	2	2	5	11	4	5
CG14235-PB, isoform B COX6B	Q8IQW2_D	9 kDa	2	1	0	1	0	1
Probable isocitrate dehydrogenase [NAD] subunit alpha, mitochondrial	IDH3A_DR	41 kDa	2	1	3	2	2	1
LDL receptor protein 1, isoform F LRP1	A0A0B4KFI	531 kDa	2	0	0	0	0	0
CG12859 ND-B15	Q6IDF5_DR	13 kDa	2	2	2	8	6	7
Multifunctional protein ADE2 ade5	PUR6_DRO	47 kDa	2	0	3	3	2	2
CG4600-PA yip2	Q9VL70_DI	42 kDa	2	1	2	6	5	2
Microtubule-associated protein 205, isoform C Map205	A0A0B4KI7	118 kDa	2	0	1	2	3	0
Cluster of Aspartyl beta-hydroxylase, isoform J Asph (D1Z397_DROME)	D1Z397_DI	45 kDa	2	0	4	6	4	3
Probable methylcrotonoyl-CoA carboxylase beta chain, mitochondrial	MCCB_DRO	63 kDa	2	0	0	2	1	2
CG1640, isoform A CG1640	Q7KV27_D	63 kDa	2	1	5	8	3	6
Anion exchange protein CG8177	M9PEQ4_D	137 kDa	2	0	0	0	1	2
Evolutionarily conserved signaling intermediate in Toll pathway, mitoc	ECSIT_DRO	47 kDa	2	1	2	11	9	5
LP07226p mge	Q9VZL1_DR	16 kDa	2	2	2	8	5	6
NADH dehydrogenase [ubiquinone] 1 subunit C2 ND-B14.5B	Q9VQM2_D	13 kDa	2	1	3	7	4	5

Maltase A1 Mal-A1	MAL1_DRO	66 kDa	2	1	0	4	3	5
CG14482, isoform A UQCR-6.4	Q500Y7_DI	6 kDa	2	1	2	2	4	4
Chitinase-like protein CG5210 CG5210	C5210_DR	50 kDa	2	0	1	3	2	2
CG42307, isoform A mus312-RD	B7Z0C9_DI	11 kDa	2	0	2	3	2	2
Alpha-actinin, sarcomeric Actn	ACTN_DRO	107 kDa	2	0	2	4	1	0
Cytochrome b-c1 complex subunit 9 ox	QCR9_DRO	6 kDa	2	2	2	3	2	2
Larval serum protein 1 alpha chain Lsp1alpha	LSP1A_DR	99 kDa	2	0	0	0	0	0
Cluster of ATP-citrate synthase ATPCL (Q7KN85_DROME)	Q7KN85_D	121 kDa	2	0	2	13	8	13
Ergic53, isoform A ergic53	Q9V3A8_D	58 kDa	2	0	1	3	2	3
Cluster of V-type proton ATPase catalytic subunit A isoform 2 Vha68-2 (V	VATA2_DR	68 kDa	2	0	3	3	1	2
LD13601p UGP	Q9VSW1_D	59 kDa	1	1	4	8	5	10
Succinate dehydrogenase [ubiquinone] flavoprotein subunit, mitochon	SDHA_DRO	72 kDa	1	0	2	3	2	2
Apolipophorins Rfabg	APLP_DRO	373 kDa	1	0	6	33	5	9
Oligosaccharide transferase delta subunit, isoform B OstDelta	A0A0B4LFR	69 kDa	1	2	7	5	4	6
Glutamate oxaloacetate transaminase 1, isoform B Got1	A1ZAA5_DI	49 kDa	1	1	1	7	3	0
Tubulin beta-1 chain betaTub56D	TBB1_DRO	50 kDa	1	1	0	1	2	1
Vacuolar protein sorting 13, isoform A Vps13	A1Z713_DI	375 kDa	1	0	0	2	1	0
60S acidic ribosomal protein P0 RpLP0	RLA0_DRO	34 kDa	1	1	2	3	2	2
Cluster of Fat body protein 2 Fbp2 (FBP2_DROME)	FBP2_DRO	29 kDa	1	0	2	7	1	0
NADH-ubiquinone oxidoreductase 75 kDa subunit, mitochondrial ND-7	NDUS1_DR	79 kDa	1	1	3	20	22	11
CG2118, isoform A CG2118	Q9V9T5_DI	77 kDa	1	0	0	2	1	2
Transmembrane protein 70 homolog, mitochondrial CG7506	TMM70_DI	27 kDa	1	0	3	1	4	1
Clumsy, isoform B clumsy	Q0E8N6_D	113 kDa	1	0	1	2	0	0
CG13887, isoform C CG13887	Q9W0M4_	26 kDa	1	0	1	5	1	0
GM23292p ND-B17	Q9V3W2_D	19 kDa	1	0	8	15	8	7
Heat shock protein 23 Hsp23	HSP23_DR	21 kDa	1	0	1	3	1	1
RPII140-upstream gene protein 140up	140U_DRO	29 kDa	1	0	1	13	10	10
Histone H2B His2B	H2B_DROM	14 kDa	1	4	2	0	2	2
CG8844 protein ND-PDSW	Q9VQR2_D	19 kDa	1	1	1	10	7	9
CG6463-PA ND-13B	Q9VTB4_DI	14 kDa	1	0	0	9	7	5
CG9297, isoform B CG9297	Q8I0D4_DI	106 kDa	0	0	1	2	1	2
Cluster of Lethal (2) 01289, isoform F l(2)01289 (E1JGY6_DROME)	E1JGY6_DR	205 kDa	0	0	2	1	0	2
Ryanodine receptor, isoform H RyR	A0A0B4K6T	581 kDa	0	0	0	3	0	0
Succinate dehydrogenase [ubiquinone] iron-sulfur subunit, mitochond	SDHB_DRO	34 kDa	0	0	0	4	4	2
Neural conserved at 73EF, isoform I Nc73EF	A8JNU6_DI	123 kDa	0	0	1	1	2	3
Cheerio, isoform M cher	A0A0B4KG	263 kDa	0	0	0	4	0	0
Bicoid stability factor bsf	Q9VJ86_DI	157 kDa	0	0	0	1	3	0
Cluster of CG16791, isoform A CG16791 (Q9VDB7_DROME)	Q9VDB7_D	121 kDa	0	0	0	0	3	0
CG17687 CG17687	Q9VU57_D	179 kDa	0	0	0	0	0	2
Cluster of MICOS complex subunit Mic60 Mitofilin (MIC60_DROME)	MIC60_DR	82 kDa	0	0	0	1	3	2
CG6512-PA, isoform A CG6512	Q8T4G5_D	90 kDa	0	0	0	3	0	1

Calnexin 99A, isoform E Cnx99A	Q0KHZ9_D	69 kDa	0	0	1	8	1	0
GH13256p Thiolase	Q9W1H8_D	51 kDa	0	0	0	2	1	0
Kazachoc, isoform F kcc	A0A0B4LHI	118 kDa	0	0	0	2	3	2
Succinyl-CoA ligase subunit beta skap	A0A0B4JCV	49 kDa	0	0	0	5	2	1
CG8888 CG8888	Q7K3N4_D	43 kDa	0	0	3	3	3	4
Protein PTCD3 homolog, mitochondrial CG4679	PTCD3_DR	74 kDa	0	1	0	2	3	0
T-complex protein 1 subunit delta CG5525	Q9VK69_D	57 kDa	0	0	0	3	1	0
GH05862p NP15.6	Q9V3L7_DI	17 kDa	0	2	3	6	2	3
CG5548, isoform B ND-B18	Q9VXZ0_DI	14 kDa	0	0	3	9	9	8
Delta-1-Pyrroline-5-carboxylate dehydrogenase 1, isoform A P5CDh1	Q9VNX4_D	64 kDa	0	0	0	2	0	1
CG7033 CG7033	Q9W392_D	58 kDa	0	0	2	3	0	0
Integrin alpha-PS2 if	ITA2_DRON	154 kDa	0	0	0	2	0	0
CG13506, isoform A CG13506-RA	Q9W259_D	57 kDa	0	0	0	3	0	0
CG1371 CG1371	A1Z843_DI	131 kDa	0	0	3	4	2	0
Fat-body protein 1 Fbp1	FBP1_DRO	120 kDa	0	0	0	2	0	0
ATP synthase-coupling factor 6, mitochondrial ATPsynCf6	ATP5J_DRO	12 kDa	0	0	3	2	2	1
Cluster of Keratin, type I microfibrillar, 47.6 kDa (K1M2_SHEEP)	K1M2_SHE	46 kDa	0	2	3	0	0	0
Tropomyosin 2, isoform E Tm2	A0A0B4KH	33 kDa	0	1	2	1	0	0
Limpet, isoform K Lmpt	Q7KUQ6_D	246 kDa	0	0	0	7	4	3
GH13725p Tcp-1zeta	Q9VXQ5_D	58 kDa	0	0	3	5	6	0
RE74917p tobi	Q9VBR6_D	75 kDa	0	6	0	0	5	4
Protein NDUFAF4 homolog CG11722	NDUF4_DR	24 kDa	0	0	1	10	2	0
CG9140, isoform B ND-51	Q9VMI3_D	52 kDa	0	0	0	5	3	2
Complex I intermediate-associated protein 30, mitochondrial CIA30	CIA30_DRO	34 kDa	0	0	0	2	3	4
CG40002, isoform A ND-AGGG	Q7PL91_DI	11 kDa	0	0	0	4	2	3
Cluster of RIC-3, isoform N RIC-3 (E1JGP2_DROME)	E1JGP2_DR	52 kDa	0	0	0	5	0	2
FI18406p1 Stim	Q7KUZ1_D	64 kDa	0	0	0	2	0	0
CG5903, isoform A CG5903	Q9VEY5_DI	24 kDa	0	0	0	2	3	0
Histone H4 His4	H4_DROME	11 kDa	0	6	0	0	0	0
CG7712, isoform A ND-B14	Q7JZK1_DI	15 kDa	0	0	0	2	1	1
Cluster of Lipophorin receptor 1, isoform K LpR1 (A8JRD0_DROME)	A8JRD0_DI	119 kDa	0	0	0	2	1	0
CG3214, isoform B ND-B17.2	Q9VQD7_D	17 kDa	0	0	0	6	0	0
FI18644p1 Hmu	Q9VB46_D	63 kDa	0	0	1	2	1	0
PHCl, isoform N pHCl	M9PI70_DI	108 kDa	0	0	0	2	0	0
Transcription factor BTF3 CG11835	Q9VPR2_D	83 kDa	0	0	0	2	0	0
Histone H2A.v His2Av	H2AV_DRO	15 kDa	0	2	0	0	0	0
CG5103 CG5103-RA	Q9VVP4_D	68 kDa	0	0	2	2	1	0
	Proteins shown in heat map							

Table 2.5: Mass spectrometry identifying constituents of the membrane arm subcomplex of CI, related to Figure 2.9.

The table shows the CI subunits and other proteins identified as part of the membrane arm subcomplex

			Mutant	Mutant	Mutant	Mutant	Wild type	Wild type		
			1FS5	1FV1	2FS5	2FV1	1WT	2WT		
Identified Proteins (450/522)	Accession Number	Molecular	tk161118_Osu	tk161118_	tk161118_	tk161118_	tk161118_	tk161118_Osuwu_2_WT		
Glycerol-3-phosphate dehydrogenase Gpo-1	Q7K569_DROME	80 kDa	130	155	144	143	152	146		
Cluster of Calcium-transporting ATPase Ca-P60A (A0A0B4LGB7_DROME	A0A0B4LGB7_DROME	109 kDa	157	162	152	149	146	135		
Probable citrate synthase, mitochondrial kdn	CISY_DROME	52 kDa	126	146	141	138	123	129		
Pyruvate kinase PyK	KPYK_DROME	57 kDa	120	123	138	113	125	129		
Sodium/potassium-transporting ATPase subunit alpha Atpalpha	ATNA_DROME	116 kDa	117	111	120	120	93	124		
Cluster of CG4389-PB, isoform B Mtpalpha (Q8IPE8_DROME)	Q8IPE8_DROME [2]	80 kDa	107	102	91	93	106	100		
Cluster of Calcium-transporting ATPase PMCA (Q9V4C7_DROME)	Q9V4C7_DROME [5]	133 kDa	82	97	90	98	84	83		
ATP synthase subunit beta, mitochondrial ATPsyn-beta	ATPB_DROME (+1)	54 kDa	96	97	98	96	101	103		
Succinate dehydrogenase [ubiquinone] flavoprotein subunit, mitochon	SDHA_DROME	72 kDa	73	87	70	75	79	80		
Cluster of ADP,ATP carrier protein sesB (ADT_DROME)	ADT_DROME [3]	34 kDa	56	65	59	62	67	70		
Cluster of Neural conserved at 73EF, isoform I Nc73EF (A8JNU6_DROM	A8JNU6_DROME [2]	123 kDa	66	73	70	60	74	64		
Cluster of Arginine kinase, isoform E Argk (A8JNP2_DROME)	A8JNP2_DROME [2]	42 kDa	80	65	68	68	78	67		
Voltage-dependent anion-selective channel porin	VDAC_DROME	31 kDa	64	84	62	72	67	67		
ATP synthase subunit alpha, mitochondrial blw	ATPA_DROME	59 kDa	65	55	67	63	70	66		
Cluster of Glutamate dehydrogenase, mitochondrial Gdh (DHE3_DROM	DHE3_DROME [2]	63 kDa	62	72	61	64	71	60		
Cluster of 60 kDa heat shock protein, mitochondrial Hsp60 (CH60_DRO	CH60_DROME [2]	61 kDa	33	55	74	69	63	57		hsp60
Trehalase Treh	A4UZR3_DROME	64 kDa	58	56	53	40	59	49		
Alpha actinin, isoform D Actn	M9MS06_DROME	104 kDa	68	51	83	57	35	34		
Pyruvate carboxylase PCB	Q0E9E2_DROME (+1)	133 kDa	54	72	46	43	59	37		
Stretchin-Mlck, isoform R Strn-Mlck	A1ZA73_DROME	215 kDa	60	67	43	84	14	48		
Cluster of Tropomyosin-1, isoforms 33/34 Tm1 (TPM4_DROME)	TPM4_DROME [4]	55 kDa	62	49	49	46	41	41		
Cluster of Proline dehydrogenase 1, mitochondrial slgA (PROD_DROME	PROD_DROME [2]	77 kDa	40	39	33	26	39	28		
Cluster of Fructose-bisphosphate aldolase Ald (ALF_DROME)	ALF_DROME [2]	39 kDa	50	57	40	35	40	44		
CG9485, isoform B CG9485	Q9W2H8_DROME	183 kDa	34	29	46	35	41	36		
Glucose-6-phosphate isomerase Pgi	G6PI_DROME	62 kDa	45	56	45	50	48	54		
Cluster of Titin sls (TITIN_DROME)	TITIN_DROME [2]	2066 kDa	24	13	36	22	0	7		
Cluster of Ryanodine receptor, isoform J RyR (A0A0B4K715_DROME)	A0A0B4K715_DROME	580 kDa	33	11	76	47	0	13		Ryr
CG7920, isoform A CG7920	Q9VAC1_DROME	52 kDa	42	41	47	36	41	50		
IP09655p Mdh2	Q9VEB1_DROME	35 kDa	37	48	45	45	41	42		
Cluster of Succinate dehydrogenase [ubiquinone] iron-sulfur subunit, m	SDHB_DROME [2]	34 kDa	31	36	40	34	35	34		
Enolase Eno	ENO_DROME	54 kDa	48	40	37	36	36	31		
Enigma Egm	Q5U117_DROME	71 kDa	49	55	40	41	28	27		Egm
Cluster of Tropomyosin-2 Tm2 (TPM2_DROME)	TPM2_DROME [2]	33 kDa	50	45	34	31	38	35		
Cluster of Aralar1, isoform F aralar1 (A0A0B4KHW3_DROME)	A0A0B4KHW3_DROM	77 kDa	38	37	32	35	43	41		
LETM1 and EF-hand domain-containing protein anon-60Da, mitochond	A60DA_DROME	114 kDa	25	36	21	30	55	29		
CG3731, isoform A UQCR-C1	Q9VFF0_DROME	52 kDa	48	45	44	43	14	42		UQCR-C1
CG10664-PA, isoform A COX4	Q9VIQ8_DROME	21 kDa	28	26	29	35	29	33		Cox4
CG11015-PA COX5B	Q9VMB9_DROME	14 kDa	35	39	42	50	39	48		Cox5B
AT02348p UQCR-C2	Q9VV75_DROME	45 kDa	49	45	46	38	17	33		UQCR-C2
GM23292p ND-B17	Q9V3W2_DROME	19 kDa	55	47	57	40	2	2		FB6
ATP synthase subunit gamma, mitochondrial ATPsyngamma	ATPG_DROME	33 kDa	38	36	42	36	34	39		

GH13256p Thiolase	Q9W1H8_DROME	51 kDa	39	39	27	31	41	34		
Cluster of Actin, larval muscle Act79B (ACT4_DROME)	ACT4_DROME [4]	42 kDa	37	33	26	33	27	37		
Cytochrome c oxidase subunit 5A, mitochondrial COX5A	COX5A_DROME	17 kDa	34	32	32	37	22	38		Cox5A
NADH dehydrogenase [ubiquinone] 1 beta subcomplex subunit 8, mitoc	Q9W3X7_DROME	20 kDa	53	46	47	45	1	3		FB8
Malic enzyme Men	Q9VG31_DROME (+1)	85 kDa	30	34	23	29	19	29		
CG8844 protein ND-PDSW	Q9VQR2_DROME	19 kDa	52	36	43	38	3	6		FB10
Neuroglian, isoform D Nrg	E1JJF9_DROME (+2)	138 kDa	28	26	20	18	18	19		
Neuromusculin, isoform E nrm	M9NE05_DROME	245 kDa	20	22	23	25	26	19		
Aconitate hydratase, mitochondrial Acon	Q9VIE8_DROME	85 kDa	17	25	19	16	27	19		
Pyruvate dehydrogenase E1 component subunit alpha l(1)G0334	Q7KVX1_DROME	49 kDa	33	31	20	22	32	18		
Cluster of Shibire, isoform L shi (E1JJA4_DROME)	E1JJA4_DROME [5]	99 kDa	22	26	20	17	24	16		
Cluster of Z band alternatively spliced PDZ-motif protein 52, isoform W	A0A0B4LGL0_DROME	227 kDa	16	23	12	22	24	17		
CG14235-PA, isoform A COX6B	Q9VWD1_DROME	11 kDa	16	14	21	18	20	23		
Cluster of Lethal (2) 01289, isoform F l(2)01289 (E1JGY6_DROME)	E1JGY6_DROME [3]	205 kDa	19	13	20	21	10	8		
Cluster of Reticulon-like protein Rtnl1 (E1JHT6_DROME)	E1JHT6_DROME [4]	65 kDa	19	17	22	28	15	16		
CG9090, isoform A CG9090-RA	Q7JUS9_DROME	41 kDa	17	24	20	19	17	24		
V-type proton ATPase subunit a Vha100-2	Q9VE75_DROME	95 kDa	25	23	24	22	0	21		
Mitochondrial import receptor subunit TOM40 homolog 1 Tom40	TO401_DROME	36 kDa	26	31	28	24	27	22		
ATP synthase subunit b, mitochondrial ATPsynB	AT5F1_DROME	27 kDa	20	22	21	19	15	20		
CG4600-PA yip2	Q9VL70_DROME	42 kDa	28	27	24	22	21	23		
Alcohol dehydrogenase Adh	ADH_DROME	28 kDa	25	25	25	24	23	26		
CG9762-PA ND-SGDH	Q9VTU2_DROME	22 kDa	35	28	30	29	4	5		FB5
Phosphoglucomutase Pgm	PGM_DROME	61 kDa	16	26	11	18	17	18		
Limpet, isoform K Lmpt	Q7KUQ6_DROME	246 kDa	13	11	15	20	8	11		
CG31233 CG5839	Q8MRN5_DROME	107 kDa	46	11	24	21	3	22		
Cluster of Fasciclin 2, isoform H Fas2 (X2JCI0_DROME)	X2JCI0_DROME [3]	93 kDa	24	21	20	20	8	13		
Probable isocitrate dehydrogenase [NAD] subunit alpha, mitochondrial	IDH3A_DROME	41 kDa	23	27	11	19	20	15		
Evolutionarily conserved signaling intermediate in Toll pathway, mitoch	ECSIT_DROME	47 kDa	18	25	14	16	11	10		
Maltase A1 Mal-A1	MAL1_DROME	66 kDa	30	24	13	20	14	11		
Cluster of Sodium/potassium-transporting ATPase subunit beta-2 nrv2	ATPB2_DROME [2]	37 kDa	21	18	17	20	18	16		
Cluster of CG11876, isoform A CG11876 (Q7K5K3_DROME)	Q7K5K3_DROME [2]	39 kDa	21	22	16	20	18	17		
Cluster of Basigin, isoform G Bsg (Q7KTJ7_DROME)	Q7KTJ7_DROME [2]	71 kDa	17	22	23	20	17	15		
CG8036, isoform B CG8036	Q9VHN7_DROME	68 kDa	14	21	12	17	15	23		
NADH dehydrogenase [ubiquinone] 1 subunit C2 ND-B14.5B	Q9VQM2_DROME	13 kDa	30	35	23	24	4	3		FC2
Fasciclin 1, isoform G Fas1	A0A0B4KH94_DROM	74 kDa	22	22	17	14	6	5		
Cluster of Multidrug-Resistance like protein 1, isoform C MRP (Q7KTC7	Q7KTC7_DROME [8]	173 kDa	11	12	14	14	12	13		
CG32230, isoform B ND-MLRQ	Q8SYJ2_DROME	9 kDa	15	16	18	18	17	21		
Cluster of Integrin beta mys (X2JE30_DROME)	X2JE30_DROME [2]	93 kDa	22	18	20	17	7	8		
CG31343 CG5839	Q8SWX4_DROME	108 kDa	33	23	10	19	0	29		
CG4769, isoform A Cyt-c1	Q9VRL0_DROME	34 kDa	19	18	22	18	7	18		
Cluster of CG9297, isoform B CG9297 (Q8I0D4_DROME)	Q8I0D4_DROME [2]	106 kDa	26	12	9	17	8	8		
Glycogen phosphorylase GlyP	PYG_DROME	97 kDa	8	14	11	6	17	9		
CG5548, isoform B ND-B18	Q9VXZ0_DROME	14 kDa	31	28	31	20	2	4		FB7
LP07226p mge	Q9VZL1_DROME	16 kDa	19	19	18	16	19	21		

Cluster of Myosin heavy chain, isoform O Mhc (E1JHJ3_DROME)	E1JHJ3_DROME [4]	225 kDa	14	3	11	10	5	6		
Bicoid stability factor bsf	Q9VJ86_DROME	157 kDa	10	16	6	14	21	10		
Cytochrome c oxidase subunit 2 mt:CoII	COX2_DROME	26 kDa	12	16	18	18	19	18		
Delta-1-Pyrroline-5-carboxylate dehydrogenase 1, isoform A P5CDh1	Q9VNX4_DROME	64 kDa	13	14	17	8	10	9		
Probable methylmalonate-semialdehyde dehydrogenase [acylating], m	MMSA_DROME	56 kDa	13	8	16	14	16	10		
CG2658, isoform A CG2658	Q9W4W8_DROME	90 kDa	14	10	11	5	16	12		
MICOS complex subunit Mic60 Mitofilin	MIC60_DROME	82 kDa	9	15	6	9	8	7		
ATP synthase subunit d, mitochondrial ATPsynD	ATP5H_DROME	20 kDa	13	7	14	15	13	16		
Acyl-CoA synthetase long-chain, isoform J Acsl	A0A0B4KFE4_DROME	82 kDa	13	12	16	13	14	9		
Cluster of FI04465p hoe1 (Q9VR47_DROME)	Q9VR47_DROME [2]	95 kDa	19	16	17	15	13	9		
Levy, isoform A levy	Q9W1N3_DROME	12 kDa	10	9	8	12	10	14		
Nucleoside diphosphate kinase awd	A0A0B4LHX6_DROME	19 kDa	15	13	13	15	15	13		
Neprilysin 2, isoform B Nep2	A0A0B4K692_DROME	88 kDa	13	10	9	18	8	8		
AT12494p ND-B22	Q9VJZ4_DROME	17 kDa	17	15	17	14	2	2		FB9
Cluster of 3-hydroxyacyl-CoA dehydrogenase type-2 scu (HCD2_DROME	HCD2_DROME [2]	27 kDa	13	18	13	14	15	11		
Fructose-1,6-bisphosphatase fbp	Q9VIS3_DROME	36 kDa	14	16	15	12	13	11		
CG6439, isoform A CG6439	Q9VD58_DROME	40 kDa	13	14	13	14	13	15		
CG1970, isoform B ND-49	Q9V4E0_DROME	53 kDa	27	4	17	2	9	6		
Serine hydroxymethyltransferase CG3011	Q9W457_DROME	59 kDa	4	11	6	10	8	4		
CG7461, isoform B CG7461	A1ZBJ2_DROME	68 kDa	10	12	14	7	16	11		
CG1824 CG1824	Q9VYL5_DROME	84 kDa	7	14	10	13	10	11		
CG1640, isoform A CG1640	Q7KV27_DROME (+1)	63 kDa	11	11	10	8	8	7		
CG32649 CG4410	Q9VYI6_DROME	74 kDa	10	11	6	4	14	5		
Succinyl-CoA ligase [ADP/GDP-forming] subunit alpha, mitochondrial Sc	SUCA_DROME	34 kDa	14	19	13	18	12	13		
Cluster of Glyceraldehyde-3-phosphate dehydrogenase 1 Gapdh1 (G3P	G3P1_DROME [2]	35 kDa	10	12	10	11	13	11		
CG9634, isoform A goe	Q9XZ14_DROME (+1)	100 kDa	13	12	7	6	8	6		
Heat shock 70 kDa protein cognate 3 Hsc70-3	HSP7C_DROME	72 kDa	13	17	11	10	13	16		
Cluster of Heat shock 70 kDa protein cognate 4 Hsc70-4 (HSP7D_DROM	HSP7D_DROME [2]	71 kDa	18	22	16	17	17	20		
CG5028, isoform C CG5028-RC	A8JRB8_DROME (+2)	43 kDa	12	8	11	6	6	9		
CG7433, isoform A CG7433	Q9VW68_DROME	55 kDa	5	11	6	11	7	4		
V-type proton ATPase subunit d 1 VhaAC39-1	VA0D1_DROME	40 kDa	12	12	12	7	2	9		
NADH-ubiquinone oxidoreductase 75 kDa subunit, mitochondrial ND-75	NDUS1_DROME	79 kDa	23	0	21	0	3	4		
Cluster of Elongation factor 1-alpha 1 Ef1alpha48D (EF1A1_DROME)	EF1A1_DROME [2]	50 kDa	6	7	4	9	6	12		
Putative apoptosis-inducing factor 1, mitochondrial AIF	AIFM1_DROME (+1)	81 kDa	13	16	6	6	13	6		
Amino acid transporter Eaat1	O77062_DROME	52 kDa	7	10	7	8	7	8		
GH21316p Ssadh	Q9VBP6_DROME	55 kDa	6	12	9	8	9	3		
Contactin Cont	CONT_DROME	158 kDa	7	6	6	7	6	4		
Cluster of Stretchin-Mlck, isoform U Strn-Mlck (A0A0B4KG35_DROME)	A0A0B4KG35_DROM	924 kDa	8	11	6	9	2	6		
CG3523, isoform C FASN1	B7Z001_DROME	278 kDa	3	6	4	2	4	3		
Na/Ca-exchange protein, isoform E Calx	A0A0B4K790_DROME	108 kDa	7	6	9	12	5	6		
BcDNA.GH11322 bdl	Q9U4G1_DROME	81 kDa	12	12	8	7	7	6		
Aldehyde dehydrogenase Aldh	Q9VLC5_DROME	57 kDa	9	16	12	10	5	4		
Glutamate oxaloacetate transaminase 1, isoform B Got1	A1ZAA5_DROME (+1)	49 kDa	5	9	7	12	7	9		
CG6851-PA, isoform A Mtch	Q9V3Y4_DROME	35 kDa	10	12	6	13	7	5		

Cytochrome b-c1 complex subunit Rieske, mitochondrial RFeSP	Q9VQ29_DROME	25 kDa	12	7	11	7	3	2		
Cluster of CG13887, isoform C CG13887 (Q9W0M4_DROME)	Q9W0M4_DROME [2	26 kDa	8	11	8	7	10	8		
Cluster of LP02262p l(1)G0255 (Q8IRQ5_DROME)	Q8IRQ5_DROME [3]	50 kDa	2	10	9	3	10	8		
Peroxiredoxin 1 Jafrac1	PRDX1_DROME	22 kDa	10	5	5	7	3	10		
CG31198 CG31198	Q8IN25_DROME	107 kDa	17	9	4	9	0	11		
CG14028-PA cype	Q9VMS1_DROME	8 kDa	7	7	7	7	8	9		
Succinyl-CoA ligase subunit beta skap	A0A0B4JCW4_DROM	49 kDa	6	18	8	4	6	5		
Catalase Cat	CATA_DROME	57 kDa	6	5	4	7	13	7		
Integrin alpha-PS3 scb	ITA3_DROME	125 kDa	11	9	7	8	3	2		
CG12859 ND-B15	Q6IDF5_DROME	13 kDa	7	12	13	12	4	3		FB4
Cluster of AMP deaminase, isoform E AMPdeam (Q9VY76_DROME)	Q9VY76_DROME [3]	89 kDa	4	6	1	0	11	1		
BcDNA.GH04962 GCS2alpha	Q7KMM4_DROME	106 kDa	7	9	3	4	7	7		
LD31742p whd	Q7JQH9_DROME (+1)	89 kDa	3	7	7	11	9	5		
CG11771 CG11771	Q9VC06_DROME	81 kDa	5	6	5	3	9	2		
Cluster of CG11700-PA CG11700 (R9PY16_DROME)	R9PY16_DROME [3]	34 kDa	4	4	5	3	4	13		
Cluster of Cytochrome b-c1 complex subunit 7 UQCR-14 (Q9VXI6_DRON	Q9VXI6_DROME [2]	14 kDa	8	3	9	4	0	6		
RH44771p SdhC	Q9VGS3_DROME	19 kDa	7	8	9	7	9	8		
Paramyosin, long form Prm	MYSP1_DROME	102 kDa	6	3	6	7	1	3		
CG6512-PA, isoform A CG6512	Q8T4G5_DROME	90 kDa	2	7	4	5	6	6		
FI01422p Spn43Ab	A1Z6V5_DROME	43 kDa	7	7	9	8	7	6		
Cluster of Beta-Tubulin at 56D, isoform A betaTub56D (A1ZBL0_DROME	A1ZBL0_DROME [6]	51 kDa	5	2	1	2	2	14		
GH04080p PPO1	Q7K2W6_DROME	79 kDa	7	7	9	5	7	4		
GH05862p NP15.6	Q9V3L7_DROME	17 kDa	11	11	10	8	4	7		FB11
Transporter Gat	Q9V4E7_DROME	72 kDa	5	4	6	4	2	8		
Complex I intermediate-associated protein 30, mitochondrial CIA30	CIA30_DROME	34 kDa	5	9	3	4	1	4		
Neurexin-4 Nrx-IV	NRX4_DROME	145 kDa	5	3	4	5	1	3		
Adenylyl cyclase-associated protein capt	Q9VPX6_DROME	84 kDa	6	4	9	8	8	7		
CG31663, isoform A CG31663	Q9VQ52_DROME	107 kDa	6	4	1	2	5	1		
Glycerol-3-phosphate dehydrogenase [NAD(+)] Gpdh	B5RIM9_DROME (+1)	39 kDa	6	8	7	8	7	4		
Glycoprotein 93 Gp93	Q9VAY2_DROME	90 kDa	6	5	1	3	7	4		
Putative ATP synthase subunit f, mitochondrial CG4692	ATPK_DROME	12 kDa	9	6	7	6	7	5		
Integrin alpha-PS2 if	ITA2_DROME	154 kDa	9	10	6	7	2	5		
Cluster of FI01544p Rab1 (O18332_DROME)	O18332_DROME [14]	23 kDa	3	2	3	3	1	2		
Malic enzyme Men-b	E1JIZ4_DROME (+2)	69 kDa	6	2	4	9	6	5		
V-type proton ATPase subunit a Vha100-1	Q6NLA3_DROME (+1)	97 kDa	5	8	4	6	0	4		
Cluster of ATP-dependent 6-phosphofructokinase Pfk (A0A0B4K7L1_DR	A0A0B4K7L1_DROME	105 kDa	1	4	6	2	9	2		
AP-2 complex subunit alpha AP-2alpha	AP2A_DROME	106 kDa	8	5	1	0	6	5		
Serine/threonine-protein phosphatase Pgam5, mitochondrial Pgam5	PGAM5_DROME (+1)	33 kDa	4	7	4	5	1	2		
Cluster of Calnexin 14D Cnx14D (Q9VXF6_DROME)	Q9VXF6_DROME [4]	73 kDa	6	5	2	3	3	1		
Flightin fln	FTN_DROME	21 kDa	7	3	6	4	4	6		
Lethal (1) G0230, isoform A ATPsyndelta	Q9W2X6_DROME	17 kDa	5	6	9	9	5	6		
CG11679 CG11679	Q9VXQ8_DROME	48 kDa	1	5	2	2	2	1		
Coracle, isoform F cora	A0A0B4LFX4_DROME	174 kDa	3	3	1	2	1	1		
Heat shock 70 kDa protein cognate 5 Hsc70-5	HSP7E_DROME	74 kDa	1	8	1	5	3	1		

Phosphoglycerate kinase Pgk	PGK_DROME	44 kDa	3	8	10	2	4	3		
Pyrroline-5-carboxylate reductase P5cr-2	A0A0B4KGC5_DROM	26 kDa	8	6	6	6	4	6		
Chitinase-like protein CG5210 CG5210	C5210_DROME	50 kDa	4	10	3	3	8	1		
CG13907, isoform A CG13907	Q9W0L6_DROME	88 kDa	4	8	5	5	5	3		
Mitochondrial import inner membrane translocase subunit TIM50-C ttn	TI50C_DROME	50 kDa	5	5	6	7	10	3		
Cluster of Cheerio, isoform M cher (A0A0B4KGT8_DROME)	A0A0B4KGT8_DROM	263 kDa	3	1	5	1	0	1		
CG13601, isoform B CG13601	A0A0B4KGV7_DROM	31 kDa	4	6	3	7	5	4		
CG2076, isoform A CG2076	Q9VZ34_DROME	36 kDa	3	5	3	6	5	2		
Cluster of Aspartyl beta-hydroxylase, isoform L Asph (A0A0B4KFS5_DRO	A0A0B4KFS5_DROME	113 kDa	5	2	3	6	1	4		
Cluster of NADH-ubiquinone oxidoreductase chain 4 ND4 (A0A075E721	A0A075E721_DROME	51 kDa	9	11	6	6	0	0		ND4
Coronin coro	A0A0B4KEJ7_DROME	58 kDa	1	5	4	2	6	1		
ATP-dependent Clp protease proteolytic subunit CG5045	Q9VKY3_DROME	28 kDa	6	5	4	3	4	0		
BcDNA.GH10614 BcDNA.GH10614	Q9Y112_DROME	36 kDa	10	4	5	2	1	7		
CG4984, isoform A CG4975-RB	A1ZAY4_DROME	51 kDa	4	7	6	5	4	2		
UDP-glucuronosyltransferase CG17323	Q9VJ46_DROME	58 kDa	2	5	4	3	4	5		
CG13220, isoform A CG13220	Q6NP72_DROME	16 kDa	6	7	7	8	3	7		
Aldehyde dehydrogenase Aldh-III	A0A0B4KEL0_DROME	56 kDa	3	4	1	3	4	3		
Phenylalanine--tRNA ligase beta subunit beta-PheRS	SYFB_DROME	66 kDa	4	4	3	0	7	1		
FI04632p nrv3	Q7JS69_DROME	36 kDa	5	5	1	1	2	2		
Dodeca-satellite-binding protein 1, isoform A Dp1	Q7KN75_DROME	144 kDa	4	3	0	0	4	1		
CG9510, isoform C CG9510	Q9VLG9_DROME	52 kDa	8	1	4	0	1	2		
Failed axon connections fax	FAXC_DROME (+1)	47 kDa	4	2	1	5	3	0		
Moesin, isoform M Moe	M9PHG2_DROME	69 kDa	5	2	2	3	0	3		
CG2943, isoform A CG2943	Q9VHY6_DROME	101 kDa	4	5	3	2	2	2		
Cluster of CG18769, isoform H CG18769 (M9NF23_DROME)	M9NF23_DROME [2]	53 kDa	7	1	1	2	6	2		
CG12079-PA ND-30	Q9VZU4_DROME	30 kDa	13	0	11	0	2	2		
Glutamine synthetase Gs2	X2JDA5_DROME	42 kDa	4	3	5	5	3	3		
Sodium/potassium-transporting ATPase subunit beta-1 nrv1	ATPB1_DROME	35 kDa	3	4	3	3	2	3		
CG40002, isoform A ND-AGGG	Q7PL91_DROME	11 kDa	3	4	6	4	0	0		FB2
CG18624, isoform B ND-MNLL	Q9W3N7_DROME	6 kDa	6	8	6	6	0	0		FB1
Cluster of Tubulin alpha-1 chain alphaTub84B (TBA1_DROME)	TBA1_DROME [3]	50 kDa	4	4	1	2	2	5		
Cluster of Protein mesh mesh (MESH_DROME)	MESH_DROME [2]	165 kDa	6	2	0	1	0	1		
Glutamine synthetase 1, mitochondrial Gs1	GLNA1_DROME	44 kDa	3	5	4	3	7	3		
NADH-ubiquinone oxidoreductase chain 5 mt:ND5	NU5M_DROME	65 kDa	10	7	7	9	1	0		ND5
CG5903, isoform A CG5903	Q9VEY5_DROME	24 kDa	5	4	4	5	1	3		
Phenylalanine--tRNA ligase alpha subunit alpha-PheRS	SYFA_DROME	56 kDa	7	2	2	0	5	2		
CG8888 CG8888	Q7K3N4_DROME	43 kDa	4	3	5	3	2	0		
Protein windpipe wdp	WDP_DROME	75 kDa	3	4	2	4	3	0		
Cluster of CG9990, isoform D CG9990 (A0A0B4JD13_DROME)	A0A0B4JD13_DROME	84 kDa	2	1	4	2	4	2		
Protein NDUFAF4 homolog CG11722	NDUF4_DROME	24 kDa	9	0	6	0	4	0		
Transferrin 1, isoform A Tsf1	Q9VWV6_DROME	72 kDa	6	6	4	6	2	0		
SAM50-like protein CG7639 CG7639	SAM50_DROME	49 kDa	8	3	2	5	2	3		
CG10320, isoform A ND-B12	Q9W2E8_DROME	12 kDa	8	7	6	4	0	0		FB3
AP complex subunit beta AP-1-2beta	Q24253_DROME	101 kDa	3	3	1	3	3	2		

Cluster of CG10737, isoform R CG10737 (B7YZL6_DROME)	B7YZL6_DROME [5]	97 kDa	1	4	2	5	4	0		
CG13392, isoform B CG13392	Q9VLM7_DROME	25 kDa	4	6	6	4	0	0		
V-type proton ATPase subunit B Vha55	VATB_DROME	55 kDa	4	6	7	4	1	3		
Zasp67, isoform H Zasp67	X2JGI5_DROME	76 kDa	3	7	4	3	3	0		
CG9603, isoform B COX7A	A0A0B4K6C3_DROME	11 kDa	4	5	4	5	4	5		
Cluster of Congested-like trachea protein colt (COLT_DROME)	COLT_DROME [2]	33 kDa	5	3	1	2	3	3		
Cluster of Synaptotagmin 1, isoform I Syt1 (X2J4C1_DROME)	X2J4C1_DROME [3]	53 kDa	5	5	2	2	5	2		
Cluster of Major heat shock 70 kDa protein Aa Hsp70Aa (HSP70_DROM	HSP70_DROME [3]	70 kDa	6	7	6	6	6	10		
CG5080, isoform A CG5080	Q7K3E2_DROME	61 kDa	4	6	2	4	4	2		
CDGSH iron-sulfur domain-containing protein 2 homolog Cisd2	CISD2_DROME	15 kDa	3	3	3	3	3	3		
CG34172, isoform A CG34172	Q6IHY5_DROME	7 kDa	3	4	4	5	4	7		
CG6105-PA ATPsynG	Q9VKM3_DROME	11 kDa	5	3	5	4	4	5		
Superoxide dismutase Sod2	A0A0B4LGQ1_DROM	25 kDa	3	4	3	2	5	3		
CG9674, isoform F CG9674	M9NFH8_DROME (+1	232 kDa	0	0	1	0	2	1		
Acyl-coenzyme A oxidase CG9527	B7Z028_DROME (+1)	81 kDa	2	2	2	1	0	2		
Cluster of CG9399, isoform A CG9399 (Q9VHB1_DROME)	Q9VHB1_DROME [2]	17 kDa	2	5	4	4	4	3		
UDP-glucuronosyltransferase BEST:LD25345	Q9VJ45_DROME	58 kDa	4	1	2	2	2	2		
RPII140-upstream gene protein 140up	140U_DROME	29 kDa	10	0	5	0	3	0		
CD98 heavy chain, isoform D CD98hc	A0A0B4KFA6_DROME	63 kDa	4	2	5	3	4	2		
Heat shock protein 83 Hsp83	HSP83_DROME	82 kDa	2	2	1	1	0	7		
CG42307, isoform A mus312-RD	B7Z0C9_DROME	11 kDa	4	3	3	3	3	2		
Syntaxin 1A, isoform B Syx1A	A0A0B4JCZ4_DROME	34 kDa	3	5	4	6	2	3		
RH64870p Ucp4A	Q9VX14_DROME	37 kDa	4	6	2	3	3	2		
ABCB7, isoform A ABCB7	Q9W0C5_DROME	80 kDa	2	2	0	1	2	2		
CG4019, isoform F CG4019	A0A0B4KFZ1_DROME	32 kDa	2	4	3	3	2	2		
FI18626p1 ZnT49B	A1Z936_DROME	72 kDa	2	3	0	1	9	2		
Stromal interaction molecule homolog Stim	STIM_DROME	65 kDa	0	2	2	6	3	0		
Actin-interacting protein 1 flr	WDR1_DROME	67 kDa	3	4	0	3	6	0		
CG31648 CG31648	Q9VMQ6_DROME	27 kDa	1	2	0	3	3	1		
UPF0389 protein CG9231 CG9231	U389_DROME	14 kDa	2	4	2	3	3	2		
Transmembrane GTPase Marf Marf	MARF_DROME	91 kDa	0	3	1	0	1	0		
Triosephosphate isomerase Tpi	TPIS_DROME	27 kDa	4	4	3	4	4	2		
LD23292p Mcr	Q9VLT3_DROME	203 kDa	5	2	2	0	1	2		
Asrij, isoform B asrij	A0A0B4KF31_DROME	29 kDa	3	3	3	1	3	3		
Uricase Uro	URIC_DROME	40 kDa	1	3	4	2	2	1		
Vitellogenin-2 Yp2	VIT2_DROME	50 kDa	1	0	0	7	4	0		
GH13304p Pglym78	Q9VAN7_DROME	29 kDa	1	4	2	4	0	1		
CG5214 CG5214	Q9VGQ1_DROME	50 kDa	2	4	6	1	5	1		
Synapsin, isoform D Syn	E2QCY9_DROME (+1)	109 kDa	2	3	2	1	2	1		
Histone H4 His4	H4_DROME	11 kDa	1	0	1	1	0	10		
10-formyltetrahydrofolate dehydrogenase CG8665-RA	Q9VIC9_DROME	100 kDa	4	2	2	3	2	1		
CG6463-PA ND-13B	Q9VTB4_DROME	14 kDa	7	0	5	0	2	0		
CG9629 CG9629	Q8SXQ1_DROME	58 kDa	2	3	2	3	4	2		
CG17734, isoform B CG17734	Q8INK7_DROME (+1)	10 kDa	4	4	3	4	5	2		

CG40042 Tim23	Q8MRW1_DROME	22 kDa	3	6	1	4	3	5		
Prohibitin 2, isoform E Phb2	A8DYI6_DROME	37 kDa	3	3	3	0	0	2		
CG4123-PA, isoform A Mipp1	Q9VV72_DROME	54 kDa	3	4	3	3	3	3		
Cytochrome c-2 Cyt-c-p	CYC2_DROME	12 kDa	4	5	3	2	3	2		
AT13736p UQCR-Q	Q9VVH5_DROME	10 kDa	3	4	4	4	2	4		
CG7382 CG7382	Q9VMR0_DROME	27 kDa	1	4	0	1	0	1		
CG1814, isoform A CG1814-RA	A1Z7V9_DROME	64 kDa	1	2	2	0	1	1		
CG34200 CG34200	Q6IGW6_DROME	6 kDa	2	3	2	1	1	2		
Protein jagunal jagn	JAGN_DROME	23 kDa	2	4	4	5	2	2		
CG33970, isoform A CG6166	Q86P18_DROME	86 kDa	2	2	2	2	0	1		
CG15096, isoform A CG15096	Q5BIE4_DROME	53 kDa	2	1	2	3	0	1		
60S acidic ribosomal protein P0 RpLP0	RLA0_DROME	34 kDa	2	2	1	2	2	3		
CG8773 CG8773-RB	Q9VFX0_DROME	111 kDa	8	3	0	2	2	5		
Glycogen [starch] synthase GlyS	GYS_DROME	82 kDa	0	1	0	1	2	1		
CG4562, isoform E CG4562	A0A0B4KGI0_DROME	158 kDa	3	0	1	1	0	2		
Peroxiredoxin 3 Prx3	Q9VEJ0_DROME	26 kDa	0	2	5	3	2	1		
CG3106, isoform A CG3106	Q9W322_DROME	84 kDa	1	4	0	2	0	3		
AT14148p CG2604	Q9VN86_DROME	47 kDa	1	3	2	2	2	2		
Cluster of Rhea, isoform B rhea (Q9VSL8_DROME)	Q9VSL8_DROME [2]	307 kDa	2	0	1	1	0	0		
CG14482, isoform A UQCR-6.4	Q500Y7_DROME	6 kDa	4	3	2	2	3	3		
FI03373p Mco1	Q9VLC3_DROME	108 kDa	2	0	0	1	0	5		
Histone H2B His2B	H2B_DROME	14 kDa	0	1	1	1	1	7		
NADH-cytochrome b5 reductase CG5946	X2JGK6_DROME	37 kDa	4	1	2	0	1	0		
Cytochrome b mt:Cyt-b	CYB_DROME (+1)	43 kDa	3	2	2	3	1	1		
Beta-alanine synthase pyd3	Q9VI04_DROME	44 kDa	2	3	1	2	0	2		
Cytochrome b-c1 complex subunit 9 ox	QCR9_DROME	6 kDa	3	4	3	4	0	3		
CG7888, isoform B CG7888	Q9VTD7_DROME	51 kDa	0	2	1	0	3	1		
40S ribosomal protein S3 RpS3	RS3_DROME	27 kDa	3	2	0	0	3	4		
CG5991, isoform A CG5991	Q9VCE0_DROME	50 kDa	2	2	0	2	1	2		
Sodium- and chloride-dependent GABA transporter ine ine	INE_DROME	104 kDa	3	1	1	1	1	1		
Vitellogenin-1 Yp1	VIT1_DROME	49 kDa	0	0	0	3	1	0		
CG4239, isoform A CG4239	Q9VXG9_DROME	30 kDa	2	3	3	4	2	1		
FI04467p Pdxk	Q7KUC2_DROME	33 kDa	2	3	2	2	2	1		
Ade5, isoform B ade5	F0JAN1_DROME (+1)	47 kDa	2	2	1	3	1	0		
Vesicle-fusing ATPase 1 comt	NSF1_DROME	83 kDa	2	0	0	0	2	2		
CG32267 CG32267	Q8IRD0_DROME	6 kDa	3	2	2	2	2	1		
G protein alpha o subunit Galphao	GNAO_DROME	40 kDa	4	1	3	3	4	3		
Protein l(2)37Cc l(2)37Cc	L2CC_DROME	30 kDa	3	0	2	0	0	2		
Aquaporin, isoform B AQP	E1JH55_DROME (+1)	29 kDa	0	1	3	3	0	1		
CG9140, isoform B ND-51	Q9VMI3_DROME	52 kDa	5	0	4	0	1	0		
Eip55E, isoform A Eip55E	Q7JXZ2_DROME	43 kDa	1	4	0	1	2	0		
CG4377 CG4377	Q9W2C4_DROME	25 kDa	4	3	0	1	1	2		
FI18644p1 Hmu	Q9VB46_DROME	63 kDa	1	1	0	3	2	2		
CG14777, isoform B EG:80H7.10	Q9W588_DROME	22 kDa	2	2	3	2	2	2		

Acyl carrier protein, mitochondrial ND-ACP	ACPM_DROME	17 kDa	3	2	2	1	0	0		FAB1
CG9715 CG9715	Q9VVA9_DROME	197 kDa	0	0	0	0	2	0		
Aromatic-L-amino-acid decarboxylase Ddc	DDC_DROME	57 kDa	0	0	0	2	0	0		
Tetraspanin Tsp5D	M9PDV2_DROME (+1	32 kDa	2	1	0	0	0	0		
Elongation factor 2 EF2	EF2_DROME	94 kDa	1	0	0	0	0	3		
CG3156 EG:171D11.2	Q8SWW9_DROME	76 kDa	0	1	2	0	0	1		
Na[+]/H[+] hydrogen antiporter 2, isoform B Nha2	A0A0B4K6G5_DROM	77 kDa	2	2	0	2	2	1		
Adenylyl cyclase 76E, isoform B Ac76E	M9NDD2_DROME	143 kDa	2	1	0	0	2	0		
Cofilin/actin-depolymerizing factor homolog tsr	CADF_DROME	17 kDa	2	3	2	2	3	0		
Delta-aminolevulinic acid dehydratase Pbgs	Q9VTV9_DROME	36 kDa	1	1	0	0	3	0		
Acetylcholinesterase Ace	ACES_DROME (+1)	72 kDa	1	0	0	1	0	3		
Cluster of GH13729p nemy (Q95T77_DROME)	Q95T77_DROME [2]	30 kDa	2	1	2	2	0	3		
Dystroglycan, isoform D Dg	A0A0C4DHF6_DROM	138 kDa	2	1	3	1	0	0		
COQ7 COQ7	Q9W3W4_DROME	24 kDa	0	1	3	1	0	0		
CG1440, isoform A CG1440	Q9W3F6_DROME	55 kDa	0	0	2	0	0	0		
Semaphorin-2b, isoform D Sema-2b	A0A0B4KG38_DROM	94 kDa	2	1	1	1	0	2		
CG10830 Ktl	Q9VDH3_DROME	26 kDa	3	1	0	2	1	0		
CG3446, isoform B ND-B16.6	Q9W402_DROME	18 kDa	2	0	4	0	1	0		
CG13506, isoform A CG13506-RA	Q9W259_DROME	57 kDa	2	1	2	2	2	0		
GM02062p ND-23	Q9VF27_DROME	25 kDa	4	0	1	0	0	0		
CG2930, isoform A CG2930-RA	Q9W4P6_DROME (+1	89 kDa	2	2	0	1	0	3		
Vacuolar protein sorting-associated protein 35 Vps35	Q7KVL7_DROME (+1)	91 kDa	1	2	0	0	0	0		
LD36265p (Fragment) UGP	A5XCL5_DROME (+3)	58 kDa	0	2	1	1	0	1		
V-type proton ATPase catalytic subunit A isoform 2 Vha68-2	VATA2_DROME	68 kDa	2	3	3	1	2	3		
Histone H3.3 His3.3A	H33_DROME (+1)	15 kDa	0	0	0	0	0	4		
AT09773p Vha68-3	Q9VK47_DROME	82 kDa	2	3	2	1	2	3		
Cluster of Axotactin, isoform D axo (M9NF15_DROME)	M9NF15_DROME [2]	229 kDa	2	0	0	0	0	0		
CG9172, isoform A ND-20	Q9VXK7_DROME	25 kDa	9	1	11	1	3	4		
V-type proton ATPase catalytic subunit A isoform 1 Vha68-1	VATA1_DROME	68 kDa	2	3	3	2	2	3		
Cluster of Histone H2A.v His2Av (H2AV_DROME)	H2AV_DROME [3]	15 kDa	0	0	0	0	0	5		
Glutactin Glt	GLT_DROME	119 kDa	1	0	0	0	4	0		
CG8132 CG8132	Q9VHE4_DROME	32 kDa	2	1	0	1	0	0		
ATP synthase subunit beta ATPsynbetaL	Q8T4C4_DROME	68 kDa	3	4	4	4	5	4		
Juvenile hormone epoxide hydrolase 1 Jheh1	Q7JRC3_DROME	55 kDa	1	3	0	0	0	0		
Alkyldihydroxyacetonephosphate synthase CG10253	ADAS_DROME	71 kDa	0	4	1	0	1	0		
Alkaline phosphatase CG1809	Q7K3X8_DROME	57 kDa	1	1	0	0	0	4		
GTP-binding nuclear protein Ran Ran	RAN_DROME	25 kDa	0	0	0	0	0	2		
Heat shock protein 23 Hsp23	HSP23_DROME	21 kDa	3	0	1	0	0	2		
NTPase, isoform F NTPase	M9PBV2_DROME (+2	58 kDa	0	2	0	1	1	1		
Transport and Golgi organization protein 11 Tango11	TNG11_DROME	32 kDa	0	0	0	0	2	0		
Sodium/potassium-transporting ATPase subunit alpha JYalpha	A8QI34_DROME	112 kDa	9	0	10	0	11	9		
40S ribosomal protein S14 RpS14a	RS14_DROME	16 kDa	0	0	0	0	0	4		
Drab11 Rab11	O18335_DROME	24 kDa	0	0	0	0	1	3		
CG12119, isoform A CG12119	Q9W373_DROME	56 kDa	2	0	0	0	0	0		

CG1092, isoform C CG1092	Q9VMZ9_DROME	47 kDa	0	0	2	0	0	0		
Chitinase-like protein Idgf4 Idgf4	IDGF4_DROME	49 kDa	2	2	0	0	2	0		
CG9577 CG9577	Q9W5W8_DROME	34 kDa	0	0	0	0	2	0		
CG3822 CG3822	Q9VDH5_DROME	96 kDa	0	0	0	2	0	0		
CG5554, isoform B CG5554	A0A0B4LHC9_DROME	37 kDa	0	0	0	0	2	0		
Neuropeptide-like 2 Nplp2	NPLP2_DROME	9 kDa	0	0	0	3	0	0		
40S ribosomal protein S15Ab RpS15Ab	RS15B_DROME	15 kDa	0	0	0	0	0	4		
LP01562p veil	Q7K0L5_DROME	65 kDa	3	0	0	0	0	0		
RE74917p tobi	Q9VBR6_DROME	75 kDa	0	0	0	2	0	0		
CG8607-PA CG8607	Q9VS44_DROME	31 kDa	2	0	0	0	1	0		
CG2014, isoform A ND-20L	Q9VAK5_DROME	24 kDa	5	1	6	0	3	4		
Calmodulin Cam	CALM_DROME (+1)	17 kDa	0	0	0	0	0	2		
Red font denotes proteins shown in heat map										

References

Abdrakhmanova, A., Zwicker, K., Kerscher, S., Zickermann, V., and Brandt, U. (2006). Tight binding of NADPH to the 39-kDa subunit of complex I is not required for catalytic activity but stabilizes the multiprotein complex. Biochim Biophys Acta *1757*, 1676-1682.

Andrews, B., Carroll, J., Ding, S., Fearnley, I.M., and Walker, J.E. (2013). Assembly factors for the membrane arm of human complex I. Proc Natl Acad Sci U S A *110*, 18934-18939.

Balsa, E., Marco, R., Perales-Clemente, E., Szklarczyk, R., Calvo, E., Landazuri, M.O., and Enriquez, J.A. (2012). NDUFA4 is a subunit of complex IV of the mammalian electron transport chain. Cell Metab *16*, 378-386.

Berger, I., Hershkovitz, E., Shaag, A., Edvardson, S., Saada, A., and Elpeleg, O. (2008). Mitochondrial complex I deficiency caused by a deleterious NDUFA11 mutation. Ann Neurol *63*, 405-408.

Brand, A.H., and Perrimon, N. (1993). Targeted gene expression as a means of altering cell fates and generating dominant phenotypes. Development *118*, 401-415.

Budde, S.M., van den Heuvel, L.P., Janssen, A.J., Smeets, R.J., Buskens, C.A., DeMeirleir, L., Van Coster, R., Baethmann, M., Voit, T., Trijbels, J.M.*, et al.* (2000). Combined enzymatic complex I and III deficiency associated with mutations in the nuclear encoded NDUFS4 gene. Biochem Biophys Res Commun *275*, 63-68.

Clason, T., Ruiz, T., Schagger, H., Peng, G., Zickermann, V., Brandt, U., Michel, H., and Radermacher, M. (2010). The structure of eukaryotic and prokaryotic complex I. J Struct Biol *169*, 81-88.

Duarte, M., Sousa, R., and Videira, A. (1995). Inactivation of genes encoding subunits of the peripheral and membrane arms of neurospora mitochondrial complex I and effects on enzyme assembly. Genetics *139*, 1211-1221.

Efremov, R.G., Baradaran, R., and Sazanov, L.A. (2010). The architecture of respiratory complex I. Nature *465*, 441-445.

Fiedorczuk, K., Letts, J.A., Degliesposti, G., Kaszuba, K., Skehel, M., and Sazanov, L.A. (2016). Atomic structure of the entire mammalian mitochondrial complex I. Nature *538*, 406-410.
Guarani, V., Paulo, J., Zhai, B., Huttlin, E.L., Gygi, S.P., and Harper, J.W. (2014). TIMMDC1/C3orf1 functions as a membrane-embedded mitochondrial complex I assembly factor through association with the MCIA complex. Mol Cell Biol *34*, 847-861.

Guerrero-Castillo, S., Baertling, F., Kownatzki, D., Wessels, H.J., Arnold, S., Brandt, U., and Nijtmans, L. (2017). The Assembly Pathway of Mitochondrial Respiratory Chain Complex I. Cell Metab *25*, 128-139.

Haynes, C.M., Fiorese, C.J., and Lin, Y.F. (2013). Evaluating and responding to mitochondrial dysfunction: the mitochondrial unfolded-protein response and beyond. Trends Cell Biol *23*, 311-318.

Heide, H., Bleier, L., Steger, M., Ackermann, J., Drose, S., Schwamb, B., Zornig, M., Reichert, A.S., Koch, I., Wittig, I.*, et al.* (2012). Complexome profiling identifies TMEM126B as a component of the mitochondrial complex I assembly complex. Cell Metab *16*, 538-549.

Hirst, J. (2013). Mitochondrial complex I. Annu Rev Biochem *82*, 551-575.

Hoefs, S.J., Dieteren, C.E., Distelmaier, F., Janssen, R.J., Epplen, A., Swarts, H.G., Forkink, M., Rodenburg, R.J., Nijtmans, L.G., Willems, P.H.*, et al.* (2008). NDUFA2 complex I mutation leads to Leigh disease. American journal of human genetics *82*, 1306-1315.

Hoefs, S.J., van Spronsen, F.J., Lenssen, E.W., Nijtmans, L.G., Rodenburg, R.J., Smeitink, J.A., and van den Heuvel, L.P. (2011). NDUFA10 mutations cause complex I deficiency in a patient with Leigh disease. European journal of human genetics : EJHG *19*, 270-274.

Hu, Y., Flockhart, I., Vinayagam, A., Bergwitz, C., Berger, B., Perrimon, N., and Mohr, S.E. (2011). An integrative approach to ortholog prediction for disease-focused and other functional studies. BMC Bioinformatics *12*, 357.

Jensen, M.B., and Jasper, H. (2014). Mitochondrial proteostasis in the control of aging and longevity. Cell Metab *20*, 214-225.

Kirby, D.M., Salemi, R., Sugiana, C., Ohtake, A., Parry, L., Bell, K.M., Kirk, E.P., Boneh, A., Taylor, R.W., Dahl, H.H.*, et al.* (2004). NDUFS6 mutations are a novel cause of lethal neonatal mitochondrial complex I deficiency. The Journal of clinical investigation *114*, 837-845.

Nehls, U., Friedrich, T., Schmiede, A., Ohnishi, T., and Weiss, H. (1992). Characterization of assembly intermediates of NADH:ubiquinone oxidoreductase (complex I) accumulated in Neurospora mitochondria by gene disruption. Journal of molecular biology *227*, 1032-1042.

Nouws, J., Nijtmans, L., Houten, S.M., van den Brand, M., Huynen, M., Venselaar, H., Hoefs, S., Gloerich, J., Kronick, J., Hutchin, T.*, et al.* (2010). Acyl-CoA dehydrogenase 9 is required for the biogenesis of oxidative phosphorylation complex I. Cell Metab *12*, 283-294.

Ostergaard, E., Rodenburg, R.J., van den Brand, M., Thomsen, L.L., Duno, M., Batbayli, M., Wibrand, F., and Nijtmans, L. (2011). Respiratory chain complex I deficiency due to NDUFA12 mutations as a new cause of Leigh syndrome. J Med Genet *48*, 737-740.

Owusu-Ansah, E., and Banerjee, U. (2009). Reactive oxygen species prime Drosophila haematopoietic progenitors for differentiation. Nature *461*, 537-541.

Owusu-Ansah, E., Song, W., and Perrimon, N. (2013). Muscle mitohormesis promotes longevity via systemic repression of insulin signaling. Cell *155*, 699-712.

Owusu-Ansah, E., Yavari, A., Mandal, S., and Banerjee, U. (2008). Distinct mitochondrial retrograde signals control the G1-S cell cycle checkpoint. Nat Genet *40*, 356-361.

Radermacher, M., Ruiz, T., Clason, T., Benjamin, S., Brandt, U., and Zickermann, V. (2006). The three-dimensional structure of complex I from Yarrowia lipolytica: a highly dynamic enzyme. J Struct Biol *154*, 269-279.

Rera, M., Bahadorani, S., Cho, J., Koehler, C.L., Ulgherait, M., Hur, J.H., Ansari, W.S., Lo, T., Jr., Jones, D.L., and Walker, D.W. (2011). Modulation of longevity and tissue homeostasis by the Drosophila PGC-1 homolog. Cell Metab *14*, 623-634.

Roy, S., and VijayRaghavan, K. (1999). Muscle pattern diversification in Drosophila: the story of imaginal myogenesis. Bioessays *21*, 486-498.

Scacco, S., Petruzzella, V., Budde, S., Vergari, R., Tamborra, R., Panelli, D., van den Heuvel, L.P., Smeitink, J.A., and Papa, S. (2003). Pathological mutations of the human NDUFS4 gene of the 18-kDa (AQDQ) subunit of complex I affect the expression of the protein and the assembly and function of the complex. The Journal of biological chemistry *278*, 44161-44167.

Stroud, D.A., Surgenor, E.E., Formosa, L.E., Reljic, B., Frazier, A.E., Dibley, M.G., Osellame, L.D., Stait, T., Beilharz, T.H., Thorburn, D.R.*, et al.* (2016). Accessory subunits are integral for assembly and function of human mitochondrial complex I. Nature *538*, 123-126.

Tuschen, G., Sackmann, U., Nehls, U., Haiker, H., Buse, G., and Weiss, H. (1990). Assembly of NADH: ubiquinone reductase (complex I) in Neurospora mitochondria. Independent pathways of nuclear-encoded and mitochondrially encoded subunits. Journal of molecular biology *213*, 845-857.

Vartak, R.S., Semwal, M.K., and Bai, Y. (2014). An update on complex I assembly: the assembly of players. J Bioenerg Biomembr *46*, 323-328.

Vinothkumar, K.R., Zhu, J., and Hirst, J. (2014). Architecture of mammalian respiratory complex I. Nature *515*, 80-84.

Vogel, R.O., Janssen, R.J., van den Brand, M.A., Dieteren, C.E., Verkaart, S., Koopman, W.J., Willems, P.H., Pluk, W., van den Heuvel, L.P., Smeitink, J.A.*, et al.* (2007). Cytosolic signaling protein Ecsit also localizes to mitochondria where it interacts with chaperone NDUFAF1 and functions in complex I assembly. Genes Dev *21*, 615-624.

Wittig, I., Braun, H.P., and Schagger, H. (2006). Blue native PAGE. Nat Protoc *1*, 418-428.
Zhu, J., Vinothkumar, K.R., and Hirst, J. (2016). Structure of mammalian respiratory complex I. Nature *536*, 354-358.

Zickermann, V., Wirth, C., Nasiri, H., Siegmund, K., Schwalbe, H., Hunte, C., and Brandt, U. (2015). Structural biology. Mechanistic insight from the crystal structure of mitochondrial complex I. Science *347*, 44-49.

.

Chapter 3: Identifying Novel Regulators of Mitochondrial Complex I Biogenesis

Garcia C.J., Khajeh J., Chen E.I.-J., Villanueva M., Rhooms S.K., and Owusu-Ansah E.

Khajeh J performed figures 3.2C and 3.2D and contributed to figure 3.3A-3.3BB

Chen E.L.-J performed mass spectrometry

Villanueva M. and Rhooms S.K. contributed to figure 3.6B-3.6D

Owusu-Ansah, E. performed figure 3.1B and discussed results

Garcia C.J. wrote the chapter and generated the rest of the

Introduction

Mitochondrial Complex I (CI) from bovine heart mitochondria has 44 distinct subunits; 14 are referred to as core subunits, as they are directly required for electron transfer from NADH to ubiquinone, or for generation of the membrane potential (Hirst, 2013). The other 30 nuclear-encoded subunits are referred to as accessory subunits, because they are not directly required for catalysis (Fiedorczuk et al., 2016). CI consists of a hydrophilic matrix arm and a hydrophobic membrane arm that project into the mitochondrial matrix and inner membrane respectively; and are oriented almost orthogonally to each other, resulting in a boot-shaped structure (Blaza et al., 2018; Zhu et al., 2016). The mechanistic assembly of the 44 distinct subunits occurs via a step-wise process. First, the subunits come together to form four assembly intermediates which then bind to each other to complete the assembly of the holoenzyme (Garcia et al., 2017; Guerrero-Castillo et al., 2017). The four assembly intermediates are named after the functional modules of the enzyme. They are the NADH binding site module (N-module), ubiquinone binding site module (Q-module) and the proton pumping module which is split into two assembly intermediates (P proximal-module (P_P) and P distal-module (P_D)).

CI assembly factors (CIAFs) are proteins that assist with the assembly process but are not found in the fully assembled complex (Formosa et al., 2018). Fifteen CIAFs have been described thus far (Formosa et al., 2018). Some CIAFs function as chaperones to stabilize specific CI assembly intermediates, or assist with the combination of two assembly intermediates to form a larger assembly intermediate (Andrews et al., 2013; Sugiana et al., 2008). Others have more specific roles, such as the posttranslational modifications of subunits (Rhein et al., 2013). The need to identify novel regulators of CI assembly is underscored by the fact that about half of CI disorders observed in patients cannot be traced to mutations in any of the 44 human CI subunits or known CIAFs (Pagliarini and Rutter, 2013; Taylor et al., 2014). This may be due to mutations happening *de novo*, occurring on sites of untranslated regions, and missing the exact variant that causes the disease after sequencing (Fassone and Rahman, 2012; Rodenburg, 2016). New sequencing technologies, such as RNA sequencing, are being used to complement the initial approach of whole exome and whole genome sequencing. One study used RNA sequencing to diagnose a patient's CI deficiency due to a mutation in a known assembly factor TIMMDC1; the expression of TIMMDC1 was

reduced due to a new exon in intron 5 which produced a frameshift introducing a premature stop codon (Kremer et al., 2017). Although RNA sequencing seems like a promising method to identify new regulators of CI, the challenge lies in the vast amount of data generated, and the dearth of genes of interest known to cause CI deficiency. As a proof of this challenge, only 10% of cases in the previous study were diagnosed using RNA sequencing. Therefore, identifying more nuclear genes that affect CI assembly is warranted for a more efficient genetic diagnosis of CI deficiency.

Here, we have utilized *Drosophila melanogaster* as a model system to study the CIAFs and their roles in CI assembly **(Figure 3.1)**. We hypothesized that some of the proteins that interact with NDUFS3, an integral core subunit of the Q-module, may serve as CIAFs. We identified 175 different interacting proteins of NDUFS3 and knocked them down individually in *Drosophila* using RNAi. Blue-native PAGE was performed to analyze the respiratory chain complexes of the knockdown flight muscle mitochondria. We discovered that knockdown of the *Drosophila* Fragile X Mental Retardation Protein (dFMRP) destabilized the structure of CI. Accordingly, we further analyzed the lifespan and in-gel activity, and characterized the assembly process, of flies lacking dFMRP. We report here that knockdown of dFMRP leads to a misassembly of CI. We further demonstrate the stalling of 815-kDa assembly intermediate and the accumulation of lower assembly intermediates. Finally, we conclude that the misassembly of CI is due to the destabilization of the P_P- or P_D-module.

Results

Complex I-interacting proteins were identified in *Drosophila* flight muscles

To identify interactors of CI, we genetically tagged the C-terminus of *Drosophila* NDUFS3 (dNDUFS3) with HA and expressed it in the fly flight muscles using Mhc-Gal4 **(Figure 3.2A)**. The C-terminus was used given that the mitochondria targeting sequence for dNDUFS3 is located at the N-terminus (Loeffen et al., 1998). This was achieved in offspring produced from a cross between two transgenic flies: one carrying the dNDUFS3-HA linked to an upstream activating sequence (i.e. UAS-dNDUFS3-HA, the Gal4 protein binds to the UAS sequence and drives expression of the dNDUFS3-HA construct), and the other with the muscle-specific Gal4 driver (e.g. Mhc-Gal4) **(Figure 3.2A)**. We found that

Mhc-Gal4<UAS-dNDUFS3-HA flies are viable and have no overt phenotypic differences from wild-type flies. The expression of dNDUFS3-HA was confirmed by SDS-PAGE and probing with an anti-HA antibody **(Figure 3.2C)**. We also confirmed that dNDUFS3-HA gets incorporated into CI using blue-native PAGE (BN-PAGE) followed by immunoblot analysis (**Figure 3.2D)**. We probed with an HA antibody and found that dNDUFS3-HA gets incorporated into the holoenzyme of CI and several assembly intermediates. These results demonstrated successful tagging of dNDUFS3 with HA and that the tagging did not alter the holoenzyme of CI and its assembly intermediates.

To identify the proteins interacting with dNDUFS3, we first isolated whole thorax lysates by permeabilizing the cellular membranes with buffer containing either 1% NP-40 or Digitonin (4g Digitonin: 1g Protein) from Mhc-Gal4<UAS-dNDUFS3-HA flies aged to 24 hours after eclosing **(Figure 3.2A)**. We chose 24 hours because CI biogenesis is active in *Drosophila* during the first 48 hours (Garcia et al., 2017). Samples were placed on ice for 30 minutes and then centrifuged at high speed to clear lysates before proceeding with co-immunoprecipitation (co-IP) **(Figure 3.2A)**. For co-IP, samples were first rotated with control agarose beads for 1 hour to control for any non-specific binding proteins. Next, the supernatant was transferred to agarose beads containing an anti-HA antibody and rotated overnight. Control agarose beads and anti-HA beads were sent for mass spectrometry to identify interacting proteins. We found a total of 385 proteins between the NP-40- and digitonin-permeabilized samples; 60% of the proteins identified were found with both buffers **(Figure 3.2A and Table 3.1)**. We identified known interactors such as dNDUFS2, dNDUFS7 and dNDUFS8 which form the 315-kDa CI assembly intermediate **(Figure 3.2B)**. We also identified other CI subunits such as dNDUFA9, dNDUFA10, dNDUFS1, dNDUFV1, and dNDUFV2 **(Figure 3.2B)**. dNDUFA9 and dNDUFA10 are found in the Q-module of CI and are known to interact closely with dNDUFS3. While dNDUFS1, dNDUFV1, and dNDUFV2 are not known to interact with dNDUFS3, they were also identified **(Figure 3.2B)**.

dFMRP was identified as a regulator for CI biogenesis by screening NDUFS3-interacting proteins

We chose to screen 175 of the proteins that interacted with dNDUFS3 after eliminating ribosomal proteins, mitochondria proteins that are known to be involved with the respiratory chain complexes, and

proteins that did not have RNA interference's (RNAi's) readily available at the time **(Table 3.1)**. The RNAi's to target these proteins were ordered from the Bloomington *Drosophila* Stock Center (BDSC) at http://flystocks.bio.indiana.edu/. If available, more than one RNAi for each protein were ordered. In total, we obtained 292 transgenic UAS-RNAi lines and tested their effect on CI assembly **(Table 3.2)**. Each UAS-RNAi line was crossed to the *Drosophila* muscle enhancing factor (Dmef2) gal4, which is known to express gal4 in flight muscles. Dmef2-Gal4<UAS-RNAi offspring were aged for 5-7 days at 25°C. If the flies died before the 5 days, they were re-crossed and dissected at an earlier time point. If offspring did not eclose to adults due to embryonic or pupae lethality, they were re-crossed to the myosin heavy chain (Mhc) gal4 which has been shown to reduce the expression of the RNAi compared to Dmef2-Gal4 (Garcia et al., 2017). In total, 53 of the UAS-RNAi lines were crossed with Mhc-Gal4. For each cross, we isolated mitochondria from 10 thoraxes, solubilized their membranes with 4g of digitonin to 1g of protein and performed BN-PAGE to resolve the oxidative phosphorylation (OXPHOS) complexes. The gels were subjected to either coomassie- or silver staining to show the effect of the RNAi on CI **(Figure 3.3A-BB)**. We focused on UAS-RNAi lines that specifically destabilized CI rather than generally affecting the other complexes, since knockdown of known CIAFs only reduce CI **(Figure 3.1E)**. After screening 292 UAS-RNAi lines, we identified three hits that destabilized CI: Cora **(Figure 3.3M Lane 107)**, CG10543 **(Figure 3.3Q Lane 166)**, and *Drosophila* Fragile Mental Retardation 1 Protein (dFMRP) **(Figure 3.3AA Lane 279)**. However, other RNAi's targeting the same proteins did not produce similar phenotypes. We speculate that this could be due to the RNAi's not effectively knocking down the protein levels.

To confirm the knockdown at protein levels, we crossed the three RNAi's that target FMR1 (Bloomington Stock #'s: 27484, 35200, and 34944) to their respective Gal4's and performed a western blot on whole cell lysates of fly thoraxes **(Figure 3.3CC)**. Before dissecting the flies, we aged them for 72 hours as the offspring of the RNAi that produced the CI phenotype died before 4 days. The RNAi that causes CI deficiency, Bloomington Stock #34944, showed a 90% knockdown efficiency in comparison to the other RNAi's which showed a 50% knockdown efficiency **(Figure 3.3CC)**. We also looked at dNDUFS3 protein levels in these flies and found it to be absent in the #34944 stock **(Figure 3.3CC)**. We were not able to find antibodies that cross-react with Cora or CG10543, therefore from here on we focused on dFMRP.

Because we were not able to confirm the CI phenotype with an alternative RNAi, we decided to try CRISPR interference (CRISPRi) in *Drosophila* flight muscles to decrease the protein levels of dFMRP. The sgRNA was designed for dead CAS9 (dCAS9) to target the first intron of dFMRP and silence transcription levels. However, protein levels of dFMRP were not significantly reduced and no CI phenotype was present **(Figure 3.4A-3.4D)**. Additionally, efforts were made to knockdown the mammalian orthologues of dFMRP (FMRP and FXR1) in cell lines, but an efficient knockdown could not be achieved for any of the proteins to observe a CI deficiency **(Figure 3.4E-3.4O)**. Ongoing collaboration with Dr. Richard Kitsis will test the mouse orthologues in vivo.

To confirm the mass spectrometry results that dFMRP interacts with NDUFS3, we followed the same co-IP protocol that was initially used to identify NDUFS3 interactors. We isolated whole tissue lysates from thoraxes of Mhc-Gal4<UAS-NDUFS3-HA offspring aged to 24 hours and 48 hours after eclosing and performed co-IP. We hypothesized that dFMRP also interacts with dNDUFS3 at 48 hours since early biogenesis of CI happens from 0 to 48 hours in adult flies (Garcia et al., 2017). Anti-HA-beads were digested with SDS-buffer, subjected to immunoblot analysis and probed with anti-dFMRP. A band between the 75 and 100 kDa marker was identified in both 24 and 48 hour time points **(Figure 3.3DD)**. The size of this band corresponds with the mass spectrometry results which identified a dFMRP isoform whose size is 81 kDa.

Knockdown of dFMRP destabilizes CI and reduces fly lifespan

MhcGal4<UAS-dFMRP$_{RNAi(BL\#34944)}$ (Henceforth referred to as Mhc<dFMRP$_{RNAi}$) offspring died within four days when incubated at 25°C. To track the exact lifespan of these flies, we monitored their survival rates after eclosing into adults. Every 12 hours, we checked the vials and recorded the percentage of flies that were still alive. At 48 hours, we began to see the survival rate decrease. By 60 hours, 50% of the offspring were dead and by 84 hours 100% of the flies had died **(Figure 3.5A)**. To assess the protein expression levels of dFMRP throughout its lifespan, cell lysates from whole thorax tissues aged to 6, 24, and 48 hours were subjected to western blot and probed with anti-dFMRP **(Figure 3.5B)**. At 6 hours, ~25% of dFMRP was present, followed by ~20% at 24 hours and ~10% at 48 hours. Next, we checked if

Mhc<dFMRP$_{RNAi}$ offspring have a reduction in the structure of CI at an earlier timepoint where ~20% of the protein is still present. We isolated mitochondria from Mhc<dFMRP$_{RNAi}$ thoraxes aged to 24 hours, solubilized their membranes in 4g of digitonin to 1g of protein, and performed BN-PAGE. Coomassie- and silver-stained native gels showed a significant reduction in CI. To further assess the extent of the CI deficiency, in-gel activity assay was performed, and revealed a reduction in CI activity in Mhc<dFMRP$_{RNAi}$ flies aged to 6, 24 and 48 hours **(Figure 3.5E)**. Altogether, these results indicate that dFMRP is essential for the viability of the flies and is important for the stability of the CI holoenzyme. Accordingly, we decided to elucidate the mechanisms of CI assembly in Mhc<dFMRP$_{RNAi}$ offspring.

Disruption of dFMRP in flight muscles impairs CI assembly

We have established a *Drosophila* model system to study the assembly of CI, where we showed the four assembly intermediates, the N-, Q-, P proximal- (P_P), and P distal-(P_D) modules, come together in a step-by-step procedure (Garcia et al., 2017). We generated individual knockdown strains of *Drosophila* for each subunit of CI and determined at which assembly step the subunit is indispensable. An antibody against NDUFS3, an early component of the Q-module, was used to track the Q-module building up from the 315-kDa assembly intermediate (Q-module) to 550-kDa (Q + P_P -modules) and then 815-kDa (Q + P_P + P_D -modules) on BN-PAGE. The stalling or accumulation of the assembly process at one of these milestones indicated that the subunit being knocked down is essential to advance to the next step. We also reported a new 700-kDa assembly intermediate in the process between 550- and 815-kDa, where we speculate individual subunits rather than an entire module bound the 550-kDa before the P_D was added.

Using this model, we examined whether dFMRP is an assembly factor required for the CI assembly. To test, we isolated mitochondria from Mhc<dFMRP$_{RNAi}$ offspring at the 24 hour timepoint and examined CI assembly via western blotting of native complexes. We used an antibody to NDUFS3 to track the Q-module **(Figure 3.6A)**. As expected, the protein levels of both holoenzyme CI and the CI-Complex III (CI-CIII) supercomplex were reduced in flies when dFMRP was disrupted **(Figure 3.6B)**. At a longer exposure, a reduction in the 815-kDa assembly intermediate and an increase in the 550- and 700-kDa assembly intermediates were observed, suggesting that dFMRP was the key component to achieve the 815 kDa from

the 550- and 700-kDa assembly intermediates **(Figure 3.6B)**. To better understand the misassembly of CI in dFMRP knockdown flies, we used antibodies to other CI subunits to analyze the other modules. We used an antibody to dND3, a mitochondria-encoded subunit and a part of the P_P-module assembly, to track the P_P-module **(Figure 3.6A)** (Guerrero-Castillo et al., 2017). Anti-dND3 did not detect the CI-CIII supercomplex but showed a strong reduction of the CI holoenzyme in dFMR1 knockdown flies aged to 24 hours **(Figure 3.6C)**. In a longer exposure, the 815-kDa assembly intermediate was reduced but the smaller assembly intermediates including the 700- and 550-kDa were accumulated, in agreement with the observation with anti-NDUFS3 **(Figure 3.6C)**. Additionally, anti-dND3 detected additional bands below the 550-kDa assembly intermediate that also were increased **(Figure 3.6C)**. We believe these bands are assembly intermediates that contain portions of the P_P-module. Because the exact subunits that make up these bands have not been characterized, we termed them as lower assembly intermediates (L.A.I).

The assembly intermediates for the P_D- and N-modules have not been well characterized in *Drosophila*. Therefore, we aged Mhc<dFMRP$_{RNAi}$ offspring to various times (6, 24, and 48 hours) to track bona fide assembly intermediates of these modules. To identify assembly intermediates of the P_D-module we used antibodies against the mitochondria-encoded subunit dND5 and the nuclear-encoded CI subunit dNDUFB5, previously shown to initiate the biogenesis of the P_D-module in mammalian system **(Figure 3.6A)** (Guerrero-Castillo et al., 2017). The holoenzyme CI and the CI-CIII supercomplex were reduced in Mhc<dFMRP$_{RNAi}$ offsprings when probed with these antibodies **(Figure 3.6D and 3.6E)**. Interestingly, the 48 hour time point showed the strongest reduction of CI which coincides with the time point at which these flies begin to die. Contrary to the expectation, none of the antibodies detected the 815-kDa assembly intermediate in wild-type (W1118) or dFMRP$_{RNAi}$ samples, although the P_D-module is known to be a part of it. One explanation could be that the epitopes for dND5 and dNDUFB5 were not accessible to the antibodies within the 815-kDa assembly intermediate. Alternatively, the assembly is stalled before the formation of the 815-kDa assembly intermediate due to the disruption of dFMRP. Similar to the immunoblot against dND3, several L.A.I. below the 815-kDa assembly intermediate were observed. It is possible that some or all of the L.A.I are degraded products of a larger assembly intermediate, especially when we don't observe the same size proteins in the wildtype. However, this question remains to be further investigated.

To track assembly intermediates of the N-module, we used an antibody against dNDUFV1, a CI nuclear-encoded core subunit part of the N-module **(Figure 3.6A)**. As expected, both CI and CI-CIII supercomplex were reduced in Mhc<dFMRP$_{RNAi}$ offspring **(Figure 3.6F)**. The N-module is the last piece to be added to CI to form the holoenzyme, therefore we don't expect to detect the 815-kDa assembly intermediate with this antibody. In dFMR1 knockdown flies we observed an L.A.I band at the 6 and 24 hour and faintly at 48 hour time points that were not present in wild-type flies **(Figure 3.6F)**. Again, this L.A.I may indicate that due to dFMRP disruption the N-module assembly is stalled; alternatively, there is a possibility that this L.A.I is also a degradation product, Taken together, these results indicate that dFMR1 regulates the biogenesis of CI assembly intermediates at the level of Q-, P$_P$-, P$_D$- and N-modules during CI assembly in *Drosophila* flight muscles.

The P$_D$-module regulator, Foxred1, is downregulated in Mhc<dFMRP$_{RNAi}$ offspring

We have previously shown that in *Drosophila*, the knockdown of CI subunits that form the N-module leads to an accumulation of the 815-kDa assembly intermediate vs. a reduction which has been shown in both Q- and P-modules (Garcia et al., 2017). Given that information, a reduction of the 815-kDa assembly intermediate suggested that the misregulation of CI was occurring at the Q- or P-modules in flies as a result of dFMRP disruption rather than the N-module. To identify the module that is being misregulated, we measured the protein expression levels of known CI assembly factors (CIAFs) that regulate the Q- and P-modules **(Figure 3.7A)**. We chose to test CIAFs based on the finding that the knockout of certain CIAFs in mammalian cells led to the downregulation of CI subunits that belong to the specific modules those CIAFs interact with (Stroud et al., 2016). Therefore, we hypothesized that if any assembly factor is downregulated, then the module it regulates would be affected. We aged Mhc<dFMRP$_{RNAi}$ offspring to 6, 24, and 48 hour time points, collected cell lysates from thoraxes, and performed western blot. We probed for dNDUFAF5, known to regulate the Q-module, and found a slight increase of expression at 48 hours **(Figure 3.7B)**. We also assessed the protein expression of dACAD9, dECSIT, dNDUFAF1, and dTIMMDC1, known to regulate the P$_P$-module. Minimal changes in protein levels was detected in dACAD9, dECSIT, and dNDUFAF1, however at 48 hours dTIMMDC1 was substantially reduced **(Figure 3.7C)**. Finally, the protein expression

of dFOXRED1, a regulator of the P_D-module, was measured. To our surprise, dFoxred1 was reduced at 6 and 24 hours and undetectable at 48 hours **(Figure 3.7D)**. These results indicate that the disruption of dFMRP leads to the misassembly of CI by the reduction of TIMMDC1 or Foxred1, located in either P_P- or P_D-module respectively. However, further confirmation is necessary, especially to rule out the possibility of RNAi off-target effect.

Discussion

In this chapter, we screened the interactors of NDUFS3, a Q module core subunit, to identify novel CIAFs of CI assembly. The existing models of CI assembly have considerable weaknesses especially when trying to identify novel regulators of CI biogenesis such as CIAF. For instance, CIAFs and several CI assembly intermediates found in mammalian CI are not conserved in *N. crassa* and *Arabidopsis thaliana* (Duarte et al., 1995) (Clark et al., 2006; Yun et al., 2014) (Park et al., 2006) (Hu et al., 2011).

Here we demonstrate that *Drosophila melanogaster* is an ideal model to study the regulators of CI biogenesis. (i) The flight muscles of *Drosophila* are highly enriched with mitochondria **(Figure 3.1B)**. (ii) The widely available genetic tools, relatively short lifespan and high fertility of *Drosophila* allow both loss- and gain-of function experiments to be performed rather easily **(Figure 3.1C and 3.1D).** (iii) CI assembly can be analyzed in vivo in the flight muscles. (iv) CI assembly in *Drosophila* is conserved with mammalian CI assembly and contains 42 of the 44 subunits **(Figure 3.1A)** and (v) several of the CIAFs are present in *Drosophila* and have been shown have a conserved function **(Figure 3.1E)**. Thus, we used the *Drosophila* model system to identify regulators of CI assembly.

Our approach of identifying interactors of the CI subunit NDUFS3 in *Drosophila* involved a screen of 175 proteins via RNAi knockdowns, through which we identified three potential hits that regulate the stability of CI: Cora, CG10543, and dFMRP. We followed up with dFMRP for the fact that all isoforms of dFMRP were knocked down in the Mhc>dFMRP$_{RNAi}$ thoraxes, as well as the availability of a cross-reacting antibody.

While the primary method of dFMRP knockdown in our model was RNAi, RNAi methods pose a limitation of off-target effect (OTEs), warranting confirmation of the observed phenotypes using additional RNAi of the same target or alternative knockdown methods (Mohr et al., 2014). While we tested three different RNAi against dFMRP (Bloomington Stock #'s: 27484, 35200, and 34944), only one (BI# 34944) showed a robust knockdown. **(Figure 3.3CC).** To check for OTEs of BI#34944 RNAi, the following software (https://www.flyrnai.org/up-torr/) from the Harvard Medical School DRSC/TRIP functional genomics resources was used. The BI #34944 RNAi is short hairpin with 21 base pairs in length. When we matched for sequences 15 base pairs in length or greater, no OTEs were reported. Alternatively, a query with the RNAi nucleotide sequence in NCBI Nucleotide Blast resulted in 100% match to the *Fmr1,* whereas any other matches were less than 70% and not assembly subunits.

Unfortunately, our alternative knockdown attempts using CRISPRi and loss-of-function mutation in *Drosophila* did not reproduce the reduced CI and the lethal phenotypes we saw in Mhc<dFMRP$_{RNAi}$ offspring. In *Drosophila*, there are 11 different isoforms of dFMRP with the most cited one to have 10 exons and to be approximately 81 kDa (Mila et al., 2018; Oostra and Willemsen, 2009; Weisz et al., 2018). Some CRISPRi did result in the complete absence of the 81 kDa isoform as detected by western blot, but accumulations of lower bands were observed **(Figure 3.4B)**. Considering that the sgRNA was designed to target only the first exon of d*Fmr1,* it is possible that these lower bands are isoforms of dFMRP without the first exon of *dFmr1,* and are able to compensate for the lost isoform during CI assembly. The results from the loss-of-function *dFmr1* mutant flies exhibited similar pattern as the CRISPRi flies; no reduction of CI by BN-PAGE and smaller isoforms of dFMRP detected by western blot, which could be the reason they are able to survive as opposed to the Mhc<dFMRP$_{RNAi}$ offsprings that die within three days (Dockendorff et al., 2002). The limitations of the CRISPRi and the mutant fly inherently lies in that the dFMRP has so many isoforms. One way to combat this limitation would be to generate knockout lines using CRISPR-Cas9 or TALENs to ensure that the all isoforms of FMRP are knocked out. However, I expect that these flies would not eclose into adults since a strong knockdown of FMRP results in lethality shortly after hatching. Alternatively, advances in CRISPRi technology have allowed for multiple sgRNA's to be used concurrently (up to 5) to target different nucleotide sequences on a gene. In the case where the knockout results in lethality, this method could prove to be a better option given that CRISPRi can be inducible in flies. On the

other hand, exogenous *Drosophila* FMRP or its respective mammalian orthologues can be overexpressed in Mhc<dFMRP$_{RNAi}$ offspring to see if it rescues the CI deficit. This could also help predict which mammalian orthologue is important for CI function.

In addition, we used shRNA in mammalian cell culture to test the effect of knockdown in mammalian CI assembly. dFMRP has three mammalian orthologues: fragile X mental retardation 1 protein (FMRP) and the fragile X-related proteins 1 and 2 (FXR1 and FXR2) (Oostra and Willemsen, 2009). We did not observe a CI reduction phenotype, which could be due to the fact that a strong enough knockdown could not be achieved in any of the orthologs. An alternate method would be to assess the CI assembly in mice, as whole body knockout mice are readily available for FMRP and FXR2 (Spencer et al., 2006). Additionally, creating a double knockout of FMRP and FXR2 might be necessary if a CI phenotype is not seen in the single knockout mice, since compensation mechanisms between these two proteins have been characterized (Spencer et al., 2006). For FXR1, another mammalian orthologue of dFMRP, the whole body knockout mouse is embryonic lethal; however, mice with loxP sites targeting FXR1 are available and can be crossed to Cre mice to create tissue specific knockouts (Mientjes et al., 2004). Since FXR1 is highly expressed in the muscle and heart, FXR1 should be knocked out in these tissues and CI should be analyzed by BN-PAGE (Mientjes et al., 2004). Overall, these future experiments will be crucial for confirming whether FMRP regulates CI function.

The observation of Foxred1 being absent from 6 to 48 hours was unexpected. Foxred1, an assembly factor, has been hypothesized to regulate the P_D-module as revealed by complexome profiling (Guerrero-Castillo et al., 2017). The subunits that Foxred1 interacts with are NDUFB6, NDUFB5, NDUFB10, NDUFB11, NDUFB1 and the mitochondria-encoded subunit ND4. Interestingly, knockdown of each of these subunits by RNAi in flies revealed a similar pattern of assembly intermediates compared to that of Mhc<dFMRP$_{RNAi}$ offspring when tracking the CI assembly via NDUFS3. In Mhc<dFMRP$_{RNAi}$ offspring, BN-PAGE followed by immunoblot analysis with anti-NDUFS3 showed a stalling at the 815-kDa assembly intermediate which led to the accumulation of the 700-, 550-, and 315-kDa assembly intermediates (Garcia et al., 2017). In addition, in patients mutations in *Foxred1,* a decrease in the 815-kDa assembly intermediate and an accumulation of L.A.I has been shown, similar to the pattern of

Mhc<dFMRP$_{RNAi}$ offspring (Formosa et al., 2015). These results overall have suggested that the destabilization of CI in Mhc<dFMRP$_{RNAi}$ offspring is due to the mis-assembly of the P_D-module. To further characterize this, it would be interesting to see if dFMRP interacts with Foxred1 or any other subunits that Foxred1 makes an assembly intermediate with. If it does, one could hypothesize that dFMRP forms an assembly intermediate with Foxred1 and the subunits that interact with Foxred1. This could be tested by performing complexome profiling to check if dFMRP co-migrates with the P_D-module. Alternatively, it would be interesting to test if FMRP binds to and regulates the transcripts of the P_D-module subunits, given that FMRP is an RNA binding protein.

In summary, we have identified three potential new regulators of CI assembly in *Drosophila* flight muscles, and described the mis-assembly process for dFMRP. To fully characterize the role of dFMRP, it will be important to analyze whether it directly interacts with CI in the mitochondria or it regulates its subunits from the outside of the mitochondria. In conclusion, it will be important to confirm that each of these hits are true regulators for CI before claiming them to be a bona fide assembly factor.

Materials and Methods

Drosophila Strains and Genetics.

The following fly stocks were used: y w; Dmef2-Gal4 and w; mhc-Gal4 were the Gal4 transgenic lines used to express RNAi lines in muscles. w1118/mhc-Gal4 flies were used as wildtype (wt) controls. To test CI assembly factors, the following fly stocks were ordered from the Bloomington Drosophila Stock Center (https://bdsc.indiana.edu/): 55660 (dNDUFAF1^{RNAi}), 31160 (dNDUFAF2^{RNAi}), 51894 (dNDUFAF3^{RNAi}), 51879 (dNDUFAF4^{RNAi}), 55332 (dNDUFAF6^{RNAi}), 51873 (dNUBPL^{RNAi}), and 42608 (dFoxred1^{RNAi}). Other assembly factors were ordered from the National Institute of Genetics (NIG, Japan) Drosophila Stock Center https://shigen.nig.ac.jp/fly/nigfly/: 17726R-3 (dNDUFAF5^{RNAi}), 9852R-1 (dTIMMDC1^{RNAi}). The UAS-NDUFS3-HA stock was ordered from FLYORF at https://www.flyorf.ch/imlskonakart/SelectProd.do;jsessionid=43121D3655A6E110BCEAE6AC49E7C416?prodId=4620&manufacturer=IMLS&category=all&name=F003000&model=Fruitfly. Stocks that were screened were ordered from the Bloomington Drosophila Stock Center (https://bdsc.indiana.edu/). The Bloomington stock number can be found in table 3.2 for each respective protein.

Mitochondria Purification.

Mitochondrial purification was performed essentially as described by Rera et al 2012 (Rera et al., 2011). Thoraxes were dissected and gently crushed with a pestle homogenizer in 500µl of pre-chilled mitochondrial isolation buffer containing 250 mM sucrose and 0.15 mM MgCl2 in 10 mM Tris.HCl, pH 7.4, on ice. After two rounds of centrifugation at 500g for 5 minutes at 4°C to remove insoluble material, the supernatant was recovered and centrifuged at 5000g for 5 minutes at 4°C. The pellet which is enriched for mitochondria was washed twice in the mitochondrial isolation buffer and stored at -80°C until further processing.

Blue Native Polyacrylamide Gel Electrophoresis (BN-PAGE).

BN-PAGE was performed using NativePAGE gels from Life Technologies, following the manufacturer's instructions. Essentially, mitochondria were suspended in native PAGE sample buffer (Life Technologies) supplemented with 1% digitonin and protease inhibitors, and incubated on ice for 20 minutes. Following centrifugation at 20,000g for 30 minutes, the supernatant was recovered, mixed with the G-250 sample additive (Life Technologies) and Native PAGE Sample Buffer (Life Technologies), and loaded onto 3–12% pre-cast Bis–Tris Native PAGE gels (Life Technologies). The NativeMark Protein standard (Life Technologies), run together with the samples, was used to estimate the molecular weight of the protein complexes. Electrophoreses was performed using the Native PAGE Running buffer (as anode buffer, from Life technologies) and the Native PAGE Running buffer containing 0.4% Coomassie G-250 (cathode buffer). Gels were stained with the Novex Colloidal Blue staining kit (Life Technologies) to reveal the protein complexes.

Silver Staining.

Silver staining of native gels was performed with the SilverXpress staining kit from Life Technologies, following the manufacturer's protocol.

In-gel Complex I Activity.

Complex I activity in native gels was performed by incubating the native gels in 0.1 mg/ml NADH, 2.5 mg/ml Nitrotetrazolium Blue Chloride, 5 mM Tris-HCl (pH 7.4) overnight at room temperature.

In-gel Complex II Activity.

Complex II activity in native gels was performed by incubating the native gels in 50 mM sodium phosphate pH 7.2, 0.05% DAB, 50 uM mouse heart cytochrome C.

Immunoblotting

For immunoblotting of samples in native gels, protein complexes from native gels were transferred to PVDF membranes (BIORAD). For immunoblotting of samples in whole tissue lysates, thoraxes were homogenized in RIPA buffer (150 mM NaCl, 1% Triton X-100, 0.5% Sodium Deoxycholate, 0.1% SDS, 50mM Tris HCl, pH 8) supplemented with Halt protease inhibitors (Pierce), resolved on mini-PROTEAN TGX stain-free gels from BIO-RAD, and transferred to PVDF membranes. In both instances (native and non-native gels), the membrane was subsequently blocked in 5% (w/v) non-fat dry milk in Tris-buffered saline (TBS) for 30minutes, and incubated in the appropriate primary antibody dissolved in 2% BSA, 0.1% Tween 20 in TBS (TBST) overnight at 4°C. Following the overnight incubation, the blot was rinsed 4X10 minutes in 0.1%TBST, blocked for 30 minutes in 5% (w/v) non-fat dry milk in TBST and incubated for two hours with the appropriate HRP-conjugated secondary antibody dissolved in 2% BSA, 0.1% Tween 20 in TBS (TBST). After incubation in the secondary antibody, samples were rinsed 4X10 minutes in 0.1%TBST. Immunoreactivity was detected by enhanced chemiluminescence (ECL) and analyzed by a ChemiDoc Gel imaging system from BIO-RAD. Antibodies used were anti-NDUFS3 (abcam, ab14711), anti-ND1 (abcam, ab74257), anti-HA (Thermofisher PA1-985), anti-dFMRP (abcam, ab10299), and anti-actin (EMD Millipore, MAB1501). Additional antibodies used were anti-dSDHA, anti-dND5, anti-dNDUFB5, anti-dNDUFV1, anti-dTIMMDC1, anti-dNDUFAF1, anti-dECSIT, anti-dACAD9, anti-dNDUFAF5, and anti-dFoxred1 which were generated by the Edward Owusu-Ansah lab.

LC-MS/MS Analysis

The concentrated peptide mix was reconstituted in a solution of 2 % ACN, 2 % Formic acid (FA) for MS analysis. Peptides were eluted from the column using a Dionex Ultimate 3000 Nano LC system with a 10 min gradient from 2% buffer B to 35 % buffer B (100 % ACN, 0.1 % FA). The gradient was switched from 35 % to 85 % buffer B over 1 min and held constant for 2 min. Finally, the gradient was changed from 85 % buffer B to 98 % buffer A (100% water, 0.1% FA) over 1 min, and then held constant at 98 % buffer A for 5 more minutes. The application of a 2.0 kV distal voltage electrosprayed the eluting peptides directly into the Thermo Fusion Tribrid mass spectrometer equipped with an EASY-Spray source (Thermo Scientific).

Mass spectrometer-scanning functions and HPLC gradients were controlled by the Xcalibur data system (Thermo Finnigan, San Jose, CA).

Database Search And Interpretation Of MS/MS Data

Tandem mass spectra from raw files were searched against a Drosophila protein database using the Proteome Discoverer 1.4 software (Thermo Finnigan, San Jose, CA). The Proteome Discoverer application extracts relevant MS/MS spectra from the .raw file and determines the precursor charge state and the quality of the fragmentation spectrum. The Proteome Discoverer probability-based scoring system rates the relevance of the best matches found by the SEQUEST algorithm. The Drosophila protein database was downloaded as FASTA-formatted sequences from Uniprot protein database (database released in May, 2015). The peptide mass search tolerance was set to 10ppm. A minimum sequence length of 7 amino acids residues was required. Only fully tryptic peptides were considered. To calculate confidence levels and false positive rates (FDR), Proteome Discoverer generates a decoy database containing reverse sequences of the non-decoy protein database and performs the search against this concatenated database (non-decoy + decoy). Scaffold (Proteome Software) was used to visualize searched results. The discriminant score was set at less than 1% FDR determined based on the number of accepted decoy database peptides to generate protein lists for this study. Spectral counts were used for estimation of relative protein abundance between samples.

Survival Assay

60 flies per genotype were collected and placed in 3 vials of food with approximately 20 flies each. The amount of flies alive was recorded for in each vial every 12 hours. The survival rate was calculated by (the amount of flies alive in each vial / 20 (initial amount of flies in the vial)). The average was taken from the 3 vials at each time point for each genotype and was plotted using GraphPad Prism software.

Co-Immunoprecipitation (co-IP) Analysis

20 whole fly thoraxes were blended in 200 ul of NP-40 lysis buffer (25 mM Tris-HCL [pH 7.5], 150 mM NaCl, 5 mM EDTA, 1% (v/v) NP-40, 5% (v/v) Glycerol, 1 mM DTT supplemented with protease inhibitors [Thermofisher]) or 200 ul of digitonin lysis buffer (50 mM Tris-HCl [pH 7.5], 150 mM NaCl, 4g:1g (digitonin : protein ratio) supplemented with protease inhibitors [Thermofisher]). Tubes were placed on ice for 30 minutes. Cell lysate was centrifuged at 20,000 x g for 10 min at 4°C. The supernatant was transferred to a a new tube and 300 ul of dilution buffer ([NP-40: 25 mM Tris-HCL [pH 7.5], 150 mM NaCl, 5 mM EDTA, 5% (v/v) Glycerol, 1 mM DTT]; [Digitonin 50 mM Tris-HCl [pH 7.5], 150 mM NaCl]) was added to the supernatant. 50 ul of control agarose beads were added and rotated for 1 hour at 4°C. Samples were centrifuged at 2500g for 2 minutes to collect control agarose beads. Lysates were pipetted into 50 ul of anti-HA beads and rotated overnight in the 4°C. The beads were washed three times with 1000ul of lysis buffer at 4°C. Control and anti-HA agarose beads were sent for mass spectrometry to identify interactors of NDUFS3-HA. To check the binding of dFMRP, samples were eluted using 60 ul of 1X SDS-loading sample buffer and heated to 95°C for 10 minutes. Samples were then subjected to immunoblot analysis and probed with anti-dFMRP.

Transfection of shRNA plasmids

shRNA plasmids were ordered from Origene (FMR1 sRNA plasmid # 312955; FXR1 shRNA plasmid #312890). Origene transfection protocol was followed step-by-step. To check transfection efficiency, cells were looked under a fluorescent microscope to analyze GFP expression.

Figure 3.1: *Drosophila* flight muscles are suitable for identifying novel regulators of complex I biogenesis.

(A) *Drosophila* complex I is comparable to mammalian complex as it contains 42 of the 44 subunits. Schematic representation of how the 44 distinct subunits of bovine or ovine CI are arranged to produce the L-shaped topology; based on recent CI structures described (Fiedorczuk et al., 2016; Vinothkumar et al., 2014; Zhu et al., 2016; Zickermann et al., 2015). The asterisk denotes subunits for which an ortholog was not identified in *Drosophila* by DIOPT. NDUFAB1 occurs twice in the complex, giving rise to a total of 45 subunits.

(B) *Drosophila* flight muscles are rich in mitochondria. Drosophila flight muscles from wildtype flies stained with phalloidin (red) to mark the sarcomeres, and expressing GFP tagged with a nuclear localization signal in (A) or GFP with a mitochondrial targeting signal in (B). (C) Adult fly showing position of flight muscles (thorax) in region demarcated.

(C) *Drosophila* have a short life cycle. Schematic representation showing the life cycle of flies. Flies take 10 days from egg to eclose into adult flies. The survival span of flies is approximately 3 months.

(D) Several advanced genetic tools have been established by the *Drosophila* community. This includes access to 1000s of RNAi's available from stock centers around the world, easy manipulation of genes using the Gal4/UAS system, as well as cost efficiency compared to mammalian models.

(E) Several assembly factors in mammalian systems are functionally conserved in *Drosophila.* BN-PAGE (left panel) and Silver staining (right panel) of samples from thoraxes following RNAi-mediated knockdown of assembly factor proteins, dNDUFAF1, dNDUFAF2, dNDUFAF3, dNDUFAF4, dNDUFAF5, dNDUFAF6, dNUBPL, dTIMMDC1, dFoxred1. CI-CIII denotes the complex I-complex III supecomplex, CV2 denotes a dimer of complex V respectively, CI denotes complex I, CV denotes complex V, CIII denotes complex III, CIV denotes complex IV, and CII denotes complex II**.**

A

1. Comparable to Mammalian CI

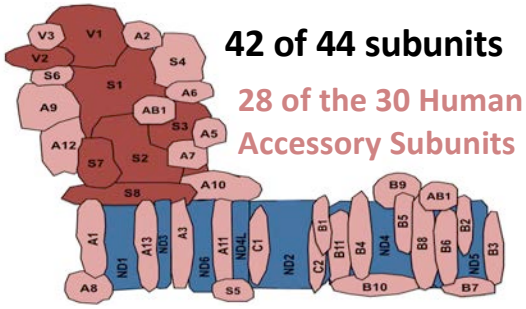

42 of 44 subunits

28 of the 30 Human Accessory Subunits

B

2. Rich in Mitochondria

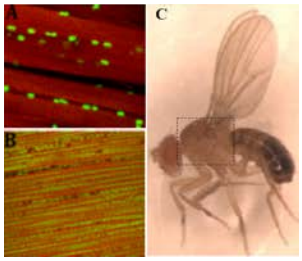

C

3. Short Life Cycle

D

4. Advanced Genetic Tools

a) 1000s of RNAi's available from Stock Center
b) Gal4/UAS system
   a) Knockdown, overexpression, temporal
c) Cost efficient

E

5. Several Assembly Factors Are Conserved

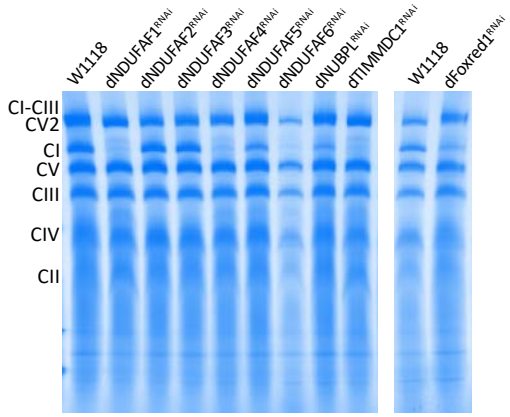

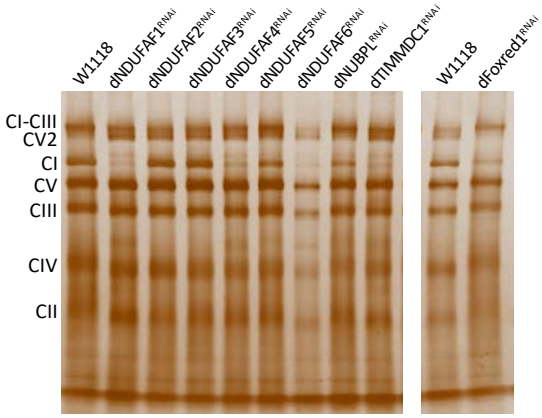

Figure 3.2: Identifying interactors of CI in *Drosophila* flight muscles.

(A) Summary of the experimental procedure for identifying interactors of the CI nuclear-encoded subunit dNDUFS3. (1) dNDUFS3-HA flies were generated using the Gal4-UAS system. (2) dNDUFS3-HA was expressed in the *Drosophila* thoraxes and dissected for co-immunoprecipitation (Co-IP). (3) Co-IP was performed with anti-HA agarose beads to identify interactors to NDUFS3. (4) Two different lysis buffers (NP-40 and digitonin) identified a total of 385 putative interactors. 237 were identified in both buffers, 68 were found in NP-40 buffer and 80 were present in the digitonin buffer. (5) Of these 385, 175 proteins were selected to be screened. (6) In total 292 RNAi's were ordered from the Bloomington Drosophila Stock Center. More than 1 RNAi was ordered for each protein if available.

(B) Schematic representation of mammalian CI representing the CI subunits that interacted with NDUFS3 after mass spectrometry analysis. The subunits in red indicate that they interacted with NDUFS3. They are NDUFV1, NDUFV2, NDUFS1, NDUFA9, NDUFS7, NDUFS2, NDUFS8, and NDUFA10. NDUFS3 is encoded in yellow.

(C) To check the expression of HA in Mhc-Gal4<UAS-dNDUFS3-HA flies aged to 24 hours, 10 thoraxes were lysed in SDS-PAGE buffer and subjected to western blot and probed with an HA antibody.

(D) To check to see if NDUFS3-HA gets incorporated into the holoenzyme of CI during CI biogenesis, we isolated mitochondria from 10 Mhc-Gal4<UAS-dNDUFS3-HA thoraxes aged to 6 or 24 hours, permeabilized their membranes in 1% digitonin and performed a BN-PAGE. To track the assembly of CI we performed a western blot and probed with anti-ND1 (middle panel) and anti-NDUFS3 (right panel) to track the CI-CIII supercomplex, CI, 815 kDa-, 550 kDa- and 315 kDa assembly intermediates respectively. To see if NDUFS3-HA gets incorporated into the complex, we probed with anti-HA (left panel) and compared it to the western blots of anti-ND1 and anti-NDUFS3.

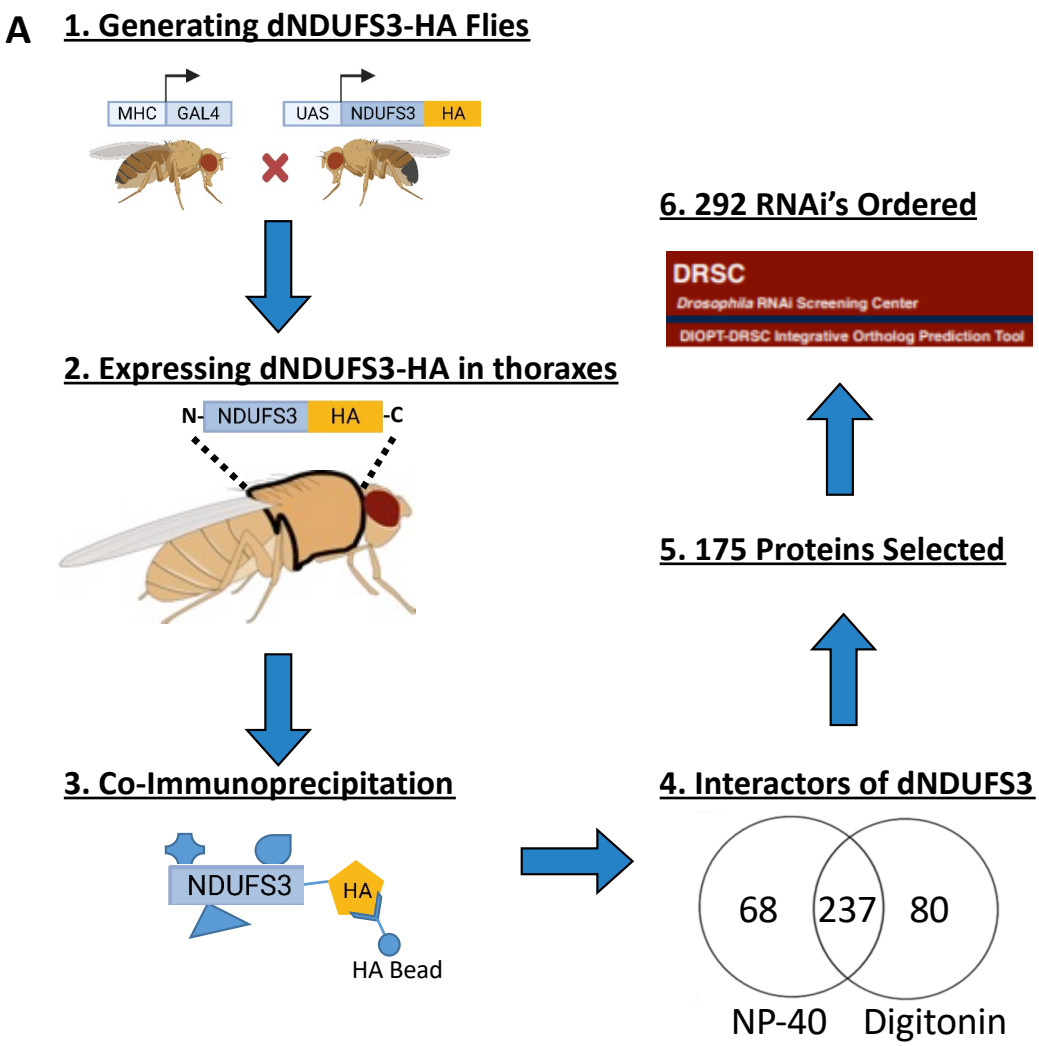
A
1. Generating dNDUFS3-HA Flies
MHC
GAL4
UAS
NDUFS3
HA
2. Expressing dNDUFS3-HA in thoraxes
N-
NDUFS3
HA
-C
3. Co-Immunoprecipitation
NDUFS3
HA
HA Bead
4. Interactors of dNDUFS3
68
237
80
NP-40
Digitonin
5. 175 Proteins Selected
6. 292 RNAi's Ordered
DRSC
Drosophila RNAi Screening Center
DIOPT-DRSC Integrative Ortholog Prediction Tool

B

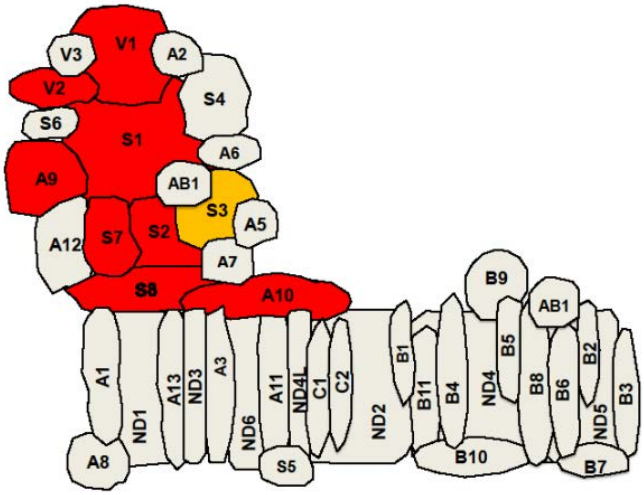
V3
V1
A2
V2
S4
S6
S1
A6
A9
AB1
S3
A5
A12
S7
S2
A7
S8
A10
B9
AB1
A1
ND1
A13
ND3
A3
ND6
A11
ND4L
C1
C2
S5
ND2
B1
B11
B4
ND4
B5
B8
B6
B2
ND5
B3
A8
B10
B7

C

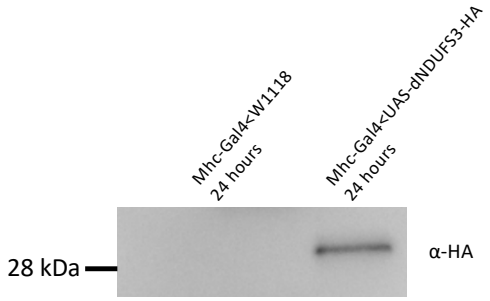
Mhc-Gal4<W1118
24 hours
Mhc-Gal4<UAS-dNDUFS3-HA
24 hours
28 kDa
α-HA

D

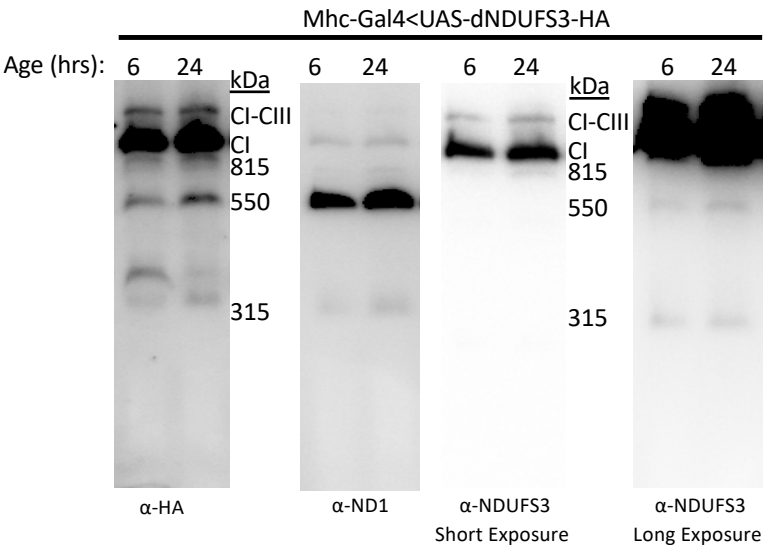
Mhc-Gal4<UAS-dNDUFS3-HA
Age (hrs):
6
24
kDa
CI-CIII
CI
815
550
315
α-HA
α-ND1
α-NDUFS3
Short Exposure
α-NDUFS3
Long Exposure

Figure 3.3: Screening interactors of the dNDUFS3 CI subunit identifies dFMRP as a regulator for CI biogenesis.

(A-BB) 292 RNAi's to interacting proteins of dNDUFS3 were expressed in flight thoraxes using either the Dmef2- or Mhc- Gal4 and aged for 5-7 days. We isolated mitochondria from 10 thoraxes, permeabilized their membranes in 1% digitonin and performed BN-PAGE. The complexes were resolved by either coomassie- or silver staining. Each lane is numbered and corresponds to the RNAi's ordered from the Bloomington Stock Center found in Table 3.2. CI-CIII denotes the complex I-complex III supecomplex, CV2 denotes a dimer of complex V respectively, CI denotes complex I, CV denotes complex V, CIII denotes complex III, CIV denotes complex IV, and CII denotes complex II.

(CC) Western blot showing the protein levels of FMRP in flies expressing RNAi's that target FMRP in the flight muscles. All flies were aged for 72 hours. The protein expression levels of dNDUFS3 and the complex II subunit dSDHA were also analyzed in these flies.

(DD) The interaction between dNDUFS3-HA and dFMRP was confirmed via western blot analysis. Co-IP was performed using anti-HA agarose beads in NP-40 lysis buffer on thoraxes from Mhc-Gal4<UAS-dNDUFS3-HA aged to 24 hours and 48 hours. Beads were lysed in SDS-PAGE buffer, subjected to immunoblot analysis and probed with anti-dFMRP.

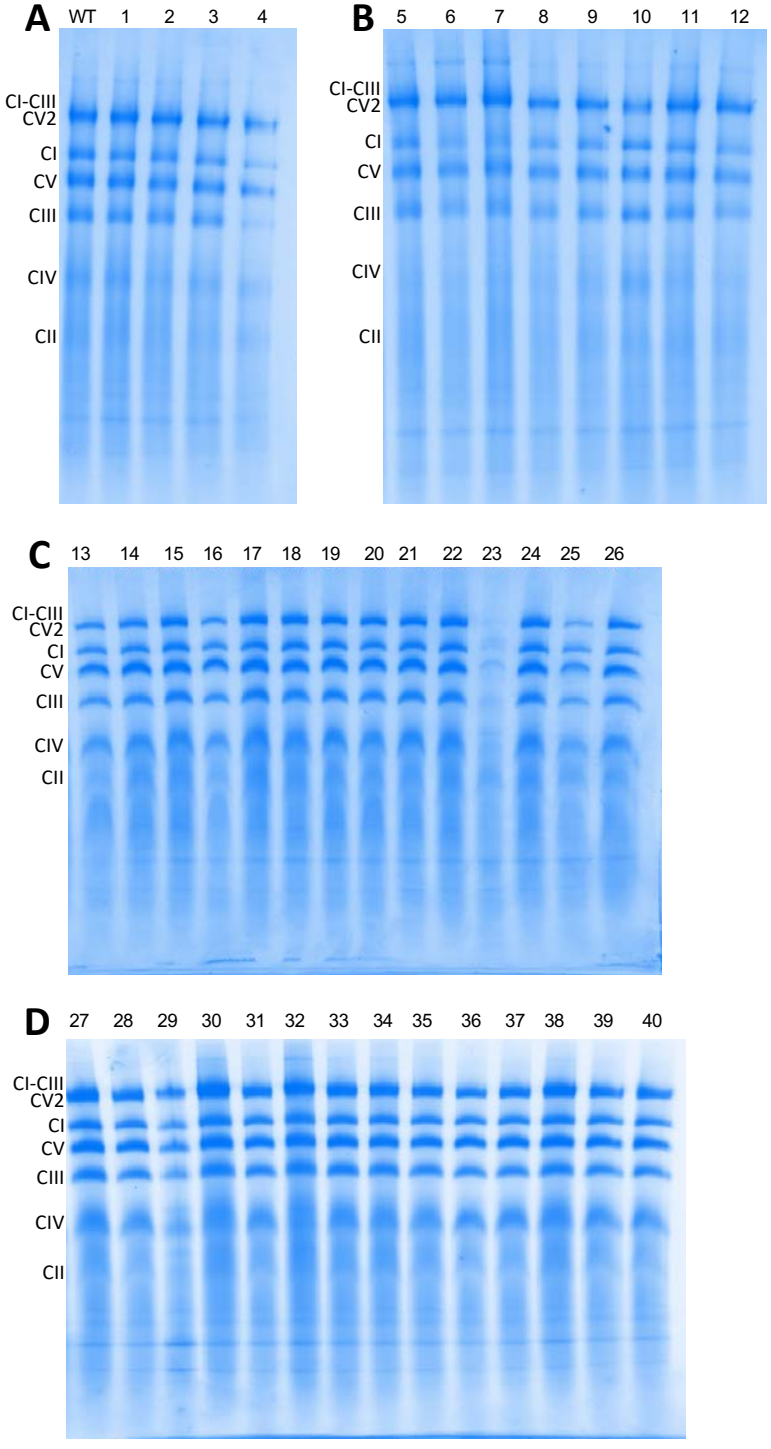
A
WT 1 2 3 4
CI-CIII
CV2
CI
CV
CIII
CIV
CII
B
5 6 7 8 9 10 11 12
CI-CIII
CV2
CI
CV
CIII
CIV
CII
C
13 14 15 16 17 18 19 20 21 22 23 24 25 26
CI-CIII
CV2
CI
CV
CIII
CIV
CII
D
27 28 29 30 31 32 33 34 35 36 37 38 39 40
CI-CIII
CV2
CI
CV
CIII
CIV
CII

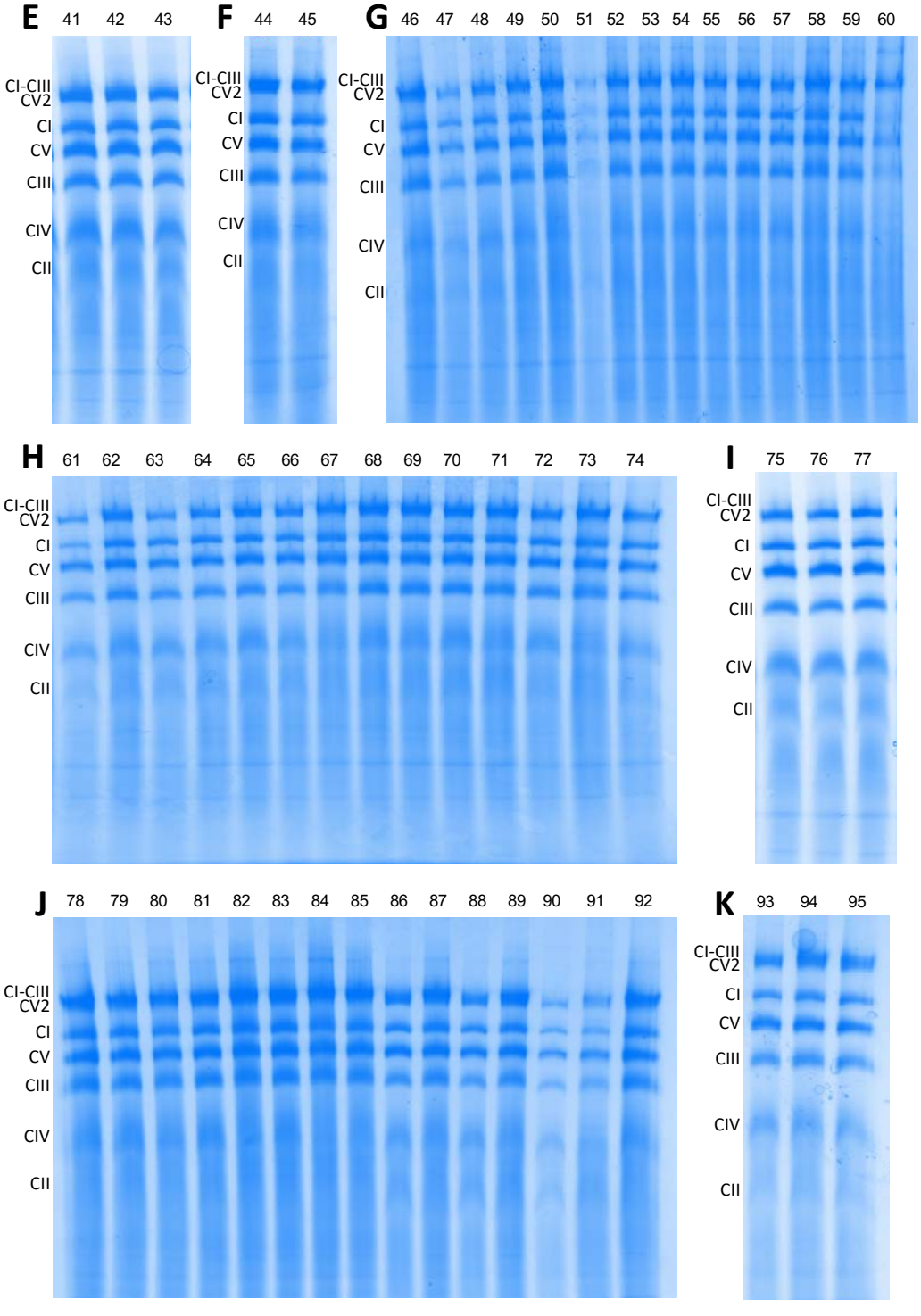
E
41 42 43
F
44 45
G
46 47 48 49 50 51 52 53 54 55 56 57 58 59 60
CI-CIII CV2
CI
CV
CIII
CIV
CII
H
61 62 63 64 65 66 67 68 69 70 71 72 73 74
I
75 76 77
J
78 79 80 81 82 83 84 85 86 87 88 89 90 91 92
K
93 94 95

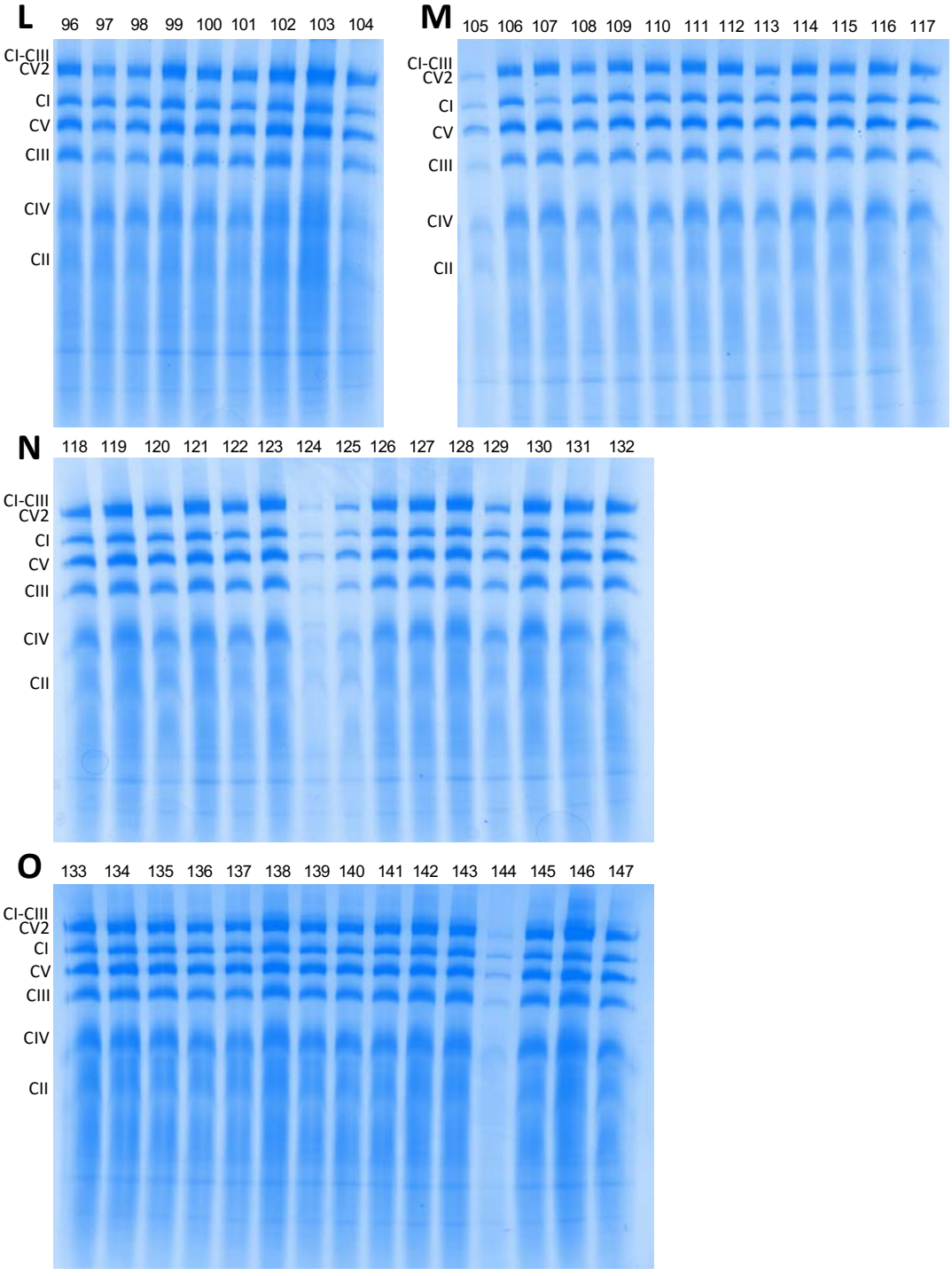
L
96 97 98 99 100 101 102 103 104
CI-CIII
CV2
CI
CV
CIII
CIV
CII
M
105 106 107 108 109 110 111 112 113 114 115 116 117
CI-CIII
CV2
CI
CV
CIII
CIV
CII
N
118 119 120 121 122 123 124 125 126 127 128 129 130 131 132
CI-CIII
CV2
CI
CV
CIII
CIV
CII
O
133 134 135 136 137 138 139 140 141 142 143 144 145 146 147
CI-CIII
CV2
CI
CV
CIII
CIV
CII

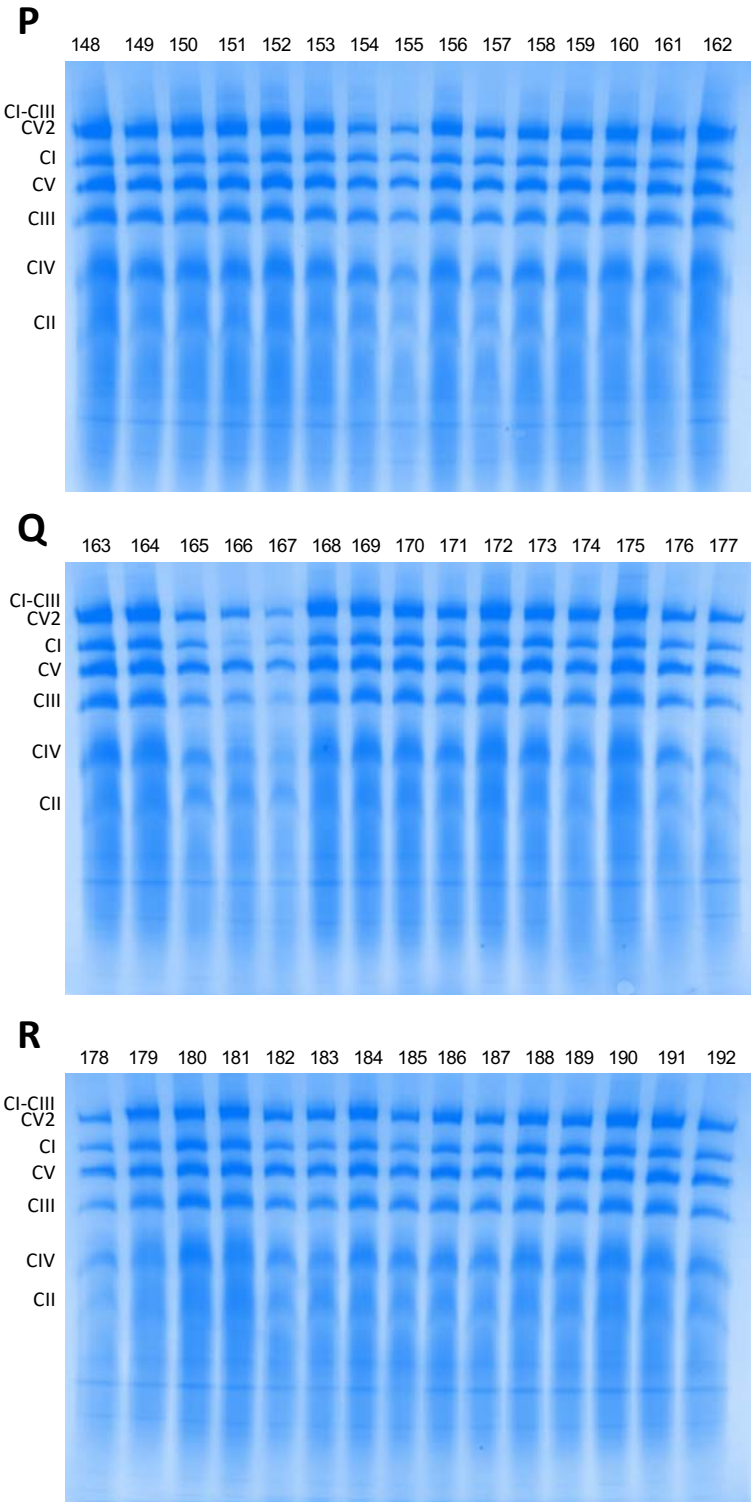
P
148 149 150 151 152 153 154 155 156 157 158 159 160 161 162
CI-CIII CV2
CI
CV
CIII
CIV
CII
Q
163 164 165 166 167 168 169 170 171 172 173 174 175 176 177
CI-CIII CV2
CI
CV
CIII
CIV
CII
R
178 179 180 181 182 183 184 185 186 187 188 189 190 191 192
CI-CIII CV2
CI
CV
CIII
CIV
CII

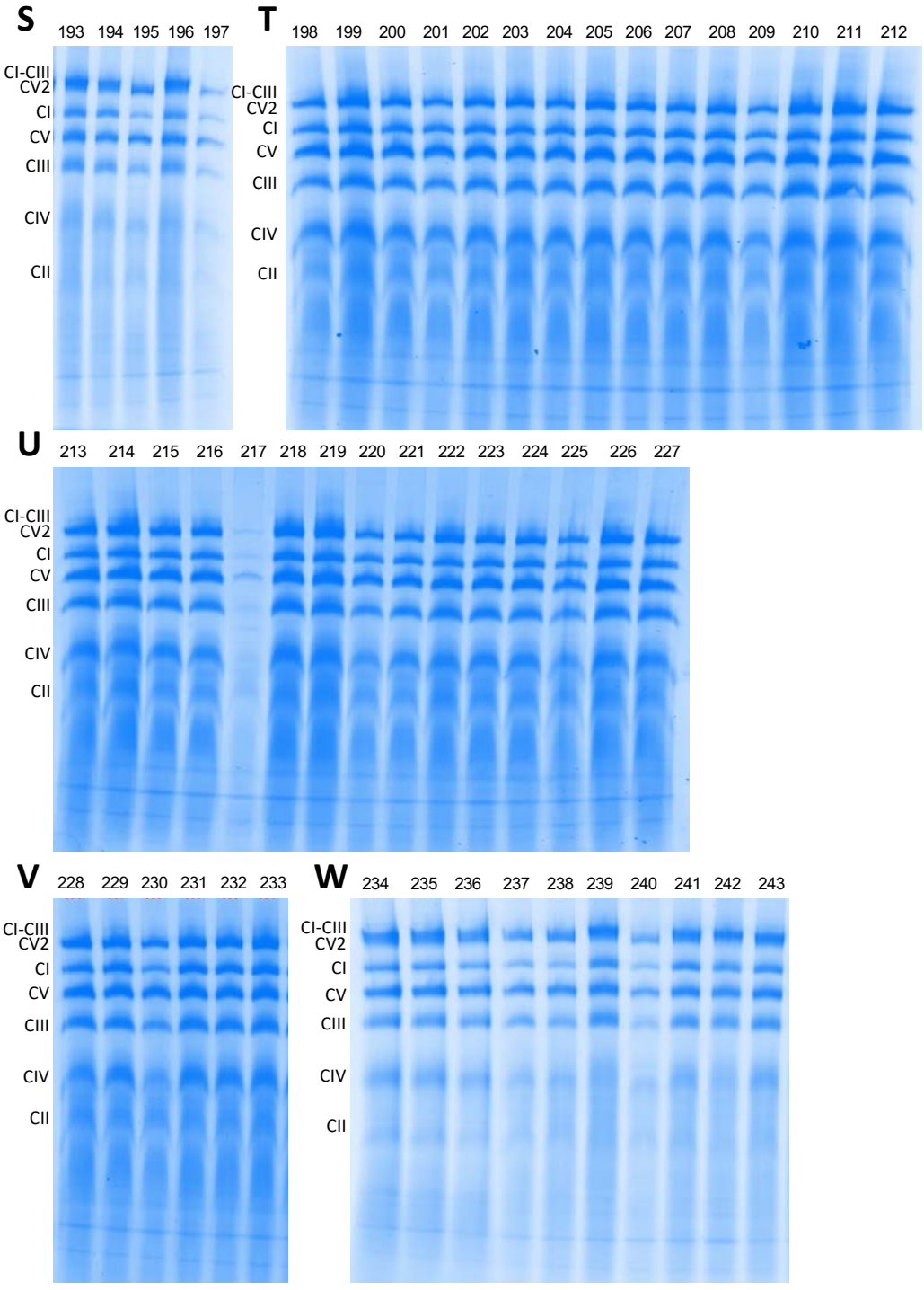
S
193 194 195 196 197
CI-CIII
CV2
CI
CV
CIII
CIV
CII
T
198 199 200 201 202 203 204 205 206 207 208 209 210 211 212
CI-CIII
CV2
CI
CV
CIII
CIV
CII
U
213 214 215 216 217 218 219 220 221 222 223 224 225 226 227
CI-CIII
CV2
CI
CV
CIII
CIV
CII
V
228 229 230 231 232 233
CI-CIII
CV2
CI
CV
CIII
CIV
CII
W
234 235 236 237 238 239 240 241 242 243
CI-CIII
CV2
CI
CV
CIII
CIV
CII

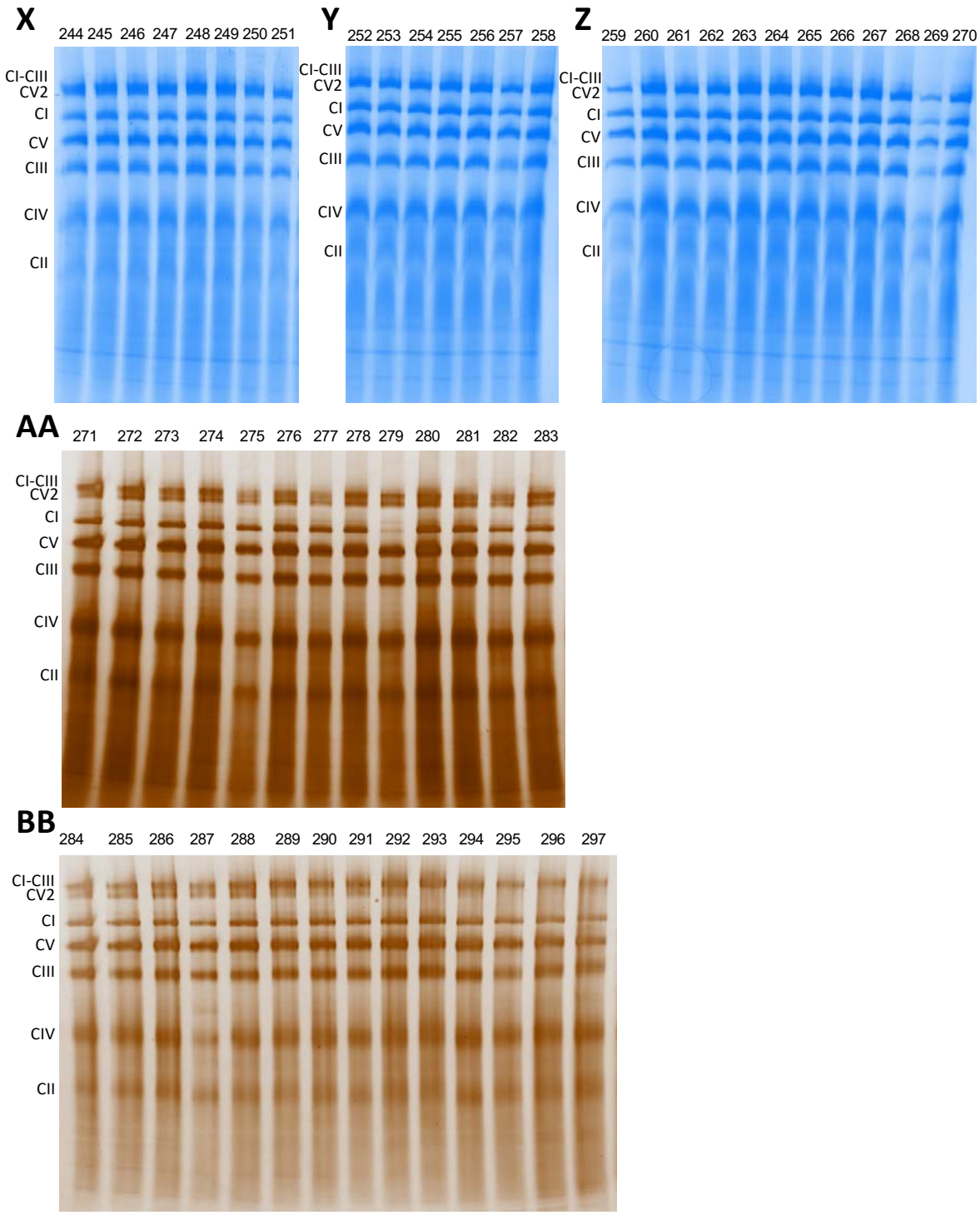
X
244 245 246 247 248 249 250 251
CI-CIII
CV2
CI
CV
CIII
CIV
CII
Y
252 253 254 255 256 257 258
CI-CIII
CV2
CI
CV
CIII
CIV
CII
Z
259 260 261 262 263 264 265 266 267 268 269 270
CI-CIII
CV2
CI
CV
CIII
CIV
CII
AA
271 272 273 274 275 276 277 278 279 280 281 282 283
CI-CIII
CV2
CI
CV
CIII
CIV
CII
BB
284 285 286 287 288 289 290 291 292 293 294 295 296 297
CI-CIII
CV2
CI
CV
CIII
CIV
CII

CC

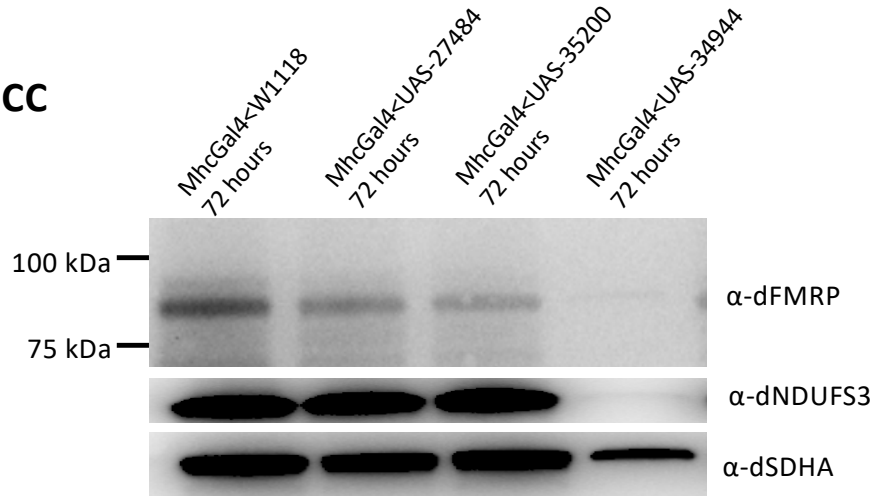
MhcGal4<W1118
72 hours
MhcGal4<UAS-27484
72 hours
MhcGal4<UAS-35200
72 hours
MhcGal4<UAS-34944
72 hours
100 kDa
75 kDa
α-dFMRP
α-dNDUFS3
α-dSDHA

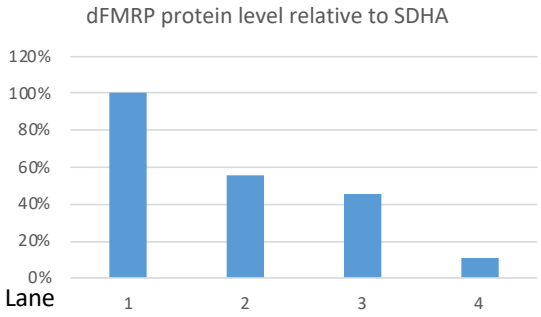
dFMRP protein level relative to SDHA
120%
100%
80%
60%
40%
20%
0%
Lane
1
2
3
4

DD

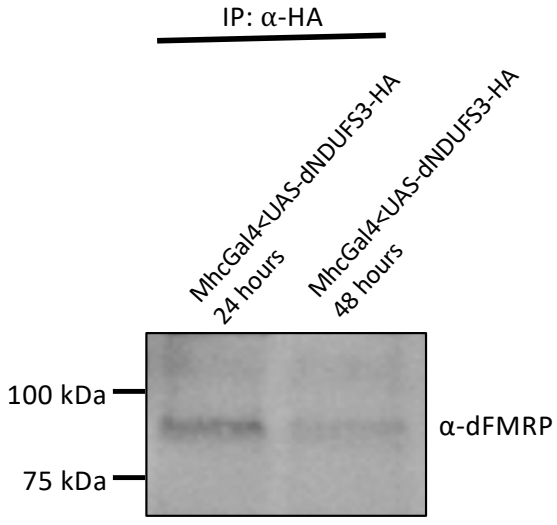
IP: α-HA
MhcGal4<UAS-dNDUFS3-HA
24 hours
MhcGal4<UAS-dNDUFS3-HA
48 hours
100 kDa
75 kDa
α-dFMRP

Figure 3.4: Alternative methods used to disrupt dFMRP and mammalian orthologues to confirm CI phenotype.

(A) Table of the lane number of each genotype to be used as reference for Figures 3.7B-3.7D. MhcGal4<UAS-cas9 was used as control.

(B) SDS-PAGE of whole lysates to check FMRP expression. Note lane 4 shows a reduction in the 81 kDa isoform of dFMRP that causes an increase in lower isoforms. Actin was used as a loading control.

(C) Natve PAGE followed by silver-staining of mitochondria isolated from thoraxes in 4g:1g protein to digitonin ratio (protein:digitonin) to analyze respiratory chain complexes

(D) Native PAGE followed by western blot probed with anti-NDUFS3 to analyze holoenzyme CI and assembly intermediates. Anti-SDHA (CII) is used as a loading control

(E-F) Knockdown of FXR1 after a transfection of 48 and 72 hours in HeLa cell lines. SC=scrambled shRNA; A,B,C,D= different shRNA plasmids targeting FXR1; Mix = 1:1:1:1 ratio of A-D shRNAs; NT = cells not treated with any shRNA. Actin was used as a loading control.

(G-H) Knockdown of FXR1 after a transfection of 48 and 72 hours in C2C12 cell lines. SC=scrambled shRNA; A,B,C,D= different shRNA plasmids targeting FXR1; NT = cells not treated with any shRNA. Actin was used as a loading control.

(I-K) Knockdown of FMR1 after a transfection of 24, 48, and 72 hours hours in C2C12 Cell lines. SC=scrambled shRNA; A,B,C,D= different shRNA plasmids targeting FXR1; Mix = 1:1:1:1 ratio of A-D shRNAs; NT = cells not treated with any shRNA. Actin was used as a loading control.

(L-M) Knockdown of FMR1 after a transfection of 48 and 72 hours in HeLa cell lines. SC=scrambled shRNA; A,B,C,D= different shRNA plasmids targeting FXR1; Mix = 1:1:1:1 ratio of A-D shRNAs; NT = cells not treated with any shRNA. Actin was used as a loading control.

(N-O) Knockdown of FMR1 after a transfection of 48 and 72 hours in C2C12 cell lines. SC=scrambled shRNA; A,B,C,D= different shRNA plasmids targeting FXR1; NT = cells not treated with any shRNA. Actin was used as a loading control.

A

Lane

1. MhcGal4<UAS-cas9 (aged 10 days)
2. MhcGal4<UAS-Cas9; UAS-sgFMR1 RNA (aged 10 days)
3. MhcGal4<UAS-cas9 (aged 10 days)
4. MhcGal4<UAS-Cas9; UAS-sgFMR1 RNA (aged 10 days)
5. MhcGal4<UAS-cas9 (aged 10 days)
6. MhcGal4<UAS-Cas9; UAS-sgFMR1 RNA (aged 10 days)

B

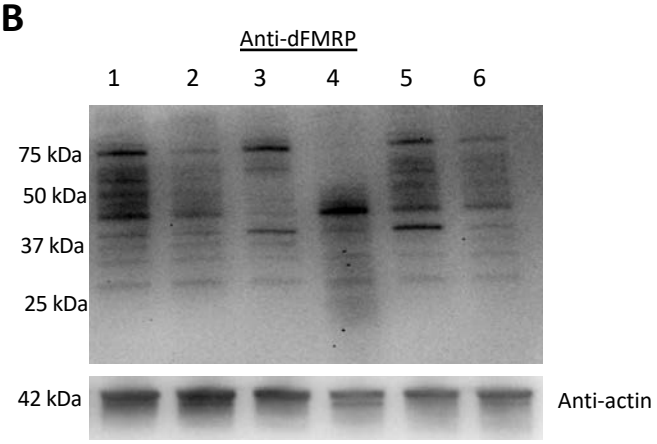

C

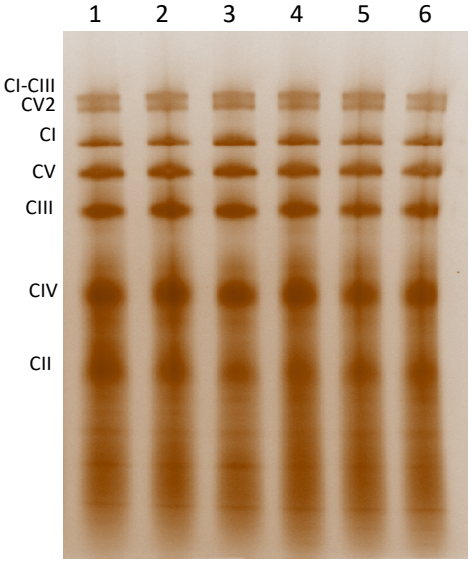

D

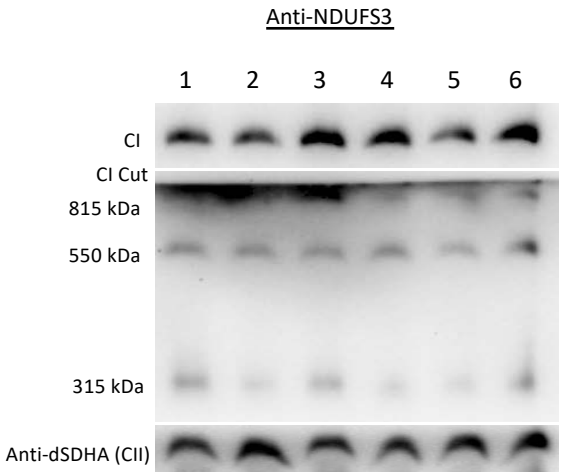

E

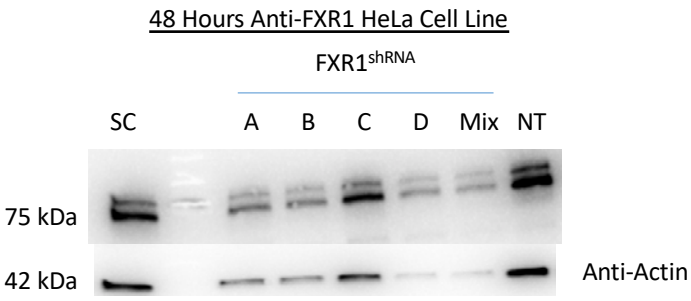
48 Hours Anti-FXR1 HeLa Cell Line
FXR1shRNA
SC
A
B
C
D
Mix
NT
75 kDa
42 kDa
Anti-Actin

F

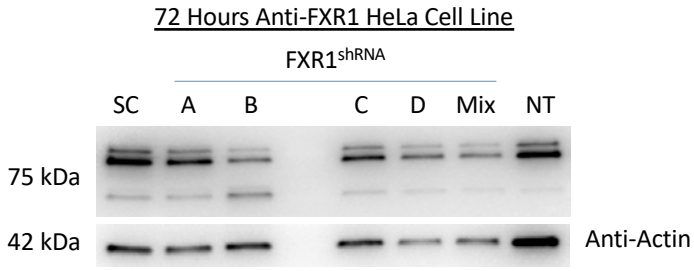
72 Hours Anti-FXR1 HeLa Cell Line
FXR1shRNA
SC
A
B
C
D
Mix
NT
75 kDa
42 kDa
Anti-Actin

G

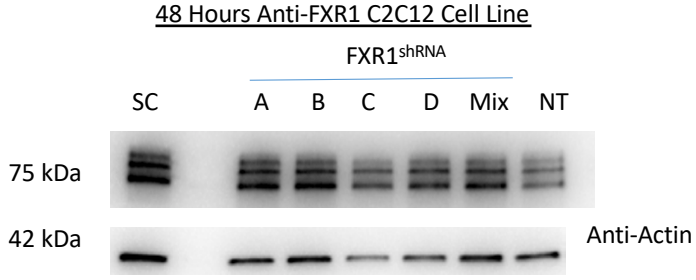
48 Hours Anti-FXR1 C2C12 Cell Line
FXR1shRNA
SC
A
B
C
D
Mix
NT
75 kDa
42 kDa
Anti-Actin

H

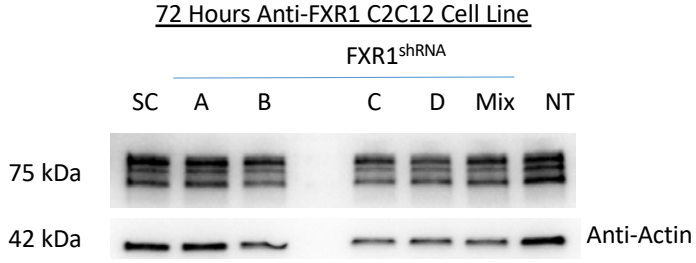
72 Hours Anti-FXR1 C2C12 Cell Line
FXR1shRNA
SC
A
B
C
D
Mix
NT
75 kDa
42 kDa
Anti-Actin

I

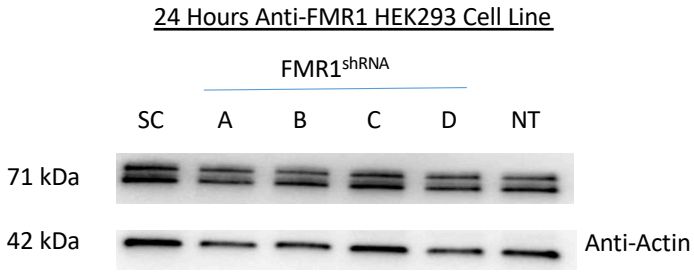
24 Hours Anti-FMR1 HEK293 Cell Line
FMR1shRNA
SC
A
B
C
D
NT
71 kDa
42 kDa
Anti-Actin

J

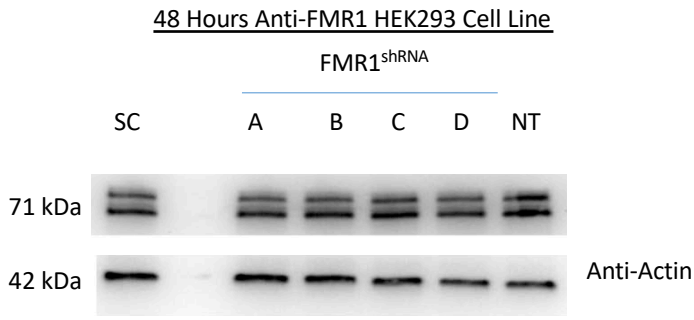
48 Hours Anti-FMR1 HEK293 Cell Line
FMR1shRNA
SC
A
B
C
D
NT
71 kDa
42 kDa
Anti-Actin

K

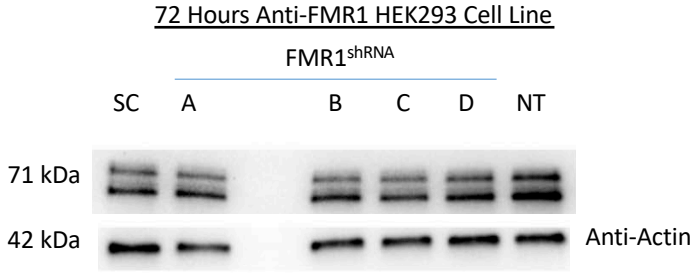
72 Hours Anti-FMR1 HEK293 Cell Line
FMR1shRNA
SC
A
B
C
D
NT
71 kDa
42 kDa
Anti-Actin

L

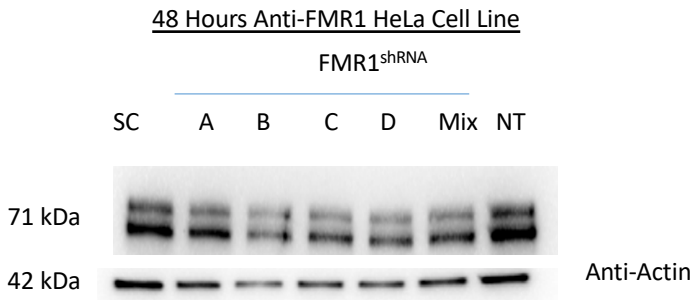
48 Hours Anti-FMR1 HeLa Cell Line
FMR1shRNA
SC A B C D Mix NT
71 kDa
42 kDa
Anti-Actin

M

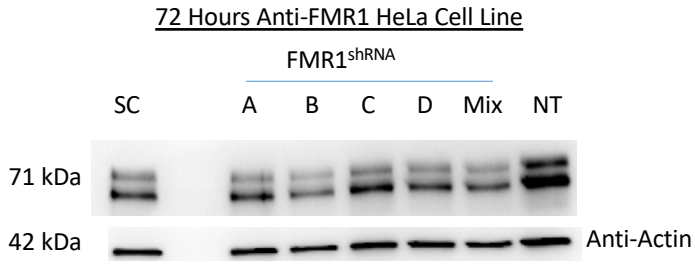
72 Hours Anti-FMR1 HeLa Cell Line
FMR1shRNA
SC A B C D Mix NT
71 kDa
42 kDa
Anti-Actin

N


48 Hours Anti-FMR1 C2C12 Cell Line
FMR1shRNA
SC A B C D Mix NT
71 kDa
42 kDa
Anti-Actin

O

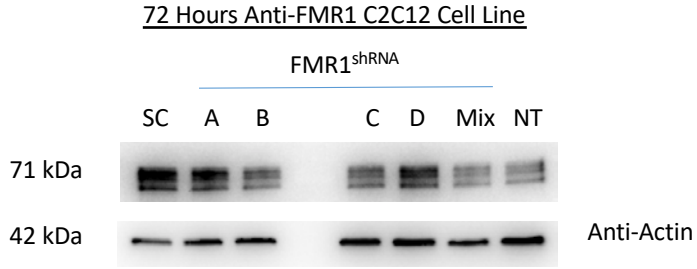
72 Hours Anti-FMR1 C2C12 Cell Line
FMR1shRNA
SC A B C D Mix NT
71 kDa
42 kDa
Anti-Actin

Figure 3.5: Knockdown of dFMRP destabilizes CI and reduces lifespan.

(A) Survival curve showing the percentage of flies surviving per hours. The blue bar indicates Mhc<dFMRP$_{RNAi}$ and the green bar indicates Mhc<W1118.

(B) Western blot showing the protein levels of Mhc<dFMRP$_{RNAi}$ flies aged to 6, 24, and 48 hours compared to Mhc<W1118. Anti-dFMRP was used to detect dFMRP. Anti-actin was used as a loading control.

(C) BN-PAGE of Mhc<W1118 and Mhc<dFMRP$_{RNAi}$ flies aged to 24 hours. CI-CIII denotes the complex I-complex III supecomplex, CV2 denotes a dimer of complex V respectively, CI denotes complex I, CV denotes complex V, CIII denotes complex III, CIV denotes complex IV, and CII denotes complex II.

(D) Silver Stainining of Mhc<W1118 and Mhc<dFMRP$_{RNAi}$ flies aged to 24 hours. CI-CIII denotes the complex I-complex III supecomplex, CV2 denotes a dimer of complex V respectively, CI denotes complex I, CV denotes complex V, CIII denotes complex III, CIV denotes complex IV, and CII denotes complex II.

(E) CI in-gel activity of Mhc<W1118 and Mhc<dFMRP$_{RNAi}$ aged to 6, 24, and 48 hours. CII in-gel activity was also detected for loading control. CI-CIII denotes the complex I-complex III supecomplex, , CI denotes complex I, and CII denotes complex II.

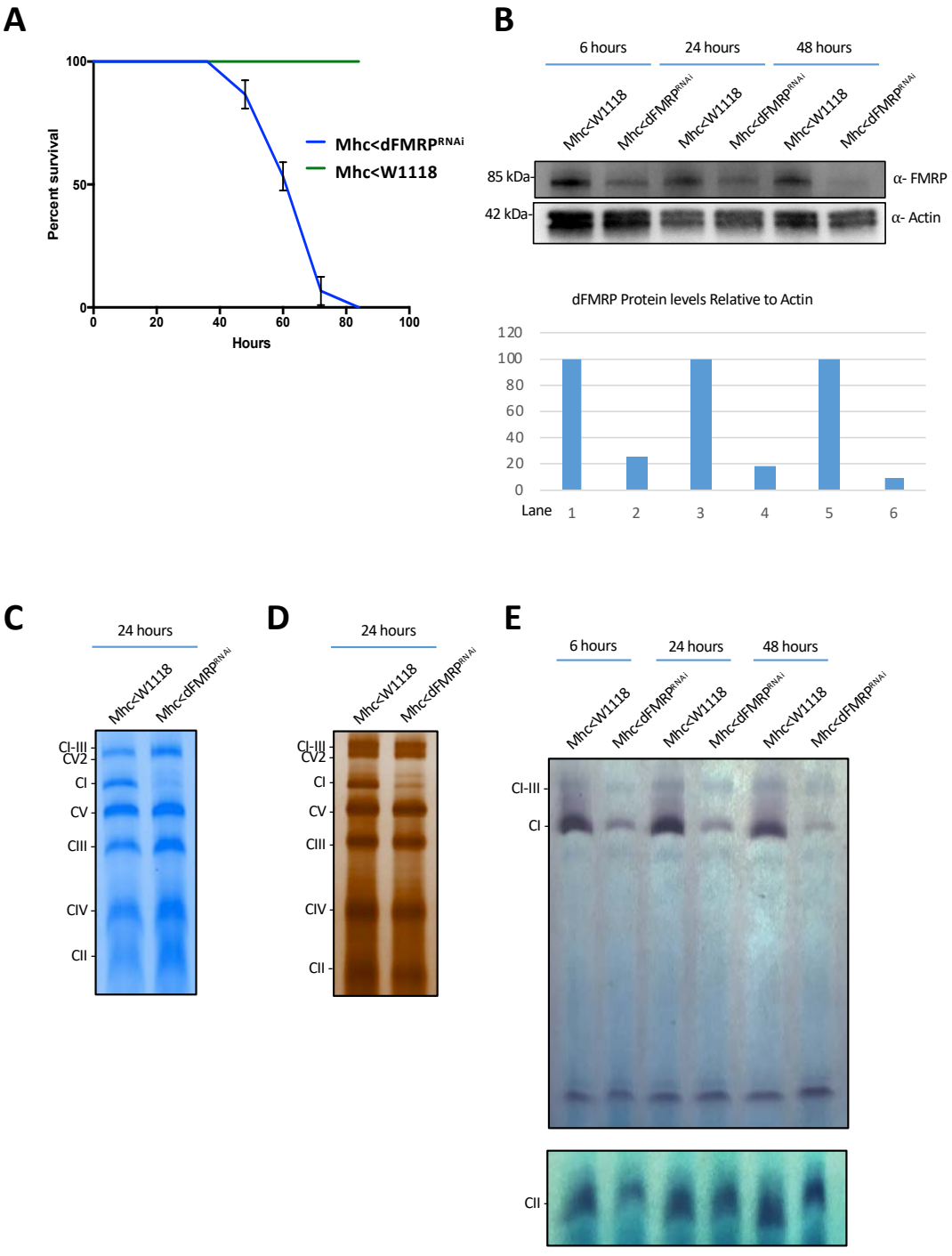
A
Percent survival
Hours
Mhc<dFMRP^RNAi
Mhc<W1118
B
6 hours
24 hours
48 hours
Mhc<W1118
Mhc<dFMRP^RNAi
85 kDa
42 kDa
α- FMRP
α- Actin
dFMRP Protein levels Relative to Actin
Lane
C
24 hours
CI-III
CV2
CI
CV
CIII
CIV
CII
D
24 hours
E
6 hours
24 hours
48 hours
CI-III
CI
CII

Figure 3.6: Disruption of dFMRP in flight muscles impairs CI assembly.

(A) Schematic representation of mammalian CI representing the antibodies to CI subunits (depicted in red) used to track the assembly of the modules of CI. dNDUFV1 was used to detect the N-module, dNDUFS3 was used to detect the Q-module, dND3 was used to detect the P_P-module, and dNDUFB5 and dND5 were used to detect the P_D-module.

(B) Immunoblots probed with anti-NDUFS3 of samples obtained from wildtype and mhc>dFMRP^{RNAi} thoraxes of flies aged for 24 hours after eclosure. Left panel shows short exposure timepoint. Note a decrease in the CI-CIII supercomplex and holoenzyme of CI in mhc>dFMRP^{RNAi} thoraxes. Right panel shows long exposure timepoint to reveal assembly intermediates. 815-, 700-, 550-, and 315 kDa assembly intermediates were detected. Note a decrease in the 815 kDa assembly intermediate and increase in the 700- and 550 kDa assembly intermediates in mhc>dFMRP^{RNAi} thoraxes. Anti-SDHA was used as a loading control.

(C) Immunoblots probed with anti-dND3 of samples obtained from wildtype and mhc>dFMRP^{RNAi} thoraxes of flies aged for 24 hours after eclosure. Left panel shows short exposure time point. Note a decrease in the holoenzyme of CI in mhc>dFMRP^{RNAi} thoraxes. Right panel shows long exposure time point to reveal assembly intermediates. 815-, 700-, and 550 kDa assembly intermediates were detected. Note a decrease in the 815 kDa assembly intermediate and increase in the 700- and 550 kDa assembly intermediates in mhc>dFMRP^{RNAi} thoraxes. Also, additional assembly intermediates were detected and termed lower assembly intermediates (L.A.I.). Anti-SDHA was used as a loading control.

(D) Immunoblots probed with anti-dND5 of samples obtained from wildtype and mhc>dFMRP^{RNAi} thoraxes of flies aged for 6, 24, and 48 hours after eclosure. Left panel shows short exposure time point. Note a decrease in the holoenzyme of CI and CI-CIII supercomplex in mhc>dFMRP^{RNAi} thoraxes. Right panel shows long exposure time point to reveal lower assembly intermediates (L.A.I.). Note an overall increase in L.A.I. along with additional bands that may be degradation products from L.A.I. Anti-SDHA was used as a loading control.

(E) Immunoblots probed with anti-dNDUFB5 of samples obtained from wildtype and mhc>dFMRP^{RNAi} thoraxes of flies aged for 6, 24, and 48 hours after eclosure. Left panel shows short exposure time point. Note a decrease in the holoenzyme of CI and CI-CIII supercomplex in mhc>dFMRP^{RNAi} thoraxes. Right

panel shows long exposure time point to reveal lower assembly intermediates (L.A.I.). Note an overall increase in L.A.I. along with additional bands that may be degradation products from L.A.I. Anti-SDHA was used as a loading control.

(F) Immunoblots probed with anti-dNDUFV1 of samples obtained from wildtype and mhc>dFMRP$_{RNAi}$ thoraxes of flies aged for 6, 24, and 48 hours after eclosure. Left panel shows short exposure time point. Note a decrease in the holoenzyme of CI and CI-CIII supercomplex in mhc>dFMRP$_{RNAi}$ thoraxes. Right panel shows long exposure time point to reveal lower assembly intermediates (L.A.I.). Note an overall increase in L.A.I. Anti-SDHA was used as a loading control.

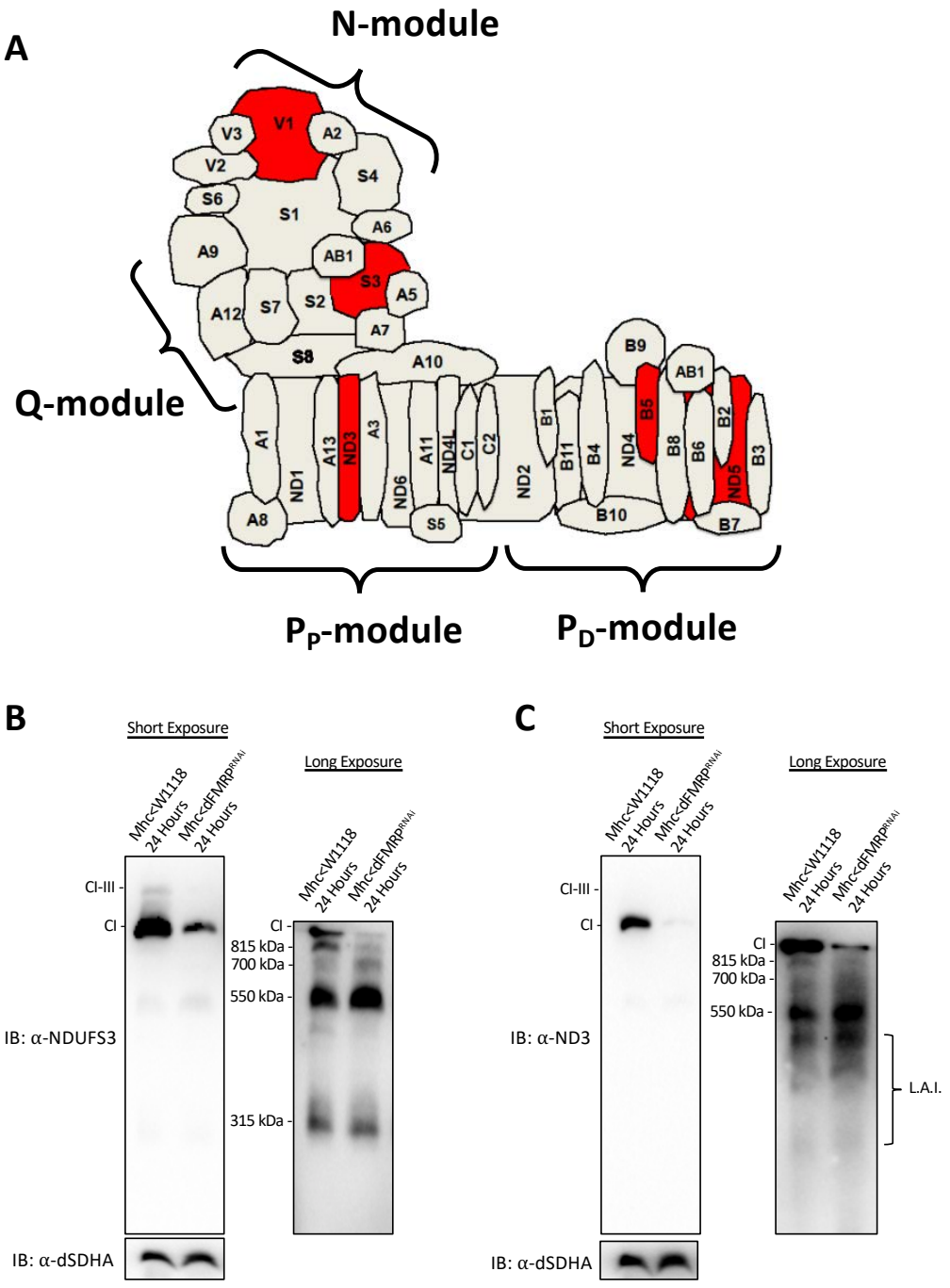
A
N-module
Q-module
V1
V3
A2
V2
S4
S6
S1
A6
A9
AB1
S3
A5
A12
S7
S2
A7
S8
A10
B9
AB1
B5
B2
A1
A13
ND3
A3
A11
ND4L
C1
C2
ND2
B1
B11
B4
ND4
B8
B6
ND5
B3
ND1
ND6
A8
S5
B10
B7
PP-module
PD-module
B
Short Exposure
Long Exposure
Mhc<W1118 24 Hours
Mhc<dFMRPRNAi 24 Hours
CI-III
CI
815 kDa
700 kDa
550 kDa
315 kDa
IB: α-NDUFS3
IB: α-dSDHA
C
Short Exposure
Long Exposure
Mhc<W1118 24 Hours
Mhc<dFMRPRNAi 24 Hours
CI-III
CI
815 kDa
700 kDa
550 kDa
IB: α-ND3
L.A.I.
IB: α-dSDHA

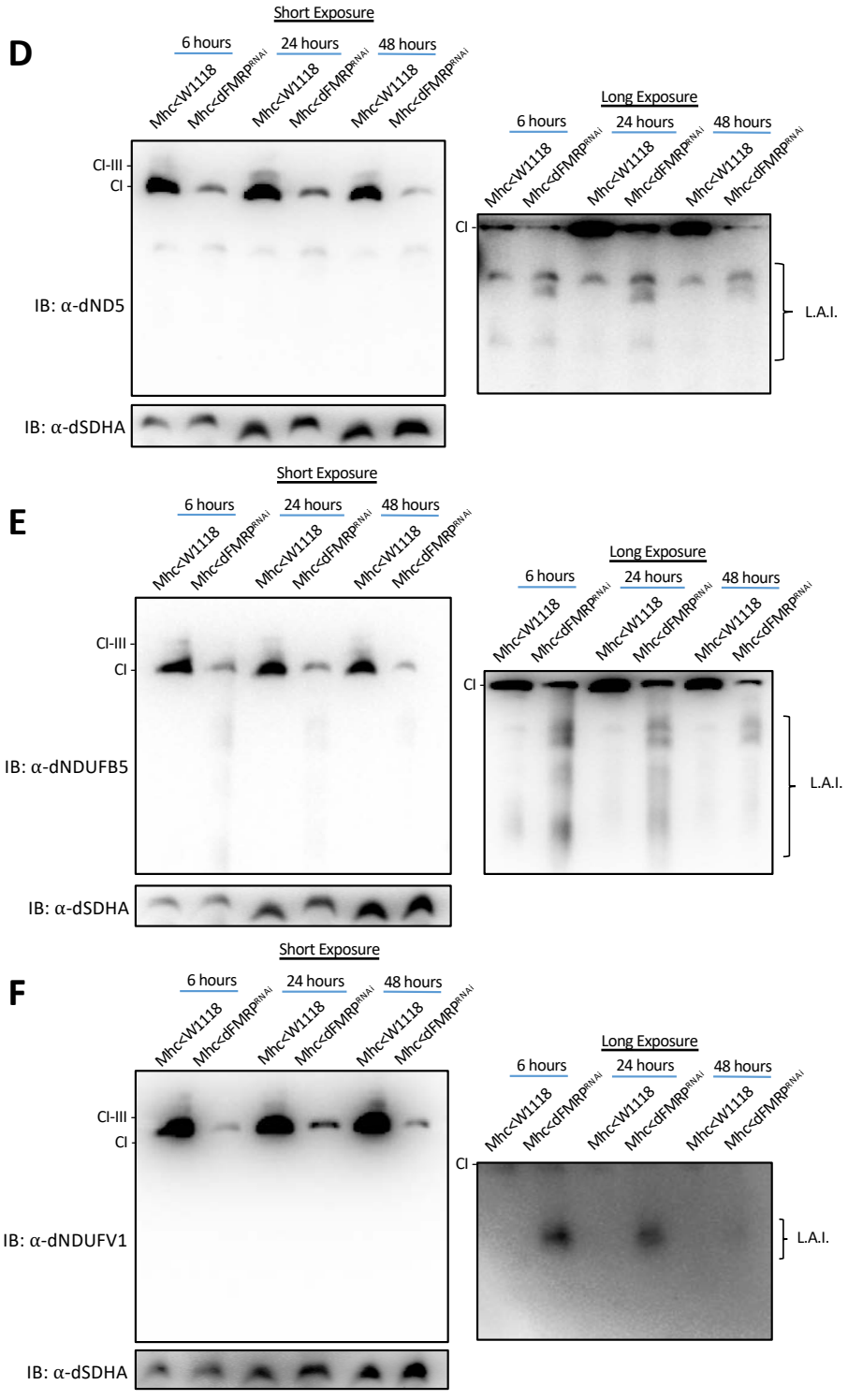
D
Short Exposure
6 hours
24 hours
48 hours
Mhc<W1118
Mhc<dFMRP^RNAi
CI-III
CI
IB: α-dND5
IB: α-dSDHA
Long Exposure
L.A.I.
E
IB: α-dNDUFB5
F
IB: α-dNDUFV1

Figure 3.7: The P_D-module regulator, Foxred1, is downregulated in Mhc<dFMRP$_{RNAi}$ offspring.

(A) Schematic representation of the assembly of mammalian CI. The Q module binds to the P_P-module followed by the addition of the P_D-module. Finally, the N-module binds to the Q+P module to form the fully assembled holoenzyme of CI. Red dots depict the modules that known CIAFs are predicted to bind and regulate.

(B) SDS-PAGE Immunoblots probed with known CIAFs that bind to the P_P-module (anti-dTIMMDC1, anti-dNDUFAF1, anti-dECSIT, and anti-dACAD9) of samples obtained from wildtype and mhc>dFMRP$_{RNAi}$ thoraxes of flies aged for 6, 24, and 48 hours after eclosure. Note a slight decrease in dTIMMDC1 at 48 hours.

(C) SDS-PAGE Immunoblots probed with known CIAFs that bind to the Q-module (anti-dNDUFAF5) of samples obtained from wildtype and mhc>dFMRP$_{RNAi}$ thoraxes of flies aged for 6, 24, and 48 hours after eclosure.

(D) SDS-PAGE Immunoblots probed with known CIAFs that bind to the P_D-module (anti-dFoxred1) of samples obtained from wildtype and mhc>dFMRP$_{RNAi}$ thoraxes of flies aged for 6, 24, and 48 hours after eclosure. Note a decrease in dFoxred1 at every time point.

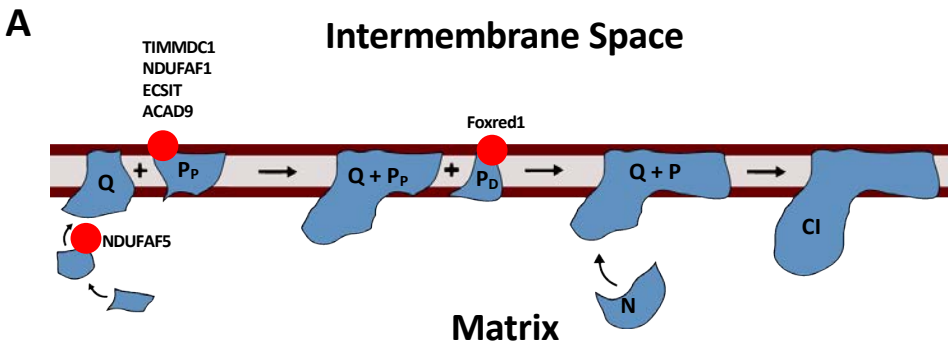
A
Intermembrane Space
TIMMDC1
NDUFAF1
ECSIT
ACAD9
Foxred1
Q
+
PP
Q + PP
+
PD
Q + P
CI
NDUFAF5
N
Matrix

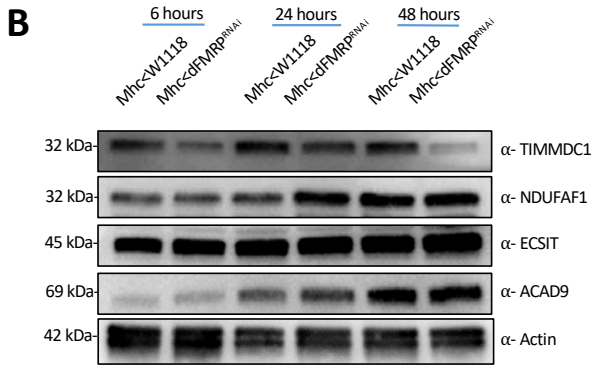
B
6 hours
24 hours
48 hours
Mhc<W1118
Mhc<dFMRPRNAi
32 kDa
α- TIMMDC1
32 kDa
α- NDUFAF1
45 kDa
α- ECSIT
69 kDa
α- ACAD9
42 kDa
α- Actin

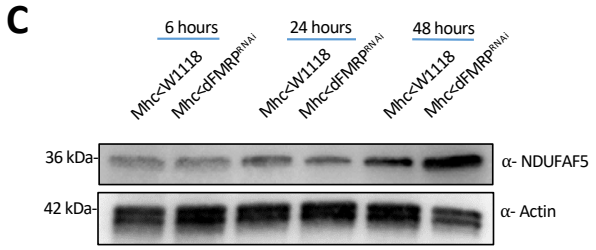
C
6 hours
24 hours
48 hours
Mhc<W1118
Mhc<dFMRPRNAi
36 kDa
α- NDUFAF5
42 kDa
α- Actin

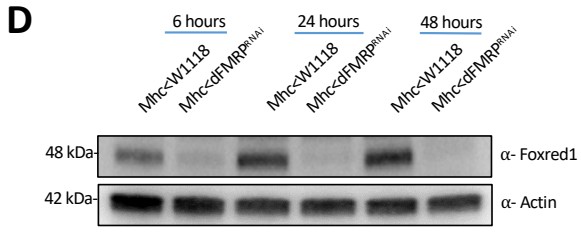
D
6 hours
24 hours
48 hours
Mhc<W1118
Mhc<dFMRPRNAi
48 kDa
α- Foxred1
42 kDa
α- Actin

Table 3.1: Proteins identified by mass spectrometry after co-IP with dNDUFS3-HA.

The table shows all the peptides identified after co-IP with dNDUFS3-HA. Peptides highlighted in blue are CI subunits. Peptides highlighted in green are proteins we ordered Bloomington stocks for.

			IP with Digitonin	IP with NP40		Bloomington #			
Identified Proteins (493/509)	Accession Number	Molecular Weigh	ND-30_Dig	ND_30_NP					
14-3-3 protein zeta 14-3-3zeta	1433Z_DROME	28 kDa	0	3		31498	28327		
26S proteasome non-ATPase regulatory subunit 11 Rpn6	PSD11_DROME	47 kDa	4	0		29385			
26S proteasome regulatory complex subunit p48B Rpt1	Q7KMQ0_DROME	49 kDa	4	1		33930			
26S proteasome regulatory complex subunit p50 Rpt5	Q9V3V6_DROME	48 kDa	3	0		53886	32422		
26S proteasome regulatory complex subunit p97 Rpn1	Q9VW54_DROME	102 kDa	2	0		34348			
39S ribosomal protein L28, mitochondrial mRpL28	RM28_DROME	35 kDa	4	0		36076			
40S ribosomal protein S13 RpS13	RS13_DROME	17 kDa	6	0					
40S ribosomal protein S14 RpS14a	RS14_DROME	16 kDa	3	6					
40S ribosomal protein S16 RpS16	RS16_DROME	17 kDa	4	6					
40S ribosomal protein S17 RpS17	RS17_DROME	15 kDa	2	3		42656			
40S ribosomal protein S18 RpS18	RS18_DROME	18 kDa	9	6					
40S ribosomal protein S19a RpS19a	RS19A_DROME	17 kDa	2	4		42774			
40S ribosomal protein S2 RpS2	RS2_DROME	29 kDa	7	5					
40S ribosomal protein S3 RpS3	RS3_DROME	27 kDa	6	4					
40S ribosomal protein S3a RpS3A	RS3A_DROME	30 kDa	16	11					
40S ribosomal protein S4 RpS4	RS4_DROME	29 kDa	4	14					
40S ribosomal protein S6 RpS6	RS6_DROME	28 kDa	8	1					
40S ribosomal protein S7 RpS7	RS7_DROME	22 kDa	2	10					
40S ribosomal protein S8 RpS8	RS8_DROME	24 kDa	8	7					
40S ribosomal protein S9 RpS9	RS9_DROME	23 kDa	17	3					
40S ribosomal protein SA sta	RSSA_DROME (+1)	35 kDa	1	2					
60S acidic ribosomal protein P0 RpLP0	RLA0_DROME	34 kDa	7	5					
60S ribosomal protein L10 RpL10	RL10_DROME	26 kDa	5	3					
60S ribosomal protein L13 RpL13	RL13_DROME	25 kDa	4	0					
60S ribosomal protein L13a RpL13A	RL13A_DROME	24 kDa	6	0					
60S ribosomal protein L14 RpL14	RL14_DROME	19 kDa	3	3					
60S ribosomal protein L17 RpL17	RL17_DROME	22 kDa	1	2		54048			
60S ribosomal protein L18 RpL18	RL18_DROME	22 kDa	6	2					
60S ribosomal protein L18a RpL18A	RL18A_DROME	21 kDa	6	0					
60S ribosomal protein L19 RpL19	RL19_DROME	24 kDa	11	2					
60S ribosomal protein L22 RpL22	RL22_DROME	31 kDa	1	4					
60S ribosomal protein L23 RpL23	RL23_DROME	15 kDa	0	3		53300			
60S ribosomal protein L27 RpL27	Q9VBN5_DROME	16 kDa	5	1					
60S ribosomal protein L27a RpL27A	RL27A_DROME	17 kDa	5	0					
60S ribosomal protein L28 RpL28	RL28_DROME	16 kDa	3	1					
60S ribosomal protein L3 RpL3	RL3_DROME	47 kDa	11	3					
60S ribosomal protein L32 RpL32	RL32_DROME	16 kDa	3	0		51746			
60S ribosomal protein L4 RpL4	RL4_DROME	45 kDa	38	16					
60S ribosomal protein L5 RpL5	RL5_DROME	34 kDa	8	13					
60S ribosomal protein L7 RpL7	RL7_DROME	30 kDa	22	6					
60S ribosomal protein L7a RpL7A	RL7A_DROME	31 kDa	5	2					
60S ribosomal protein L8 RpL8	RL8_DROME	28 kDa	2	4		50610			
60S ribosomal protein L9 RpL9	RL9_DROME	21 kDa	0	3					
AAA family protein Bor bor	Q9VEX6_DROME	68 kDa	15	10					
Acetyl-CoA carboxylase, isoform A ACC	A1Z784_DROME	279 kDa	3	1					
Acyl-CoA synthetase long-chain, isoform J Acsl	A0A0B4KFE4_DROME	82 kDa	1	3		43268	41885	27729	
Adenylyl cyclase-associated protein capt	Q9VPX6_DROME	84 kDa	5	0		33010			
AF4/FMR2 family member 4 lilli	AFF4_DROME	180 kDa	2	0		26314	34592		

Alanine--tRNA ligase, cytoplasmic Aats-ala	SYAC_DROME	108 kDa	6	0					
Aldehyde dehydrogenase Aldh	Q9VLC5_DROME	57 kDa	17	10					
Aldehyde dehydrogenase Aldh-III	A0A0B4KEE1_DROME	56 kDa	3	0		51820			
ALG-2 interacting protein X ALiX	Q9VB05_DROME	93 kDa	3	2		50904	33417		
Alpha spectrin, isoform C alpha-Spec	M9PBI5_DROME (+3)	281 kDa	36	4					
Alpha-actinin, sarcomeric Actn	ACTN_DROME (+2)	107 kDa	89	59					
Amphiphysin, isoform B Amph	A0A0B4KEW6_DROM	55 kDa	12	6		53971	39015		
Ankyrin, isoform B Ank	Q0KIE7_DROME	170 kDa	2	0		43965	31115		
AP-2 complex subunit alpha AP-2alpha	AP2A_DROME	106 kDa	0	5		32866			
Apolipophorins Rfabg	APLP_DROME	373 kDa	747	204					
Arginine kinase, isoform E Argk	A8JNP2_DROME (+1)	42 kDa	19	4		35221	41697		
Argonaute-1, isoform A AGO1	Q32KD4_DROME (+1	110 kDa	0	35		31700	33727	53293	
Aspartyl-tRNA synthetase, isoform A Aats-asp	Q7K0E6_DROME	59 kDa	1	5					
AT02348p UQCR-C2	Q9VV75_DROME	45 kDa	43	33					
AT21758p CG5261	Q9VM14_DROME	54 kDa	10	7		40922	44439		
AT27578p rin	Q9VFT4_DROME	75 kDa	0	20		33392			
AT27789p glo	Q9VGH5_DROME	61 kDa	0	45		33668	36066		
Ataxin-2 binding protein 1, isoform L A2bp1	M9ND74_DROME (+2	85 kDa	3	0		32476	27286		
Ataxin-2 homolog Atx2	ATX2_DROME	118 kDa	0	16		44012			
ATP synthase subunit alpha, mitochondrial blw	ATPA_DROME	59 kDa	95	37					
ATP synthase subunit b, mitochondrial ATPsynB	AT5F1_DROME	27 kDa	3	2					
ATP synthase subunit beta ATPsynbetaL	Q8T4C4_DROME	68 kDa	18	4					
ATP synthase subunit beta, mitochondrial ATPsyn-beta	ATPB_DROME (+1)	54 kDa	180	65					
ATP synthase subunit d, mitochondrial ATPsynD	ATP5H_DROME	20 kDa	5	3					
ATP synthase subunit gamma, mitochondrial ATPsyngamma	ATPG_DROME	33 kDa	29	22					
ATP synthase subunit O, mitochondrial ATPsynO	ATPO_DROME	22 kDa	4	1					
ATP-citrate synthase ATPCL	E2QCF1_DROME	120 kDa		0					
ATP-dependent 6-phosphofructokinase Pfk	A0A0B4K7L1_DROME	105 kDa	29	8					
ATP-dependent helicase brm brm	BRM_DROME (+2)	185 kDa	0	5		31712	34520	35211	
ATP-dependent RNA helicase p62 Rm62	DDX17_DROME	79 kDa	1	5		58150	34829	31395	
B52, isoform O B52	A0A0C4DHG5_DROM	40 kDa	3	0		37519			
Belle, isoform B bel	A0A0B4KGU4_DROM	85 kDa	7	43		35185	35302		
Beta spectrin, isoform B beta-Spec	M9PF16_DROME	268 kDa	23	21					
Beta-Tubulin at 97EF, isoform B betaTub97EF	Q8MST5_DROME (+1	51 kDa	16	11					
Bicoid stability factor bsf	Q9VJ86_DROME	157 kDa	8	1		31078	34550		
Brahma associated protein 155 kDa mor	Q9VF03_DROME	131 kDa	0	10		34919	35630	35662	
Brahma associated protein 55kD Bap55	Q7K012_DROME	47 kDa	0	7		31708			
Brahma-associated protein of 60 kDa Bap60	BAP60_DROME	58 kDa	0	10		31337	32503	33954	
Calcium-transporting ATPase Ca-P60A	A0A0B4LGB7_DROM	109 kDa	36	48					
Carboxylic ester hydrolase alpha-Est7	Q9VIB5_DROME	65 kDa	3	0					
Catalase Cat	CATA_DROME	57 kDa	4	3					
CG10077, isoform D CG10077	Q8MZI3_DROME	88 kDa	4	21		32388	32981		
CG10543, isoform D CG10543	Q86BG2_DROME	183 kDa	0	2		54816	31964		
CG10732-PA, isoform A cmb	Q9VU76_DROME	184 kDa	12	8					
CG10737, isoform R CG10737	B7YZL6_DROME (+2)	97 kDa	4	8					
CG10777, isoform B CG10777	Q9W3M7_DROME	100 kDa	3	45					
CG10932, isoform A CG10932	Q9W3N9_DROME	43 kDa	2	1		51785			
CG11395, isoform A CG11395	Q7K533_DROME	49 kDa	0	4					
CG11423 ND-51L1	A1ZAW7_DROME	77 kDa	0	3					
CG11504, isoform A CG11504-RA	Q7K4R2_DROME	46 kDa	2	0		42509	31917		

CG11771 CG11771	Q9VC06_DROME	81 kDa	3	0					
CG12079-PA ND-30	Q9VZU4_DROME	30 kDa	5	35	NDUFS3				
CG12105, isoform A CG12105	Q9W0C9_DROME	168 kDa	2	0					
CG14607 CG14607-RB	Q9VI81_DROME	41 kDa	0	3					
CG15006-PA Cpr64Aa	Q9VZG2_DROME	20 kDa	6	8					
CG1648, isoform B CG1648	A1Z7Z4_DROME (+1)	24 kDa	3	0					
CG16885 CG16885	Q8SZM2_DROME	29 kDa	0	5					
CG1970, isoform B ND-49	Q9V4E0_DROME	53 kDa	3	33	NDUFS2				
CG2233 CG2233	Q9W3L4_DROME	47 kDa	2	0					
CG30069 CG30069	A1Z9M5_DROME	461 kDa	4	6		57820	61925		
CG30122, isoform B CG30122	A1ZBB4_DROME (+2)	140 kDa	4	1		55209			
CG32479, isoform A Usp10	Q9W0L7_DROME	165 kDa	1	4					
CG33521, isoform C CG33521	Q59DP3_DROME (+1	75 kDa	10	3					
CG34417, isoform T CG34417	M9PDW8_DROME	580 kDa	7	4		58278	62945		
CG3523, isoform A FASN1	Q9VQL7_DROME	266 kDa	6	0		28930	35775		
CG3731, isoform A UQCR-C1	Q9VFF0_DROME	52 kDa	9	5					
CG3902-PA CG3902-RA	Q9VVU1_DROME	45 kDa	5	1		56880			
CG4461 CG4461	Q9VSX2_DROME	24 kDa	2	0		53298			
CG4769, isoform A Cyt-c1	Q9VRL0_DROME	34 kDa	0	8					
CG4882, isoform A CG4882	O77477_DROME	46 kDa	5	1					
CG5028, isoform C CG5028-RC	A8JRB8_DROME (+2)	43 kDa	39	18					
CG5214 CG5214	Q9VGQ1_DROME	50 kDa	10	5		50650			
CG5215-PB, isoform B Zn72D	Q86BI3_DROME	96 kDa	3	0					
CG5703, isoform A ND-24	Q9VX36_DROME	27 kDa	0	2	NDUFV2				
CG5787, isoform A CG5787	Q9VK59_DROME	100 kDa	2	23					
CG6020, isoform A ND-39	Q9VPE2_DROME	47 kDa	1	19	NDUFA9				
CG6439, isoform A CG6439	Q9VD58_DROME	40 kDa	32	20		44475			
CG7033 CG7033	Q9W392_DROME	58 kDa	2	0					
CG7409 CG7409	Q9VSA9_DROME	18 kDa	5	1		51433			
CG7470, isoform A CG7470	Q9VNW6_DROME	84 kDa	3	1		51911			
CG7920, isoform A CG7920	Q9VAC1_DROME	52 kDa	33	11					
CG8036, isoform B CG8036	Q9VHN7_DROME	68 kDa	12	3		32884	60371		
CG8108, isoform A CG8108	Q9VT61_DROME	103 kDa	3	0		32930	27562		
CG8258 CG8258	Q7K3J0_DROME	59 kDa	3	0					
CG8288-PA mRpL3	Q9VXQ0_DROME	41 kDa	6	0					
CG8520, isoform A CG8520	Q7K4T8_DROME	52 kDa	3	0		51749	44533		
CG8547, isoform C CG8547	Q0E980_DROME	68 kDa	2	4					
CG8963, isoform E CG8963	A0A0B4K891_DROME	58 kDa	0	8		31756			
CG9090, isoform A CG9090-RA	Q7JUS9_DROME	41 kDa	1	6		44495			
CG9140, isoform B ND-51	Q9VMI3_DROME	52 kDa	0	12	NDUFV1				
CG9297, isoform B CG9297	Q8I0D4_DROME (+1)	106 kDa	10	1					
CG9485, isoform B CG9485	Q9W2H8_DROME	183 kDa	15	74		58313	34333		
CG9572, isoform B CG9572-RB	E8NH67_DROME (+1)	47 kDa	0	2		58340			
Chip, isoform B Chi	Q7KVG9_DROME	65 kDa	0	3		35435	25225	31049	
Chitinase-like protein Idgf4 Idgf4	IDGF4_DROME	49 kDa	3	0		55381			
Cht5 Cht5	Q9VFR3_DROME	67 kDa	0	10		38984	51157		
Clathrin heavy chain Chc	CLH_DROME	191 kDa	10	0					
Cluster of 26S protease regulatory subunit 8 Rpt6 (PRS8_DROME)	PRS8_DROME	46 kDa	3	0		34712			
Cluster of 60 kDa heat shock protein, mitochondrial Hsp60 (CH60_DROME)	CH60_DROME [2]	61 kDa	9	25		34729			

Cluster of Aconitate hydratase, mitochondrial Acon (Q9VIE8_DROME)	Q9VIE8_DROME [2]	85 kDa	49	28					
Cluster of Actin, larval muscle Act79B (ACT4_DROME)	ACT4_DROME [4]	42 kDa	160	122					
Cluster of ADP,ATP carrier protein sesB (ADT_DROME)	ADT_DROME [3]	34 kDa	30	36					
Cluster of Bent, isoform I bt (L0MN91_DROME)	L0MN91_DROME [2]	993 kDa	188	222					
Cluster of Calcium-transporting ATPase PMCA (Q9V4C7_DROME)	Q9V4C7_DROME [2]	133 kDa	12	1		31572			
Cluster of Calcium/calmodulin-dependent protein kinase type II alpha chain CaMKII (KCC2A_	KCC2A_DROME [4]	60 kDa	2	1					
Cluster of CAP, isoform B CAP (A1Z871_DROME)	A1Z871_DROME [4]	197 kDa	6	0		30506	36613	36663	
Cluster of CG11321, isoform I CG11321 (M9PCS0_DROME)	M9PCS0_DROME [2]	315 kDa	7	0					
Cluster of CG11876, isoform A CG11876 (Q7K5K3_DROME)	Q7K5K3_DROME	39 kDa	12	10		55619			
Cluster of CG14995, isoform I CG14995-RC (F0JAM2_DROME)	F0JAM2_DROME [3]	48 kDa	0	16					
Cluster of CG1674, isoform K CG1674 (H9XVM8_DROME)	H9XVM8_DROME [3]	96 kDa	82	16					
Cluster of CG17597, isoform B CG17597 (Q9VJ44_DROME)	Q9VJ44_DROME [2]	44 kDa	5	0		52886			
Cluster of CG18304, isoform B CG18304 (M9NCS3_DROME)	M9NCS3_DROME [4]	205 kDa	2	2					
Cluster of CG42492, isoform A CG11473 (Q9W4A6_DROME)	Q9W4A6_DROME	99 kDa	2	0					
Cluster of CG42540, isoform F CG42540 (Q9VZA5_DROME)	Q9VZA5_DROME [3]	57 kDa	1	2					
Cluster of CG43078, isoform G CG43078 (M9NE59_DROME)	M9NE59_DROME [4]	275 kDa	56	8					
Cluster of CG43143, isoform I CG43143 (A0A0B4KFP5_DROME)	A0A0B4KFP5_DROME	277 kDa	8	0		35194	31885		
Cluster of CG43897, isoform M CG43897 (M9PF57_DROME)	M9PF57_DROME [4]	155 kDa	18	10		31560			
Cluster of CG44085, isoform O CG44085 (M9PDE7_DROME)	M9PDE7_DROME [3]	267 kDa	1	47					
Cluster of CG6455, isoform E Mitofilin (A0A0B4KGN2_DROME)	A0A0B4KGN2_DROM	83 kDa	56	6		63994	43245		
Cluster of CG6512-PA, isoform A CG6512 (Q8T4G5_DROME)	Q8T4G5_DROME [2]	90 kDa	6	9		34343	50524		
Cluster of CG7766, isoform D CG7766 (B7Z134_DROME)	B7Z134_DROME [3]	138 kDa	3	0		42890	42510		
Cluster of CG8086, isoform G CG8086 (M9NCS7_DROME)	M9NCS7_DROME [5]	171 kDa	26	8					
Cluster of CG9172, isoform A ND-20 (Q9VXK7_DROME)	Q9VXK7_DROME [2]	25 kDa	0	6	NDUFS7				
Cluster of Cheerio, isoform M cher (A0A0B4KGT8_DROME)	A0A0B4KGT8_DROM	263 kDa	3	3					
Cluster of Darkener of apricot, isoform P Doa (Q86B73_DROME)	Q86B73_DROME [4]	227 kDa	9	3		50903	55908		
Cluster of Disks large 1 tumor suppressor protein dlg1 (DLG1_DROME)	DLG1_DROME [2]	107 kDa	1	2					
Cluster of Elongation factor 1-alpha 2 Ef1alpha100E (EF1A2_DROME)	EF1A2_DROME [2]	51 kDa	20	35					
Cluster of Eukaryotic initiation factor 4A eIF-4a (IF4A_DROME)	IF4A_DROME	46 kDa	13	10					
Cluster of FI21236p1 rump (Q9VHC7_DROME)	Q9VHC7_DROME	67 kDa	3	5					
Cluster of Flotillin 2, isoform G Flo2 (E1JJL2_DROME)	E1JJL2_DROME [6]	38 kDa	4	5		55212	40833		
Cluster of GH17761p Ubi-p5E (Q9W418_DROME)	Q9W418_DROME [5]	60 kDa	21	15		38967			
Cluster of GH19182p Zasp66 (Q95TZ7_DROME)	Q95TZ7_DROME [3]	44 kDa	18	10					
Cluster of Glyceraldehyde-3-phosphate dehydrogenase 1 Gapdh1 (G3P1_DROME)	G3P1_DROME [2]	35 kDa	34	29					
Cluster of Heat shock 70 kDa protein cognate 4 Hsc70-4 (HSP7D_DROME)	HSP7D_DROME [2]	71 kDa	38	41		35684	34836		
Cluster of Heat shock protein 68 Hsp68 (HSP68_DROME)	HSP68_DROME [4]	70 kDa	5	6		50637			
Cluster of Hu li tai shao, isoform P hts (A8DYJ2_DROME)	A8DYJ2_DROME [2]	205 kDa	7	4		38283			
Cluster of Isocitrate dehydrogenase [NADP] Idh (Q7KUB1_DROME)	Q7KUB1_DROME [2]	53 kDa	7	4		41708			
Cluster of Lethal (2) 01289, isoform M l(2)01289 (A0A0B4K7H1_DROME)	A0A0B4K7H1_DROM	137 kDa	12	34					
Cluster of Lingerer, isoform H lig (A0A0B4K7U5_DROME)	A0A0B4K7U5_DROM	134 kDa	28	49		61857			
Cluster of Mf4 protein Mf (Q70VI1_DROME)	Q70VI1_DROME [3]	42 kDa	38	20					
Cluster of Muscle LIM protein Mlp84B Mlp84B (MLP2_DROME)	MLP2_DROME	54 kDa	0	15		31558			
Cluster of Myosin heavy chain-like, isoform G Mhcl (Q0KI67_DROME)	Q0KI67_DROME	242 kDa	2	0					
Cluster of Myosin heavy chain, isoform T Mhc (M9NEP1_DROME)	M9NEP1_DROME [4]	224 kDa	3190	520					
Cluster of Neural conserved at 73EF, isoform I Nc73EF (A8JNU6_DROME)	A8JNU6_DROME [2]	123 kDa	145	31		33686			
Cluster of Paramyosin, long form Prm (MYSP1_DROME)	MYSP1_DROME [3]	102 kDa	213	100					
Cluster of PDZ and LIM domain protein Zasp Zasp52 (ZASP_DROME)	ZASP_DROME [4]	238 kDa	135	126					
Cluster of Polychaetoid, isoform J pyd (Q9VHK1_DROME)	Q9VHK1_DROME [4]	188 kDa	0	7		28920	33386		
Cluster of Protein 4.1 homolog cora (41_DROME)	41_DROME [2]	184 kDa	7	8		28933	35003	51845	
Cluster of Protein anoxia up-regulated fau (FAU_DROME)	FAU_DROME [2]	69 kDa	48	13					

Cluster of Protein elav elav (ELAV_DROME)	ELAV_DROME [3]	51 kDa	0	7					
Cluster of Protein no-on-transient A nonA (NONA_DROME)	NONA_DROME	77 kDa	15	29		52933	56944	61279	
Cluster of Rbp1-like, isoform B Rbp1-like (M9MS48_DROME)	M9MS48_DROME [2]	26 kDa	3	0		50574	55362	44100	
Cluster of Reticulon-like protein Rtnl1 (E1JHT6_DROME)	E1JHT6_DROME [2]	65 kDa	7	1					
Cluster of RH48056p RpL34b (Q9VHE5_DROME)	Q9VHE5_DROME [2]	18 kDa	6	0					
Cluster of RNA-binding protein cabeza caz (CAZ_DROME)	CAZ_DROME	39 kDa	0	5		34839	32990		
Cluster of Ryanodine receptor, isoform E RyR (A0A0B4K837_DROME)	A0A0B4K837_DROM	580 kDa	47	28					
Cluster of Sallimus, isoform T sls (M9PDS3_DROME)	M9PDS3_DROME [3]	2051 kDa	232	361					
Cluster of Shibire, isoform L shi (E1JJA4_DROME)	E1JJA4_DROME [2]	99 kDa	9	4		36921	28513		
Cluster of Short stop, isoform H shot (A1Z9J3_DROME)	A1Z9J3_DROME [3]	990 kDa	24	32					
Cluster of Sodium/potassium-transporting ATPase subunit alpha Atpalpha (A0A0B4KGG8_D	A0A0B4KGG8_DROM	111 kDa	77	13					
Cluster of Syncrip, isoform J Syp (A0A0B4KHT5_DROME)	A0A0B4KHT5_DROM	83 kDa	16	16					
Cluster of TER94, isoform E TER94 (A0A0B4LFZ4_DROME)	A0A0B4LFZ4_DROME	92 kDa	3	2					
Cluster of Terribly reduced optic lobes, isoform AI trol (M9NET2_DROME)	M9NET2_DROME [4]	432 kDa	6	61		42783	38298		
Cluster of Thin, isoform C tn (B7YZK8_DROME)	B7YZK8_DROME [3]	164 kDa	8	3		31588	42826		
Cluster of Tropomyosin 2, isoform E Tm2 (A0A0B4KHJ9_DROME)	A0A0B4KHJ9_DROME	33 kDa	21	43					
Cluster of Tropomyosin-1, isoforms 33/34 Tm1 (TPM4_DROME)	TPM4_DROME [3]	55 kDa	13	47					
Cluster of Troponin I wupA (TNNI_DROME)	TNNI_DROME	30 kDa	15	15					
Cluster of Tubulin alpha-1 chain alphaTub84B (TBA1_DROME)	TBA1_DROME [3]	50 kDa	21	15					
Cluster of Tubulin beta-1 chain betaTub56D (TBB1_DROME)	TBB1_DROME [4]	50 kDa	47	30					
Cluster of Unc-89, isoform E Unc-89 (A0A0B4LGI5_DROME)	A0A0B4LGI5_DROME	473 kDa	273	53					
Cluster of Upheld, isoform P up (M9PHJ0_DROME)	M9PHJ0_DROME [5]	47 kDa	19	20					
Cluster of Zipper, isoform F zip (A0A0B4JD57_DROME)	A0A0B4JD57_DROME	228 kDa	83	13					
Cluster of Zormin, isoform J zormin (M9PBJ1_DROME)	M9PBJ1_DROME [3]	413 kDa	11	7		34039			
Coatomer subunit beta' beta'COP	COPB2_DROME	103 kDa	2	1		33741	31709		
Collagen alpha-1(IV) chain Cg25C	CO4A1_DROME	174 kDa	2	3					
Contactin Cont	CONT_DROME	158 kDa	2	0		34867	28923		
Cuticular protein 100A Cpr100A	Q9VA32_DROME	27 kDa	1	4		57845			
Cuticular protein 47Ef, isoform C Cpr47Ef	A1Z8H7_DROME	51 kDa	0	17					
Cuticular protein 76Bd, isoform C Cpr76Bd	M9PFX4_DROME (+1	123 kDa	0	4					
Cuticular protein 97Eb Cpr97Eb	Q9VB81_DROME	27 kDa	11	5					
Cytochrome b-c1 complex subunit Rieske, mitochondrial RFeSP	Q9VQ29_DROME	25 kDa	0	4					
DALAO protein dalao	Q9W384_DROME	79 kDa	0	6		35242	26218		
Delta-1-Pyrroline-5-carboxylate dehydrogenase 1, isoform A P5CDh1	Q9VNX4_DROME	64 kDa	6	2		41833			
Dipeptidase B, isoform A Dip-B	Q9VFQ9_DROME	56 kDa	5	2					
DNA-directed RNA polymerase II subunit RPB1 RpII215	RPB1_DROME	209 kDa	3	0					
Dodeca-satellite-binding protein 1, isoform A Dp1	Q7KN75_DROME	144 kDa	1	4		32872			
Dynactin subunit 1 Gl	DCTN1_DROME	141 kDa	10	0		27721	24761	24760	
Elongation factor 1-gamma Ef1gamma	EF1G_DROME	49 kDa	5	16					
Elongation factor 2 EF2	EF2_DROME	94 kDa	7	4					
Elongation factor Tu EfTuM	A1Z9E3_DROME	54 kDa	5	14					
Encore, isoform E enc	A8JNJ9_DROME (+2)	200 kDa	2	4		42797			
Enolase Eno	ENO_DROME	54 kDa	8	2					
Eukaryotic translation initiation factor 2 subunit 3 eIF-2gamma	IF2G_DROME	51 kDa	0	4					
Eukaryotic translation initiation factor 3 subunit A eIF3-S10	EIF3A_DROME	134 kDa	6	7		27565	34353		
Eukaryotic translation initiation factor 3 subunit C eIF3-S8	EIF3C_DROME	106 kDa	3	6					
Eukaryotic translation initiation factor 3 subunit I Trip1	EIF3I_DROME	36 kDa	0	4		34978			
Eukaryotic translation initiation factor 4G, isoform B eIF4G	A8DZ29_DROME (+1)	211 kDa	6	23					
F-box-like/WD repeat-containing protein ebi ebi	EBI_DROME	72 kDa	0	7		44443	34981	8390	
Facilitated trehalose transporter Tret1-1 Tret1-1	TRE11_DROME	95 kDa	3	0					

Fasciclin 1, isoform G Fas1	A0A0B4KH94_DROM	74 kDa	3	1		42887	41854		
Fat-body protein 1 Fbp1	FBP1_DROME	120 kDa	60	25					
Ferrochelatase, mitochondrial FeCh	HEMH_DROME	44 kDa	8	2		55146			
FI01544p Rab1	O18332_DROME	23 kDa	3	0		23236	34670	27299	9757
FI01658p RpL23A	Q9W0A8_DROME	29 kDa	12	4					
FI21274p1 Trap1	A1Z6L9_DROME	78 kDa	4	1					
Flightin fln	FTN_DROME	21 kDa	35	23					
Flotillin-1 Flo1	FLOT1_DROME	47 kDa	5	4					
Fmr1, isoform G Fmr1	A0A0B4K618_DROM	81 kDa	0	8		35200	34944	27484	
Fondue, isoform D fon	M9PDP3_DROME	58 kDa	5	13					
GH05406p mRpS30	Q9VXP3_DROME	65 kDa	13	0					
GH13256p Thiolase	Q9W1H8_DROME	51 kDa	13	6		34546			
GH13304p Pglym78	Q9VAN7_DROME	29 kDa	5	1		57503	26303		
GH13725p Tcp-1zeta	Q9VXQ5_DROME	58 kDa	10	0		43146			
GH15296p Scp1	Q8MSI2_DROME	22 kDa	0	11		51406	31957		
Glucose-6-phosphate isomerase Pgi	G6PI_DROME	62 kDa	12	4					
Glutactin Glt	GLT_DROME	119 kDa	2	13		55929			
Glutamine synthetase 2 cytoplasmic Gs2	GLNA2_DROME (+1)	41 kDa	8	5		26037			
Glutamyl-tRNA(Gln) amidotransferase subunit A, mitochondrial gatA	GATA_DROME	56 kDa	2	0		50553			
Glutathione S transferase S1, isoform D GstS1	A0A0B4KFT5_DROM	28 kDa	0	4		53238	28885		
Glycerol-3-phosphate dehydrogenase Gpo-1	Q7K569_DROME	80 kDa	16	7					
Glycogen [starch] synthase GlyS	GYS_DROME	82 kDa	14	13					
Glycogen phosphorylase GlyP	PYG_DROME	97 kDa	49	11					
GM02062p ND-23	Q9VF27_DROME	25 kDa	1	4	NDUFS8				
Guanine nucleotide-binding protein subunit beta-like protein Rack1	GBLP_DROME	36 kDa	6	2		34694	38198		
Heat shock 70 kDa protein cognate 3 Hsc70-3	HSP7C_DROME	72 kDa	7	20		32402			
Heat shock 70 kDa protein cognate 5 Hsc70-5	HSP7E_DROME	74 kDa	20	13					
Heat shock protein 23 Hsp23	HSP23_DROME	21 kDa	3	4					
Heat shock protein 26 Hsp26	HSP26_DROME	23 kDa	5	3					
Heat shock protein 27 Hsp27	HSP27_DROME	24 kDa	3	1		33922	33007		
Heat shock protein 83 Hsp83	HSP83_DROME	82 kDa	19	12					
Hepatocyte growth factor-regulated tyrosine kinase substrate Hrs	HRS_DROME	85 kDa	3	0		34086	33900	28026	
Heterogeneous nuclear ribonucleoprotein 27C Hrb27C	RB27C_DROME	45 kDa	13	52					
Heterogeneous nuclear ribonucleoprotein 87F Hrb87F	RB87F_DROME	39 kDa	0	36		31244	31472	52937	
Heterogeneous nuclear ribonucleoprotein at 98DE, isoform F Hrb98DE	A4V3J6_DROME	39 kDa	1	36		32351			
Histone H2B His2B	H2B_DROME	14 kDa	4	4					
Hsc70Cb, isoform G Hsc70Cb	M9MSL3_DROME (+1	92 kDa	3	0		53728	56497	33742	
Jak pathway signal transduction adaptor molecule Stam	Q9XTL2_DROME	75 kDa	3	1		35016	27487		
Kinesin heavy chain Khc	KINH_DROME	110 kDa	11	1					
Kinesin light chain, isoform C Klc	M9PFG7_DROME	58 kDa	6	0					
Klaroid, isoform A koi	A0A0B4KEE4_DROM	110 kDa	6	1		40924			
Klarsicht, isoform E klar	M9PGK7_DROME (+2	246 kDa	2	0		36721			
La-related protein CG11505 CG11505	Y1505_DROME	162 kDa	0	30		58201			
Lamin Dm0 Lam	LAM0_DROME	71 kDa	0	7					
Lamin-C LamC	LAMC_DROME	70 kDa	9	3					
Laminin subunit alpha LanA	LAMA_DROME	411 kDa	0	7		28071			
Laminin subunit beta-1 LanB1	LAMB1_DROME	198 kDa	0	3		42616			
Laminin subunit gamma-1 LanB2	LAMC1_DROME	182 kDa	0	4		55388	62002		
Larval serum protein 1 alpha chain Lsp1alpha	LSP1A_DROME	99 kDa	7	0					
Larval serum protein 1 beta chain Lsp1beta	LSP1B_DROME	96 kDa	9	0					

Larval serum protein 1 gamma chain Lsp1gamma	LSP1G_DROME	93 kDa	14	0					
LD21345p ssx	Q8IH14_DROME	49 kDa	0	4		42881			
LD30155p lost	Q9VN21_DROME	60 kDa	9	9		38931	55201		
LD35640p Psi	A1ZAK7_DROME (+1)	82 kDa	1	9		34825	31301	31683	
Lethal (3) 03670 l(3)03670	Q9VA18_DROME	24 kDa	4	0					
Levy, isoform A levy	Q9W1N3_DROME	12 kDa	6	0					
LIM and SH3 domain protein Lasp Lasp	LASP1_DROME (+1)	74 kDa	0	11		26305			
Limpet, isoform K Lmpt	Q7KUQ6_DROME	246 kDa	22	0		28790			
Lon protease homolog, mitochondrial Lon	LONM_DROME	115 kDa	3	1		34586			
Mauve mv	Q9W060_DROME	400 kDa	2	0					
Mediator of RNA polymerase II transcription subunit 1 MED1	MED1_DROME	150 kDa	0	8		50525	34662		
Mediator of RNA polymerase II transcription subunit 12 kto	MED12_DROME	279 kDa	0	4		34588			
Mediator of RNA polymerase II transcription subunit 14 MED14	MED14_DROME	172 kDa	0	6		34575			
Mediator of RNA polymerase II transcription subunit 17 MED17	MED17_DROME	72 kDa	0	2		34664			
Mediator of RNA polymerase II transcription subunit 23 MED23	MED23_DROME	167 kDa	0	7		52871	51153	34658	56970
Mediator of RNA polymerase II transcription subunit 24 MED24	MED24_DROME	112 kDa	0	3		33755			
Mediator of RNA polymerase II transcription subunit 25 MED25	MED25_DROME	97 kDa	0	4		33595	42501		
Mitochondrial import inner membrane translocase subunit TIM44 CG11779	Q9VDZ7_DROME (+1	53 kDa	10	0					
Molecule interacting with CasL, isoform L Mical	A0A0B4K6D5_DROM	527 kDa	31	0		31148			
Multiple ankyrin repeats single KH domain, isoform C mask	A0A0B4K725_DROM	424 kDa	5	0		34571			
Muscle-specific protein 300 kDa, isoform D Msp300	M9MRD1_DROME (+	1405 kDa	77	6					
Muscle-specific protein 300 kDa, isoform E Msp300	M9MSG3_DROME	1064 kDa	5	0					
Myosin light chain alkali Mlc1	MLC1_DROME	18 kDa	10	7					
Myosin regulatory light chain 2 Mlc2	MLR_DROME	24 kDa	54	16					
NADH dehydrogenase [ubiquinone] 1 alpha subcomplex subunit 10, mitochondrial ND-42	NDUAA_DROME	47 kDa	9	19	NDUFA10				
NADH-ubiquinone oxidoreductase 75 kDa subunit, mitochondrial ND-75	NDUS1_DROME	79 kDa	17	64	NDUFS1				
NAT1 ortholog, isoform A Nat1	Q9VWI2_DROME	103 kDa	0	4		32357	27302		
Nejire, isoform C nej	M9MS40_DROME (+2	341 kDa	0	3		36682	31728	27724	
Neurochondrin homolog Neurochondrin	NCDN_DROME	82 kDa	0	4		40903			
Neuroglian, isoform D Nrg	E1JJF9_DROME (+2)	138 kDa	5	0		38215	37496	36897	
NF-kappa-B inhibitor cactus cact	CACT_DROME	54 kDa	0	4		37484	34775	31713	
No circadian temperature entrainment, isoform D nocte	M9PE74_DROME (+1	235 kDa	6	54		28895			
Nucleoporin 358kD, isoform B Nup358	A0A0B4K7J2_DROME	299 kDa	29	0		34710			
Optic atrophy 1 ortholog, isoform D Opa1	A0A0B4LFB8_DROME	107 kDa	17	2		32358			
Osa, isoform F osa	A0A0B4KGD1_DROM	269 kDa	0	14		35447	38285		
Pericardin prc	Q9VTR6_DROME	163 kDa	0	3					
Peroxiredoxin 1 Jafrac1	PRDX1_DROME	22 kDa	2	3					
PERQ amino acid-rich with GYF domain-containing protein CG11148 CG11148	PERQ1_DROME	174 kDa	2	0		28896			
Phosphoglucomutase Pgm	PGM_DROME	61 kDa	11	3					
Polyadenylate-binding protein pAbp	PABP_DROME	70 kDa	54	68					
Pre-mRNA-processing factor 39 CG1646	PRP39_DROME	121 kDa	4	0					
Probable 2-oxoglutarate dehydrogenase E1 component DHKTD1 homolog, mitochondrial CG	DHTK1_DROME	104 kDa	3	0		43310			
Probable isocitrate dehydrogenase [NAD] subunit alpha, mitochondrial l(1)G0156	IDH3A_DROME	41 kDa	55	36					
Probable medium-chain specific acyl-CoA dehydrogenase, mitochondrial CG12262	ACADM_DROME	46 kDa	11	6					
Probable methylmalonate-semialdehyde dehydrogenase [acylating], mitochondrial CG1789	MMSA_DROME	56 kDa	3	0		55323			
Prohibitin 2, isoform E Phb2	A8DYI6_DROME (+2)	37 kDa	9	2					
Proline dehydrogenase 1, mitochondrial sIgA	PROD_DROME	77 kDa	9	4		43172	51811		
Protein alan shepard shep	SHEP_DROME	62 kDa	3	2		43545	38218	33996	
Protein BCL9 homolog lgs	BCL9_DROME	154 kDa	0	4		41983			
Protein clueless clu	CLU_DROME	161 kDa	1	11					

Protein Gawky gw	GAWKY_DROME	143 kDa	2	70					
Protein l(2)37Cc l(2)37Cc	L2CC_DROME	30 kDa	4	0		32912			
Protein tumorous imaginal discs, mitochondrial l(2)tid	TID_DROME	56 kDa	0	3		28594			
Putative ATP synthase subunit f, mitochondrial CG4692	ATPK_DROME	12 kDa	2	0					
Pyruvate carboxylase PCB	Q0E9E2_DROME (+1)	133 kDa	38	1		56883			
Pyruvate dehydrogenase E1 component subunit alpha l(1)G0334	Q7KVX1_DROME (+1)	49 kDa	26	14					
Pyruvate kinase PyK	KPYK_DROME	57 kDa	47	26					
RE08669p RpL6	Q9V9W3_DROME	30 kDa	4	0					
Rhea, isoform G rhea	M9PBW9_DROME (+	305 kDa	7	4		33913	32999		
Sec13 ortholog, isoform A Sec13	Q9V3J4_DROME	40 kDa	0	5		32468			
Sec16 ortholog, isoform E Sec16	A8JUU1_DROME (+2)	220 kDa	2	18		53917			
Sequence-specific single-stranded DNA-binding protein, isoform A Ssdp	Q9VEB9_DROME	45 kDa	0	6		62167			
Skuld, isoform E skd	A8JNW4_DROME	296 kDa	0	11		34630			
Smrter, isoform G Smr	M9PGZ8_DROME (+1	380 kDa	0	3		34528	34087	27068	57464
Staufen, isoform C stau	E1JGK6_DROME	110 kDa	1	5		43187	35690	31247	
Stretchin-Mlck, isoform R Strn-Mlck	A1ZA73_DROME	215 kDa	185	96					
Stretchin-Mlck, isoform S Strn-Mlck	A0A0B4KF84_DROME	919 kDa	29	15					
Succinate dehydrogenase [ubiquinone] flavoprotein subunit, mitochondrial SdhA	SDHA_DROME	72 kDa	60	20					
Succinate dehydrogenase [ubiquinone] iron-sulfur subunit, mitochondrial SdhB	SDHB_DROME	34 kDa	3	1					
Succinyl-CoA ligase subunit beta skap	A0A0B4JCW4_DROM	49 kDa	9	16		55168			
Superoxide dismutase Sod2	A0A0B4LGQ1_DROM	25 kDa	3	1		36871	32983	32496	25969
Tiggrin Tig	TIG_DROME	257 kDa	6	1		31570			
Trailer hitch, isoform G tral	M9PCB7_DROME (+7	68 kDa	5	9		28542	38909	53961	
Transporter Gat	Q9V4E7_DROME	72 kDa	2	0		29422			
Triosephosphate isomerase Tpi	TPIS_DROME	27 kDa	4	2		51829	26304		
Unc-115a, isoform F Unc-115a	A0A0B4LI11_DROME	92 kDa	6	2					
V-type proton ATPase catalytic subunit A isoform 1 Vha68-1	VATA1_DROME	68 kDa	4	0		50726	42888		
V-type proton ATPase catalytic subunit A isoform 2 Vha68-2	VATA2_DROME	68 kDa	9	0					
V-type proton ATPase subunit a Vha100-2	Q9VE75_DROME	95 kDa	2	0					
V-type proton ATPase subunit B Vha55	VATB_DROME	55 kDa	7	1					
V-type proton ATPase subunit E Vha26	VATE_DROME	26 kDa	11	2					
V-type proton ATPase subunit H VhaSFD	VATH_DROME	54 kDa	7	2					
Viking, isoform A vkg	Q9VMV5_DROME	194 kDa	2	12		50895			
Vinculin Vinc	VINC_DROME	106 kDa	3	1					
Voltage-dependent anion-selective channel porin	VDAC_DROME	31 kDa	2	3					
Ypsilon schachtel, isoform B yps	M9NFR5_DROME (+1	37 kDa	0	5		38250	30810		
Zasp67, isoform E Zasp67	M9PEZ7_DROME (+1	80 kDa	28	1					
Zinc finger protein on ecdysone puffs Pep	PEP_DROME	78 kDa	5	2					

Table 3.2: Table for figure 3.3 listing the RNAi's that were screened.

Column 1: The number that corresponds with the lane numbered in figure 3.3.

Column 2: The Bloomington Stock ordered

Column 3: The *Drosophila* gene that is being knocked down by RNAi

Column 4: The Gal4 used to express the UAS-RNAi lines in *Drosophila* flight muscles.

Number	Bloomington Stock #	Drosophila Gene	Gal4
1	28071	Laminin subunit alpha	Dmef2
2	28542	Trailer Hitch	Dmef2
3	28790	Limpet	Dmef2
4	28895	Nocte	Dmef2
5	28920	Polychaetoid	Dmef2
6	28930	FASN1	Dmef2
7	30506	isoform B CAP	Dmef2
8	31078	Bicoid Stability Factor	Dmef2
9	31148	Mical	Dmef2
10	31558	Muscle LIM protein Mlp84B	Dmef2
11	31560	CG43897	Dmef2
12	31683	LD35640p Psi	Dmef2
13	31712	ATP-dependent helicase brm	Dmef2
14	32388	CG10077	Dmef2
15	32503	Brahma-associated protein 60 kDa	Dmef2
16	32884	CG8036	Dmef2
17	32981	CG10077	Dmef2
18	33386	Polychaetoid	Dmef2
19	33392	AT27578p rin	Dmef2
20	33668	AT27789p glo	Dmef2
21	35003	Cora	Dmef2
22	34825	LD35640p Psi	Dmef2
23	34550	Bicoid Stability Factor	Dmef2
24	35630	Brahma associated protein 155 kDa mor	Dmef2
25	35684	Heat schock 70 kDa protein cognate 4 Hsc70-4	Dmef2
26	36066	AT27789p glo	Dmef2
27	38967	GH17761p Ubi-p5E	Dmef2
28	40922	CG5261	Dmef2
29	41697	Arginine Kinase	Dmef2
30	41708	Isocitrate Dehydrogenase	Dmef2
31	42783	Terribly reduced obtic lobes	Dmef2
32	42826	Thin	Dmef2
33	43172	Proline Dehydrogenase 1, mitochondrial sIgA	Dmef2
34	44012	Ataxin-2 homolog	Dmef2
35	44475	CG6439	Dmef2
36	34546	Thiolase	Dmef2
37	34520	ATP-dependent helicase brm	Dmef2
38	33727	Argonaute-1	Dmef2
39	35185	Belle	Dmef2
40	35211	ATP-dependent helicase brm	Dmef2
41	35221	Arginine Kinase	Dmef2
42	35302	Belle	Dmef2
43	35447	Osa	Dmef2
44	35775	FASN1	Dmef2
45	38285	Osa	Dmef2

46	38283	Hts	Dmef2
47	38198	Guanine nucleotide-binding protein subunit beta-like pr	Dmef2
48	36663	isoform B CAP	Dmef2
49	43245	CG6455	Dmef2
50	38909	Trailer Hitch	Dmef2
51	50524	CG6512	Dmef2
52	50650	CG5214	Dmef2
53	51811	Proline Dehydrogenase 1, mitochondrial slgA	Dmef2
54	51845	Cora	Dmef2
55	52933	nonA	Dmef2
56	52937	Hrb87F	Dmef2
57	53293	Ago1	Dmef2
58	53917	Sec16	Dmef2
59	53961	Trailer Hitch	Dmef2
60	53971	Amphiphysin	Dmef2
61	55908	Darkener of Apricot	Dmef2
62	55929	Glutactin	Dmef2
63	56883	Pyruvate Carboxylase PCB	Dmef2
64	56944	Protein no-on-transient A nonA	Dmef2
65	57820	CG30069	Dmef2
66	58201	CG11505	Dmef2
67	58278	CG34417	Dmef2
68	58313	CG9485	Dmef2
69	42509	CG11504	Dmef2
70	60371	CG8036	Dmef2
71	61279	Protein no-on-transient A nonA	Dmef2
72	61857	Lingerer	Dmef2
73	61925	CG30069	Dmef2
74	62002	Laminin subunit gamma-1	Dmef2
75	62945	CG34417	Dmef2
76	63994	CG6455	Dmef2
77	32872	Dodeca-satellite-binding protein 1	Dmef2
78	55201	LD30155p lost	Dmef2
79	55168	Succinyl-CoA ligase subunit beta skap	Dmef2
80	55388	Laminin subunit gamma-1	Dmef2
81	55619	CG11876	Dmef2
82	42774	RpS19a	Dmef2
83	42888	Vha68-1	Dmef2
84	43965	Ank	Dmef2
85	44100	Rbp1-like	Dmef2
86	44533	CG8520	Dmef2
87	50553	GatA	Dmef2
88	50574	Rbp1-like	Dmef2
89	50610	RpL8	Dmef2
90	29422	Gat	Dmef2
91	30810	yps	Dmef2

92	31115	Ank	Dmef2
93	57464	smr	Dmef2
94	56970	med23	Dmef2
95	62167	ssdp	Dmef2
96	8390	ebi	Dmef2
97	24760	DCTN1	Dmef2
98	24761	DCTN1	Dmef2
99	26037	cyp4d2	Dmef2
100	26305	lasp	Dmef2
101	27484	FMR1	Dmef2
102	27565	Eukaryotic translation inititation factor 3 subunit A	Dmef2
103	27721	DCTN1	Dmef2
104	27729	Acsl	Dmef2
105	28885	Gsts1	Dmef2
106	28896	GYF	Dmef2
107	28933	Cora	Dmef2
108	31049	Chi	Dmef2
109	31244	Hrb87F	Dmef2
110	31247	stau	Dmef2
111	31301	LD35640p Psi	Dmef2
112	31472	Hrb87F	Dmef2
113	31570	Tig	Dmef2
114	31700	Argonaute-1	Dmef2
115	31708	bap55	Dmef2
116	31728	nej	Dmef2
117	31957	scp1	Dmef2
118	31964	CG10543	Dmef2
119	32402	Hsc70-3	Dmef2
120	32990	caz	Dmef2
121	33417	AliX	Dmef2
122	33996	shep	Dmef2
123	34333	CG9485	Dmef2
124	34528	smr	Dmef2
125	34571	mask	Dmef2
126	34630	Skuld	Dmef2
127	34658	med23	Dmef2
128	34662	Med1	Dmef2
129	34694	Guanine nucleotide-binding protein subunit beta-like pr	Dmef2
130	34729	HSP60	Dmef2
131	34839	caz	Dmef2
132	35200	FMR1	Dmef2
133	25225	Chi	Dmef2
134	35435	Chi	Dmef2
135	35690	Stau	Dmef2
136	36613	isoform B CAP	Dmef2
137	36682	Nej	Dmef2

138	36721	Klar	Dmef2
139	36897	Nrg	Dmef2
140	38215	Nrg	Dmef2
141	38218	Shep	Dmef2
142	40833	Flo2	Dmef2
143	40903	Neurochondrin	Dmef2
144	41833	P5CDh1	Dmef2
145	41854	Fas1	Dmef2
146	42510	CG7766	Dmef2
147	42616	lanB1	Dmef2
148	42797	enc	Dmef2
149	42887	Fas1	Dmef2
150	42890	cg7766	Dmef2
151	43146	tcp-1zeta	Dmef2
152	43187	Stau	Dmef2
153	43268	Acsl	Dmef2
154	43545	Shep	Dmef2
155	44439	CG5261	Dmef2
156	44443	Ebi	Dmef2
157	44495	CG9090	Dmef2
158	50525	Med1	Dmef2
159	50904	AliX	Dmef2
160	51153	Med23	Dmef2
161	51406	Scp1	Dmef2
162	51433	CG7409	Dmef2
163	51911	CG7470	Dmef2
164	52871	Med23	Dmef2
165	53238	GstS1	Dmef2
166	54816	CG10543	Dmef2
167	55146	FeCh	Dmef2
168	55209	CG30122	Dmef2
169	55212	Flo2	Dmef2
170	34039	Zormin	Dmef2
171	38298	Terribly reduced obtic lobes	Dmef2
172	38931	LD30155p lost	Dmef2
173	40924	Koi	Dmef2
174	27286	A2bp1	Dmef2
175	27302	NAT1	Dmef2
176	28327	14-3-3zeta	Dmef2
177	27487	Stam	Dmef2
178	28026	Hrs	Dmef2
179	29422	Gat	Dmef2
180	30810	yps	Dmef2
181	31115	Ank	Dmef2
182	31498	14-3-3zeta	Dmef2
183	31713	cact	Dmef2

184	31756	CG8963	Dmef2
185	31917	CG11504	Dmef2
186	32357	NAT1	Dmef2
187	32422	Rpt5	Dmef2
188	32476	A2bp1	Dmef2
189	32496	sod2	Dmef2
190	32930	CG8108	Dmef2
191	33007	hsp27	Dmef2
192	33010	capt	Dmef2
193	33741	betaCOP	Dmef2
194	33755	med24	Dmef2
195	33900	hrs	Dmef2
196	33922	hsp27	Dmef2
197	34086	hrs	Dmef2
198	34592	lilli	Dmef2
199	34664	Med17	Dmef2
200	34670	Rab1	Dmef2
201	34775	cact	Dmef2
202	34978	eIF3i	Dmef2
203	35016	Stam	Dmef2
204	36076	Rpl28	Dmef2
205	26304	Tpi	Dmef2
206	26314	lilli	Dmef2
207	33742	HSC70Cb	Dmef2
208	34586	Lon	Dmef2
209	37484	cact	Dmef2
210	37519	B52	Dmef2
211	42888	Vha68-1	Dmef2
212	42881	Ssx	Dmef2
213	42501	MED25	Dmef2
214	43310	CG1544	Dmef2
215	50637	Hsp68	Dmef2
216	50726	Vha68-1	Dmef2
217	51157	Cht5	Dmef2
218	51749	CG8520	Dmef2
219	51785	CG10932	Dmef2
220	51820	Aldh-III	Dmef2
221	51829	Tpi	Dmef2
222	52886	CG17597	Dmef2
223	53298	CG4461	Dmef2
224	53728	HSC70Cb	Dmef2
225	54048	RpL17	Dmef2
226	55323	CG17896	Dmef2
227	55362	Rbp1-like	Dmef2
228	56880	CG3902	Dmef2
229	57845	CPR100A	Dmef2

230	58150	Rm62	Dmef2
231	58340	CG9572	Dmef2
232	55381	Idgf4	Dmef2
233	56497	HSC70Cb	Dmef2
234	23236	Rab1	Dmef2
235	28923	cont	Dmef2
236	32468	Sec13	Dmef2
237	33595	MED25	Dmef2
238	34867	cont	Dmef2
239	36871	sod2	Dmef2
240	38250	yps	Dmef2
241	38984	Cht5	Dmef2
242	42774	RpS19a	Dmef2
243	42656	RpS17	Dmef2
244	31588	Thin	Mhc
245	32351	Hrb98DE	Mhc
246	34919	Brahma associated protein 155 kDa mor	Mhc
247	33686	Nc73EF	Mhc
248	34353	Eukaryotic translation inititation factor 3 subunit A	Mhc
249	34836	Heat schock 70 kDa protein cognate 4 Hsc70-4	Mhc
250	34343	CG6512	Mhc
251	36921	Shibire	Mhc
252	26218	dalao	Mhc
253	27068	smr	Mhc
254	27724	nej	Mhc
255	31337	Brahma-associated protein 60 kDa	Mhc
256	31885	CG43143	Mhc
257	32358	Opa1	Mhc
258	32866	AP-2alpha	Mhc
259	33954	Brahma-associated protein 60 kDa	Mhc
260	34087	smr	Mhc
261	34575	Med14	Mhc
262	34981	ebi	Mhc
263	35194	CG43143	Mhc
264	35242	dalao	Mhc
265	35662	Brahma associated protein 155 kDa mor	Mhc
266	41885	Acsl	Mhc
267	50895	Viking	Mhc
268	9757	rab1	Mhc
269	25969	sod2	Mhc
270	31572	Calcium-Transporting ATPase PMCA	Mhc
271	32999	Rhea	Mhc
272	32912	l(2)37Cc	Mhc
273	39015	Amphiphysin	Mhc
274	41983	bcl9	Mhc
275	51746	RpL32	Mhc

276	53300	RpL23	Mhc
277	53886	Rpt5	Mhc
278	57503	pglym78	Mhc
279	34944	FMR1	Mhc
280	28513	Shibire	Mhc
281	33913	Rhea	Mhc
282	34588	kto	Mhc
283	37496	Nrg	Mhc
284	26303	Pglym78	Mhc
285	27299	Rab1	Mhc
286	27562	CG8108	Mhc
287	28594	l(2)tid	Mhc
288	29385	Rpn6	Mhc
289	31395	Rm62	Mhc
290	31709	betaCOP	Mhc
291	32983	sod2	Mhc
292	33930	rpt1	Mhc
293	34348	rpn1	Mhc
294	34710	nup358	Mhc
295	34712	Rpt6	Mhc
296	34829	Rm62	Mhc
297	50903	Doa	Mhc

References

Andrews, B., Carroll, J., Ding, S., Fearnley, I.M., and Walker, J.E. (2013). Assembly factors for the membrane arm of human complex I. Proc. Natl. Acad. Sci. USA *110*, 18934–18939.

Blaza, J.N., Vinothkumar, K.R., and Hirst, J. (2018). Structure of the deactive state of mammalian respiratory complex I. Structure *26*, 312–319.e3.

Clark, I.E., Dodson, M.W., Jiang, C., Cao, J.H., Huh, J.R., Seol, J.H., Yoo, S.J., Hay, B.A., and Guo, M. (2006). Drosophila pink1 is required for mitochondrial function and interacts genetically with parkin. Nature *441*, 1162–1166.

Dockendorff, T.C., Su, H.S., McBride, S.M.J., Yang, Z., Choi, C.H., Siwicki, K.K., Sehgal, A., and Jongens, T.A. (2002). Drosophila lacking dfmr1 activity show defects in circadian output and fail to maintain courtship interest. Neuron *34*, 973–984.

Duarte, M., Sousa, R., and Videira, A. (1995). Inactivation of genes encoding subunits of the peripheral and membrane arms of neurospora mitochondrial complex I and effects on enzyme assembly. Genetics *139*, 1211–1221.

Fassone, E., and Rahman, S. (2012). Complex I deficiency: clinical features, biochemistry and molecular genetics. J. Med. Genet. *49*, 578–590.

Fiedorczuk, K., Letts, J.A., Degliesposti, G., Kaszuba, K., Skehel, M., and Sazanov, L.A. (2016). Atomic structure of the entire mammalian mitochondrial complex I. Nature *538*, 406–410.

Formosa, L.E., Mimaki, M., Frazier, A.E., McKenzie, M., Stait, T.L., Thorburn, D.R., Stroud, D.A., and Ryan, M.T. (2015). Characterization of mitochondrial FOXRED1 in the assembly of respiratory chain complex I. Hum. Mol. Genet. *24*, 2952–2965.

Formosa, L.E., Dibley, M.G., Stroud, D.A., and Ryan, M.T. (2018). Building a complex complex: Assembly of mitochondrial respiratory chain complex I. Semin. Cell Dev. Biol. *76*, 154–162.

Garcia, C.J., Khajeh, J., Coulanges, E., Chen, E.I.-J., and Owusu-Ansah, E. (2017). Regulation of mitochondrial complex I biogenesis in drosophila flight muscles. Cell Rep. *20*, 264–278.

Guerrero-Castillo, S., Baertling, F., Kownatzki, D., Wessels, H.J., Arnold, S., Brandt, U., and Nijtmans, L. (2017). The assembly pathway of mitochondrial respiratory chain complex I. Cell Metab. *25*, 128–139.

Hirst, J. (2013). Mitochondrial complex I. Annu. Rev. Biochem. *82*, 551–575.

Hu, Y., Flockhart, I., Vinayagam, A., Bergwitz, C., Berger, B., Perrimon, N., and Mohr, S.E. (2011). An integrative approach to ortholog prediction for disease-focused and other functional studies. BMC Bioinformatics *12*, 357.

Kremer, L.S., Bader, D.M., Mertes, C., Kopajtich, R., Pichler, G., Iuso, A., Haack, T.B., Graf, E., Schwarzmayr, T., Terrile, C., et al. (2017). Genetic diagnosis of Mendelian disorders via RNA sequencing. Nat. Commun. *8*, 15824.

Loeffen, J., van den Heuvel, L., Smeets, R., Triepels, R., Sengers, R., Trijbels, F., and Smeitink, J. (1998). cDNA sequence and chromosomal localization of the remaining three human nuclear encoded iron sulphur protein (IP) subunits of complex I: the human IP fraction is completed. Biochem. Biophys. Res. Commun. *247*, 751–758.

Mientjes, E.J., Willemsen, R., Kirkpatrick, L.L., Nieuwenhuizen, I.M., Hoogeveen-Westerveld, M., Verweij, M., Reis, S., Bardoni, B., Hoogeveen, A.T., Oostra, B.A., et al. (2004). Fxr1 knockout mice show a striated muscle phenotype: implications for Fxr1p function in vivo. Hum. Mol. Genet. *13*, 1291–1302.

Mila, M., Alvarez-Mora, M.I., Madrigal, I., and Rodriguez-Revenga, L. (2018). Fragile X syndrome: An overview and update of the FMR1 gene. Clin. Genet. *93*, 197–205.

Mohr, S.E., Smith, J.A., Shamu, C.E., Neumüller, R.A., and Perrimon, N. (2014). RNAi screening comes of age: improved techniques and complementary approaches. Nat. Rev. Mol. Cell Biol. *15*, 591–600.

Oostra, B.A., and Willemsen, R. (2009). FMR1: a gene with three faces. Biochim. Biophys. Acta *1790*, 467–477.

Pagliarini, D.J., and Rutter, J. (2013). Hallmarks of a new era in mitochondrial biochemistry. Genes Dev. *27*, 2615–2627.

Park, J., Lee, S.B., Lee, S., Kim, Y., Song, S., Kim, S., Bae, E., Kim, J., Shong, M., Kim, J.-M., et al. (2006). Mitochondrial dysfunction in Drosophila PINK1 mutants is complemented by parkin. Nature *441*, 1157–1161.

Rhein, V.F., Carroll, J., Ding, S., Fearnley, I.M., and Walker, J.E. (2013). NDUFAF7 methylates arginine 85 in the NDUFS2 subunit of human complex I. J. Biol. Chem. *288*, 33016–33026.

Rodenburg, R.J. (2016). Mitochondrial complex I-linked disease. Biochim. Biophys. Acta *1857*, 938–945.

Spencer, C.M., Serysheva, E., Yuva-Paylor, L.A., Oostra, B.A., Nelson, D.L., and Paylor, R. (2006). Exaggerated behavioral phenotypes in Fmr1/Fxr2 double knockout mice reveal a functional genetic interaction between Fragile X-related proteins. Hum. Mol. Genet. *15*, 1984–1994.

Stroud, D.A., Surgenor, E.E., Formosa, L.E., Reljic, B., Frazier, A.E., Dibley, M.G., Osellame, L.D., Stait, T., Beilharz, T.H., Thorburn, D.R., et al. (2016). Accessory subunits are integral for assembly and function of human mitochondrial complex I. Nature *538*, 123–126.

Sugiana, C., Pagliarini, D.J., McKenzie, M., Kirby, D.M., Salemi, R., Abu-Amero, K.K., Dahl, H.-H.M., Hutchison, W.M., Vascotto, K.A., Smith, S.M., et al. (2008). Mutation of C20orf7 disrupts complex I assembly and causes lethal neonatal mitochondrial disease. Am. J. Hum. Genet. *83*, 468–478.

Taylor, R.W., Pyle, A., Griffin, H., Blakely, E.L., Duff, J., He, L., Smertenko, T., Alston, C.L., Neeve, V.C., Best, A., et al. (2014). Use of whole-exome sequencing to determine the genetic basis of multiple mitochondrial respiratory chain complex deficiencies. JAMA *312*, 68–77.

Weisz, E.D., Towheed, A., Monyak, R.E., Toth, M.S., Wallace, D.C., and Jongens, T.A. (2018). Loss of Drosophila FMRP leads to alterations in energy metabolism and mitochondrial function. Hum. Mol. Genet. *27*, 95–106.

Yun, J., Puri, R., Yang, H., Lizzio, M.A., Wu, C., Sheng, Z.-H., and Guo, M. (2014). MUL1 acts in parallel to the PINK1/parkin pathway in regulating mitofusin and compensates for loss of PINK1/parkin. Elife *3*, e01958.

Zhu, J., Vinothkumar, K.R., and Hirst, J. (2016). Structure of mammalian respiratory complex I. Nature *536*, 354–358.

Chapter 4: Conclusions and Future Directions

Garcia C.J., Varriano J., Tafader M., Gilani R. and Owusu-Ansah E.

Varriano J., Tafader M., and Gilani R. contributed to figure 4.1

Owusu-Ansah E. designed experiments

Garcia C.J. performed rest of figures and wrote the chapter

The *Drosophila* model has proven to be valuable for understanding the regulation of CI biogenesis. In this body of work, we have established the mechanism of CI assembly in *Drosophila* to help delineate the assembly process of CI in mammals. We also utilized our model to identify new regulators of CI biogenesis that led to the identification of dFMRP playing a role in the stabilization and activity of CI. In this chapter, I will summarize our findings and discuss the results collectively, as well as suggest future directions.

New roles for accessory subunits

From our studies, we were able to address a big question in the CI field: whether the accessory subunits are required for the biogenesis of CI. We demonstrated that the knockdown of each CI accessory subunit in the fly by RNAi resulted in CI misassembly and loss of activity (Garcia et al., 2017). Additionally, when these RNAi lines targeting the accessory subunits were crossed to a Gal4 that increases the expression of the RNAi during the pupae stage none of the flies' eclosed to adults suggesting that these accessory subunits are critical for CI activity and subsequently the survival of the flies. Our results were in agreement with those of studies in mammalian cells that have also shown that knockout of these subunits resulted in dysfunctional CI (Stroud et al., 2016). All together, these findings provided strong evidence that these accessory subunits are indispensable for CI biogenesis and activity. Given the importance of the accessory subunits, it is worth questioning why these subunits are not a part of the core subunits, and the evolutionary purpose to understand their roles. One hypothesis could be that they evolved to act as sensors for CI in higher-order organisms to respond to the changes in environment. Recent cyro-EM structures have uncovered cofactor binding sites on accessory subunits, which enable direct regulation of redox reactions, fatty acid synthesis and oxygen sensing. it would be interesting to investigate how these sites are regulated during different environmental stresses such as high fat diet, hypoxia, or aging (Dunham-Snary et al., 2019; Fiedorczuk et al., 2016; Letts et al., 2017; Zhu et al., 2016). In other words, understanding these binding sites may link how CI and the accessory subunits adjust to environmental pressures. Another hypothesis is that the accessory subunits tightly regulate the catalytic core subunits. Cryo-EM structures in the ovine model have revealed that the coupling between electron transfer and proton translocation is tightly

controlled by accessory subunits, by regulating ubiquinone entry to the Q site (Fiedorczuk et al., 2016). Whether the accessory subunits play a role in regulation of NADH binding to FMN, proton pumping across the IMM, or the transition between active and inactive state of CI, are all questions of interest. Although the mechanism of CI activity has been studied for several decades, the accessory subunits have remained largely elusive. New technologies such as cryo-EM allow us to define the accessory subunits at the atomic resolution, and combining the new tools with a strong genetic model such as *Drosophila* we will be able to address these questions and further elucidate our understanding of the accessory subunits. To do this, the structure of CI in the fly would need to be solved. Given the abundance of mitochondria in fly thoraxes and the availability of mammalian structures for reference this would be a simple but vital task to be resolved in the near future. Undoubtedly, the *Drosophila* model will shed light on the roles of the accessory subunits.

Using *Drosophila* to study human CI diseases

CI in *Drosophila* is an attractive model to understand human CI diseases as it contains 42 of the 44 human CI subunits and the assembly mechanism is very similar (Garcia et al., 2017). In vivo models that recapitulate the phenotypes of patients with mitochondria CI deficiency are scarce due to the lethality in many CI subunit knockout mice (Lee et al., 2019; Mimaki et al., 2012). Recently, models of CI deficiency in the *Drosophila* were generated using the Gal4-UAS system to knockdown specific CI proteins ubiquitously (Foriel et al., 2019). A broad range of phenotypes in the flies were scored, similar to the polymorphic phenotypes found in CI deficiency patients (Foriel et al., 2019). This work is the first to arise from our foundational work from 2017 and would be the first of many *Drosophila* models to study the CI deficiency in humans. The available genetic information and the advancing gene editing technology such as CRISPR/Cas9 will allow researchers to replicate the mutations found in patients and to simulate the phenotypes in *Drosophila*. Moreover, *Drosophila* models can be used to screen candidate drug molecules in a time- and cost-effective manner. While patient samples can be scarce, these models could foster our insight of the mitochondrial functions such as ATP production, oxygen consumption, OXPHOS activity assays, mitochondria morphology, and assembly of CI.

Defining the mechanisms of discovered regulators of CI biogenesis

Finding novel regulators of CI or novel CI-regulating roles of known proteins are important tasks to improve diagnosis of CI deficiency in patients. To identify target proteins, we have developed a strategy to screen those that interact with the NDUFS3 subunit of CI. In addition, I also screened proteins that interacted with other subunits of CI or assembly factors. These screens identified the fly proteins Sterol Carrier Protein X-related thiolase (Scpx) and Malic Enzyme b (Men-b) as potential regulators of CI **(Figure 4.1L Lane 98 and Figure 4.1I Lane 56).** Scpx is localized in the peroxisome and is important for peroxisomal beta oxidation by converting 3-ketoacyl-CoA into acyl-CoA, which can then be made into acyl-carnitine for the mitochondria to use (Faust et al., 2012; Ruiz-Ramírez et al., 2015). One hypothesis linking Scpx to CI is through the alterations in the NAD+/NADH ratio. NAD+ is required for converting 3-hydroxyacyl-CoA into 3-ketocyl-CoA. Therefore, if Scpx is absent, an accumulation of 3-ketoacyl-CoA would stall several reactions before the conversion of 3-hydroxyacyl-CoA into 3-ketocyl-CoA. The increased NAD+ would then lead to the mitochondria shutting down CI. On another note, to my knowledge, this is the first time a link has been made between peroxisomal beta oxidation and CI (Fransen et al., 2017). Thus, it would be interesting to follow up what other parts along the pathway are involved with CI deficiency. Men-b is a protein localized in the mitochondria matrix that converts malate into pyruvate using the cofactor NAD+ (Hasan et al., 2015; Weeda, 1981). Similar to Scpx, the CI deficiency phenotype we see in flies without men-b is presumably due to a change in the NAD+/NADH ratio, and possibly its downstream effects on the TCA cycle.

Another screen I took part of in the lab was to test proteins found in the MitoCarta list to see if they regulate CI. The Mitocarta is a list of proteins that have been identified to localize to the mitochondria (Calvo et al., 2016; Pagliarini et al., 2008). In our screen, I identified that disrupting the *NFU1* gene by RNAi causes a destabilization of the holoenzyme CI **(Figure 4.1A Lane 5)**. NFU1 is an iron-sulfur cluster scaffold protein for CI, and this result suggests that iron-sulfur cluster may also contribute to the regulation of CI biogenesis (Navarro-Sastre et al., 2011). Future studies analyzing other iron sulfur cluster scaffold proteins may help to us to elucidate the mechanism of when and how iron sulfur cluster affects the CI biogenesis.

Calcium accumulation in the mitochondria is an essential part of cell activity. We tested if proteins known to regulate calcium signaling in the cell have any effect on CI. Mitochondrial calcium uptake 1 (Micu1), a protein that regulates the calcium uptake into the matrix and a part of the mitochondria calcium uniporter complex (MCUC), caused CI deficiency when knocked down by RNAi **(Figure 4.1S Lane 98)** (Antony et al., 2016; Marchi and Pinton, 2014). Interestingly, knocking down other subunits that are part of the MCUC did not result in a reduction or loss of activity of CI. Future studies will be necessary to analyze the relationship of MICU1 and the regulation of CI.

Overall, I screened over ~500 different proteins to analyze their effects on CI biogenesis. These included knocking down or overexpressing proteins that interact with CI subunits or CIAFs, proteins from the MitoCarta, and calcium signaling proteins **(Figure 4.1)**. As more and more proteins are identified to regulate CI in the fly system, it will be important to test if the mammalian orthologues produce the same phenotype. All in all, these findings have allowed us to broaden our perspective on how the regulation of CI is not confined to CI, let alone the mitochondria, in terms of the genes involved (mtDNA and nDNA) and the space it takes place in (mitochondria and cytoplasm).

Alternative methods to identifying novel regulators of CI biogenesis

Assembly factors are transient interactors to CI subunits and assembly intermediates that assist with the assembly of the holoenzyme. As a first approach, we tagged the CI subunits or CIAFs and cataloged their interacting proteins to test if they are potential assembly factors. Although this method provided a decent list of proteins to screen, transient interactors are overlooked. In the past decade, a method known as BioID has proven to be reliable for the identification of transient protein-protein interactions (Roux et al., 2013). This method works by tagging a protein of interest to a biotin ligase, that when expressed in cells biotinylate any proteins in close proximity. In flies, this method is applied in the Gal4-UAS system by expressing the biotin ligase (BirA) enzyme from *E. Coli* with the protein of interest (Ramirez et al., 2015) **(Figure 4.2)**. Another method to identify transient interactors with the CI subunits and assembly intermediates would be to trap the assembly intermediates themselves and analyze the proteins bound to it. We have shown that disrupting the subunits of CI can result in the accumulation of

assembly intermediates (Garcia et al., 2017). It would be interesting to isolate these accumulating assembly intermediate and visualize it by cryo-EM to grasp the bound and interacting proteins, and to test their potentials as regulators of CI biogenesis.

Elucidating mechanisms of supercomplexes in *Drosophila*

. A growing body of literature in supercomplexes reflect the interest and the importance to elucidate the physiological function of these massive complexes as well as their regulation (Greggio et al., 2017; Letts and Sazanov, 2017; Letts et al., 2017, 2019; Signes and Fernandez-Vizarra, 2018). Several studies have suggested that they are involved in stabilizing the individual complexes, providing a more efficient transfer of electrons between the complexes, and preventing ROS formation (Milenkovic et al., 2017). Mammalian CI is primarily found in supercomplexes with either complex III (CIII) or CIII-complex IV. In flies, we have shown that the CI-CIII supercomplex is present and can be analyzed by BN-PAGE. We have also confirmed that NDUFA11 is important for the stabilization of the CI-CIII supercomplex, as reported in mammalian models (Letts and Sazanov, 2017; Letts et al., 2017). Future studies should test the different components of CI and CIII under different physiological conditions in the context of supercomplex stabilization. Thus far, only one regulator of supercomplexes, super complex assembly factor 1 (SCAF1), has been discovered (Cogliati et al., 2016). From our screens, we identified that knockdown of CP1 causes a reduction in the CI-CIII supercomplex **(Figure 4.1L Lane 103)**. CP1 is a cysteine proteinase that is involved in the degradation of proteins. Future studies to elucidate how CP1 regulates the CI-CIII supercomplex will be needed. Lastly, studies have revealed that changes in physiological conditions such as exercise can alter supercomplex formation in in human skeletal muscle (Greggio et al., 2017). *Drosophila* model is suitable for testing various conditions (i.e. diet, aging) and would be useful in understanding the physiological roles of supercomplexes.

Concluding Remarks

In conclusion, recent advancements in technology and the addition of new models will help further our knowledge of CI. As the field moves forward in understanding the formation and function of the holoenzyme, it is now an exciting time to start exploring the possibility of CI beyond the main contributor of OXPHOS but as a central mediator of the metabolic processes in general, happening inside and outside the mitochondria. This not only includes advancing our knowledge of CI as one enzyme, but also as a structure that is made up 44 different pieces, with each piece potentially serving as a signaling molecule. Additionally, it will be important to increase our understanding of the transient interactors of CI and address how CI is regulated under different environmental pressures. In closing, as we begin to shed light on the role of CI as a regulator of metabolism in the mitochondria, this will hopefully help to delineate the role of mitochondria in several chronic diseases.

Materials and Methods

Drosophila Strains and Genetics.

The following fly stocks were used: y w; Dmef2-Gal4 ; w; mhc-Gal4 ; w; Ubi-Gal4 and w; myo1a-Gal4. W1118 were used as wildtype (wt) controls. Stocks that were screened were ordered from the Bloomington Drosophila Stock Center (https://bdsc.indiana.edu/). The Bloomington stock number can be found in table 4.1 for each respective protein. UAS-BirA and UAS-Ubi6-BirA were ordered from the Bloomington Drosophila Stock Center (https://bdsc.indiana.edu/.

Mitochondria Purification.

Mitochondrial purification was performed essentially as described by Rera et al 2012 (Rera et al., 2011). Thoraxes were dissected and gently crushed with a pestle homogenizer in 500µl of pre-chilled mitochondrial isolation buffer containing 250 mM sucrose and 0.15 mM MgCl2 in 10 mM Tris.HCl, pH 7.4, on ice. After two rounds of centrifugation at 500g for 5 minutes at 4°C to remove insoluble material, the supernatant was recovered and centrifuged at 5000g for 5 minutes at 4°C. The pellet which is enriched for mitochondria was washed twice in the mitochondrial isolation buffer and stored at -80°C until further processing.

Blue Native Polyacrylamide Gel Electrophoresis (BN-PAGE).

BN-PAGE was performed using NativePAGE gels from Life Technologies, following the manufacturer's instructions. Essentially, mitochondria were suspended in native PAGE sample buffer (Life Technologies) supplemented with 1% digitonin and protease inhibitors, and incubated on ice for 20 minutes. Following centrifugation at 20,000g for 30 minutes, the supernatant was recovered, mixed with the G-250 sample additive (Life Technologies) and Native PAGE Sample Buffer (Life Technologies), and loaded onto 3–12% pre-cast Bis–Tris Native PAGE gels (Life Technologies). The NativeMark Protein standard (Life Technologies), run together with the samples, was used to estimate the molecular weight of the protein complexes. Electrophoreses was performed using the Native PAGE Running buffer (as anode buffer, from

Life technologies) and the Native PAGE Running buffer containing 0.4% Coomassie G-250 (cathode buffer). Gels were stained with the Novex Colloidal Blue staining kit (Life Technologies) to reveal the protein complexes.

Silver Staining.

Silver staining of native gels was performed with the SilverXpress staining kit from Life Technologies, following the manufacturer's protocol.

Immunoblotting

For immunoblotting of samples in native gels, protein complexes from native gels were transferred to PVDF membranes (BIORAD). For immunoblotting of samples in whole tissue lysates, thoraxes were homogenized in RIPA buffer (150 mM NaCl, 1% Triton X-100, 0.5% Sodium Deoxycholate, 0.1% SDS, 50mM Tris HCl, pH 8) supplemented with Halt protease inhibitors (Pierce), resolved on mini-PROTEAN TGX stain-free gels from BIO-RAD, and transferred to PVDF membranes. In both instances (native and non-native gels), the membrane was subsequently blocked in 5% (w/v) non-fat dry milk in Tris-buffered saline (TBS) for 30minutes, and incubated in the appropriate primary antibody dissolved in 2% BSA, 0.1% Tween 20 in TBS (TBST) overnight at 4°C. Following the overnight incubation, the blot was rinsed 4X10 minutes in 0.1%TBST, blocked for 30 minutes in 5% (w/v) non-fat dry milk in TBST and incubated for two hours with the appropriate HRP-conjugated secondary antibody dissolved in 2% BSA, 0.1% Tween 20 in TBS (TBST). After incubation in the secondary antibody, samples were rinsed 4X10 minutes in 0.1%TBST. Immunoreactivity was detected by enhanced chemiluminescence (ECL) and analyzed by a ChemiDoc Gel imaging system from BIO-RAD. Antibodies used were anti-streptavidin to detect biotinylated proteins.

Figure 4.1: Screens performed to Identify Novel Regulators of Complex I Biogenesis

(A-E) RNAi Knockdown of MitoCarta Proteins Screen; **(F-L)** RNAi Knockdown of Proteins that interacted with dNDUFS3, dFoxred1, and dNDUFAF7 after knockdown of dNDUFS5 and Ion protease Screen; **(M-U)** RNAi knockdown of Calcium Signaling Proteins Screen; **(V-GG)** UAS-Protein Overexpression Screen. We isolated mitochondria from 10 thoraxes, permeabilized their membranes in 1% digitonin and performed BN-PAGE. The complexes were resolved by either coomassie- or silver staining. Each lane is numbered and corresponds to the RNAi's ordered from the Bloomington Stock Center found in Table 4.1. CI-CIII denotes the complex I-complex III supecomplex, CV2 denotes a dimer of complex V respectively, CI denotes complex I, CV denotes complex V, CIII denotes complex III, CIV denotes complex IV, and CII denotes complex II.

RNAi Knockdown - MitoCarta Protein Screen

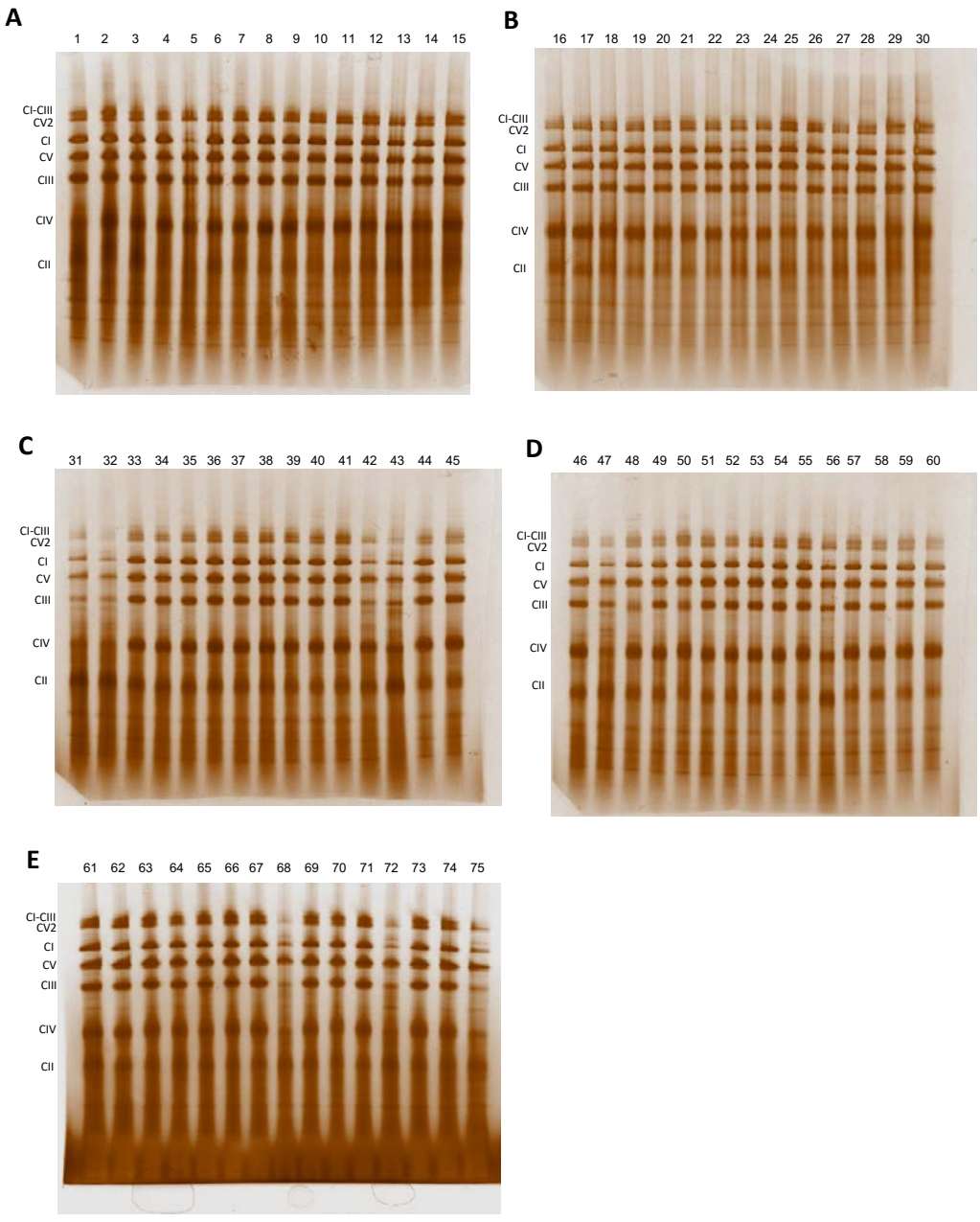

RNAi Knockdown of Proteins that interacted with dNDUFS3, dFoxred1, and dDUFAF7 after knockdown of dNDUFS5 and lon protease

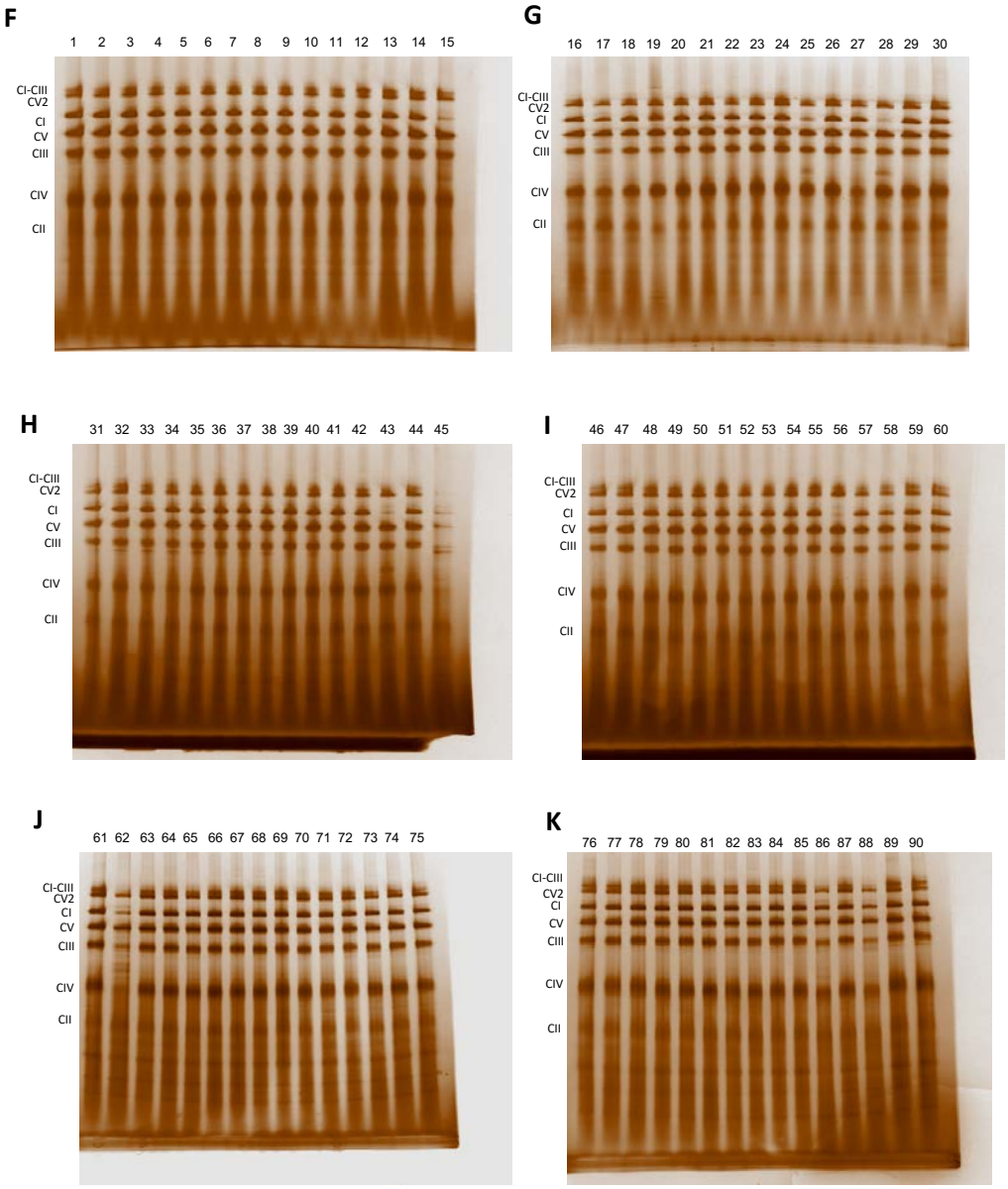

RNAi Knockdown of Proteins that interacted with dNDUFS3, dFoxred1, and dNDUFAF7 after knockdown of dNDUFS5 and lon protease

L

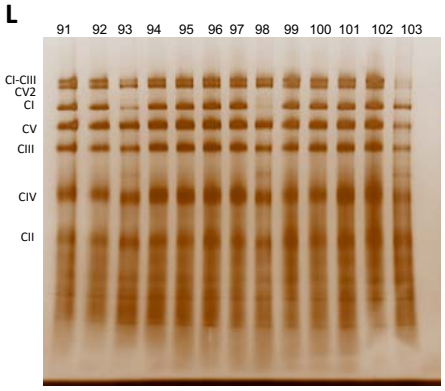

RNAi Knockdown of Calcium Signaling Proteins

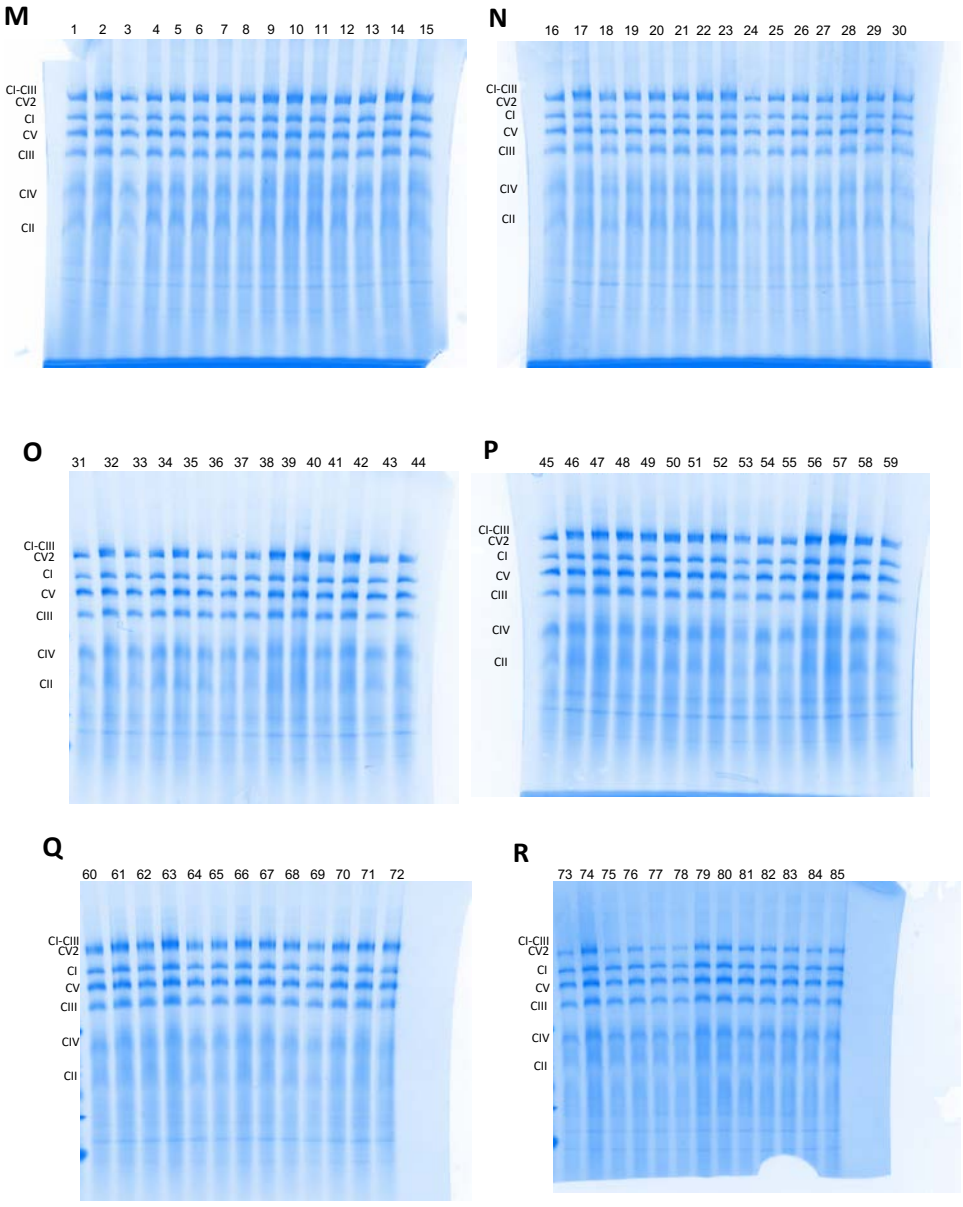

RNAi Knockdown of Calcium Signaling Proteins

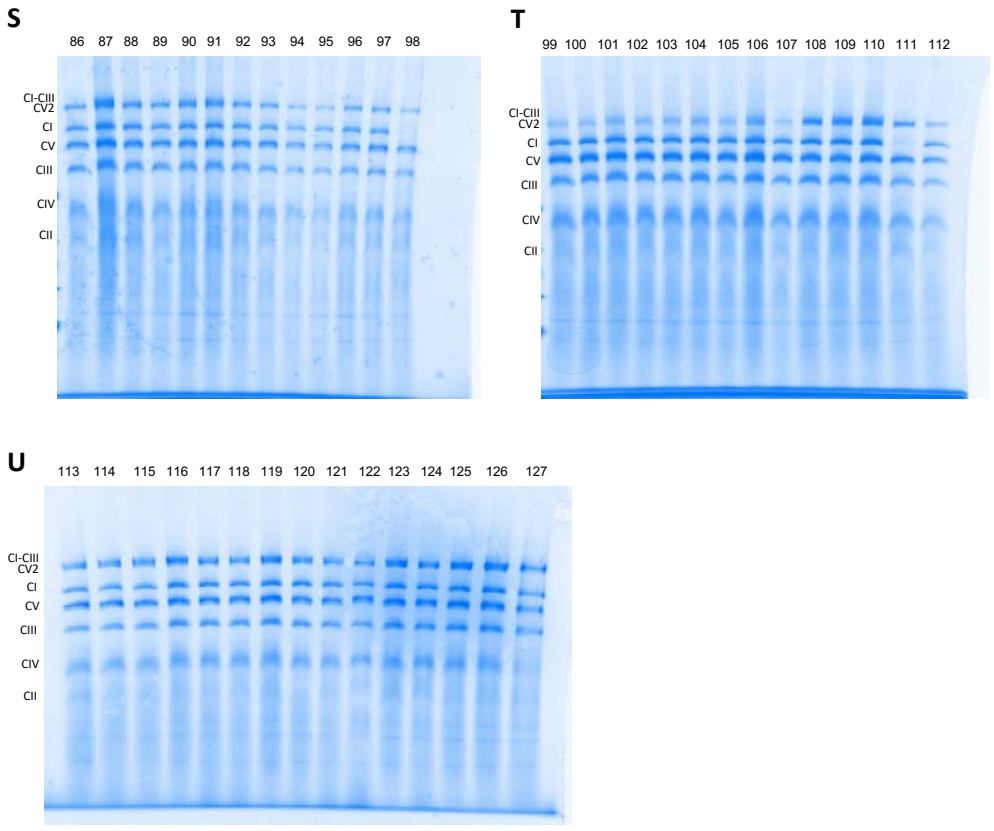

UAS-Protein Overexpression

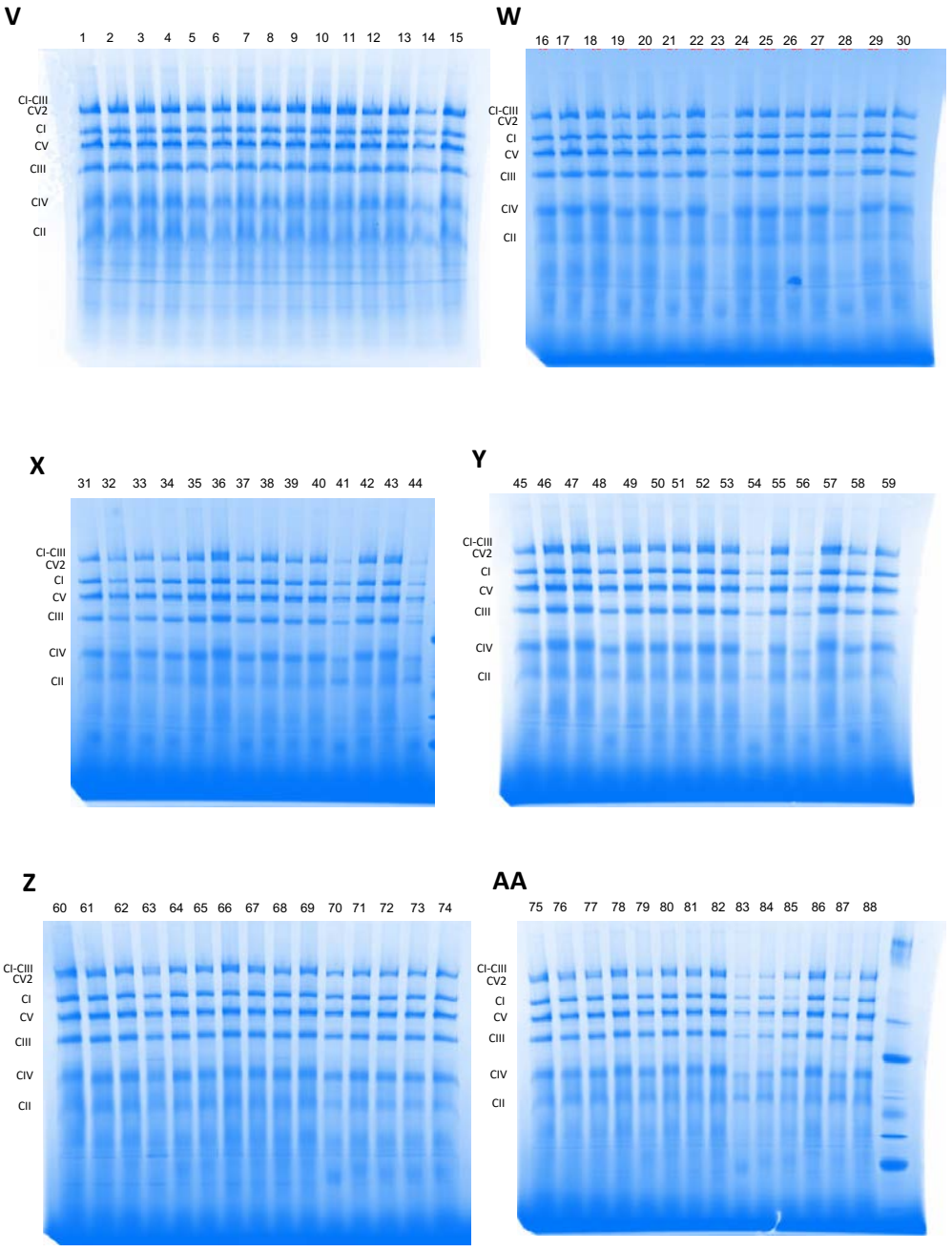

UAS-Protein Overexpression

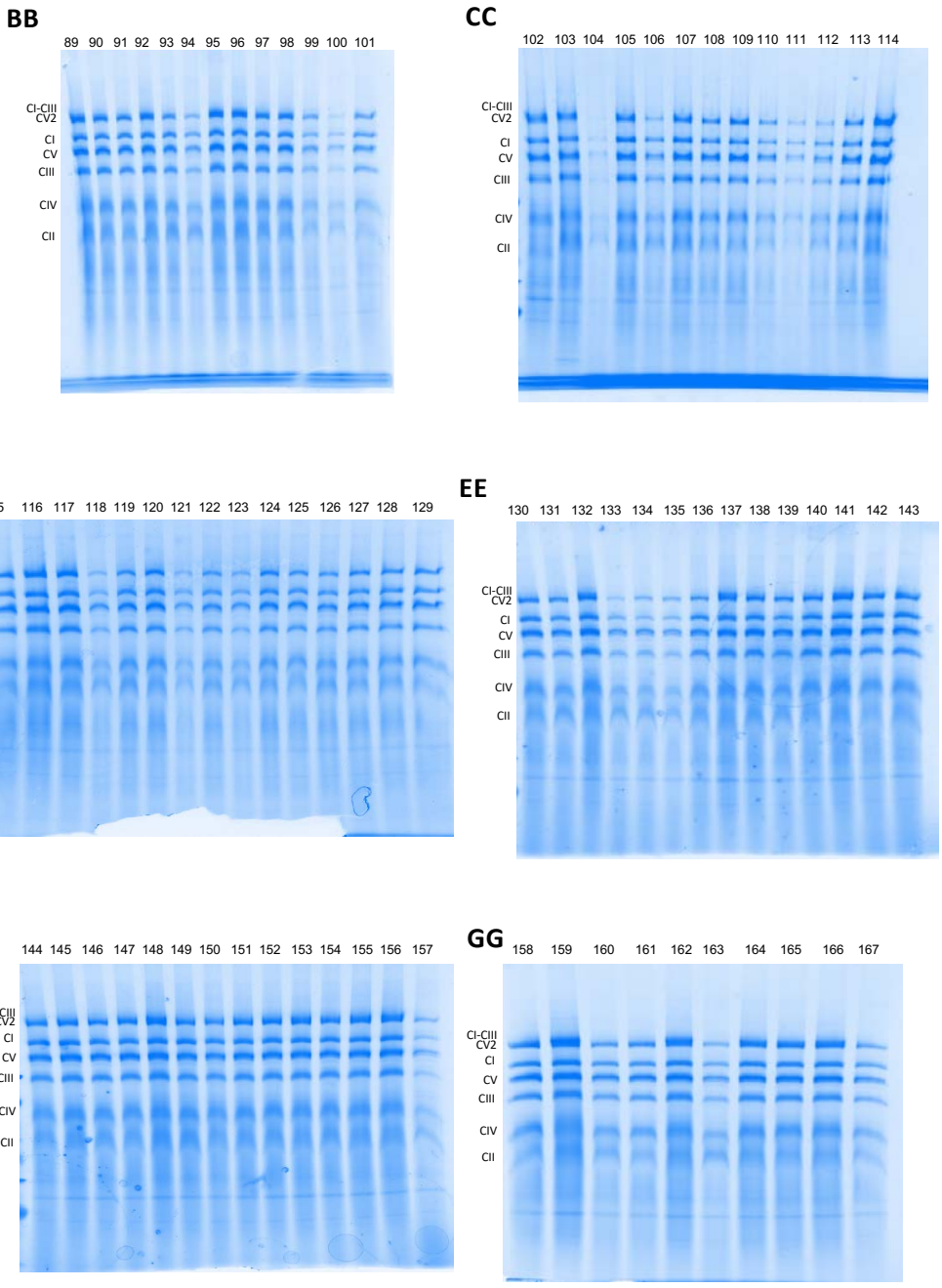

Figure 4.2: The potential to use BioID in the *Drosophila* gut and thorax.

(A) SDS-PAGE of *Drosophila* gut samples to measure the amount of biotinylated proteins. Myo1aGal4<W1118 was used as a control. Two different UAS-BirA lines were used to control expressed under the gut driver Myo1aGal4 for non-specific proteins that BirA may biotinylate. Myo1aGal4<UAS-Ubi6-BirA is used to identify proteins that were biotinylated by BirA since they came in close proximity to Ubi6.

(B) SDS-PAGE of *Drosophila* flight thoraxes to measure the amount of biotinylated proteins. Myo1aGal4<W1118 was used as a control. Two different UAS-BirA lines were used to control expressed under the gut driver Myo1aGal4 for non-specific proteins that BirA may biotinylate. Myo1aGal4<UAS-Ubi6-BirA is used to identify proteins that were biotinylated by BirA since they came in close proximity to Ubi6.

A

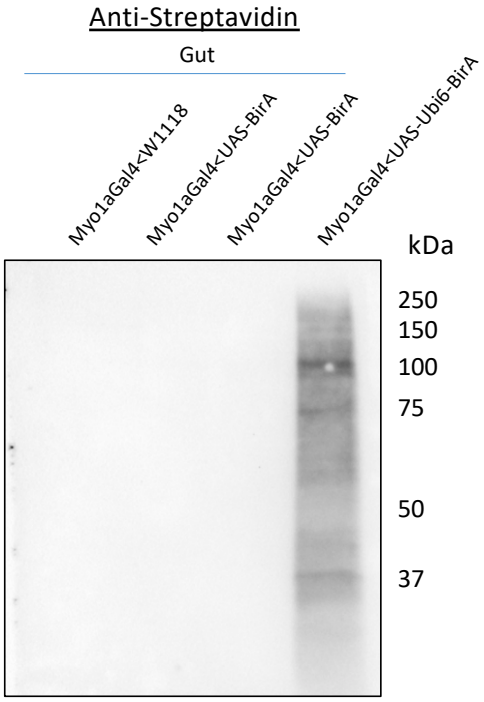
Anti-Streptavidin
Gut
Myo1aGal4<W1118
Myo1aGal4<UAS-BirA
Myo1aGal4<UAS-BirA
Myo1aGal4<UAS-Ubi6-BirA
kDa
250
150
100
75
50
37

B

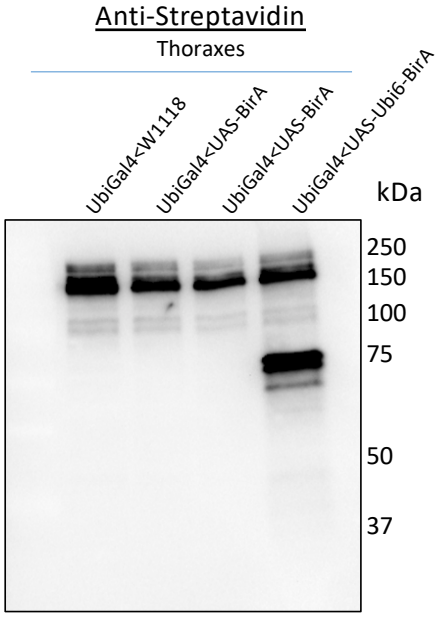
Anti-Streptavidin
Thoraxes
UbiGal4<W1118
UbiGal4<UAS-BirA
UbiGal4<UAS-BirA
UbiGal4<UAS-Ubi6-BirA
kDa
250
150
100
75
50
37

Table 4.1: Table for Figure 4.1 listing the RNAi's that were screened

Column 1: The screen type for each RNAi

Column 2: The number that corresponds with the lane numbered in figure 3.3.

Column 3: The Bloomington Stock ordered.

Column 4: The Gal4 used to express the UAS-RNAi lines in *Drosophila* flight muscles.

Column 5: X denotes if it is a hit

Column 6: Protein name is listed if identified as a hit.

Screen Type	Lane Number	Bloomington Stock #	Gal4	Hit	Protein
MitoCarta	1	42595	Dmef2		
MitoCarta	2	43155	Dmef2		
MitoCarta	3	52922	Dmef2		
MitoCarta	4	42591	Dmef2		
MitoCarta	5	52907	Dmef2	X	NFU1
MitoCarta	6	52920	Dmef2		
MitoCarta	7	64025	Dmef2		
MitoCarta	8	57572	Dmef2		
MitoCarta	9	43245	Dmef2		
MitoCarta	10	36671	Dmef2		
MitoCarta	11	64489	Dmef2		
MitoCarta	12	64564	Dmef2		
MitoCarta	13	67030	Dmef2		
MitoCarta	14	57557	Dmef2		
MitoCarta	15	67425	Dmef2		
MitoCarta	16	67585	Dmef2		
MitoCarta	17	43297	Dmef2		
MitoCarta	18	43278	Dmef2		
MitoCarta	19	60133	Dmef2		
MitoCarta	20	60360	Dmef2		
MitoCarta	21	60404	Dmef2		
MitoCarta	22	60475	Dmef2		
MitoCarta	23	60873	Dmef2	X	NDUFV2 (internal control)
MitoCarta	24	62272	Dmef2		
MitoCarta	25	62373	Dmef2		
MitoCarta	26	62455	Dmef2		
MitoCarta	27	56864	Dmef2		
MitoCarta	28	63035	Dmef2	X	NDUFV2
MitoCarta	29	56880	Dmef2		
MitoCarta	30	56885	Dmef2		
MitoCarta	31	34971	Dmef2	X	PRDX2
MitoCarta	32	44037	Dmef2	X	NFS1
MitoCarta	33	44429	Dmef2		
MitoCarta	34	34974	Dmef2		
MitoCarta	35	26007	Dmef2		
MitoCarta	36	41857	Dmef2		
MitoCarta	37	26007	Dmef2		
MitoCarta	38	40936	Dmef2		
MitoCarta	39	44475	Dmef2		
MitoCarta	40	36871	Dmef2		
MitoCarta	41	36740	Dmef2		
MitoCarta	42	36911	Dmef2	X	COQ10A
MitoCarta	43	34588	Dmef2	X	MED12L
MitoCarta	44	25886	Dmef2		
MitoCarta	45	28664	Dmef2		
MitoCarta	46	34028	Dmef2		
MitoCarta	47	31157	Dmef2	X	MFN2
MitoCarta	48	31074	Dmef2	X	BCS1L
MitoCarta	49	38332	Dmef2		
MitoCarta	50	31075	Dmef2	X	BCS1L
MitoCarta	51	29573	Dmef2		
MitoCarta	52	52917	Dmef2		
MitoCarta	53	30500	Dmef2		

MitoCarta	54	31077	Dmef2		
MitoCarta	55	58074	Dmef2		
MitoCarta	56	28294	Dmef2	X	MTCH2
MitoCarta	57	58148	Dmef2		
MitoCarta	58	60107	Dmef2		
MitoCarta	59	58084	Dmef2		
MitoCarta	60	28635	Dmef2		
MitoCarta	61	56043	Dmef2		
MitoCarta	62	27725	Dmef2		
MitoCarta	63	31076	Dmef2		
MitoCarta	64	51900	Dmef2		
MitoCarta	65	52989	Dmef2		
MitoCarta	66	44512	Dmef2		
MitoCarta	67	51876	Dmef2		
MitoCarta	68	55146	Dmef2	X	FECH
MitoCarta	69	51798	Dmef2		
MitoCarta	70	53355	Dmef2		
MitoCarta	71	53287	Dmef2		
MitoCarta	72	50939	Dmef2	X	SUCLG2
MitoCarta	73	53325	Dmef2		
MitoCarta	74	54465	Dmef2		
MitoCarta	75	56858	Dmef2	X	ACAT2
FS5/Lon KD Interactors	1	52913	Dmef2		
FS5/Lon KD Interactors	2	55168	Dmef2		
FS5/Lon KD Interactors	3	18121	Dmef2		
FS5/Lon KD Interactors	4	40874	Dmef2		
FS5/Lon KD Interactors	5	38926	Dmef2		
FS5/Lon KD Interactors	6	35608	Dmef2		
FS5/Lon KD Interactors	7	36071	Dmef2		
FS5/Lon KD Interactors	8	35348	Dmef2		
FS5/Lon KD Interactors	9	35486	Dmef2		
FS5/Lon KD Interactors	10	33765	Dmef2		
FS5/Lon KD Interactors	11	33696	Dmef2		
FS5/Lon KD Interactors	12	33950	Dmef2		
FS5/Lon KD Interactors	13	31100	Dmef2		
FS5/Lon KD Interactors	14	34936	Dmef2		
FS5/Lon KD Interactors	15	52907	Dmef2	X	NFU1
FS5/Lon KD Interactors	16	31237	Dmef2		
FS5/Lon KD Interactors	17	31223	Dmef2		
FS5/Lon KD Interactors	18	36775	Dmef2		
FS5/Lon KD Interactors	19	36072	Dmef2		
FS5/Lon KD Interactors	20	38256	Dmef2		
FS5/Lon KD Interactors	21	36820	Dmef2		
FS5/Lon KD Interactors	22	34729	Dmef2		
FS5/Lon KD Interactors	23	34554	Dmef2		
FS5/Lon KD Interactors	24	33976	Dmef2		
FS5/Lon KD Interactors	25	31240	Dmef2	X	NDUFAF5
FS5/Lon KD Interactors	26	32405	Dmef2		
FS5/Lon KD Interactors	27	31222	Dmef2		
FS5/Lon KD Interactors	28	31102	Dmef2	X	NDUFAF5
FS5/Lon KD Interactors	29	33001	Dmef2		
FS5/Lon KD Interactors	30	35034	Dmef2		
FS5/Lon KD Interactors	31	51807	Dmef2		

FS5/Lon KD Interactors	32	51797	Dmef2		
FS5/Lon KD Interactors	33	51785	Dmef2		
FS5/Lon KD Interactors	34	51783	Dmef2		
FS5/Lon KD Interactors	35	51749	Dmef2		
FS5/Lon KD Interactors	36	51714	Dmef2		
FS5/Lon KD Interactors	37	51359	Dmef2		
FS5/Lon KD Interactors	38	44512	Dmef2		
FS5/Lon KD Interactors	39	44475	Dmef2		
FS5/Lon KD Interactors	40	51899	Dmef2		
FS5/Lon KD Interactors	41	53894	Dmef2		
FS5/Lon KD Interactors	42	53334	Dmef2		
FS5/Lon KD Interactors	43	51879	Dmef2	X	NDUFAF5
FS5/Lon KD Interactors	44	50555	Dmef2		
FS5/Lon KD Interactors	45	51157	Dmef2	X	CHCHD3
FS5/Lon KD Interactors	46	57843	Dmef2		
FS5/Lon KD Interactors	47	55323	Dmef2		
FS5/Lon KD Interactors	48	38332	Dmef2		
FS5/Lon KD Interactors	49	40874	Dmef2		
FS5/Lon KD Interactors	50	41625	Dmef2		
FS5/Lon KD Interactors	51	57252	Dmef2		
FS5/Lon KD Interactors	52	55347	Dmef2		
FS5/Lon KD Interactors	53	41698	Dmef2		
FS5/Lon KD Interactors	54	42007	Dmef2		
FS5/Lon KD Interactors	55	57407	Dmef2		
FS5/Lon KD Interactors	56	57489	Dmef2	X	Men-b
FS5/Lon KD Interactors	57	42005	Dmef2		
FS5/Lon KD Interactors	58	43172	Dmef2		
FS5/Lon KD Interactors	59	35142	Dmef2		
FS5/Lon KD Interactors	60	57736	Dmef2		
FS5/Lon KD Interactors	61	61183	Dmef2		
FS5/Lon KD Interactors	62	62362	Dmef2	X	MARS2
FS5/Lon KD Interactors	63	64489	Dmef2		
FS5/Lon KD Interactors	64	64614	Dmef2		
FS5/Lon KD Interactors	65	64919	Dmef2		
FS5/Lon KD Interactors	66	65243	Dmef2		
FS5/Lon KD Interactors	67	66328	Dmef2		
FS5/Lon KD Interactors	68	65215	Dmef2		
FS5/Lon KD Interactors	69	66929	Dmef2		
FS5/Lon KD Interactors	70	28968	Dmef2		
FS5/Lon KD Interactors	71	28930	Dmef2		
FS5/Lon KD Interactors	72	28749	Dmef2		
FS5/Lon KD Interactors	73	28317	Dmef2		
FS5/Lon KD Interactors	74	27682	Dmef2		
FS5/Lon KD Interactors	75	27650	Dmef2		
FS5/Lon KD Interactors	76	25953	Dmef2		
FS5/Lon KD Interactors	77	67601	Dmef2		
FS5/Lon KD Interactors	78	67003	Dmef2		
FS5/Lon KD Interactors	79	29399	Dmef2		
FS5/Lon KD Interactors	80	31150	Dmef2		
FS5/Lon KD Interactors	81	31205	Dmef2		
FS5/Lon KD Interactors	82	31660	Dmef2		
FS5/Lon KD Interactors	83	31470	Dmef2		
FS5/Lon KD Interactors	84	31666	Dmef2		
FS5/Lon KD Interactors	85	31661	Dmef2		

FS5/Lon KD Interactors	86	32934	Dmef2	X	RELA
FS5/Lon KD Interactors	87	31966	Dmef2		
FS5/Lon KD Interactors	88	34347	Dmef2	X	ADSL
FS5/Lon KD Interactors	89	34346	Dmef2		
FS5/Lon KD Interactors	90	34913	Dmef2		
FS5/Lon KD Interactors	91	53894	Dmef2		
FS5/Lon KD Interactors	92	31660	Dmef2		
FS5/Lon KD Interactors	93	51479	Dmef2	X	ScpX
FS5/Lon KD Interactors	94	31205	Dmef2		
FS5/Lon KD Interactors	95	28317	Dmef2		
FS5/Lon KD Interactors	96	43172	Dmef2		
FS5/Lon KD Interactors	97	38332	Dmef2		
FS5/Lon KD Interactors	98	36691	Dmef2	X	Dumpy
FS5/Lon KD Interactors	99	51899	Dmef2		
FS5/Lon KD Interactors	100	31100	Dmef2		
FS5/Lon KD Interactors	101	52913	Dmef2		
FS5/Lon KD Interactors	102	31666	Dmef2		
FS5/Lon KD Interactors	103	41939	Dmef2	X	Cp1
Calcium Signaling Proteins	1	W1118	Mhc		
Calcium Signaling Proteins	2	25830	Mhc		
Calcium Signaling Proteins	3	25928	Mhc		
Calcium Signaling Proteins	4	26012	Mhc		
Calcium Signaling Proteins	5	26172	Mhc		
Calcium Signaling Proteins	6	26251	Mhc		
Calcium Signaling Proteins	7	27053	Mhc		
Calcium Signaling Proteins	8	58971	Mhc		
Calcium Signaling Proteins	9	27244	Mhc		
Calcium Signaling Proteins	10	35362	Mhc		
Calcium Signaling Proteins	11	37502	Mhc		
Calcium Signaling Proteins	12	39029	Mhc		
Calcium Signaling Proteins	13	28919	Mhc		
Calcium Signaling Proteins	14	29401	Mhc		
Calcium Signaling Proteins	15	29445	Mhc		
Calcium Signaling Proteins	16	W1118	Mhc		
Calcium Signaling Proteins	17	29662	Mhc		
Calcium Signaling Proteins	18	29663	Mhc		
Calcium Signaling Proteins	19	29665	Mhc		
Calcium Signaling Proteins	20	29666	Mhc		
Calcium Signaling Proteins	21	58972	Mhc		
Calcium Signaling Proteins	22	31540	Mhc		
Calcium Signaling Proteins	23	58973	Mhc		
Calcium Signaling Proteins	24	31695	Mhc		
Calcium Signaling Proteins	25	44581	Mhc		
Calcium Signaling Proteins	26	64003	Mhc		
Calcium Signaling Proteins	27	58974	Mhc		
Calcium Signaling Proteins	28	34609	Mhc		
Calcium Signaling Proteins	29	35330	Mhc		
Calcium Signaling Proteins	30	41900	Mhc		
Calcium Signaling Proteins	31	W1118	Mhc		
Calcium Signaling Proteins	32	25830	Mhc		
Calcium Signaling Proteins	33	25928	Mhc		
Calcium Signaling Proteins	34	26012	Mhc		
Calcium Signaling Proteins	35	26172	Mhc		

Calcium Signaling Proteins	36	26251	Mhc		
Calcium Signaling Proteins	37	27053	Mhc		
Calcium Signaling Proteins	38	58971	Mhc		
Calcium Signaling Proteins	39	27244	Mhc		
Calcium Signaling Proteins	40	35362	Mhc		
Calcium Signaling Proteins	41	37502	Mhc		
Calcium Signaling Proteins	42	39029	Mhc		
Calcium Signaling Proteins	43	28918	Mhc		
Calcium Signaling Proteins	44	29401	Mhc		
Calcium Signaling Proteins	45	29445	Mhc		
Calcium Signaling Proteins	46	29662	Mhc		
Calcium Signaling Proteins	47	29663	Mhc		
Calcium Signaling Proteins	48	29665	Mhc		
Calcium Signaling Proteins	49	29666	Mhc		
Calcium Signaling Proteins	50	58972	Mhc		
Calcium Signaling Proteins	51	31540	Mhc		
Calcium Signaling Proteins	52	58973	Mhc		
Calcium Signaling Proteins	53	31695	Mhc		
Calcium Signaling Proteins	54	44581	Mhc		
Calcium Signaling Proteins	55	64003	Mhc		
Calcium Signaling Proteins	56	58974	Mhc		
Calcium Signaling Proteins	57	34609	Mhc		
Calcium Signaling Proteins	58	35330	Mhc		
Calcium Signaling Proteins	59	41900	Mhc		
Calcium Signaling Proteins	60	W1118	Mhc		
Calcium Signaling Proteins	61	53893	Mhc		
Calcium Signaling Proteins	62	63021	Mhc		
Calcium Signaling Proteins	63	33923	Mhc		
Calcium Signaling Proteins	64	41909	Mhc		
Calcium Signaling Proteins	65	31676	Mhc		
Calcium Signaling Proteins	66	26726	Mhc		
Calcium Signaling Proteins	67	33413	Mhc		
Calcium Signaling Proteins	68	63025	Mhc		
Calcium Signaling Proteins	69	40835	Mhc		
Calcium Signaling Proteins	70	32404	Mhc		
Calcium Signaling Proteins	71	41900	Mhc		
Calcium Signaling Proteins	72	31471	Mhc		
Calcium Signaling Proteins	73	W1118	Dmef2		
Calcium Signaling Proteins	74	26172	Dmef2		
Calcium Signaling Proteins	75	26251	Dmef2		
Calcium Signaling Proteins	76	39029	Dmef2		
Calcium Signaling Proteins	77	29401	Dmef2		
Calcium Signaling Proteins	78	35330	Dmef2		
Calcium Signaling Proteins	79	58974	Dmef2		
Calcium Signaling Proteins	80	41900	Dmef2		
Calcium Signaling Proteins	81	42580	Dmef2		
Calcium Signaling Proteins	82	26726	Dmef2		
Calcium Signaling Proteins	83	31676	Dmef2		
Calcium Signaling Proteins	84	31471	Dmef2		
Calcium Signaling Proteins	85	63021	Dmef2		
Calcium Signaling Proteins	86	W1118	Dmef2		
Calcium Signaling Proteins	87	26012	Dmef2		
Calcium Signaling Proteins	88	29662	Dmef2		
Calcium Signaling Proteins	89	29663	Dmef2		

Calcium Signaling Proteins	90	27053	Dmef2		
Calcium Signaling Proteins	91	27244	Dmef2		
Calcium Signaling Proteins	92	35362	Dmef2		
Calcium Signaling Proteins	93	29666	Dmef2		
Calcium Signaling Proteins	94	58972	Dmef2		
Calcium Signaling Proteins	95	58973	Dmef2		
Calcium Signaling Proteins	96	63025	Dmef2		
Calcium Signaling Proteins	97	53893	Dmef2		
Calcium Signaling Proteins	98	41909	Dmef2	X	Micu1
Calcium Signaling Proteins	99	W1118	Daughterless		
Calcium Signaling Proteins	100	29665	Daughterless		
Calcium Signaling Proteins	101	25839	Daughterless		
Calcium Signaling Proteins	102	28919	Daughterless		
Calcium Signaling Proteins	103	25928	Daughterless		
Calcium Signaling Proteins	104	33413	Daughterless		
Calcium Signaling Proteins	105	31549	Daughterless		
Calcium Signaling Proteins	106	31695	Daughterless		
Calcium Signaling Proteins	107	29445	Daughterless		
Calcium Signaling Proteins	108	W1118	Dmef2;tub80		
Calcium Signaling Proteins	109	38919	Dmef2;tub80		
Calcium Signaling Proteins	110	W1118	Dmef2		
Calcium Signaling Proteins	111	41909	Dmef2	X	Micu1
Calcium Signaling Proteins	112	CG4495	Dmef2		
Calcium Signaling Proteins	113	W1118	Dmef2;tub80		
Calcium Signaling Proteins	114	31540	Dmef2;tub80		
Calcium Signaling Proteins	115	31695	Dmef2;tub80		
Calcium Signaling Proteins	116	29445	Dmef2;tub80		
Calcium Signaling Proteins	117	25928	Dmef2;tub80		
Calcium Signaling Proteins	118	58971	Dmef2;tub80		
Calcium Signaling Proteins	119	28919	Dmef2;tub80		
Calcium Signaling Proteins	120	44581	Dmef2;tub80		
Calcium Signaling Proteins	121	25830	Dmef2;tub80		
Calcium Signaling Proteins	122	64003	Dmef2;tub80		
Calcium Signaling Proteins	123	34609	Dmef2;tub80		
Calcium Signaling Proteins	124	32404	Dmef2;tub80		
Calcium Signaling Proteins	125	33923	Dmef2;tub80		
Calcium Signaling Proteins	126	33413	Dmef2;tub80		
Calcium Signaling Proteins	127	29664	Dmef2;tub80		
UAS-Protein Overexpression	1	W1118	Mhc		
UAS-Protein Overexpression	2	63079	Mhc		
UAS-Protein Overexpression	3	53753	Mhc		
UAS-Protein Overexpression	4	55073	Mhc		
UAS-Protein Overexpression	5	56495	Mhc		
UAS-Protein Overexpression	6	56752	Mhc		
UAS-Protein Overexpression	7	51636	Mhc		
UAS-Protein Overexpression	8	58460	Mhc		
UAS-Protein Overexpression	9	57355	Mhc		
UAS-Protein Overexpression	10	59085	Mhc		
UAS-Protein Overexpression	11	59055	Mhc		
UAS-Protein Overexpression	12	32330	Mhc		
UAS-Protein Overexpression	13	32110	Mhc		
UAS-Protein Overexpression	14	51380	Mhc	X	br
UAS-Protein Overexpression	15	53716	Mhc		

UAS-Protein Overexpression	16	W1118	Mhc		
UAS-Protein Overexpression	17	58723	Mhc		
UAS-Protein Overexpression	18	63058	Mhc		
UAS-Protein Overexpression	19	59843	Mhc		
UAS-Protein Overexpression	20	63229	Mhc		
UAS-Protein Overexpression	21	51671	Mhc		
UAS-Protein Overexpression	22	53758	Mhc		
UAS-Protein Overexpression	23	58357	Mhc	X	debcl
UAS-Protein Overexpression	24	59844	Mhc		
UAS-Protein Overexpression	25	63050	Mhc		
UAS-Protein Overexpression	26	51668	Mhc		
UAS-Protein Overexpression	27	34048	Mhc		
UAS-Protein Overexpression	28	56826	Mhc	X	dbx
UAS-Protein Overexpression	29	59053	Mhc		
UAS-Protein Overexpression	30	57336	Mhc		
UAS-Protein Overexpression	31	W1118	Mhc		
UAS-Protein Overexpression	32	63150	Mhc		
UAS-Protein Overexpression	33	53756	Mhc		
UAS-Protein Overexpression	34	63216	Mhc		
UAS-Protein Overexpression	35	58877	Mhc		
UAS-Protein Overexpression	36	63059	Mhc		
UAS-Protein Overexpression	37	44386	Mhc		
UAS-Protein Overexpression	38	44597	Mhc		
UAS-Protein Overexpression	39	43645	Mhc		
UAS-Protein Overexpression	40	53760	Mhc		
UAS-Protein Overexpression	41	44224	Mhc	X	dsx
UAS-Protein Overexpression	42	44609	Mhc		
UAS-Protein Overexpression	43	44600	Mhc		
UAS-Protein Overexpression	44	56197	Mhc	X	dronc
UAS-Protein Overexpression	45	W1118	Mhc		
UAS-Protein Overexpression	46	39741	Mhc		
UAS-Protein Overexpression	47	39749	Mhc		
UAS-Protein Overexpression	48	39706	Mhc		
UAS-Protein Overexpression	49	59048	Mhc		
UAS-Protein Overexpression	50	58992	Mhc		
UAS-Protein Overexpression	51	42222	Mhc		
UAS-Protein Overexpression	52	44237	Mhc		
UAS-Protein Overexpression	53	41802	Mhc		
UAS-Protein Overexpression	54	9582	Mhc	X	sima
UAS-Protein Overexpression	55	39713	Mhc		
UAS-Protein Overexpression	56	51190	Mhc	X	br
UAS-Protein Overexpression	57	39743	Mhc		
UAS-Protein Overexpression	58	impL2	Mhc		
UAS-Protein Overexpression	59	wImp	Mhc		
UAS-Protein Overexpression	60	W1118	Mhc		
UAS-Protein Overexpression	61	42227	Mhc		
UAS-Protein Overexpression	62	50891	Mhc		
UAS-Protein Overexpression	63	44234	Mhc		
UAS-Protein Overexpression	64	39703	Mhc		
UAS-Protein Overexpression	65	41791	Mhc		
UAS-Protein Overexpression	66	63077	Mhc		
UAS-Protein Overexpression	67	63052	Mhc		
UAS-Protein Overexpression	68	56766	Mhc		
UAS-Protein Overexpression	69	55067	Mhc		

UAS-Protein Overexpression	70	51645	Mhc		
UAS-Protein Overexpression	71	63078	Mhc		
UAS-Protein Overexpression	72	58787	Mhc		
UAS-Protein Overexpression	73	55046	Mhc		
UAS-Protein Overexpression	74	53750	Mhc		
UAS-Protein Overexpression	75	W1118	Mhc		
UAS-Protein Overexpression	76	58359	Mhc		
UAS-Protein Overexpression	77	59050	Mhc		
UAS-Protein Overexpression	78	56769	Mhc		
UAS-Protein Overexpression	79	32570	Mhc		
UAS-Protein Overexpression	80	58712	Mhc		
UAS-Protein Overexpression	81	38410	Mhc		
UAS-Protein Overexpression	82	34490	Mhc		
UAS-Protein Overexpression	83	37291	Mhc	X	da
UAS-Protein Overexpression	84	36496	Mhc	X	FRT
UAS-Protein Overexpression	85	33911	Mhc	X	ND-75 RNAi (internal control)
UAS-Protein Overexpression	86	37540	Mhc		
UAS-Protein Overexpression	87	32572	Mhc	X	crebA
UAS-Protein Overexpression	88	33603	Mhc		
UAS-Protein Overexpression	89	W1118	Mhc		
UAS-Protein Overexpression	90	9453	Mhc		
UAS-Protein Overexpression	91	8710	Mhc		
UAS-Protein Overexpression	92	8711	Mhc		
UAS-Protein Overexpression	93	27324	Mhc		
UAS-Protein Overexpression	94	23639	Mhc	X	ab
UAS-Protein Overexpression	95	23878	Mhc		
UAS-Protein Overexpression	96	26681	Mhc		
UAS-Protein Overexpression	97	9895	Mhc		
UAS-Protein Overexpression	98	26698	Mhc		
UAS-Protein Overexpression	99	9233	Mhc		
UAS-Protein Overexpression	100	9929	Mhc	X	exex
UAS-Protein Overexpression	101	9522	Mhc		
UAS-Protein Overexpression	102	W1118	Mhc		
UAS-Protein Overexpression	103	28810	Mhc		
UAS-Protein Overexpression	104	23143	Mhc	X	gr63a
UAS-Protein Overexpression	105	9160	Mhc		
UAS-Protein Overexpression	106	9533	Mhc	X	egfr
UAS-Protein Overexpression	107	9764	Mhc		
UAS-Protein Overexpression	108	26675	Mhc		
UAS-Protein Overexpression	109	8377	Mhc		
UAS-Protein Overexpression	110	8784	Mhc	X	DCTN2
UAS-Protein Overexpression	111	6931	Mhc	X	FMR1
UAS-Protein Overexpression	112	5790	Mhc	X	aop
UAS-Protein Overexpression	113	8384	Mhc		
UAS-Protein Overexpression	114	8380	Mhc		
UAS-Protein Overexpression	115	W1118	Mhc		
UAS-Protein Overexpression	116	8202	Mhc		
UAS-Protein Overexpression	117	24465	Mhc		
UAS-Protein Overexpression	118	913	Mhc	X	Abd-B
UAS-Protein Overexpression	119	9417	Mhc		
UAS-Protein Overexpression	120	6631	Mhc		
UAS-Protein Overexpression	121	4774	Mhc	X	E2f1
UAS-Protein Overexpression	122	26269	Mhc		
UAS-Protein Overexpression	123	36318	Mhc		

UAS-Protein Overexpression	124	24504	Mhc		
UAS-Protein Overexpression	125	9524	Mhc		
UAS-Protein Overexpression	126	26881	Mhc		
UAS-Protein Overexpression	127	9534	Mhc		
UAS-Protein Overexpression	128	7073	Mhc		
UAS-Protein Overexpression	129	26679	Mhc		
UAS-Protein Overexpression	130	W1118	Mhc		
UAS-Protein Overexpression	131	7086	Mhc		
UAS-Protein Overexpression	132	6492	Mhc		
UAS-Protein Overexpression	133	7221	Mhc	X	cbz
UAS-Protein Overexpression	134	5364	Mhc	X	egfr
UAS-Protein Overexpression	135	6846	Mhc	X	disco
UAS-Protein Overexpression	136	6705	Mhc		
UAS-Protein Overexpression	137	29962	Mhc		
UAS-Protein Overexpression	138	7107	Mhc		
UAS-Protein Overexpression	139	7220	Mhc		
UAS-Protein Overexpression	140	29663	Mhc		
UAS-Protein Overexpression	141	30553	Mhc		
UAS-Protein Overexpression	142	25102	Mhc		
UAS-Protein Overexpression	143	5368	Mhc		
UAS-Protein Overexpression	144	W1118	Mhc		
UAS-Protein Overexpression	145	8553	Mhc		
UAS-Protein Overexpression	146	29008	Mhc		
UAS-Protein Overexpression	147	8861	Mhc		
UAS-Protein Overexpression	148	39679	Mhc		
UAS-Protein Overexpression	149	26878	Mhc		
UAS-Protein Overexpression	150	8566	Mhc		
UAS-Protein Overexpression	151	6489	Mhc		
UAS-Protein Overexpression	152	6847	Mhc		
UAS-Protein Overexpression	153	32105	Mhc		
UAS-Protein Overexpression	154	6490	Mhc		
UAS-Protein Overexpression	155	26649	Mhc		
UAS-Protein Overexpression	156	6809	Mhc		
UAS-Protein Overexpression	157	7219	Mhc	X	crebB
UAS-Protein Overexpression	158	W1118	Mhc		
UAS-Protein Overexpression	159	6468	Mhc		
UAS-Protein Overexpression	160	9319	Mhc	X	dl
UAS-Protein Overexpression	161	59052	Mhc	X	CG33156
UAS-Protein Overexpression	162	36325	Mhc		
UAS-Protein Overexpression	163	56821	Mhc	X	fd59A
UAS-Protein Overexpression	164	8187	Mhc		
UAS-Protein Overexpression	165	27647	Mhc		
UAS-Protein Overexpression	166	5397	Mhc		
UAS-Protein Overexpression	167	25080	Mhc	X	Gr64a

References

Antony, A.N., Paillard, M., Moffat, C., Juskeviciute, E., Correnti, J., Bolon, B., Rubin, E., Csordás, G., Seifert, E.L., Hoek, J.B., et al. (2016). MICU1 regulation of mitochondrial Ca(2+) uptake dictates survival and tissue regeneration. Nat. Commun. *7*, 10955.

Calvo, S.E., Clauser, K.R., and Mootha, V.K. (2016). MitoCarta2.0: an updated inventory of mammalian mitochondrial proteins. Nucleic Acids Res. *44*, D1251–7.

Cogliati, S., Calvo, E., Loureiro, M., Guaras, A.M., Nieto-Arellano, R., Garcia-Poyatos, C., Ezkurdia, I., Mercader, N., Vázquez, J., and Enriquez, J.A. (2016). Mechanism of super-assembly of respiratory complexes III and IV. Nature *539*, 579–582.

Dunham-Snary, K.J., Wu, D., Potus, F., Sykes, E.A., Mewburn, J.D., Charles, R.L., Eaton, P., Sultanian, R.A., and Archer, S.L. (2019). Ndufs2, a Core Subunit of Mitochondrial Complex I, Is Essential for Acute Oxygen-Sensing and Hypoxic Pulmonary Vasoconstriction. Circ. Res. *124*, 1727–1746.

Faust, J.E., Verma, A., Peng, C., and McNew, J.A. (2012). An inventory of peroxisomal proteins and pathways in Drosophila melanogaster. Traffic *13*, 1378–1392.

Fiedorczuk, K., Letts, J.A., Degliesposti, G., Kaszuba, K., Skehel, M., and Sazanov, L.A. (2016). Atomic structure of the entire mammalian mitochondrial complex I. Nature *538*, 406–410.

Foriel, S., Renkema, G.H., Lasarzewski, Y., Berkhout, J., Rodenburg, R.J., Smeitink, J.A.M., Beyrath, J., and Schenck, A. (2019). A drosophila mitochondrial complex I deficiency phenotype array. Front. Genet. *10*, 245.

Fransen, M., Lismont, C., and Walton, P. (2017). The Peroxisome-Mitochondria Connection: How and Why? Int. J. Mol. Sci. *18*.

Garcia, C.J., Khajeh, J., Coulanges, E., Chen, E.I.-J., and Owusu-Ansah, E. (2017). Regulation of mitochondrial complex I biogenesis in drosophila flight muscles. Cell Rep. *20*, 264–278.

Greggio, C., Jha, P., Kulkarni, S.S., Lagarrigue, S., Broskey, N.T., Boutant, M., Wang, X., Conde Alonso, S., Ofori, E., Auwerx, J., et al. (2017). Enhanced respiratory chain supercomplex formation in response to exercise in human skeletal muscle. Cell Metab. *25*, 301–311.

Hasan, N.M., Longacre, M.J., Stoker, S.W., Kendrick, M.A., and MacDonald, M.J. (2015). Mitochondrial malic enzyme 3 is important for insulin secretion in pancreatic β-cells. Mol. Endocrinol. *29*, 396–410.

Lee, C.F., Caudal, A., Abell, L., Nagana Gowda, G.A., and Tian, R. (2019). Targeting NAD+ metabolism as interventions for mitochondrial disease. Sci. Rep. *9*, 3073.

Letts, J.A., and Sazanov, L.A. (2017). Clarifying the supercomplex: the higher-order organization of the mitochondrial electron transport chain. Nat. Struct. Mol. Biol. *24*, 800–808.

Letts, J.A., Fiedorczuk, K., and Sazanov, L.A. (2017). The architecture of respiratory supercomplexes. Biophys. J. *112*, 278a.

Letts, J.A., Fiedorczuk, K., Degliesposti, G., Skehel, M., and Sazanov, L.A. (2019). Structures of respiratory supercomplex I+III2 reveal functional and conformational crosstalk. Mol. Cell.

Marchi, S., and Pinton, P. (2014). The mitochondrial calcium uniporter complex: molecular components, structure and physiopathological implications. J. Physiol. (Lond.) *592*, 829–839.

Milenkovic, D., Blaza, J.N., Larsson, N.-G., and Hirst, J. (2017). The enigma of the respiratory chain supercomplex. Cell Metab. *25*, 765–776.

Mimaki, M., Wang, X., McKenzie, M., Thorburn, D.R., and Ryan, M.T. (2012). Understanding mitochondrial complex I assembly in health and disease. Biochim. Biophys. Acta *1817*, 851–862.

Navarro-Sastre, A., Tort, F., Stehling, O., Uzarska, M.A., Arranz, J.A., Del Toro, M., Labayru, M.T., Landa, J., Font, A., Garcia-Villoria, J., et al. (2011). A fatal mitochondrial disease is associated with defective NFU1 function in the maturation of a subset of mitochondrial Fe-S proteins. Am. J. Hum. Genet. *89*, 656–667.

Pagliarini, D.J., Calvo, S.E., Chang, B., Sheth, S.A., Vafai, S.B., Ong, S.-E., Walford, G.A., Sugiana, C., Boneh, A., Chen, W.K., et al. (2008). A mitochondrial protein compendium elucidates complex I disease biology. Cell *134*, 112–123.

Ramirez, J., Martinez, A., Lectez, B., Lee, S.Y., Franco, M., Barrio, R., Dittmar, G., and Mayor, U. (2015). Proteomic analysis of the ubiquitin landscape in the drosophila embryonic nervous system and the adult photoreceptor cells. PLoS One *10*, e0139083.

Roux, K.J., Kim, D.I., and Burke, B. (2013). BioID: a screen for protein-protein interactions. Curr Protoc Protein Sci *74*, Unit 19.23.

Ruiz-Ramírez, A., Barrios-Maya, M.-A., López-Acosta, O., Molina-Ortiz, D., and El-Hafidi, M. (2015). Cytochrome c release from rat liver mitochondria is compromised by increased saturated cardiolipin species induced by sucrose feeding. Am. J. Physiol. Endocrinol. Metab. *309*, E777–86.

Signes, A., and Fernandez-Vizarra, E. (2018). Assembly of mammalian oxidative phosphorylation complexes I-V and supercomplexes. Essays Biochem *62*, 255–270.

Stroud, D.A., Surgenor, E.E., Formosa, L.E., Reljic, B., Frazier, A.E., Dibley, M.G., Osellame, L.D., Stait, T., Beilharz, T.H., Thorburn, D.R., et al. (2016). Accessory subunits are integral for assembly and function of human mitochondrial complex I. Nature *538*, 123–126.

Weeda, E. (1981). Some properties of mitochondrial NAD+ linked malic enzyme and malate dehydrogenase from the flight muscles of Leptinotarsa decemlineata. Insect Biochemistry *11*, 679–684.

Zhu, J., Vinothkumar, K.R., and Hirst, J. (2016). Structure of mammalian respiratory complex I. Nature *536*, 354–358.

Resource

Cell Reports

Regulation of Mitochondrial Complex I Biogenesis in *Drosophila* Flight Muscles

Graphical Abstract

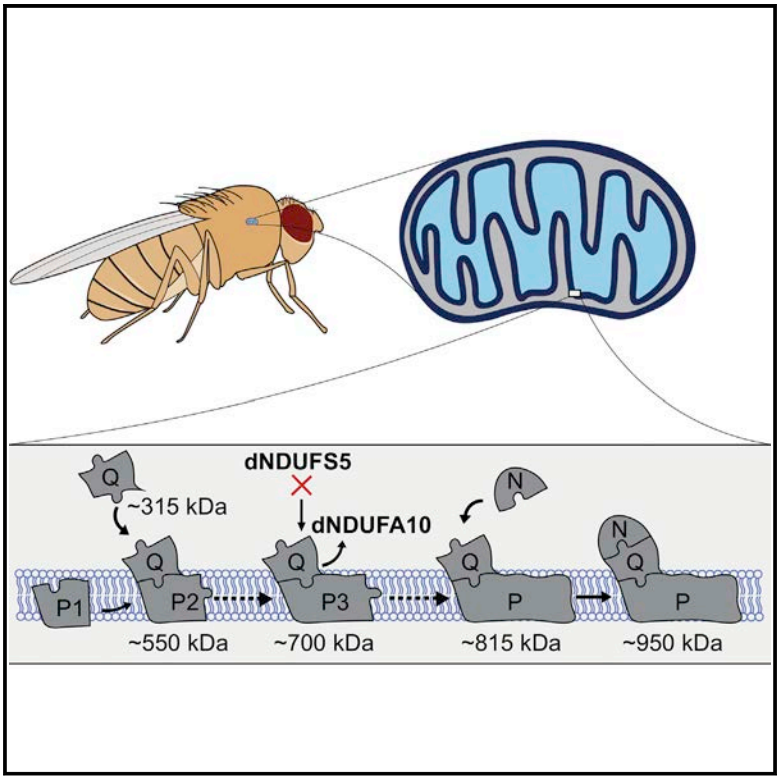

Authors

Christian Joel Garcia, Jahan Khajeh, Emmanuel Coulanges, Emily I-ju Chen, Edward Owusu-Ansah

Correspondence

eo2364@cumc.columbia.edu

In Brief

Garcia et al. establish *Drosophila* as a suitable resource for studying mitochondrial complex I biogenesis. They find that at least 42 of the 44 distinct human complex I subunits are conserved in *Drosophila*, and many of these subunits have specific roles in complex I assembly in vivo.

Highlights

- Mitochondrial complex I (CI) biogenesis can be studied in *Drosophila* flight muscles
- Subcomplexes of ~315, ~550, and ~815 kDa are formed during CI assembly in *Drosophila*
- dNDUFS5 is required for converting an ~700 kDa subcomplex into the ~815 kDa subcomplex
- dNDUFS5 is required to stabilize or promote incorporation of dNDUFA10 into the complex

Garcia et al., 2017, Cell Reports *20*, 264–278
July 5, 2017
http://dx.doi.org/10.1016/j.celrep.2017.06.015

CellPress

OPEN ACCESS
CellPress

Cell Reports
Resource

Regulation of Mitochondrial Complex I Biogenesis in *Drosophila* Flight Muscles

Christian Joel Garcia,[1,4] Jahan Khajeh,[1,4] Emmanuel Coulanges,[1] Emily I-ju Chen,[2] and Edward Owusu-Ansah[1,3,5,*]
[1]Department of Physiology and Cellular Biophysics
[2]Proteomics Shared Resource at the Herbert Irving Comprehensive Cancer Center and Department of Pharmacology
[3]The Robert N. Butler Columbia Aging Center
Columbia University Medical Center, New York, NY 10032, USA
[4]These authors contributed equally
[5]Lead Contact
*Correspondence: eo2364@cumc.columbia.edu
http://dx.doi.org/10.1016/j.celrep.2017.06.015

SUMMARY

The flight muscles of *Drosophila* are highly enriched with mitochondria, but the mechanism by which mitochondrial complex I (CI) is assembled in this tissue has not been described. We report the mechanism of CI biogenesis in *Drosophila* flight muscles and show that it proceeds via the formation of ~315, ~550, and ~815 kDa CI assembly intermediates. Additionally, we define specific roles for several CI subunits in the assembly process. In particular, we show that dNDUFS5 is required for converting an ~700 kDa transient CI assembly intermediate into the ~815 kDa assembly intermediate. Importantly, incorporation of dNDUFS5 into CI is necessary to stabilize or promote incorporation of dNDUFA10 into the complex. Our findings highlight the potential of studies of CI biogenesis in *Drosophila* to uncover the mechanism of CI assembly in vivo and establish *Drosophila* as a suitable model organism and resource for addressing questions relevant to CI biogenesis in humans.

INTRODUCTION

Mitochondrial complex I (CI) (NADH: ubiquinone oxidoreductase) is the first and largest of the electron transport chain complexes in the mitochondrion and has a molecular mass approaching 1 MDa (reviewed in Hirst, 2013). Human CI has 44 distinct subunits (Table S1), 14 of which are directly involved in transferring electrons from NADH to ubiquinone or in generation of the membrane potential. Because these 14 subunits are conserved from bacteria to humans and form the catalytic centers of the enzyme, they are referred to as the core or central subunits. The 30 remaining subunits are referred to as accessory or supernumerary subunits because they are not directly involved in catalysis and are expressed to varying extents among eukaryotes (Table S1) (reviewed in Hirst, 2013). A current hypothesis is that the accessory subunits may regulate reactive oxygen species (ROS) formation, complex assembly or stability, and cellular homeostasis in vivo. Of note, disease-causing mutations in several accessory subunits have been identified (Berger et al., 2008; Budde et al., 2000; Hoefs et al., 2008, 2011; Kirby et al., 2004; Ostergaard et al., 2011; Scacco et al., 2003), and genetic disruption of some accessory subunits in cell lines impairs CI assembly (Guerrero-Castillo et al., 2017; Stroud et al., 2016). However, a definitive role for many of the accessory subunits in vivo remains to be established.

CI has two major arms: a hydrophobic membrane arm and a hydrophilic peripheral arm that juts into the mitochondrial matrix. The two arms are oriented almost perpendicularly to each other, resulting in a characteristic boot or L-shaped structure (Clason et al., 2010; Efremov et al., 2010; Radermacher et al., 2006; Zickermann et al., 2015). Several cryoelectron microscopy density maps and higher resolution atomic structures of CI from various eukaryotes have recently been described (Fiedorczuk et al., 2016; Vinothkumar et al., 2014; Zhu et al., 2016; Zickermann et al., 2015). The accessory subunits were found to form a cage around the core subunits and were particularly concentrated around the membrane domain. These observations lend further credence to the hypothesis that the accessory subunits may be involved in stabilizing the complex during or after biogenesis in vivo.

Surprisingly, despite the outstanding genetic capabilities of *Drosophila*, a systematic genetic analysis of CI assembly has not been described in this organism. Instead, previous in vivo genetic analyses of the regulation of eukaryotic CI assembly have been performed, primarily in the aerobic fungus *Neurospora crassa* (Duarte et al., 1995). Although the *N. crassa* model of CI assembly is renowned for being the first system for which a model of CI assembly was described, there are notable deviations from the assembly pathway in mammalian systems (Nehls et al., 1992; Tuschen et al., 1990). Thus, it is important to develop additional genetically tractable CI assembly model systems that more closely resemble and recapitulate the human system. Importantly, *Drosophila* has a comparable number of CI subunits (similar to the human and bovine enzymes) and more than a dozen putative assembly factors, all of which have clear human orthologs, making it a suitable model organism for studying CI assembly. Studying CI assembly in *Drosophila* has the added advantage of being in an in vivo context, in which the effects of both developmental signals and environmental perturbations can be examined. Accordingly,

we have analyzed the role of several nuclear-encoded CI subunits in CI assembly in *Drosophila* muscles.

We describe the mechanism of CI assembly in *Drosophila* flight muscles. Specifically, we show that many of the accessory subunits regulate specific stages of CI biogenesis in vivo, such that when their levels of expression are reduced, CI activity is diminished because of impaired CI assembly. We demonstrate that CI biogenesis in *Drosophila* involves the formation of ~315, ~550, and ~815 kDa assembly intermediates, and that RNAi-mediated knockdown of either dNDUFS2 or dNDUFS3 decreases the amount of the ~315 kDa assembly intermediate that is formed. Furthermore, we show that a specific accessory subunit, dNDUFA5, is required for the formation and/or stabilization of the ~315 kDa assembly intermediate in vivo. Additionally, we define a specific role for another accessory subunit (dNDUFS5) and show that it is required for converting a transient CI assembly intermediate (an ~700 kDa assembly intermediate) into the ~815 kDa assembly intermediate, during one of the terminal steps of CI assembly. Four components of the mitochondrial CI assembly (MCIA) complex (dECSIT, dNDUFAF1, dACAD9, and dTIMMDC1) are associated with the ~700 kDa assembly intermediate, further confirming that it is a true assembly intermediate in CI biogenesis. Importantly, incorporation of dNDUFS5 into CI is necessary to stabilize or promote incorporation of dNDUFA10 into the complex. We also identify several roles for many of the dNDUFB subunits. Altogether, our analyses reveal how studies of CI biogenesis in *Drosophila* can uncover mechanisms of CI assembly in vivo and establish *Drosophila* as an important genetically pliable model organism for addressing questions relevant to mammalian CI biogenesis.

RESULTS

Drosophila Flight Muscles Are Suitable for Studying CI Assembly

CI consists of a hydrophilic matrix arm and a hydrophobic membrane arm that are oriented almost orthogonally to each other (Figure 1A). Subunits with the prefix NDUFA (NDUFA1-3 and NDUFA5-13) were so named as they were originally thought to be part of the matrix arm, whereas the NDUFB subunits (NDUFB1–NDUFB11) are part of the membrane arm. In addition, subunits that are found in the vicinity of the eight Fe-S clusters (NDUFS) or single flavoprotein (NDUFV) are also localized in the matrix. All the NDUFA and NDUFB subunits are accessory subunits (Figure 1A). We used the *Drosophila* RNAi Screening Center Integrative Ortholog Prediction Tool (DIOPT) to identify 42 putative orthologs of the 44 human CI subunits (Figure 1B; Table S1) (Hu et al., 2011). To facilitate comparison with their human orthologs, in this paper we refer to *Drosophila* orthologs of the human CI subunits as dNDUFS1, dNDUFS2, and so on. Their designated gene nomenclature in *Drosophila* is shown in Table S1.

To confirm whether the putative CI orthologs identified by DIOPT were bona fide CI subunits in *Drosophila* flight muscles, we isolated mitochondria from thoraxes of wild-type flies, solubilized their membranes in 1% digitonin, and resolved their oxidative phosphorylation (OXPHOS) complexes into various bands using blue native PAGE (BN-PAGE) (Rera et al., 2011; Wittig et al., 2006). We solubilized the mitochondrial membranes in 1% digitonin because we found that 1% digitonin was the optimal detergent concentration for isolating and resolving OXPHOS complexes in their native state in *Drosophila* (Figure S1), as has been reported previously (Rera et al., 2011; Wittig et al., 2006). Subsequently, we cut out each of the bands detected by Coomassie staining of the gel and identified their composition by mass spectrometry (Figure 1C). We confirmed the existence of 37 of the 42 putative CI orthologs on the basis of their presence in the band corresponding to the CI holoenzyme (band B) and/or supercomplex (band A) (Figure 1C; Tables S1 and S2). Notably, the *Drosophila* ortholog of NDUFA4 (NDMNLL), a protein that was previously considered a CI subunit but has been reassigned as a complex IV (CIV) subunit (Balsa et al., 2012), co-migrated with the CIV band (band E) (Figure 1C; Table S2). In addition, four of the subunits we were unable to detect are highly hydrophobic membrane-embedded core subunits encoded in the mitochondrion (ND2, ND3, ND4L, and ND6); thus they may have escaped detection because of their highly hydrophobic nature. Interestingly, these subunits were not identified in a previous proteomic analysis of CI in mouse cell lines (Balsa et al., 2012).

Coomassie- or silver-stained native gels containing mitochondrial protein complexes from flies expressing RNAi to CI, complex III (CIII), CIV, and complex V (CV) proteins further confirmed the identities of the bands cut for mass spectrometry (Figure 1D). Because our mass spectrometry data suggested that a portion of CI might be co-migrating with CV and possibly CIII, we tested whether this co-migration was the result of supercomplex formation. We were unable to find antibodies that cross-react with any of the *Drosophila* CIII proteins, but antibodies that cross-react with dNDUFS3 (a CI protein) and dATPsynβ (a CV protein) were commercially available and were used to examine the identity of "band A" via western blotting. As is evident in the silver staining gel (Figure 1D), immunoblotting revealed that "band A" was actually a doublet, and the lower band in the doublet corresponds to a dimer of CV, as has been observed in other contexts (Figure 1E) (Rera et al., 2011; Wittig et al., 2006). In addition, CI in flight muscles was found to exist predominantly as the holoenzyme, with a relatively small portion involved in CI-CIII supercomplex formation, which migrates as an upper band in the doublet (Figure 1E). Notably, the observation that CI in *Drosophila* flight and skeletal muscles occurs predominantly as the holoenzyme (i.e., free CI, not involved in supercomplex formation) contrasts markedly with CI in cardiac or skeletal muscles from mice, in which a significant portion of CI is trapped in supercomplex formation (Figure 1F). Thus, in addition to the genetic capabilities of *Drosophila*, and the fact that it has a comparable number of CI subunits as the human enzyme, it is a suitable model for studying CI assembly because most CI in flight muscles exists as the holoenzyme. Accordingly, a defect in CI biogenesis can easily be scored and quantified. Consequently, we decided to examine the role of the nuclear-encoded CI subunits in CI assembly.

Disruption of Several CI Subunits in Flight Muscles Impairs CI Assembly

We found that loss-of-function alleles for many *Drosophila* CI genes are lethal (not shown). Therefore, to ascertain which CI

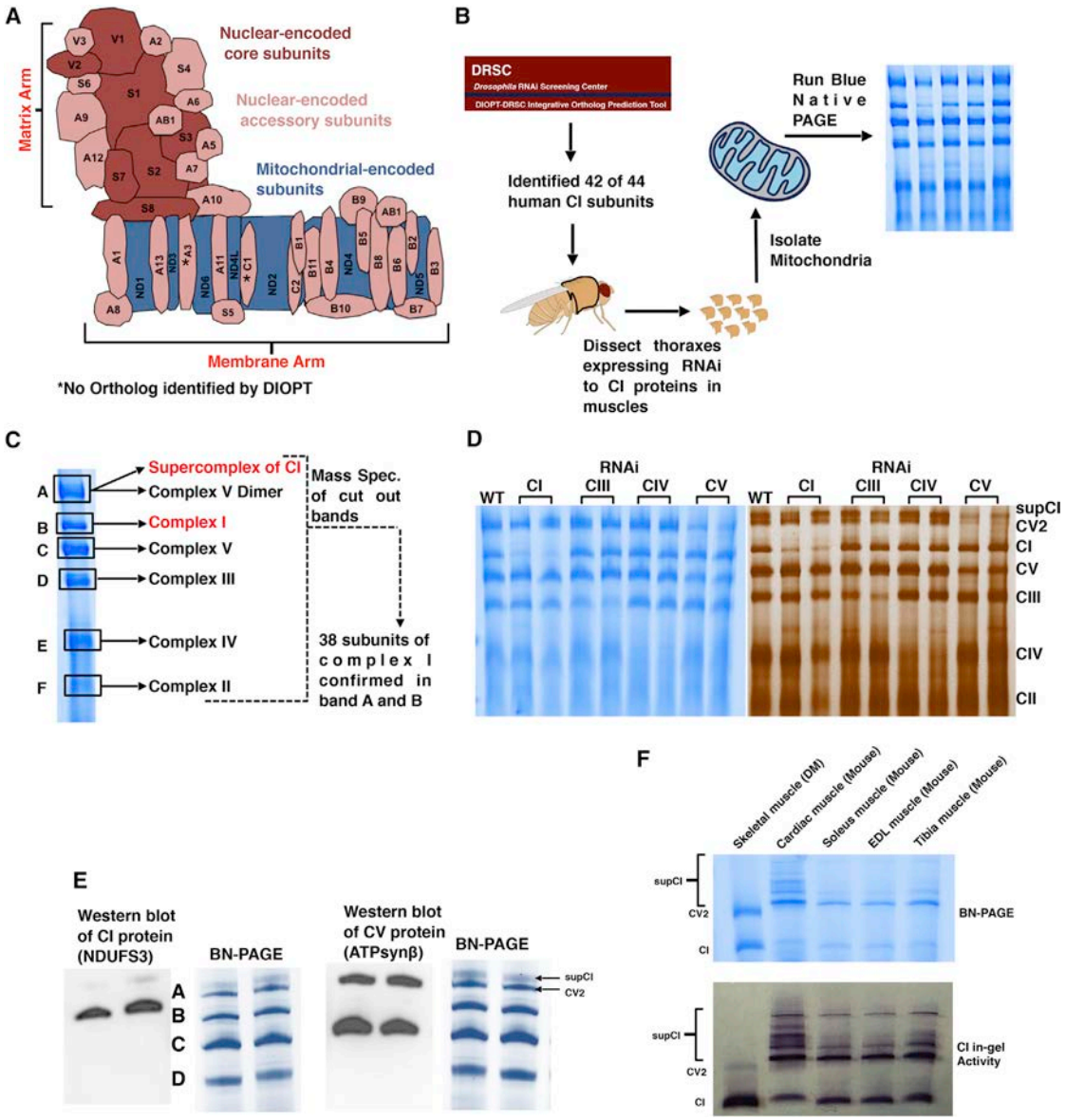

Figure 1. *Drosophila* Flight Muscles Are Suitable for Studying Complex I Assembly

(A) Schematic representation of how the 44 distinct subunits of bovine or ovine CI are arranged to produce the L-shaped topology; based on recent CI structures described (Fiedorczuk et al., 2016; Vinothkumar et al., 2014; Zhu et al., 2016; Zickermann et al., 2015). The asterisk denotes subunits for which an ortholog was not identified in *Drosophila* by DIOPT. NDUFAB1 occurs twice in the complex, giving rise to a total of 45 subunits.

(B) Summary of the experimental procedure for studying CI assembly in *Drosophila*. Transgenic RNAi constructs to the nuclear-encoded subunits were expressed specifically in thoracic muscles using the *mhc-Gal4* driver. Mitochondria were isolated from thoraxes of 1-week-old flies, solubilized in 1% digitonin, and analyzed by blue native PAGE (BN-PAGE).

(C) The constituents of each of the six major bands observed during BN-PAGE was analyzed by MS. Thirty-eight subunits of *Drosophila* CI were confirmed by MS. The 38 subunits correspond to 37 different orthologs of human CI. Two paralogs of human NDUFV1 were confirmed by MS (see Table S1). See Table S2 for all the peptides identified in the six major bands shown.

(D) BN-PAGE (left) and silver staining (right) of samples from thoraxes following RNAi-mediated knockdown of complex I (CI), complex III (CIII), complex IV (CIV), and complex V (CV) proteins to confirm the identities of the bands. SupCI and CV2 denote a supercomplex of CI and a dimer of CV, respectively. The exact RNAi constructs expressed starting from left to right were to the white gene (wild-type [WT]), dNDUFV1 (CI), dNDUFS1 (CI), dUQCRC-2 (CIII), dUQCRC-Q (CIII), dCox5A (CIV), cyclope (CIV), dATPsyn-β (CV), and ATPsyn-b (CV).

(E) Immunoblotting with anti-NDUFS3 and anti-ATPsynβ antibodies of native gels to detect CI and CV, respectively. Note that band A is a doublet consisting predominantly of a dimer of CV and a supercomplex of CI.

(F) BN-PAGE (top) and CI in-gel enzyme activity (bottom) indicate that most of CI exists as the holoenzyme in *Drosophila melanogaster* (DM) skeletal muscles, in contrast to cardiac, soleus, extensor digitorum longus (EDL), and tibia muscles from mice where a significant portion of CI exists as a supercomplex.

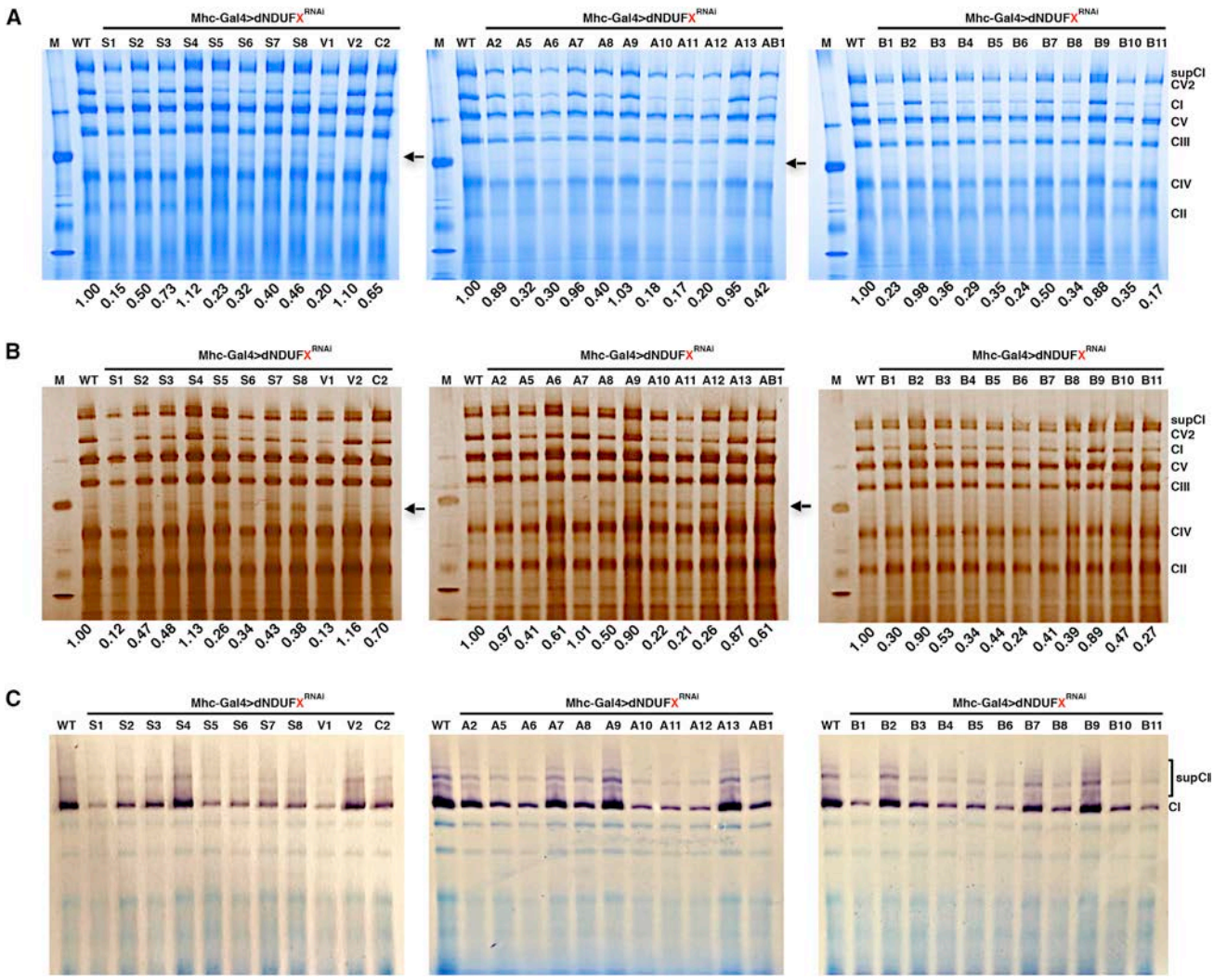

Figure 2. Disruption of Several CI Core and Supernumerary Subunits Impairs CI Assembly in *Drosophila*

(A) BN-PAGE, (B) silver staining, and (C) CI in-gel enzyme activity of mitochondria isolated from thoraxes following RNAi-mediated knockdown of the CI proteins indicated (*mhc-Gal4>dNDUFX^{RNAi}*). The values listed below each lane indicate the residual amount of CI normalized to the amount in the wild-type (*mhc-Gal4>w^{1118}*) lane.

subunits are required for CI biogenesis in *Drosophila*, we used the Gal4/UAS system to express transgenic RNAi constructs (henceforth referred to as *UAS-RNAi* lines) to both core and accessory CI subunits (Brand and Perrimon, 1993). We examined the effect of knocking down the subunits specifically in muscles (using either *Dmef2-Gal4* or *mhc-Gal4*). Transgenic expression of many of the *UAS-RNAi* constructs using *Dmef2-Gal4*, a muscle-restricted Gal4 driver that is expressed strongly throughout development, caused lethality (not shown). However, a genetic cross between each of the *UAS-RNAi* lines and *mhc-Gal4* produced viable flies, as the *mhc-Gal4* driver has a weaker expression relative to *Dmef2-Gal4* during the initial larval stages (Figure S2). Accordingly, we decided to analyze CI assembly in mitochondria isolated from thoraxes of *mhc-Gal4/UAS-CI^{RNAi}* flies (henceforth referred to as *mhc>CI^{RNAi}* flies) using BN-PAGE.

We observed that in general, both core and accessory subunits produced CI assembly defects whenever the extent of transcript knockdown was more than 50% (Figure 2A). To further assess the extent of the CI assembly deficit for each subunit, we quantified the amount of CI relative to the amount of CV in each lane and normalized it to the corresponding value in the wild-type lane. Interestingly, this revealed that some of the most robust CI assembly deficits were observed when accessory or supernumerary subunits (such as dNDUFA10–12 and dNDUFB4–6) were genetically impaired (Figures 2A and 2B). Similar results were obtained with silver staining of the protein complexes in the native gels (Figure 2B). Finally, in-gel CI enzyme activity assay revealed that the assembly deficits correlated with a reduction in CI activity (Figure 2C). Altogether, these results indicate that many of the core and accessory subunits are essential for viability and biogenesis of the CI holoenzyme or

supercomplex in flight muscles. Accordingly, we turned our attention toward elucidating the mechanism of CI assembly in *Drosophila* flight muscles.

Proteomic Analyses and Immunoblotting Identify Assembly Intermediates of CI

Studies from some mammalian cell lines have shown that CI biogenesis proceeds via a series of assembly intermediates that combine with each other, or other subunits, to form the ~950 kDa boot-shaped holoenzyme. The assembly intermediates generally correspond to partial or complete domains of the three functional modules of CI. The NADH dehydrogenase module (N module) is located at the tip of the matrix arm and is the site of NADH oxidation. Situated between the N module and the membrane is the Q module, which is responsible for ubiquinone reduction. The proton-conducting P module in the membrane arm can be subdivided into a proximal P_P module (roughly corresponding to the first half of the P module that connects with the Q module) and a distal P_D module (Figure 3A).

The current model posits that CI assembly in mammalian systems begins with the formation of a small assembly intermediate containing NDUFS2 and NDUFS3, which combines with NDUFS7 and NDUFS8 (Figure 3B). This assembly intermediate is the primary component of the Q module and ultimately combines with ND1 to form an ~315 kDa assembly intermediate that is anchored to the mitochondrial inner membrane. The ~315 kDa assembly intermediate combines with an independently formed ~370 kDa assembly intermediate to form an ~550 kDa assembly intermediate (Figure 3B). The ~550 kDa assembly intermediate, which consists of the complete Q module and a portion of the P module, grows by the addition of more subunits to form the ~815 kDa assembly intermediate, via mechanisms that are very poorly defined. At this point, the ~815 kDa assembly intermediate is generally considered to be composed of the complete Q and P modules. Finally, an independently formed assembly intermediate consisting of NDUFS1, NDUFV1, NDUFV2, NDUFV3, NDUFS4, NDUFS6, and NDUFA12, which together form the N module, is added as a "cap" to the ~815 kDa assembly intermediate to produce the ~950 kDa holoenzyme (Figure 3B; the ~315, ~370, ~550, and ~815 kDa assembly intermediates were previously estimated as ~400, ~460, ~650, and ~830 kDa subcomplexes, respectively; Andrews et al., 2013; Vartak et al., 2014).

Because some flight muscles are formed by 24 hr after pupal formation (Roy and VijayRaghavan, 1999), we decided to ascertain the extent of CI biogenesis starting at 48 hr (i.e., 2 days) postpupariation. Specifically, we isolated mitochondria at various time points and examined CI assembly via western blotting of the native complexes. Because current models of mammalian CI assembly postulate that NDUFS3 and ND1 are both part of the ~815, ~550, and ~315 kDa assembly intermediates, western blot with anti-NDUFS3 or anti-ND1 antibodies will be expected to detect these three assembly intermediates and possibly lower molecular weight assembly intermediates (if the respective epitopes are not masked when the assembly intermediate is formed). In addition, the fully assembled CI and CI-containing supercomplexes will be expected to be detected as well. Indeed, immunoblotting with anti-NDUFS3 revealed that a portion of CI is assembled during pupal development and continues during the first 48 hr after flies eclose (emerge as adults from pupae) (Figure 3C). Although we were able to detect the ~315 and ~550 kDa assembly intermediates with the anti-ND1 antibody (Figure 3C), the higher molecular weight bands were only weakly detectable, conceivably because the epitope to which this antibody was raised for this hydrophobic subunit becomes less exposed to the aqueous environment during the final stages of CI biogenesis (Figure 3C). Moreover, although we were able to detect subcomplexes of CV that migrate with an apparent mass of about 100 kDa at this stage of development (Figure S3), we were unable to detect dNDUFS3-containing assembly intermediates with an apparent mass of less than 200 kDa. There are at least two possible explanations for this result: (1) the smaller NDUFS3-containing assembly intermediates may not be present at this stage, or (2) the epitope of dNDUFS3 in the smaller assembly intermediates was inaccessible to the antibody, perhaps as a result of being masked by bound assembly factors and/or other interactors. Therefore, we used proteomic analyses to distinguish between these two possibilities.

Mitochondria were isolated from thoraxes of wild-type flies that had been aged for 24 hr after eclosure and subjected to BN-PAGE. Subsequently, the region of the gel between ~50 and ~350 kDa was excised and divided into 14 slices (labeled fractions A1–A14) for in-gel digestion and subsequent proteomics analyses (Figure 3D). We observed that dNDUFS2, dNDUFS3, and dNDUFS7 co-migrated in fractions corresponding to a mass of approximately 280–320 kDa (Figure 3D; Table S3). Interestingly, the CI assembly factor, dNDUFAF4, was also found in these fractions (Figure 3D; Table S3). In addition, dNDUFA5 co-migrated with dNDUFS2, dNDUFS3, and dNDUFS7 (Figure 3D), confirming that it is a component of the ~315 kDa assembly intermediate in vivo. Importantly, although several other CI subunits migrated in fractions corresponding to a mass of approximately 50–250 kDa, neither dNDUFS2 nor dNDUFS3 was found in these fractions. Thus, it appears that in an in vivo context, in *Drosophila* flight muscles, the constituents of the ~315 kDa assembly intermediate are combined almost synchronously.

Specific Subunits Regulate the Biogenesis or Stability of Specific Assembly Intermediates of CI

If the assembly intermediates observed are bona fide intermediates in the pathway of CI assembly in *Drosophila*, then at least some of these assembly intermediates will stall and accumulate, or they may disintegrate when specific CI subunits that are required for CI assembly are disrupted (Figure 4A). To test this hypothesis, we analyzed the CI assembly intermediates from thoraxes of *Mhc>CI^{RNAi}* flies 24 hr after eclosure using an anti-NDUFS3 antibody. As expected, the various subunits that produced CI assembly deficits in Figure 2 also resulted in a reduction of the level of the holoenzyme or the CI-containing supercomplex (Figures 4B–4F).

Disruption of dNDUFS1 and dNDUFV1, which are components of the N module of CI and are thus expected to be added as part of the "cap" during the final step in CI assembly, resulted in a stalling and accumulation of the ~815 kDa assembly

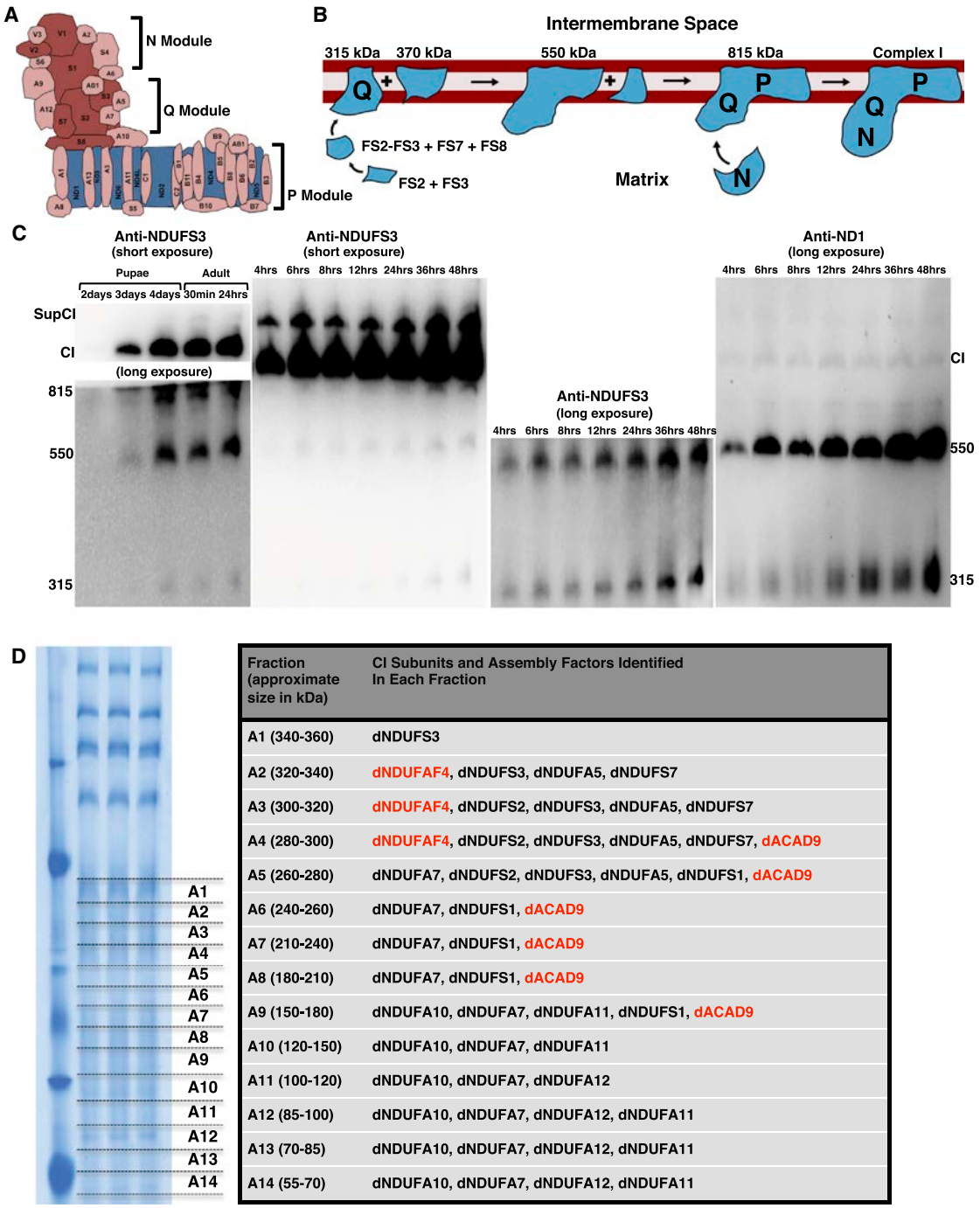

Fraction (approximate size in kDa)	CI Subunits and Assembly Factors Identified In Each Fraction
A1 (340-360)	dNDUFS3
A2 (320-340)	dNDUFAF4, dNDUFS3, dNDUFA5, dNDUFS7
A3 (300-320)	dNDUFAF4, dNDUFS2, dNDUFS3, dNDUFA5, dNDUFS7
A4 (280-300)	dNDUFAF4, dNDUFS2, dNDUFS3, dNDUFA5, dNDUFS7, dACAD9
A5 (260-280)	dNDUFA7, dNDUFS2, dNDUFS3, dNDUFA5, dNDUFS1, dACAD9
A6 (240-260)	dNDUFA7, dNDUFS1, dACAD9
A7 (210-240)	dNDUFA7, dNDUFS1, dACAD9
A8 (180-210)	dNDUFA7, dNDUFS1, dACAD9
A9 (150-180)	dNDUFA10, dNDUFA7, dNDUFA11, dNDUFS1, dACAD9
A10 (120-150)	dNDUFA10, dNDUFA7, dNDUFA11
A11 (100-120)	dNDUFA10, dNDUFA7, dNDUFA12
A12 (85-100)	dNDUFA10, dNDUFA7, dNDUFA12, dNDUFA11
A13 (70-85)	dNDUFA10, dNDUFA7, dNDUFA12, dNDUFA11
A14 (55-70)	dNDUFA10, dNDUFA7, dNDUFA12, dNDUFA11

Figure 3. Proteomic Analyses and Immunoblotting Identify Assembly Intermediates of CI

(A) Schematic of CI showing the three modules of the enzyme. The NADH dehydrogenase module (N module) is located at the tip of the matrix arm and is the site of NADH oxidation. Situated between the N module and the membrane arm is the Q module, which is responsible for ubiquinone reduction. The proton-conducting P module is in the membrane arm.

(B) The current model of CI assembly in mammalian systems (reviewed in Vartak et al., 2014). The assembly process begins with the formation of an assembly intermediate containing NDUFS2 and NDUFS3, which combines with NDUFS7 and NDUFS8. The subcomplex of NDUFS2, NDUFS3, NDUFS7, and NDUFS8 ultimately combines with ND1 to form the ~315 kDa assembly intermediate that is anchored to the membrane. The ~315 kDa subcomplex (also called the Q module) combines with an independently formed ~370 kDa assembly intermediate to form an ~550 kDa assembly intermediate. This assembly intermediate that consists of the Q module and part of the P module grows by the addition of more subunits to form the ~815 kDa assembly intermediate, via mechanisms that are very poorly defined. The ~815 kDa assembly intermediate now consists of the complete Q and P modules. Finally, the N module is added to produce the 950 kDa

(legend continued on next page)

intermediate (Figure 4B). However, unexpectedly, disruption of dNDUFA6 and dNDUFA12 also stalled the ~815 kDa subcomplex (Figure 4C). RNAi-mediated knockdown of dNDUFS2, dNDUFS3, dNDUFS5, dNDUFS7, and dNDUFS8 led to a reduction in the amount of the ~815 kDa assembly intermediate (relative to wild-type), as they impaired some of the initial steps of CI biogenesis (Figure 4B). In addition, the amount of the ~315 kDa assembly intermediate was drastically reduced when the expression of dNDUFS2, dNDUFS3, or dNDUFS7 was impaired (Figure 4B), in line with our proteomic results in Figure 3D and current mammalian CI assembly models that show that the first step in CI biogenesis involves the formation of an assembly intermediate consisting of NDUFS2 and NDUFS3 (Figure 3B) (reviewed in Vartak et al., 2014). Notably, we found that RNAi-mediated knockdown of dNDUFA5 depleted the ~315 kDa assembly intermediate (Figure 4C). Combining this result, with our proteomic data showing that dNDUFA5 co-migrates with dNDUFS2, dNDUFS3, and dNDUFS7 (Figure 3D), we conclude that although dNDUFA5 is an accessory subunit, it is a critical component of, and required for formation or stabilization of the ~315 kDa assembly intermediate (i.e., the Q module) in vivo.

Disruption of most of the dNDUFB subunits did not markedly alter the stability or extent of accretion of the CI assembly intermediates 24 hr after eclosion (Figure 4D), but by 48 and 72 hr after eclosion some notable and consistent phenotypes between the two time points were observed (Figures 4E and 4F). For instance, RNAi-mediated disruption of dNDUFB3 decreased the extent of accumulation of all the assembly intermediates, and the 550 kDa assembly intermediate accumulated when dNDUFB1, dNDUFB8, and dNDUFB11 were impaired at both time points (i.e., 48 and 72 hr post-eclosion). Surprisingly, although none of the NDUFB subunits are known to be part of the 315 kDa assembly intermediate, the extent of accumulation of the 315 kDa assembly intermediate was diminished when the expression of dNDUFB1, dNDUFB4, dNDUFB5, dNDUFB6, and dNDUFB10 were reduced (Figures 4E and 4F). Taken together, these results indicate that specific subunits regulate the biogenesis or stability of specific CI assembly intermediates during CI assembly in *Drosophila* thoraxes.

Identification of an ~700 kDa Assembly Intermediate of CI in *Drosophila*

An assembly intermediate that accumulates between the ~550 and ~815 kDa assembly intermediates was detected on immunoblots of samples from *mhc>dNDUFS5^{RNAi}* and *mhc>dNDUFC2^{RNAi}* thoraxes (Figure 4B). We estimate its size to be ~700 kDa because it co-migrates with CV, previously estimated to be ~700 kDa in blue native gels (Figure 5A) (Abdrakhmanova et al., 2006). The accumulation of the ~700 kDa assembly intermediate in samples from *mhc>dNDUFS5^{RNAi}* thoraxes was notable, because it suggested that this could be the point of entry of dNDUFS5 during CI assembly. NDUFS5 is a membrane-associated accessory subunit that extends into the intermembrane space; it is currently unclear at what point it becomes incorporated into CI. In contrast to the ~315, ~550, and ~815 kDa assembly intermediates, the ~700 kDa assembly intermediate was not readily perceptible by anti-NDUFS3 immunoblotting in the wild-type sample or most of the other mutant samples isolated 24 hr after eclosure (Figure 4B). This raised the possibility that it could simply be a degradation product, perhaps emanating from the ~815 kDa assembly intermediate.

To determine whether the ~700 kDa assembly intermediate is a true assembly intermediate, we decided to look at earlier time points (6 and 12 hr post-eclosion) to ascertain whether it ever appears in wild-type samples. Immunoblotting at these time points revealed that accumulation of the ~700 kDa assembly intermediate in *mhc>dNDUFS5^{RNAi}* thoraxes is present by the 6 hr time point and gradually tapers off afterward (Figure 5B). Importantly, at the 6 hr time point, a faint band corresponding to the ~700 kDa assembly intermediate can be observed in wild-type samples, indicating that the ~700 kDa assembly intermediate exists in wild-type samples and rapidly matures to the ~815 kDa assembly intermediate. The stalling of the ~700 kDa assembly intermediate in *mhc>dNDUFS5^{RNAi}* thoraxes occurred concurrently with an accumulation of both the ~550 and ~315 kDa assembly intermediates, and a diminution of the ~815 kDa assembly intermediate relative to wild-type levels. Thus, dNDUFS5 may be required for converting the ~700 kDa assembly intermediate into the ~815 kDa assembly intermediate, such that when this fails, there is a backlog of the ~700, ~550, and ~315 kDa assembly intermediates. To test this hypothesis, we compared the assembly intermediates that accumulate in *mhc>dNDUFS5^{RNAi}, dNDUFS1^{RNAi}* and *mhc>dNDUFS5^{RNAi},dNDUFV1^{RNAi}* thoraxes with that in *mhc>dNDUFS1^{RNAi}* and *mhc>dNDUFV1^{RNAi}* thoraxes, respectively. We reasoned that because the ~815 kDa assembly intermediate accumulates in *mhc>dNDUFS1^{RNAi}* and *mhc>dNDUFV1^{RNAi}* thoraxes (Figure 4B), if dNDUFS5 is required for converting the ~700 kDa assembly intermediate into the ~815 kDa assembly intermediate, then the extent of accumulation of the ~815 kDa assembly intermediate in either *mhc>dNDUFS5^{RNAi},dNDUFS1^{RNAi}* and/or *mhc>dNDUFS5^{RNAi}, dNDUFV1^{RNAi}* thoraxes should be reduced relative to *mhc>dNDUFS1^{RNAi}* and *mhc>dNDUFV1^{RNAi}*, respectively. In agreement with this proposition, we observed that the accumulation of the ~815 kDa assembly intermediate was significantly

fully assembled complex. Assembly factors or chaperones that assist in this process but are not present in the fully assembled complex have been omitted for clarity.

(C) Western blot of samples obtained from thoraxes from pupae aged between 2 and 4 days after pupariation and of flies from 0.5 to 48 hr post-eclosure to detect the assembly intermediates, fully assembled CI, and a supercomplex containing complex I (supCI) after BN-PAGE. The anti-NDUFS3 antibody strongly detects CI and supCI and weakly detects the ~315, ~550, and ~815 kDa assembly intermediates after a short exposure. However, after a longer exposure, the ~315 and ~550 kDa assembly intermediates can clearly be seen. At right, the membrane was stripped and re-probed with anti-NDI. Anti-ND1 detects the ~315 and ~550 kDa assembly intermediates and a very faint band corresponding to CI. (D) Proteomic analyses of assembly intermediates that form in the native gel sized between ~50 and ~350 kDa. See Table S3 for all the peptides identified. 220

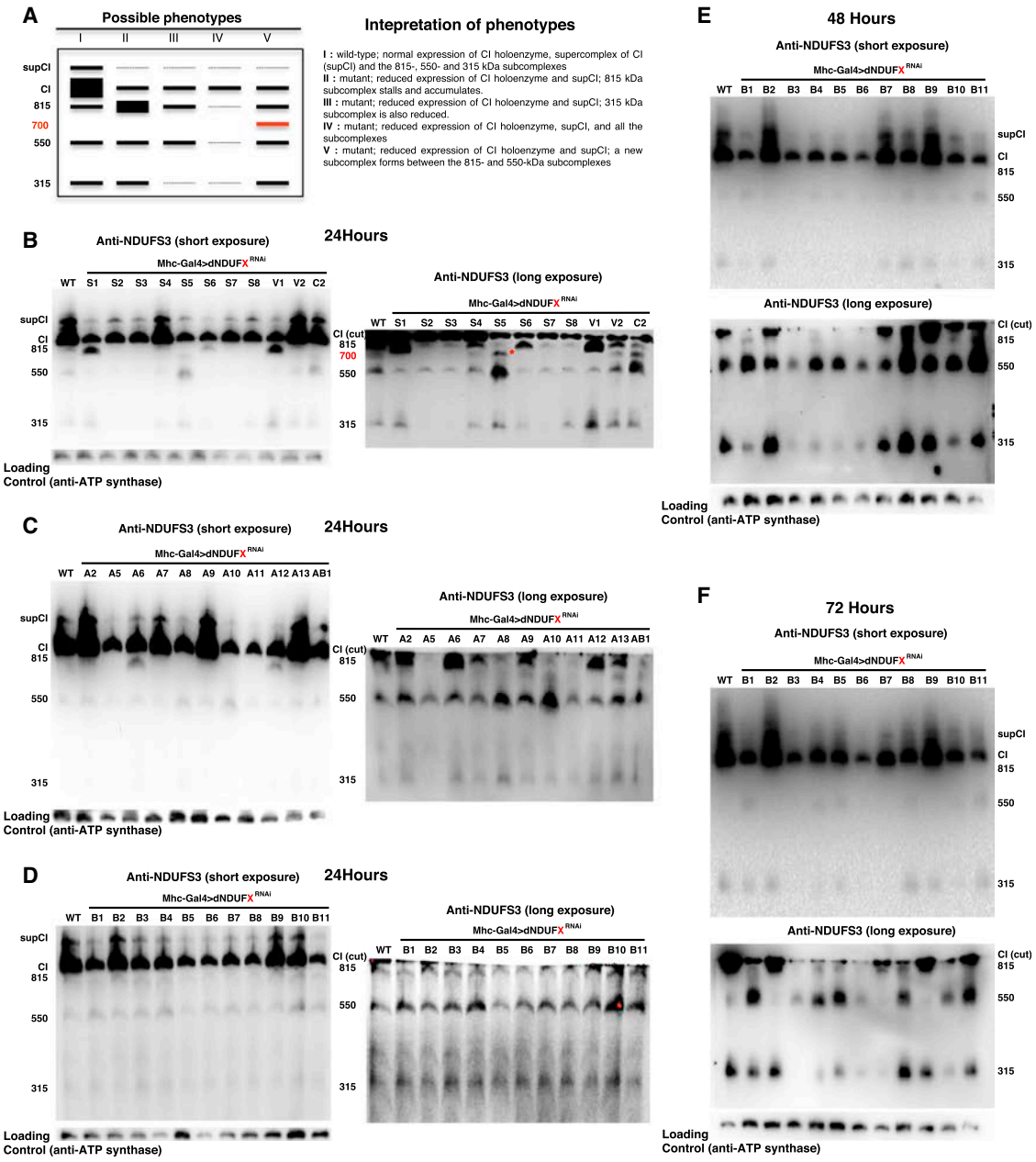

Figure 4. Specific Subunits Regulate the Biogenesis or Stability of Specific Assembly Intermediates of CI

(A) Left: schematic of the distribution of assembly intermediates on immunoblots as a result of RNAi-mediated disruption of various CI subunits. Right: description of how various results can be interpreted.

(B–D) Distribution of assembly intermediates in thoraxes dissected 24 hr after eclosion with transgenic RNAi expression of the CI subunits shown. In panels labeled "long exposure," the region of the membrane just at or below CI was cut and imaged.

(B) The ~815 kDa assembly intermediate accumulates in thoraxes expressing transgenic RNAi to dNDUFS1 and dNDUFV1; and the ~315 kDa assembly intermediate is decreased in thoraxes expressing transgenic RNAi of dNDUFS2, dNDUFS3, and dNDUFS7. In addition, another assembly intermediate accumulates in thoraxes expressing RNAi to dNDUFS5 and dNDUFC2 (denoted by an asterisk).

(C) The ~815 kDa assembly intermediate stalls in thoraxes expressing transgenic RNAi to dNDUFA6 and dNDUFA12; and the ~315 kDa assembly intermediate is attenuated in thoraxes expressing transgenic RNAi of dNDUFA5.

(D) There were no overt alterations in assembly intermediates at this time point when the dNDUFB subunits were disrupted.

(E and F) Distribution of assembly intermediates in thoraxes dissected 48 hr (E) and 72 hr (F) after eclosion with transgenic RNAi expression of the NDUFB subunits shown. RNAi-mediated knockdown of the expression of dNDUFB3 decreased the extent of accumulation of all the assembly intermediates, and the 550 kDa assembly intermediate accumulated when the expression of dNDUFB1, dNDUFB8 and dNDUFB11 were reduced. In addition, the extent of accumulation of the 315 kDa assembly intermediate was diminished following RNAi-mediated disruption of dNDUFB1, dNDUFB4, dNDUFB5, dNDUFB6, and dNDUFB10 at both the 48 and 72 hr time points.

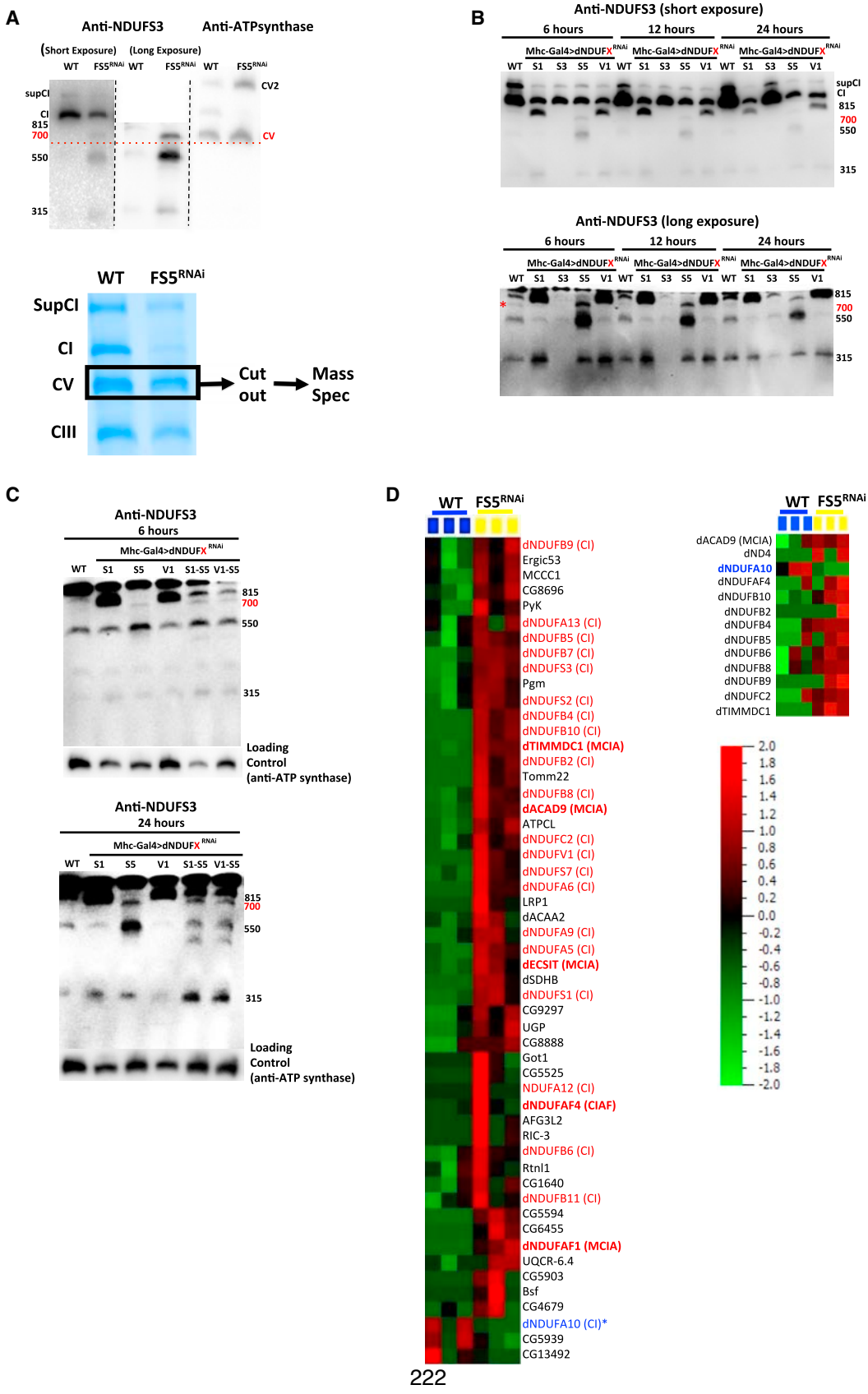

(legend on next page)

attenuated in *mhc>dNDUFS5^{RNAi},dNDUFS1^{RNAi}* thoraxes relative to *mhc>dNDUFS1^{RNAi}* thoraxes (Figure 5C). This was also accompanied by an accumulation of the ~700 kDa assembly intermediate (Figure 5C). Similar results were obtained by comparing *mhc>dNDUFS5^{RNAi},dNDUFV1^{RNAi}* and *mhc>dNDUFV1^{RNAi}* thoraxes (Figure 5C). Accordingly, we deduce from these results that when dNDUFS5 expression levels are impaired, the transient ~700 kDa assembly intermediate stalls and accumulates, impeding progression of CI biogenesis and ultimately resulting in a bottleneck of the ~550 and ~315 kDa assembly intermediates as well.

To gain further insight into the identity of the ~700 kDa assembly intermediate, a single gel slice encompassing the region shown in Figure 5A was excised from native gels containing samples from wild-type and *mhc>dNDUFS5^{RNAi}* thoraxes. Proteins from the gel slice were digested and analyzed by liquid chromatography (LC) mass spectrometry (MS), and a label-free spectral counting approach was used to generate a heatmap for some of the proteins that showed altered expression levels between the samples. In agreement with our results showing a stalling and accumulation of the ~700 kDa assembly intermediate in this portion of the gel, we observed that several CI subunits were upregulated in the *mhc>dNDUFS5^{RNAi}* sample relative to wild-type (Figure 5D). However, in stark contrast to the other CI subunits, we consistently observed (in six biological replicates taken at different time points of the day to control for circadian regulation) that dNDUFA10 was downregulated in the *mhc>dNDUFS5^{RNAi}* sample, indicating that incorporation of dNDUFS5 into CI is necessary to stabilize or promote incorporation of dNDUFA10 into the complex (Figure 5D). In mammalian systems, at least five CI assembly factors—ECSIT, TMEM126B, NDUFAF1, ACAD9, and TIMMDC1—are typically found associated with CI assembly intermediates and have been dubbed the mitochondrial complex I assembly (MCIA) complex (Guarani et al., 2014; Heide et al., 2012; Nouws et al., 2010; Vogel et al., 2007). We found four of these assembly factors (dECSIT, dNDUFAF1, dACAD9, and dTIMMDC1) associated with the 700 kDa assembly intermediate that were upregulated in the *mhc>dNDUFS5^{RNAi}* samples, further confirming that it is a true assembly intermediate in CI biogenesis (Figure 5D; Table S4).

The Distal Portion of the Membrane Arm of CI Is Assembled Independently of the Matrix Arm

We noticed that in some instances in which CI assembly was impaired, an additional band accumulated between the CIII and CIV bands in both the Coomassie- and silver-stained gels (arrows in Figures 2A and 2B). A closer examination revealed that the accumulation of this intermediate was more readily evident in samples in which subunits localized to the hydrophilic matrix domain were disrupted (i.e., the dNDUFS, dNDUFV, and dNDUFA subunits) (Figure 1A). In line with our observations described in Figures 3, 4, and 5, we hypothesized that this band was likely another CI assembly intermediate that had stalled and accumulated as a result of a block in CI biogenesis. We decided to identify the constituents of this putative assembly intermediate via MS.

We cut out the region of the gel corresponding to the stalled assembly intermediate in the wild-type, *mhc>dNDUFS5^{RNAi}*, and *mhc>dNDUFV1^{RNAi}* thoraxes (Figure 6A) and used label-free quantification of peptides to ascertain which subunits and possibly assembly factors were altered between the two samples. Several components of the ETC machinery were downregulated, but there was a dramatic increase in CI subunits that are part of the distal membrane domain (i.e., all the dNDUFB subunits as well as dNDUFAB1, dNDUFC2, ND4, and ND5) (Figures 6B and 6C; Table S5). We note that there was no obvious accumulation of this assembly intermediate in blue native or silver-stained gels when any of these subunits (i.e., the dNDUFB subunits or NDUFAB1 and NDUFC2 subunits) were disrupted (Figures 2A and 2B). Notably, many of these membrane-associated subunits were present in the corresponding gel slice from the wild-type samples (although at lower levels). All the components of the MCIA complex (i.e., dECSIT, dNDUFAF1, dACAD9, dTMEM126B, and dTIMMDC1) were also found associated with this assembly intermediate. Based on current assignments of the various CI subunits, this assembly intermediate is clearly the distal portion of the membrane arm (Fiedorczuk et al., 2016; Vinothkumar et al., 2014; Zhu et al., 2016; Zickermann et al., 2015).

Figure 5. Identification of an ~700 kDa Assembly Intermediate of CI in *Drosophila*

(A) Top: immunoblots of samples obtained from wild-type and mhc>dNDUFS5^{RNAi} thoraxes of flies aged for 6 hr after eclosure depicting co-migration of the ~700 kDa intermediate and CV. Left and middle: anti-NDUFS3 antibodies detect the fully assembled CI, the ~700 kDa subcomplex, and other assembly intermediates in dNDUFS5^{RNAi} thoraxes. Note that in the middle, the region of the membrane just below CI was cut and imaged. Right: anti-ATPsynβ detects the CV monomer (700 kDa) and dimer as shown. Bottom: mitochondrial protein complexes from wild-type and *mhc>dNDUFS5^{RNAi}* thoraxes were resolved by BN-PAGE, and the region corresponding to the ~700 kDa assembly intermediate (i.e., CV, demarcated) was cut out, subjected to tryptic digestion, and analyzed by label-free quantitative LC-MS/MS.

(B) Immunoblots from samples obtained after 6, 12, and 24 hr post-eclosure from thoraxes in which NDUFS1, NDUFS3, NDUFS5, and NDUFV1 were knocked down as a result of transgenic RNAi expression. Note that the ~815 kDa assembly intermediate accumulates as a result of disruption of NDUFS1 and NDUFV1, and the ~700 kDa assembly intermediate stalls and accumulates in NDUFS5 mutants at all time points. Importantly, upon prolonged exposure of the immunoblot, a band corresponding to the ~700 kDa assembly intermediate can also be observed in wild-type samples (denoted with the asterisk in the bottom panel), which confirms that it is an authentic, albeit transient assembly intermediate.

(C) The accumulation of the ~815 kDa assembly intermediate was significantly attenuated *in mhc>dNDUFS5^{RNAi},dNDUFS1^{RNAi}* thoraxes relative to *mhc>dNDUFS1^{RNAi}* thoraxes; instead there is an accumulation of the ~700 kDa assembly intermediate. Similar results were obtained when samples from *mhc>dNDUFS5^{RNAi},dNDUFV1^{RNAi}* thoraxes were compared with samples from *mhc>dNDUFV1^{RNAi}* thoraxes.

(D) Proteomic changes in the gel slice sample from wild-type and *mhc>dNDUFS5^{RNAi}* thoraxes corresponding to the ~700 kDa assembly intermediate. Relative protein abundance among biological samples is expressed by spectral counts on a log scale. Several CI subunits and CIAFs, most notably components of the MCIA complex, are upregulated in the ~700 kDa assembly intermediate. However, the amount of dNDUFA10 (denoted with an asterisk) is reduced in *mhc>dNDUFS5^{RNAi}* thoraxes relative to wild-type. See Table S4 for all the peptides identified.

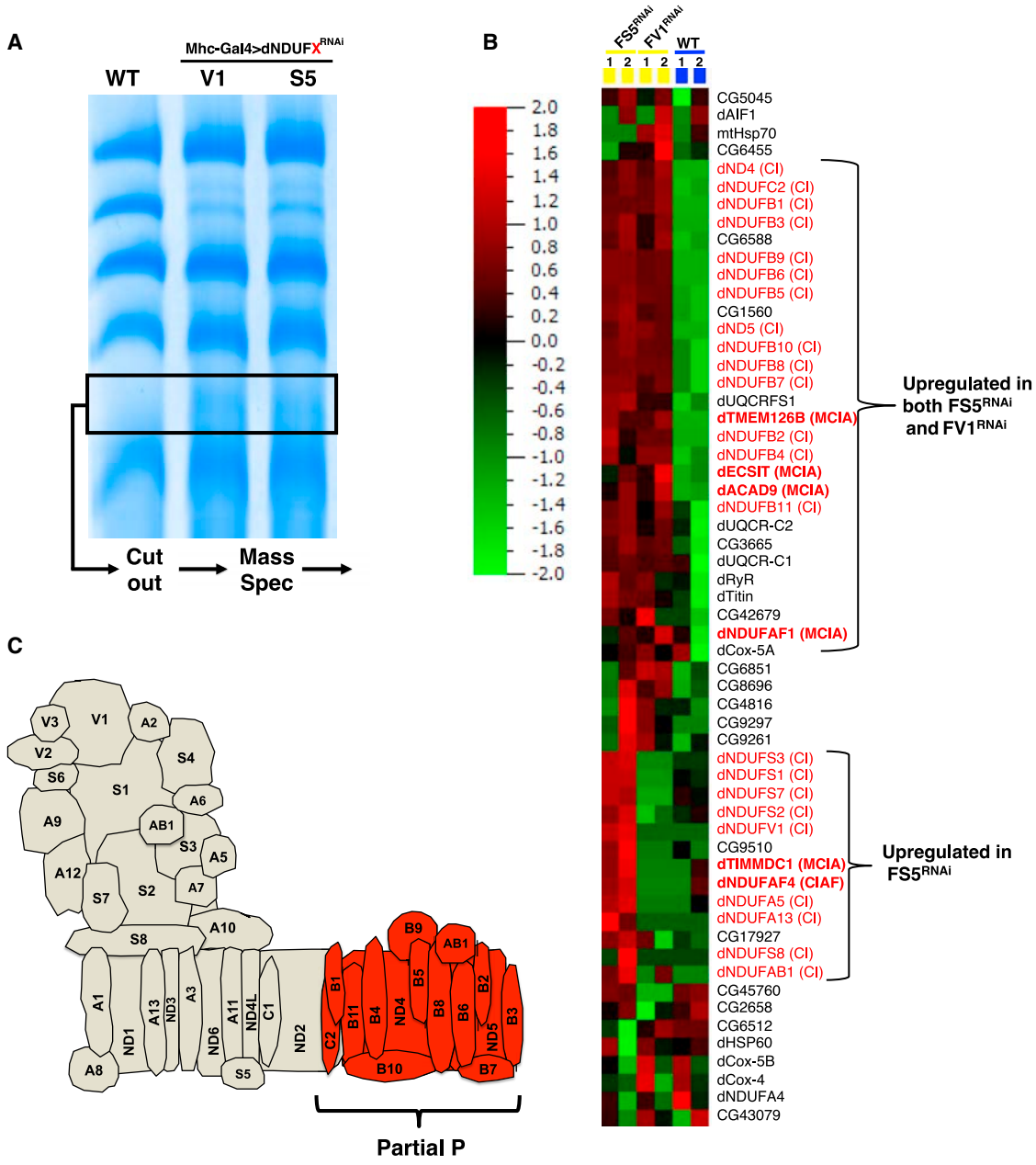

Figure 6. CI Assembly in *Drosophila* Involves an Assembly Intermediate Containing Several Membrane-Associated Accessory Subunits

(A) Mitochondrial protein complexes from wild-type, *mhc>dNDUFS5*^{RNAi}, and *mhc>dNDUFV1*^{RNAi} thoraxes were separated by BN-PAGE, and the region corresponding to the accumulated assembly intermediate (demarcated) was cut out, subjected to tryptic digestion, and analyzed by label-free quantitative LC-MS/MS.

(B) Proteomic changes in the gel slice samples from wild-type, *mhc>dNDUFS5*^{RNAi}, and *mhc>dNDUFV1*^{RNAi} thoraxes. Relative protein abundance among biological samples is expressed by spectral counts on a log scale. The color scale bar indicates the range of protein expression levels. See additional information in Table S5.

(C) Schematic representation highlighting the membrane subunits that are upregulated in the gel slice (shown in red font) from the *mhc>dNDUFS5*^{RNAi} and *mhc>dNDUFV1*^{RNAi} thoraxes.

Proposed Model of CI Assembly in *Drosophila* Muscle

We propose a model for CI assembly in *Drosophila* flight muscles in which dNDUFS2, dNDUFS3, dNDUFS7, dNDUFS8, and dNDUFA5 are combined in essentially one step to form the Q module, which is anchored to the membrane by dND1 (Figure 7). This assembly intermediate corresponds to the assembly intermediate in mammalian systems that was previously referred to as the ~400 kDa subcomplex but has recently been

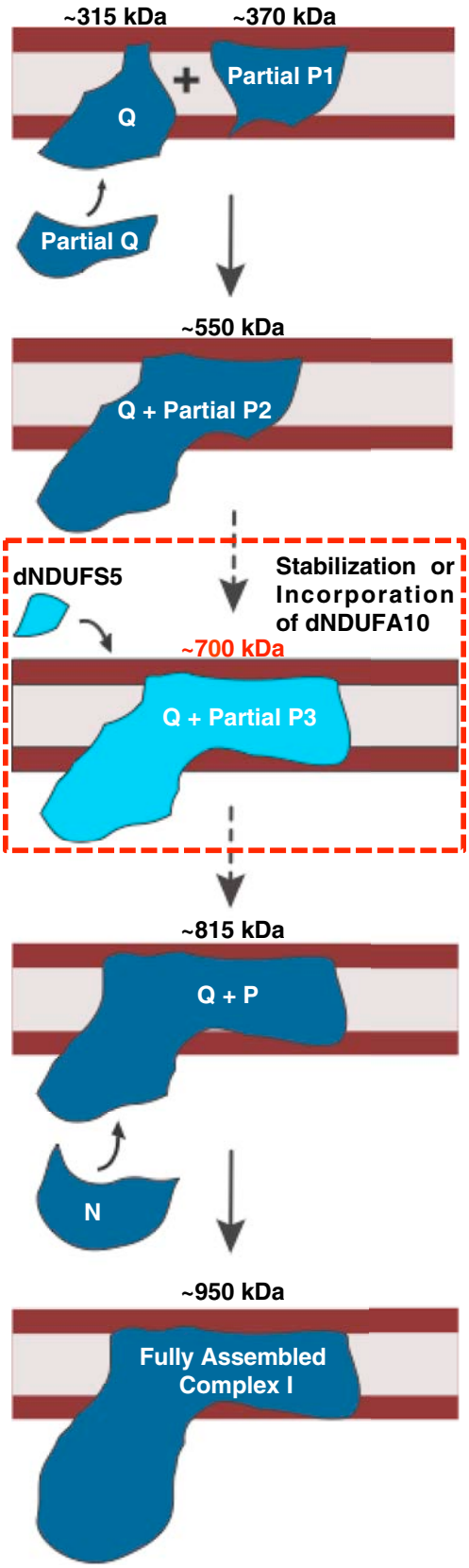

Figure 7. Proposed Model of CI Assembly in *Drosophila* Flight Muscle

An assembly intermediate consisting of dNDUFS2, dNDUS3, dNDUFS7, dNDUFS8, and dNDUFA5 combined in essentially one step to form the Q module, which is anchored to the membrane by ND1. Subsequently, an independently formed subcomplex comprising membrane-associated subunits (partial P1) is conjugated to the Q module, and possibly other subunits, to form an assembly intermediate comprised of the Q module and part of the P module (Q + partial P2). This grows by the addition of more subunits to form a transient assembly intermediate of ~700 kDa (Q + partial P3). We propose that dNDUFS5 is then incorporated at this step, to promote incorporation or stabilization of dNDUFA10. Subsequently, the transient ~700 kDa assembly intermediate is rapidly converted to the ~815 kDa assembly intermediate, consisting of the complete P and Q modules (Q + P). Finally, the N module is added to produce the CI holoenzyme.

re-estimated as the ~315 kDa subcomplex (Andrews et al., 2013; Vartak et al., 2014). This is consistent with the observation that assembly intermediates containing dNDUFS2, dNDUFS3, dNDUFS7, dNDUFS8, and dNDUFA5 co-migrate in blue native gels (Table S2) and that immunoblotting with both anti-ND1 and anti-NDUFS3 detects the ~315 kDa assembly intermediate (Figure 3C).

Subsequently, another assembly intermediate consisting of some of the subunits in the membrane domain is formed. This assembly intermediate comprises part of the P module (i.e., partial P1) and is conjugated to the Q module to form an assembly intermediate that corresponds to the ~550 kDa (formerly ~650 kDa) assembly intermediate previously described in mammalian systems (Figure 7). Although proteomic analyses of the assembly intermediate that accumulates in *mhc>dNDUFS5*^{RNAi} and *mhc>dNDUFV1*^{RNAi} thoraxes shows that all the dNDUFB subunits as well as dNDUFC1, dNDUFAB1, ND4, and ND5 subunits are present in the subcomplex (see Table S5), it is unlikely that all the membrane subunits are incorporated into the complex at this stage under normal (wild-type) conditions. We hypothesize that the accumulation of the membrane accessory subunits in response to genetic disruption of the matrix subunits may be a compensatory mitochondrial stress signaling mechanism impinging on the nucleus and resulting in a system that is poised to rapidly resume CI biogenesis if and when the missing matrix subunit becomes available. The accretion of the partial P module under conditions in which other components of the CI assembly machinery are impaired provides further evidence that the various modules of the complex (i.e., the Q, P, and N modules) are assembled largely independently of each other in vivo.

The ~550 kDa assembly intermediate grows by the addition of more subunits to form a transient assembly intermediate of ~700 kDa (Figure 7); we postulate that dNDUFS5 is then incorporated at or just prior to this stage together with possibly dNDUFA10 to rapidly convert the ~700 kDa assembly intermediate to the ~815 kDa assembly intermediate, consisting of the complete P and Q modules (Figure 7). Finally, the N module is added to produce the CI holoenzyme (Figure 7).

DISCUSSION

We have exploited the genetic capabilities of *Drosophila* to uncover the mechanism of CI assembly in vivo in *Drosophila* flight

muscles. Our immunoblotting and proteomic analyses reveal that during CI assembly in *Drosophila*, the first membrane-bound major assembly intermediate that forms contains at least the following six subunits: dND1, dNDUFS2, dNDUFS3, dNDUFS7, dNDUFS8, and dNDUFA5. On the basis of its constituents and migration pattern in native PAGE, we conclude that this assembly intermediate is the same assembly intermediate traditionally referred to as the ~315 kDa assembly intermediate from studies on mammalian CI assembly and corresponds to the Q module of CI (Andrews et al., 2013; Vartak et al., 2014). Consistent with their roles in regulating formation of the Q module, we found that genetic disruption of dNDUFS2, dNDUFS3, dNDUFA5, and dNDUFS7 attenuated the amount of the ~315 kDa assembly intermediate formed.

Unexpectedly, we found an ~700 kDa assembly intermediate that is short-lived (at least relative to the ~315, ~550, and ~815 kDa assembly intermediates), as it is rapidly converted into the ~815 kDa assembly intermediate. Importantly, our proteomic analyses revealed that incorporation of dNDUFS5 into CI around this stage is necessary to stabilize or promote incorporation of dNDUFA10 into the complex. Similar to the ~315, ~550, and ~815 kDa assembly intermediates, the ~700 kDa subcomplex is a true assembly intermediate, as it can be detected in wild-type muscles as well. Additionally, components of the MCIA complex are associated with the ~700 kDa assembly intermediate, as has been reported for other assembly intermediates observed in mammalian systems. RNAi-mediated disruption of dNDUFS5 led to a stalling and accumulation of this otherwise transient assembly intermediate, to a point at which it is readily detectable by western blots, most likely because this is the stage at or around which dNDUFS5 is incorporated into the complex.

It is possible that mutations in some accessory subunits will have both primary and secondary effects. As a case in point, dNDUFS5 disruption may first impair conversion of the ~700 kDa assembly intermediate to the ~815 kDa assembly intermediate and consequently impair CI assembly (as we have shown), but ultimately, the accumulation of the ~700 kDa assembly intermediate can activate the mitochondrial unfolded protein response as well as other stress signaling cascades, with far-reaching consequences (Haynes et al., 2013; Jensen and Jasper, 2014; Owusu-Ansah and Banerjee, 2009; Owusu-Ansah et al., 2008, 2013). As another example, when dNDUFB3 was disrupted, no specific assembly intermediates were stalled or disintegrated. Instead, there was a general reduction in the level of expression of all assembly intermediates. It is possible that disruption of dNDUFB3 activates stress signaling pathways that induce apoptosis or culminate in a general reduction of protein synthesis, leading to a reduction in CI assembly.

We find that at least 42 of the 44 distinct human CI proteins are conserved in *Drosophila*. The two human CI proteins for which a clear ortholog was not readily identified in *Drosophila* by DIOPT are NDUFA3 (9 kDa) and NDUFC1 (6 kDa), which are two of the smallest subunits of the complex. Interestingly, obvious orthologs of NDUFC1 are not found in *C. elegans* or *Yarrowia lipolytica*, and the orthologs in vertebrates such as zebrafish and *Xenopus* have very weak homology (DIOPT score of 1) to the human protein. Therefore it is possible that this subunit has significant sequence diversion in *Drosophila* and although present was not recognized by DIOPT. For most of the CI subunits in which multiple paralogs were identified by DIOPT (i.e., NDUFS2, NDUFS7, NDUFV2, NDUFA7, and NDUFB2), only one of the paralogs was detected as a bona fide CI subunit in flight muscles. However, as an exception to this general rule, two of the three paralogs of NDUFV1 were detected as part of CI in skeletal muscles via MS. ND-51 (CG9140) appears to be the authentic ortholog of human NDUFV1, as it is highly expressed in skeletal muscles relative to ND-51L (CG11423) and is comparable in size to the human ortholog (both are about 51 kDa). ND-51L is a 77 kDa protein with a stretch of about 200 amino acids at the N terminus that is not present in either the *Drosophila* paralog (ND-51) or human ortholog (NDUFV1). It remains to be determined whether the expression of the subunits with multiple paralogs are regulated in a tissue-specific manner to generate mitochondria with varied CI activities or whether they are regulated in the same tissue in response to different environmental conditions to fine-tune the activity of CI.

In summary, we have described the mechanism of CI assembly in *Drosophila* flight muscles and defined specific roles for some of the accessory subunits in CI assembly. Importantly, although CI dysfunction has been implicated in a large number of pathologies, we find that knocking down the expression of various antioxidant enzymes or mitochondrial protein quality control genes does not solely impair CI assembly, indicating that destabilization of CI may not be the sole underlying factor in many mitochondrial disorders (Figure S4). In addition, our proteomic analyses established that incorporation of dNDUFS5 into CI is necessary to stabilize or promote incorporation of dNDUFA10 into the complex. We note that our analyses of CI assembly in an in vivo setting, in which CI biogenesis is subject to both developmental and environmental cues, revealed that many of the accessory subunits are required for both assembly and viability. Moreover, several NDUFB subunits (dNDUFB1, dNDUFB4, dNDUFB5, dNDUFB6, and dNDUFB10) seem to regulate the stability of the 315 kDa assembly intermediate, in apparent deviation from what will be expected from current models of mammalian CI assembly. However, the mechanism of CI biogenesis in *Drosophila* flight muscles is remarkably similar to what has been described in mammalian systems, and the differences observed here may be due to the fact that we have analyzed CI assembly in an in vivo setting. Accordingly, *Drosophila* is a suitable organism for addressing questions relevant to mammalian CI biogenesis. We anticipate that future studies using the full repertoire of genetic tools and resources in *Drosophila* should foster the discovery of paradigms for regulating CI assembly in humans.

EXPERIMENTAL PROCEDURES

Drosophila Strains and Genetics

For a list of stocks used and detailed experimental procedures, see Supplemental Experimental Procedures.

BN-PAGE

BN-PAGE was performed using NativePAGE gels from Life Technologies, following the manufacturer's instructions.

Silver Staining

Silver staining of native gels was performed with the SilverXpress staining kit from Life Technologies, following the manufacturer's protocol.

In-Gel CI Activity

CI activity in native gels was assayed by incubating the native gels in 0.1 mg/ml NADH, 2.5 mg/ml nitrotetrazolium blue chloride, and 5 mM Tris-HCl (pH 7.4) at room temperature.

Immunoblotting

For immunoblotting of samples in native gels, protein complexes from native gels were transferred to polyvinylidene fluoride (PVDF) membranes (Bio-Rad) and probed with the relevant antibodies using standard procedures.

MS Analyses

After MS with a Thermo Fusion Tribrid mass spectrometer, tandem mass spectra from raw files were searched against a *Drosophila* protein database using the Proteome Discoverer 1.4 software (Thermo Finnigan). The Proteome Discoverer application extracts relevant MS/MS spectra from the .raw file and determines the precursor charge state and the quality of the fragmentation spectrum. The Proteome Discoverer probability-based scoring system rates the relevance of the best matches found by the SEQUEST algorithm. The *Drosophila* protein database was downloaded as FASTA-formatted sequences from Uniprot protein database (database released in May 2015). The peptide mass search tolerance was set to 10 ppm. A minimum sequence length of seven amino acids residues was required. Only fully tryptic peptides were considered. To calculate confidence levels and false discovery rates (FDR), Proteome Discoverer generates a decoy database containing reverse sequences of the non-decoy protein database and performs the search against this concatenated database (non-decoy + decoy). Scaffold (Proteome Software) was used to visualize searched results. The discriminant score was set at less than 1% FDR determined on the basis of the number of accepted decoy database peptides to generate protein lists for this study. Spectral counts were used for estimation of relative protein abundance between samples.

SUPPLEMENTAL INFORMATION

Supplemental Information includes Supplemental Experimental Procedures, four figures, and five tables and can be found with this article online at http://dx.doi.org/10.1016/j.celrep.2017.06.015.

AUTHOR CONTRIBUTIONS

E.O.-A. conceived the project, designed experiments, and secured funding for the work. C.J.G., J.K., E.C., and E.O.-A. performed all experiments, except mass spectrometry. E.I.C. performed mass spectrometry. E.O.-A., C.J.G., J.K., and E.I.C. analyzed and discussed results. E.O.-A. wrote the manuscript with feedback from E.I.C. C.J.G., and J.K.

ACKNOWLEDGMENTS

We thank members of the Owusu-Ansah lab for general discussions; Eric Schon, Estela Area-Gomez, Henry Colecraft, Barbara Corneo, Wes Grueber, Laura Johnston, Richard Kitsis, Andrew Marks, Martin Picard, Liza Pon, Mimi Shirasu-Hiza, and David Walker for fly stocks, reagents, and critical discussions; and Stavroula Kousteni for critical discussions and for providing skeletal and cardiac muscle samples from mice. We acknowledge the Bloomington *Drosophila* Stock Center, the National Institute of Genetics (Japan), and the Vienna Drosophila Resource Center for various fly strains. We appreciate Steven Shikhel's technical assistance in dissecting cardiac and skeletal muscles from mice and the technical assistance obtained from the Proteomics Shared Resource at the Herbert Irving Comprehensive Cancer Center, Columbia University Medical Center. This work was supported by an Institutional Cardiovascular Research Training Grant (T32 HL120826) to C.J.G. and J.K. and a NIH R21 grant (DK112074), a pilot grant from the Robert N. Butler Columbia Aging Center, and institutional startup funds from the Department of Physiology and Cellular Biophysics, Columbia University Medical Center, to E.O.-A.

Received: December 19, 2016
Revised: May 18, 2017
Accepted: June 1, 2017
Published: July 5, 2017

REFERENCES

Abdrakhmanova, A., Zwicker, K., Kerscher, S., Zickermann, V., and Brandt, U. (2006). Tight binding of NADPH to the 39-kDa subunit of complex I is not required for catalytic activity but stabilizes the multiprotein complex. Biochim. Biophys. Acta *1757*, 1676–1682.

Andrews, B., Carroll, J., Ding, S., Fearnley, I.M., and Walker, J.E. (2013). Assembly factors for the membrane arm of human complex I. Proc. Natl. Acad. Sci. U S A *110*, 18934–18939.

Balsa, E., Marco, R., Perales-Clemente, E., Szklarczyk, R., Calvo, E., Landázuri, M.O., and Enríquez, J.A. (2012). NDUFA4 is a subunit of complex IV of the mammalian electron transport chain. Cell Metab. *16*, 378–386.

Berger, I., Hershkovitz, E., Shaag, A., Edvardson, S., Saada, A., and Elpeleg, O. (2008). Mitochondrial complex I deficiency caused by a deleterious NDUFA11 mutation. Ann. Neurol. *63*, 405–408.

Brand, A.H., and Perrimon, N. (1993). Targeted gene expression as a means of altering cell fates and generating dominant phenotypes. Development *118*, 401–415.

Budde, S.M., van den Heuvel, L.P., Janssen, A.J., Smeets, R.J., Buskens, C.A., DeMeirleir, L., Van Coster, R., Baethmann, M., Voit, T., Trijbels, J.M., and Smeitink, J.A. (2000). Combined enzymatic complex I and III deficiency associated with mutations in the nuclear encoded NDUFS4 gene. Biochem. Biophys. Res. Commun. *275*, 63–68.

Clason, T., Ruiz, T., Schägger, H., Peng, G., Zickermann, V., Brandt, U., Michel, H., and Radermacher, M. (2010). The structure of eukaryotic and prokaryotic complex I. J. Struct. Biol. *169*, 81–88.

Duarte, M., Sousa, R., and Videira, A. (1995). Inactivation of genes encoding subunits of the peripheral and membrane arms of neurospora mitochondrial complex I and effects on enzyme assembly. Genetics *139*, 1211–1221.

Efremov, R.G., Baradaran, R., and Sazanov, L.A. (2010). The architecture of respiratory complex I. Nature *465*, 441–445.

Fiedorczuk, K., Letts, J.A., Degliesposti, G., Kaszuba, K., Skehel, M., and Sazanov, L.A. (2016). Atomic structure of the entire mammalian mitochondrial complex I. Nature *538*, 406–410.

Guarani, V., Paulo, J., Zhai, B., Huttlin, E.L., Gygi, S.P., and Harper, J.W. (2014). TIMMDC1/C3orf1 functions as a membrane-embedded mitochondrial complex I assembly factor through association with the MCIA complex. Mol. Cell. Biol. *34*, 847–861.

Guerrero-Castillo, S., Baertling, F., Kownatzki, D., Wessels, H.J., Arnold, S., Brandt, U., and Nijtmans, L. (2017). The assembly pathway of mitochondrial respiratory chain complex I. Cell Metab. *25*, 128–139.

Haynes, C.M., Fiorese, C.J., and Lin, Y.F. (2013). Evaluating and responding to mitochondrial dysfunction: the mitochondrial unfolded-protein response and beyond. Trends Cell Biol. *23*, 311–318.

Heide, H., Bleier, L., Steger, M., Ackermann, J., Dröse, S., Schwamb, B., Zörnig, M., Reichert, A.S., Koch, I., Wittig, I., and Brandt, U. (2012). Complexome profiling identifies TMEM126B as a component of the mitochondrial complex I assembly complex. Cell Metab. *16*, 538–549.

Hirst, J. (2013). Mitochondrial complex I. Annu. Rev. Biochem. *82*, 551–575.

Hoefs, S.J., Dieteren, C.E., Distelmaier, F., Janssen, R.J., Epplen, A., Swarts, H.G., Forkink, M., Rodenburg, R.J., Nijtmans, L.G., Willems, P.H., et al. (2008). NDUFA2 complex I mutation leads to Leigh disease. Am. J. Hum. Genet. *82*, 1306–1315.

Hoefs, S.J., van Spronsen, F.J., Lenssen, E.W., Nijtmans, L.G., Rodenburg, R.J., Smeitink, J.A., and van den Heuvel, L.P. (2011). NDUFA10 mutations cause complex I deficiency in a patient with Leigh disease. Eur. J. Hum. Genet. *19*, 270–274.

Hu, Y., Flockhart, I., Vinayagam, A., Bergwitz, C., Berger, B., Perrimon, N., and Mohr, S.E. (2011). An integrative approach to ortholog prediction for disease-focused and other functional studies. BMC Bioinformatics *12*, 357.

Jensen, M.B., and Jasper, H. (2014). Mitochondrial proteostasis in the control of aging and longevity. Cell Metab. *20*, 214–225.

Kirby, D.M., Salemi, R., Sugiana, C., Ohtake, A., Parry, L., Bell, K.M., Kirk, E.P., Boneh, A., Taylor, R.W., Dahl, H.H., et al. (2004). NDUFS6 mutations are a novel cause of lethal neonatal mitochondrial complex I deficiency. J. Clin. Invest. *114*, 837–845.

Nehls, U., Friedrich, T., Schmiede, A., Ohnishi, T., and Weiss, H. (1992). Characterization of assembly intermediates of NADH:ubiquinone oxidoreductase (complex I) accumulated in Neurospora mitochondria by gene disruption. J. Mol. Biol. *227*, 1032–1042.

Nouws, J., Nijtmans, L., Houten, S.M., van den Brand, M., Huynen, M., Venselaar, H., Hoefs, S., Gloerich, J., Kronick, J., Hutchin, T., et al. (2010). Acyl-CoA dehydrogenase 9 is required for the biogenesis of oxidative phosphorylation complex I. Cell Metab. *12*, 283–294.

Ostergaard, E., Rodenburg, R.J., van den Brand, M., Thomsen, L.L., Duno, M., Batbayli, M., Wibrand, F., and Nijtmans, L. (2011). Respiratory chain complex I deficiency due to NDUFA12 mutations as a new cause of Leigh syndrome. J. Med. Genet. *48*, 737–740.

Owusu-Ansah, E., and Banerjee, U. (2009). Reactive oxygen species prime Drosophila haematopoietic progenitors for differentiation. Nature *461*, 537–541.

Owusu-Ansah, E., Yavari, A., Mandal, S., and Banerjee, U. (2008). Distinct mitochondrial retrograde signals control the G1-S cell cycle checkpoint. Nat. Genet. *40*, 356–361.

Owusu-Ansah, E., Song, W., and Perrimon, N. (2013). Muscle mitohormesis promotes longevity via systemic repression of insulin signaling. Cell *155*, 699–712.

Radermacher, M., Ruiz, T., Clason, T., Benjamin, S., Brandt, U., and Zickermann, V. (2006). The three-dimensional structure of complex I from Yarrowia lipolytica: a highly dynamic enzyme. J. Struct. Biol. *154*, 269–279.

Rera, M., Bahadorani, S., Cho, J., Koehler, C.L., Ulgherait, M., Hur, J.H., Ansari, W.S., Lo, T., Jr., Jones, D.L., and Walker, D.W. (2011). Modulation of longevity and tissue homeostasis by the Drosophila PGC-1 homolog. Cell Metab. *14*, 623–634.

Roy, S., and VijayRaghavan, K. (1999). Muscle pattern diversification in Drosophila: the story of imaginal myogenesis. BioEssays *21*, 486–498.

Scacco, S., Petruzzella, V., Budde, S., Vergari, R., Tamborra, R., Panelli, D., van den Heuvel, L.P., Smeitink, J.A., and Papa, S. (2003). Pathological mutations of the human NDUFS4 gene of the 18-kDa (AQDQ) subunit of complex I affect the expression of the protein and the assembly and function of the complex. J. Biol. Chem. *278*, 44161–44167.

Stroud, D.A., Surgenor, E.E., Formosa, L.E., Reljic, B., Frazier, A.E., Dibley, M.G., Osellame, L.D., Stait, T., Beilharz, T.H., Thorburn, D.R., et al. (2016). Accessory subunits are integral for assembly and function of human mitochondrial complex I. Nature *538*, 123–126.

Tuschen, G., Sackmann, U., Nehls, U., Haiker, H., Buse, G., and Weiss, H. (1990). Assembly of NADH: ubiquinone reductase (complex I) in Neurospora mitochondria. Independent pathways of nuclear-encoded and mitochondrially encoded subunits. J. Mol. Biol. *213*, 845–857.

Vartak, R.S., Semwal, M.K., and Bai, Y. (2014). An update on complex I assembly: the assembly of players. J. Bioenerg. Biomembr. *46*, 323–328.

Vinothkumar, K.R., Zhu, J., and Hirst, J. (2014). Architecture of mammalian respiratory complex I. Nature *515*, 80–84.

Vogel, R.O., Janssen, R.J., van den Brand, M.A., Dieteren, C.E., Verkaart, S., Koopman, W.J., Willems, P.H., Pluk, W., van den Heuvel, L.P., Smeitink, J.A., and Nijtmans, L.G. (2007). Cytosolic signaling protein Ecsit also localizes to mitochondria where it interacts with chaperone NDUFAF1 and functions in complex I assembly. Genes Dev. *21*, 615–624.

Wittig, I., Braun, H.P., and Schägger, H. (2006). Blue native PAGE. Nat. Protoc. *1*, 418–428.

Zhu, J., Vinothkumar, K.R., and Hirst, J. (2016). Structure of mammalian respiratory complex I. Nature *536*, 354–358.

Zickermann, V., Wirth, C., Nasiri, H., Siegmund, K., Schwalbe, H., Hunte, C., and Brandt, U. (2015). Structural biology. Mechanistic insight from the crystal structure of mitochondrial complex I. Science *347*, 44–49.